

# THE UNIVERSITY OF SHEFFIELD

Department of Chemical & Biological Engineering



The  
University  
Of  
Sheffield.

## **Twin Screw Wet Granulation of Pharmaceutical Powders: Effects of Drying on Granules and Tablet Attributes**

A Thesis Submitted in Partial Fulfilment of the Requirements  
for the Degree of Doctor of Philosophy

August 2021

**Kawther F. Kadhim**

## Abstract

Conformity to the FDA, it is of importance for pharmaceutical industries to maintain good manufacturing practice with precision. Developing the best quality tablets that meet changing demands of patients remains a key purpose for this particular study. In this project, three main stages of tablet production including granulation, drying and tableting are investigated for identifying optimum parameters in achievement of final granule and tablet quality attributes. Particular attention is given to drying process in fluidized bed using conventional batch lab-scale and continuous six-segmented industrial-scale. The Twin Screw Granulator (TSG) and Fluidized Bed (FB) dryer are the focus of this research project as they are strongly interrelated and are the key units located upstream in the process. Given the strong association between the twin-screw parameters and its effect on granules formation and consequent drying, it is timely to investigate the downstream impact of twin screw. Therefore, the uniqueness of this project is integrating twin screw granulation with fluidized bed drying process to set the parameters of processing and formulation on two scale production. This unique involvement of twin screw has further assisted in determining the subsequent transformation during fluidised bed drying process. Moreover, this project aimed at visualizing the spatial distribution of moisture content within a single granule as a function of fluidized bed drying time through a novel quantitative non-destructive NIR chemical imaging technique. This technique has the potential to determine or predict the drying stages that the granules exhibit in drying process at any point of time. The effect of formulation parameters including liquid solid (L/S) ratio, binder viscosity and Lactose primary particle size, as well as process parameter including screw configuration were examined in both scale productions. For the work conducted using small laboratory scale equipment, FB process parameters such as air temperature and air velocity were investigated with all other formulation and process variables of TSG kept constant (i.e., 150M lactose as the primary powder, water as the granulation liquid binder, L/S of 0.1, screw speed of 250rpm and 16 kneading elements (KE) in each screw). Furthermore, when TSG both formulations (i.e., varying the L/S ratio; L/S of 0.089, 0.104 and HPC binder viscosity of different concentrations; 2%, 5%, 10%, 15%) and process parameters (varying number of kneading elements, conveying element only; 0KE, 4KE, 8KE, 16KE in each screw) were investigated, all other FB process parameters (i.e., air velocity of 2m/s, air

temperature of 50°C) kept constant. In industrial scale (consgima-25 powder to tablet line), one TSG formulation parameter (varying lactose powder primary particle size) was investigated with keeping all other TSG and FB parameters fixed (i.e., water as granulation liquid binder, L/S of 0.1, screw speed of 250 rpm, 2 kneading element zones in each screw, FB drying air temperature of 50°C, air flow rate of 400 m<sup>3</sup>/hr. and FB drying time of 800 seconds). And one TSG process parameter (varying screw configurations, conveying element only, 1 zone of kneading element and 2 zones of kneading element) was investigated with keeping all other TSG and FB parameters constant (i.e., 150M lactose as the granulation primary powder, water as the granulation liquid binder, L/S of 0.1, screw speed of 250 rpm, FB drying air temperature of 50°C, air flow rate of 400 m<sup>3</sup>/hr and FB drying time of 800 seconds). Granule breakage during FB drying in laboratory scale was evident; however, minimal breakage was achieved when higher L/S ratio, more kneading elements and lower binding viscosity are used. In addition, lower L/S ratio, a smaller number of kneading elements, lower binder viscosity and smaller lactose primary particle size was shown to follow a fast-drying regime. Furthermore, tablet attributes including tensile strength and dissolution were examined. Robust quantitative NIR-CI analytical method was developed and successfully obtained a spatial moisture content distribution across the radial distance of a single granule with MATLAB image processing software.

## **Acknowledgment**

---

I would like to express my deep and sincere gratitude to my supervisor Professor Agba D. Salman for giving me the opportunity to pursue this PhD and providing invaluable guidance throughout this research. His vision, sincerity and motivation have deeply inspired me. It was a great privilege and honour to work and study under his guidance.

First and foremost, I must acknowledge and thank The Almighty Allah for blessing, protecting and guiding me throughout this period. I could never have accomplished this without the faith I have in the Almighty. It would be impossible to go any further without expressing thanks to my PPG family.

Special thanks to my Mum & Dad for their endless love, prayers and continuous support. I am extremely grateful to you. Also, I express my thanks to my sisters for their support and encouragement throughout my entire study.



## List of Abbreviation

<b>FBD</b>	<b>Fluidized bed drying</b>
<b>FDA</b>	Food and Drug Administration
<b>FFC</b>	Flow function coefficient
<b>ICH</b>	International Conference for Harmonization
<b>KE</b>	Kneading element
<b>LOD</b>	Loss on drying
<b>LPCE</b>	Long pitch conveying element
<b>NIR-CI</b>	Near infrared chemical imaging
<b>PAT</b>	Process Analytical Technologies
<b>PLS</b>	Partial least square
<b>PSD</b>	Particle size distribution
<b>QbD</b>	Quality by Design
<b>QCI</b>	Quantitative chemical imaging
<b>RMSEC</b>	Root-mean-square
<b>RST</b>	Ring shear tester
<b>SEM</b>	Scanning electron microscopy
<b>SPCE</b>	Short pitch conveying element
<b>TSG</b>	Twin screw granulator

## Table of Contents

Abstract	1
Acknowledgment	3
List of Abbreviation	4
1.0 Introduction and Literature Review	16
1.1 Introduction	16
1.1.1 Why Drying of a Granule is Significant?	19
1.1.2 Principle of Fluidized Bed Drying	20
1.1.3 Consideration of the scales and the potential challenges of using the two-unit operations (TSG and FBD) in tandem alongside with the NIR chemical imaging challenges.	23
1.2 Literature Review	26
1.2.1 Conventional Batch Fluidized Bed Drying	26
1.2.1.2 Fluidized Bed Drying Challenges	31
1.2.1.2.1 Attrition and Breakage of Granules in Fluidized Bed	31
1.2.2 Continuous Manufacturing Process	35
1.2.2.1 Continuous Powder to Tablet Line ConsiGma-25	37
1.2.2.2 Stability and Repeatability of the ConsiGma 25 Line System	39
1.2.2.3 Twin Screw Granulation in ConsiGma 25 System	43
1.2.2.4 Six-Segmented Fluidized Bed Dryer in the ConsiGma 25 System	53
1.3 Effect of Moisture on Tablet Properties	63
1.4 Conclusion on the Fluidized Bed Drying of Granules	67
1.5 Near Infrared Chemical Imaging in Pharmaceutical Industry	68
1.5.1 Introduction to Near Infrared	68
1.5.2 Near Infrared Chemical Imaging	69
1.5.2.1 Multivariate Data Analysis	71
1.5.2.2 Studies on Near Infrared Chemical Imaging	72
1.5.2.2.1 Penetration Depth of NIR-CI	74
1.5.2.2.2 Near Infrared Chemical Imaging in Drying	77
1.5.3 Conclusion of the Literature Review on NIR-CI	78
Aim of the Research	79
Thesis Overview	81
2.0 Materials and Methods	83
2.1 Materials and Method used in the lab- scale TSG and FBD	83
2.1.1 $\alpha$ - Lactose Monohydrate	83
2.1.1.1 Lactose Powder Characterization	84
2.1.1.2 Particle Size Distribution	85
2.1.1.3 Powder Morphology	85
2.1.1.4 Flowability Test	86
2.1.1.5 Differential Scanning Calorimetry (DSC)	86
2.1.1.6 Powder Humidity Conditioning	88
2.1.2 Hydroxypropyl Cellulose (binder)	88
2.2 Twin screw Granulation and Granules Production	90

2.2.1 Liquid Binder Preparation _____	90
2.2.2 Granulation Equipment _____	92
2.2.3 Granules Production in TSG _____	93
2.3 Drying Equipment _____	94
2.3.2 Fluidized Bed Drying of Granules _____	96
2.3.3 Tablet Production _____	96
2.4. Product characterization _____	98
2.4.4 Tablet _____	99
2.5 Experimental work in the Continuous ConsiGma-25 line _____	101
2.5.1 Twin Screw Granulation and Drying _____	103
2.5.2 Tablet Dissolution Measurement _____	104
<b>Chapter 3: Drying in a Batch Laboratory Scale Fluidized Bed Dryer: Effect of Fluidized Bed Process Parameters _____</b>	<b>106</b>
3.0 Introduction _____	106
3.1 Powder Behaviour Before Granulation _____	106
3.1.2 Effect of Relative Humidity on the Tableability of the Powder _____	107
3.2.0 Twin Screw Granulation _____	110
3.2.2 Moisture Content of Wet Granules _____	111
3.3 Fluidized Bed Drying of Granules _____	113
3.3.1.2 Sphericity of Granules _____	116
4.0 Drying in Batch Laboratory Scale Fluidized Bed: Effect of Twin-Screw Formulation Parameters _____	124
4.1 Introduction _____	124
4.2 Result and Discussion _____	124
4.3 Effect of Viscosity of Granulation Liquid Binder _____	132
4.3.0 Introduction _____	132
4.3.1 Results and Discussions _____	132
4.4 Conclusion _____	138
5.0 Drying in Batch Laboratory Scale Fluidized Bed: Effect of Twin-Screw Process Parameters _____	140
5.1 Introduction _____	140
5.2 Screw Configuration _____	141
5.3 Results and Discussions _____	142
5.3.1 Drying curves for granules made with different screw configurations _____	148
5.4 Conclusion _____	152
6.0 Drying in a Continuous Wet Granulation ConsiGma 25 line: Investigation of the Effect of the Screw Configuration _____	153
6.1 Introduction _____	153
6.2 Design of Experiment _____	154
6.3 Screw Configuration _____	156
6.4 Results and Discussion _____	158
6.4.1 Temperature Profiles of Granules During Drying in the Fluidized bed _____	160
6.4.2 NIR online measurements of Moisture content in Fluidized Bed _____	163
6.4.3 Tablet Evaluation _____	167
6.4.3.1 Tablet Tensile Strength _____	167
6.4.3.2 Tablet Dissolution _____	171
6.5 Conclusion _____	172

7.0 Drying in a Continuous Wet Granulation ConsiGma 25 Line: Investigation of the Effect of Using Different Primary Particle size of Lactose Powder _____	174
7.1 Introduction _____	174
7.2 Lactose Powders Used _____	175
7.2.1 Morphology of the Powder _____	176
7.3 Lactose Powders Density _____	179
7.4 Design of Experiment _____	180
7.5 Result and Discussion _____	183
7.5.1 TSG Granules Size Distribution _____	183
7.5.2 Behaviour of Granules Drying Process in the Segmented Fluidized Bed Dryer _____	185
7.5.3 NIR Online Measurements of Moisture Content in the Fluidized Bed Dryer _____	187
8.0 Investigating the Drying Mechanism Using Near Infrared Chemical Imaging (NIR-CI) _____	198
8.1 1 Introduction _____	198
8.2 Experimental Methodology on NIR-CI _____	199
9.0 Main Conclusions _____	226
9.1 Future Work _____	230
Use of NIR-CI in Further Single Granule Drying Model _____	230
9.2 References _____	231
□ 9.3 Appendix _____	244

## Tables

Table 1: Features and potential benefits of continuous manufacturing (Lee, S.L., et al 2015) _____	36
Table 2: Type of Screw elements used in the twin-screw granulation _____	94
Table 3: Variation in the tablet thickness, diameter and weight at three different screw configurations __	167
Table 4: Particle size $d_{10}$ , $d_{50}$ and $d_{90}$ of the four lactose monohydrate powders used in this study _____	176
Table 5: The measured bulk and tapped density of the four-lactose powder monohydrate _____	180
Table 6: Variation in the tablet mass, thickness and diameter as the primary particle size of the starting materials (lactose monohydrate) changes. _____	192
Table 7: Highlight of the advantages of using the NIR chemical imaging technique over LOD. _____	224

## Table of Figures

Figure 1: A simple depiction of two types of manufacturing. (a) Batch manufacturing (b) continuous manufacturing (Lee, S.L., et al 2015).	16
Figure 2: The tablet manufacturing processes including wet granulation, dry granulation and direct compression (Mangal, S., et al 2015).	18
Figure 3: Representation of the transfer of heat and mass in the drying of a particle (Syahrul, Hamdullahpur and Dincer, 2002).	20
Figure 4: Drying curve of wet granule, $X_0$ is the initial moisture content, $X_{cr}$ is the critical moisture content and $X_e$ is equilibrium moisture content] (Mezhericher, 2014).	21
Figure 5: Transport phenomena in wet granule at (a) the 1 <sup>st</sup> stage of drying (b) the 2 <sup>nd</sup> stage of drying (Mezhericher, 2014).	22
Figure 6: (a) Granule moisture content vs. time for different air velocities (b) bed temperature vs. granule moisture content (c) Air outlet temperature vs. granule moisture content (d) Air outlet temperature as a function of granule moisture content at various velocities (Briens and Bojarra, 2010).	28
Figure 7: Effect of (a) air temperature (b) air velocity (c) particle size (d) initial moisture content on the drying rate. [“C(t) is the moisture content with respect to time (kg water/ kg dry sand”] (Srinivas and Pydi Setty, 2013).	30
Figure 8: Schematic illustration of the described mechanism (Verkoeijen et al., 2002)	33
Figure 9: Schematic diagram illustrating the ConsiGma- 25 pilot plant utilized in this project (drawn not to scale).	38
Figure 10: Process variables stability with time (a) twin screw granulator torque, (b) jacket temperature of the twin-screw granulator, (c) difference in pressure over the filters of the dryer, and (d) temperature of mill screen (Vercruysse et al. 2013).	39
Figure 11: Tablet attributes stability and repeatability over time (a) tablet weight (b) tablet hardness (Vercruysse et al. 2013).	40
Figure 12: Measurements of (a)temperature profiles (b) Loss on drying for materials processed during the 1 h continuous run and the single cell runs conducted with the C25 and the C1 system (Vercruysse et al. 2015).	42
Figure 13: Impact of different twin screw granulator parameters on percentage of (a) fines (b) oversized [Numb: number of kneading elements: temperature of granulator barrel, Bind(wet): wet binder addition, Scr: speed of the screw, Angle: kneading elements angle and Thr: powder throughput] (Vercruysse et al., 2012).	44
Figure 14: Impact of number of kneading elements on the granule size distribution (Vercruysse et al., 2014).	45
Figure 15: Impact of liquid to solid ratio on the particle size for two different powder materials (a) Lactose (b) MCC. (Hwang et al., 2019).	46
Figure 16: Effect of varying different granulation parameters on (a) fines fraction (b) oversized fractions and (c) d50 of granules (Vandevivere et al., 2019).	49
Figure 17: Particle size distribution before and after wetting (a) hydrophilic blend at low L/S (b) hydrophilic blend at high L/S (c) hydrophobic blend at low L/S (d) hydrophobic blend at high L/S (Verstraeten et al., 2017).	50
Figure 18: Effect of the concentration of HPMC on the size distribution of granule [ F6 formulation contains 20% HPMC and F9 40%HPMC] (Vanhoorne et al., 2016)	51
Figure 19: Tableability of (A) 20% HPMC concentration and 20% powdered theophylline (B) 40% HPMC concentration and 20% powdered theophylline (Vanhoorne et al., 2016).	51
Figure 20: Visual illustration to show the filling cycle in the segmented fluidized bed dryer of the ConsiGma 25 system (De Leersnyder et al., 2018).	53
Figure 21: Granules size distribution derived from C25 and C1 single cell runs after drying process in the fluidized bed (Vercruysse et al. 2015).	54
Figure 22: Illustration of the two ConsiGma™-25 (left) Horizontal set-up and (right) vertical setup with the red line represents the wet transfer line (only in horizontal set-up) and the green represents the dry transfer line.	55
Figure 23: Temperature of the granules (yellow line) and outlet humidity of air (black line) for the experiments performed at a temperature of (a) 60°C (b) 70°C and (c) 80°C (Fonteyne et al., 2014).	57
Figure 24: Moisture content of granules at different size fractions and drying air temperature as measured by means of Karl Fischer (Fonteyne et al., 2014).	59

Figure 25: Effect of water activity on the strength of tablets (MADG) at a compression force of 10 kN) “◆; Amount of added water: 0.0%, 1.0%, 1.5%, 2.0% ◇; Amount of added water: 2.5%, 3.0% and 5.0% “(Takasaki et al., 2016). ____	64
Figure 26: Strength of tablet as a function of solid fraction of different moisture content; “◆ 2.12% moisture, ■ 4.02% moisture, ○ 4.56% moisture, □ 4.97% moisture, ● 5.26% moisture” (Wade, Martin and Long, 2013). _____	65
Figure 27: 3D hyperspectral data cube unfolding for the approaches of processing data. _____	70
Figure 28: Absorbance profiles of tablet scanned from top, edge and bottom. The images are displayed in the same scale, based on absorbance at 2120 nm. (Christopher et al.,2008). _____	73
Figure 29: Profile of absorbance for a lactose tablet edge blended with 0.25%MgS (Christopher et al.,2008). _____	74
Figure 30: Schematic illustration of the experimental model (established by (Clarke et al., 2002) _____	75
Figure 31: Illustration of the 7 mm melamine holder with milk powder of 3mm depth placed on the top of it. The area with light grey shows the surface of the sample (30 mm x30 mm) (Huang et al., 2016). _____	76
Figure 32: Structure formula of $\alpha$ - Lactose Monohydrate (Rowe et al. 2006). _____	83
Figure 33: Sorption isotherm curve of crystalline $\alpha$ - lactose monohydrate at different temperatures (Bronlund and Paterson, 2004). _____	84
Figure 34: Volume based particle size distribution of lactose primary powder. _____	85
Figure 35: SEM of the primary particles of lactose monohydrates (150M lactopure). _____	86
Figure 36: Thermal DSC curve for $\alpha$ - lactose monohydrate powder in which the 1 <sup>st</sup> peak of the curve represents water of crystalline (150°C) and confirms that this lactose is $\alpha$ -monohydrates, and the 2 <sup>nd</sup> peak represents the melting of lactose (220°C). _____	87
Figure 37: Structure formula of Hydroxypropyl Cellulose (Rowe, Sheskey and Owen, 2006). _____	88
Figure 38: Scanning electron microscopy of the Hydroxypropyl Cellulose (HPC) particles. _____	89
Figure 39: Pump calibration for water liquid binder _____	91
Figure 40: Pump calibration for HPC liquid binder. _____	91
Figure 41: Image of the twin-screw granulator. _____	92
Figure 42: Image of the Screw configuration used in this in this project (16 KE in each screw). _____	93
Figure 43: A photograph diagram of the fluidized bed used for drying of the granules. _____	95
Figure 44: Schematic diagram of the Fluidized bed dryer with dimensions. _____	95
Figure 45: Flow diagram summarizing the project methodology process used for this chapter. _____	97
Figure 46: Illustration of Project process diagram. _____	100
Figure 47: ConsiGma-25 Powder to Tablet line used in this project containing an integrated co-rotating twin screw granulator, six- segmented fluidized bed dryer, milling, formulation and tableting units. _____	101
Figure 48: Illustration of the filling cycle (anticlockwise direction) in the six segmented fluidized bed dryers of the ConsiGma-25 line. _____	102
Figure 49: Near infrared probe calibration curve for different moisture contents of lactose powder mixed with water manually (samples were analysed using both near infrared probe and loss on drying by moisture analyser). _____	103
Figure 50: Schematic illustration of the dissolution testing set up and the parameters used in this study was based on using the USP apparatus I (with temperature of 37°C $\pm$ 0.5, a water of volume of 200 ml and a motor stirring speed of 700rpm). _____	105
Figure 51: Moisture content of lactose powder (150M) conditioned at different relative humidities (10% to 90% RH at a step of 10%) using humidity chamber at a temperature of 25°C for three days. _____	107
Figure 52: The influence of relative humidity at which the feed powder is stored on the tablet strength for a range of compression forces (10,15,20kN). _____	108
Figure 53: Images of lactose powder stored at relative humidity for three days of (a) 10% and (b) 90% taken by Keyence microscope at the same scale/magnification (X20). _____	109
Figure 54: Size distribution of initial granules prepared by TSG with lactose powder of 150M and water as a liquid binder, L/S of 0.10, screw speed of 250rpm, powder feed rate of 2kg/hr and 16-KE in each screw (before drying in fluidized bed). _____	110

Figure 55: Moisture content of wet granules as produced directly from TSG measured with loss on drying by moisture analysers at temperature of 105°C with fully automatic mode and a sample of 2 grams of wet granules used in each measurement. _____	111
Figure 56: Moisture content of granules produced by TSG using 150M lactose powder and water as liquid binder at a L/S of 0.1, 250rpm and 16KE in each screw and dried at standard room conditions in humidity chamber at a temperature and relative humidity of 25°C and 40% respectively with moisture content measurement performed every 20 minutes using loss on drying by moisture analyser at a temperature of 105°C and fully automatic mode. _	112
Figure 57: Effect of fluidizing air velocities on the PSD of granules produced by TSG with 150M lactose powder and water as liquid binder at a L/S of 0.1, 250rpm, 16-KE in each screw and dried with air temperature of 50°C. _____	114
Figure 58: Effect of fluidizing air temperature on the PSD of granules produced by TSG with 150M lactose powder and water as a liquid binder at a L/S of 0.1, 250rpm, 16-KE in each screw and dried with air velocity of 2m/s. _____	115
Figure 59: Sphericity curves for granules produced by TSG with 150M lactose powder and water as a liquid binder at a L/S of 0.1, 250 rpm and 16-KE in each screw and dried in fluidized bed at different air velocities (2m/s, 2.6m/s, 3.4m/s) and air temperature of 50°C. _____	116
Figure 60: Sphericity curves for granules produced by TSG with 150M lactose powder and water as a liquid binder at a L/S of 0.1, 250 rpm, 16-KE in each screw and dried in fluidized bed at different air temperature (25,50 and 75 °C) and an air velocity of 2m/s. _____	117
Figure 61: Drying curves of granules produced by TSG with 150M lactose powder and water as a liquid binder at a L/S of 0.1, 250 rpm and 16-KE in each screw and dried in FB at different air velocities 2, 2.6 and 3.4 m/ s using an air temperature of 50°C. _____	118
Figure 62: Drying curves of granules produced by TSG with 150M lactose powder and water as a liquid binder at L/S of 0.1, 250 rpm and 16-KE in each screw and dried in FB at different air temperatures of 25, 50 and 75°C using an air velocity of 2 m/s. _____	119
Figure 63: X-ray images of granules produced by TSG with 150M lactose powder and water as a liquid binder at L/S of 0.1, 250rpm and 16-KE in each screw (a) Room Temperature dried granules, (b) Fluidized bed- dried lactose granules, at a temperature of 50°C, air velocity of 2 m/s and drying time of 3 minutes. _____	121
Figure 64: Relationship between the fluidized bed drying time, moisture content of granules and tensile strength of tablet made from those granules. The granules were produced by TSG with 150M lactose powder and water as a liquid binder, L/S of 0.1, 250 rpm and 16- KE in each screw, the granules were then dried in FB at temperature of 25°C and air velocity of 2 m/s. _____	122
Figure 65 :Flow diagram showing the experimental conditions and variables used in the TSG and FB in this study. _	125
Figure 66: Size distribution of granules produced by the Twin screw granulator using 150M lactose powder and water as a liquid binder with screw speed of 250rpm, 16-KE in each screw at two different liquids to solid ratios (L/S of 0.089 and 0.104) before FB drying. _____	126
Figure 67: X-ray tomographic images of undried granules produced by TSG with 150M lactose powder with water as liquid binder, screw speed of 250 rpm and 16-KE in each screw at two different L/S ratios (a) L/S 0.089 with a porosity of 48% (b) L/S 0.104 with a porosity of 40%. _____	126
Figure 68: SEM images of granules produced by TSG with 150M lactose powder and water as a liquid binder with screw speed of 250rpm, 16-KE in each screw and at two different L/S ratio (L/S of 0.089 and L/S of 0.104) as indicated above. _____	128
Figure 69: Effect of varying liquid to solid ratios on the FB drying of granules produced by TSG with 150M lactose powder and water as a liquid binder, screw speed of 250 rpm, 16-KE in each screw and dried in FB at temperature of 50°C and an air velocity of 2m/s. _____	129
Figure 70: Size distribution of granules produced by TSG with 150M lactose powder and water as a liquid binder at a screw speed of 250 rpm, 16-KE in each screw at two different liquids to solid ratios before and after fluidized bed drying (temperature of 50°C and an air velocity of 2m/s. (a) L/S 0.089 (b) L/S 0.104. _____	130
Figure 71: Particle size (d10, d50, d90) of the batch of the granules that produced by TSG with 150M and water as liquid binder, 250 rpm, 16-KE in each screw at two different liquids to solid (L/S 0.089 and 0.104) and dried in FB at a temperature of 50°C and an air velocity of 2m/s. _____	131
Figure 72: Flow diagram showing the experimental conditions and variables used in the TSG and FB in this study. _	133

Figure 73: Shear viscosity versus shear rate for water and different HPC solution concentrations _____	134
Figure 74: The average shear viscosity for different concentrations of HPC solution including distilled water. _____	134
Figure 75: Size distribution of granules produced by TSG with 150M lactose powder and water as liquid binder (0% HPC) at 250 rpm, L/S of 0.10 and conveying elements only. This plot shows the PSD of granules before and after fluidized bed drying which was performed at a temperature of 50°C and an air velocity of 2m/s. _____	135
Figure 76: Size distribution of granules produced by TSG with 150M lactose powder and HPC as liquid binder (2% HPC) at 250 rpm, L/S of 0.10 and conveying elements only. This plot shows the PSD of granules before and after fluidized bed drying which was performed at a temperature of 50°C and an air velocity of 2m/s. _____	136
Figure 77: Size distribution of granules produced by TSG with 150M lactose powder and HPC as liquid binder (5% HPC) at 250 rpm, L/S of 0.10 and conveying elements only. This plot shows the PSD of granules before and after fluidized bed drying which was performed at a temperature of 50°C and an air velocity of 2m/s. _____	136
Figure 78: Size distribution of granules produced by TSG with 150M lactose powder and HPC as liquid binder (10% HPC) at 250 rpm, L/S of 0.10 and conveying elements only. This plot shows the PSD of granules before and after fluidized bed drying which was performed at a temperature of 50°C and an air velocity of 2m/s. _____	137
Figure 79: Size distribution of granules produced by TSG with 150M lactose powder and HPC as liquid binder (15% HPC) at 250 rpm, L/S of 0.10 and conveying elements only. This plot shows the PSD of granules before and after fluidized bed drying which was performed at a temperature of 50°C and an air velocity of 2m/s. _____	137
Figure 80: PSD (d <sub>10</sub> , d <sub>50</sub> , d <sub>90</sub> ) of granules produced by TSG using 150M lactose powder with water and HPC of different concentrations were used as a liquid binder, the screw speed was 250rpm and screw configuration of conveying element only. This Figure shows PSD before and after FBD which was performed at a temperature of 50 and an air velocity of 2m/s as binder concentration varies. _____	138
<b>Figure 81: Flow diagram showing the experimental conditions and variables used in the TSG and FB in this study.</b> _____	140
Figure 82: Screw configurations used in this study with (a) 4KE in each screw (b)8 KE in each screw (c) 16 KE in each screw (d) conveying elements only (OKE). The angle at which the Kneading element are placed is 60°. _____	141
Figure 83: Size distribution of granules produced by TSG using 150M lactose monohydrate powder with water used as the liquid binder, L/S of 0.1, screw speed of 250 rpm at four different screw configurations (conveying elements only; OKE, 4KE, 8KE, 16KE in each screw). This Figure shows the PSD of granules before fluidized bed drying. _____	142
Figure 84: Particle size (d <sub>10</sub> , d <sub>50</sub> and d <sub>90</sub> ) of granules produced by TSG using 150M lactose monohydrate powder with water used as the liquid binder, L/S of 0.1, screw speed of 250 rpm at four different screw configurations (conveying elements only;OKE,4KE 8KE,16KE in each screw). This Figure shows the PSD of granules before fluidized bed drying. _____	143
Figure 85: X-Ray images of granules produced by TSG using 150M lactose monohydrate powder with water used as the liquid binder, L/S of 0.1, screw speed of 250 rpm at four different screw configurations (a)conveying elements only;OKE (b) 4KE (c) 8KE (d) 16KE in each screw. These are X-Ray images of granules before fluidized bed drying. _____	145
Figure 86: Average porosity of granules produced by TSG using 150M lactose monohydrate powder with water used as the liquid binder, L/S of 0.1, screw speed of 250 rpm at four different screw configurations (conveying elements only;OKE,4KE 8KE,16KE in each screw). The porosity was measured by using X-Ray topography for granules before fluidized bed drying. _____	146
Figure 87: Scanning electron microscopy of granules produced by TSG with 150M lactose powder and water used as a liquid binder, 250rpm and at different screw configurations (a) 0 KE (b) 4 KE (c) 8 KE (d) 16 KE before FB drying. _____	147
Figure 88: Effect of varying screw configurations (OKE, 4KE, 8KE, 16KE) on the FB drying of granules produced by TSG with 150M lactose powder and water as a liquid binder, screw speed of 250 rpm, L/S of 0.1 and dried in FB at temperature of 50°C and an air velocity of 2m/s. _____	148
Figure 89: Size distribution of granules produced by TSG with 150M lactose powder and water used as a liquid binder at a screw speed of 250 rpm, L/S of 0.1 and a screw configuration of OKE conveying elements only in each screw. This figure shows the PSD of granules before and after Fluidized bed drying which was performed at a temperature of 50°C and an air velocity of 2m/s. _____	150



Figure 90: Size distribution of granules produced by TSG with 150M lactose powder and water used as a liquid binder at a screw speed of 250 rpm, L/S of 0.1 and a screw configuration of 4 kneading elements in each screw. This figure shows the PSD of granules before and after Fluidized bed drying which was performed at a temperature of 50°C and an air velocity of 2m/s. _____	150
Figure 91: Size distribution of granules produced by TSG with 150M lactose powder and water used as a liquid binder at a screw speed of 250 rpm, L/S of 0.10 and a screw configuration of 8 kneading elements in each screw. This figure shows the PSD of granules before and after Fluidized bed drying which was performed at a temperature of 50°C and an air velocity of 2m/s. _____	151
Figure 92: Size distribution of granules produced by TSG with 150M lactose powder and water as a liquid binder at a screw speed of 250 rpm, L/S 0.1 and a screw configuration of 16kneading elements in each screw. This figure shows the PSD of granules before and after Fluidized bed drying which was performed at a temperature of 50°C and an air velocity of 2m/s. _____	151
<b>Figure 93: Flow diagram showing process parameters used in TSG, fluidized bed dryer and tablet press unit of the ConsiGma -25 line as screw configurations vary.</b> _____	155
Figure 94: Pictures of (a) Short and long pitch conveying elements (LPCE) (b) Kneading elements used in the screw configuration of this study. _____	156
Figure 95: Screw configurations used in this study (a) Conveying elements only (b) conveying and 1-kneading elements zones (c) conveying and 2-kneading elements zones. The angle at which the kneading elements are placed is 60 degree. _____	157
Figure 96: Size distribution of granules produced by the TSG of the ConsiGma line using 150M lactose powder and water used as al liquid binder with L/S of 0.1 and screw speed of 250 rpm at three different screw configurations (conveying elements only, 2 kneading zone, and one kneading zone before drying. _____	158
Figure 97: Images of granules batches produced by TSG using 150M lactose powder and water as a liquid binder, L/S of 0.1, and screw speed of 250 rpm at (a) 2-kneading zones (b) 1kneading zone (c) conveying elements before drying in the segmented fluidized bed dryer. _____	159
Figure 98: PSD ( $d_{10}$ , $d_{50}$ and $d_{90}$ ) of granules produced by the TSG of the ConsiGma line using 150M lactose powder and water used as a liquid binder with L/S of 0.1 and screw speed of 250 rpm at three different screw configurations (conveying elements only, 2 kneading zone, and one kneading zone) before drying. _____	160
Figure 99: Temperature profiles at different screw configuration (conveying element only, 1 kneading zone and 2 kneading zones) inside the dryer cell 5 of the segmented fluidized bed dryer at an air temperature of 50 (°C), an air flow rate of 400 m <sup>3</sup> /hr, cell filling time of 300 seconds and a total drying time of 800 seconds. _____	162
Figure 100: Moisture content profiles at different screw configuration (conveying element only, 1 kneading zone and 2 kneading zones) inside the dryer cell 5 of the segmented fluidized bed dryer at an air temperature of 50 (°C), an air flow rate of 400 m <sup>3</sup> /hr, cell filling time of 300 seconds and a total drying time of 800 seconds. _____	165
Figure 101:Product presence profile of granules inside the dryer cell 5 measured by the NIR probe at different screw configurations (conveying element only, 1 kneading zone and 2 kneading zones). _____	165
Figure 102: Slopes of the drying curve between time 300 seconds and 400 seconds at the dryer cell at different screw configurations (conveying element only, 1 kneading zone and 2 kneading zones). _____	166
Figure 103: The residual moisture content of granules at the dryer cell at different screw configurations (conveying element only, 1 kneading zone and 2 kneading zones). _____	166
Figure 104: Curved faced tablets geometry with the illustration of strength equation parameters. _____	168
Figure 105: Variation in the tablet hardness at three different screw configurations (conveying element only, 1 kneading zone, 2 kneading zones). The compression force used for tableting was 5kN for all the three experiments and measurement was repeated for 100 tablets of each condition. _____	169
Figure 106: Average breaking force of 100 tablets produced with three different screw configurations (conveying element only, 1 kneading zone, 2 kneading zones). The compression force used for tableting was 5kN for all the three experiments. _____	169
Figure 107: Tensile strength of 100 tablets as calculated by the equation developed by Pitt and Newton (1988) at the three different screw configurations (conveying element only, 1 kneading zone, 2 kneading zones). The compression force used for tableting was 5kN for all the three experiments. _____	170

Figure 108: Average tensile strength of 100 tablet produced with three different screw configurations (2 kneading zone, 1 kneading zones, conveying element only,). The compression force used during tableting was 5kN for all the three screw configuration experiments. _____	170
Figure 109: Dissolution profiles for the tablets produced with three different screw configurations (2 kneading zones, 1 kneading zone, conveying element only). Measurements were repeated 10 times for all the three conditions, distilled water was being used as the dissolution medium with solution temperature of 37 °C and motor speed of 700 rpm. _____	172
Figure 110: Primary Particle size distribution of lactose monohydrate with different size grades (150M,200M,450M and microfine) measured by Camsizer XT. _____	177
Figure 111: SEM of lactose monohydrate of different primary particle size. _____	178
Figure 112: Flow diagram showing the process parameters used in TSG, FBD and tableting respectively for this chapter. _____	181
Figure 113: Screw configuration used in this stud which consisted of long pitch conveying elements and two kneading zones each contain 6 kneading discs placed at an angle of 60 degree so a total of 12 kneading discs in each screw. _____	182
Figure 114: Images of granules samples produced b TSG at different lactose primary particle size (150M,200M,450M and microfine) with water used as the granulation liquid binder, screw speed of 250rpm, L/S of 0.1 and 2 kneading zones prior to drying process. _____	184
Figure 115: Size distribution of granules produced at different primary particle size of lactose (150M, 200M, 450M and microfine). All other parameters during granulation and drying kept fixed throughout i.e., water as a liquid binder, L/S of 0.1, 2 kneading zones, screw speed of 250rpm and drying air temperature, flow rates and drying time of 50°C,400 m <sup>3</sup> /hr and 800 seconds respectively. _____	184
Figure 116: d <sub>10</sub> , d <sub>50</sub> and d <sub>90</sub> of the granules produced by TSG prior to fluidized bed drying at different lactose monohydrate primary particle size (150M, 200M, 450M and microfine). All other parameters during granulation and drying kept fixed throughout i.e., water as a liquid binder, L/S of 0.1, 2 kneading zones, screw speed of 250rpm and drying air temperature, flow rates and drying time of 50°C,400 m <sup>3</sup> /hr and 800 seconds respectively. _____	185
Figure 117: Granule's temperature profiles plot at different lactose monohydrate primary particle size (150M, 200M, 450M and microfine). All other parameters during granulation and drying kept fixed throughout i.e., water as a liquid binder, L/S of 0.1, 2 kneading zones, screw speed of 250rpm and drying air temperature, flow rates and drying time of 50°C,400 m <sup>3</sup> /hr and 800 seconds respectively. _____	186
Figure 118: Granule's moisture content profiles obtained from the NIR probe at the four different lactose monohydrate particle size (150M, 200M, 450M and microfine). The black dotted line shows the end of the filling time and the start of the drying time. All other parameters during granulation and drying kept fixed throughout i.e., water as a liquid binder, L/S of 0.1, 2 kneading zones, screw speed of 250rpm and drying air temperature, flow rates and drying time of 50°C,400 m <sup>3</sup> /hr and 800 seconds respectively. _____	189
Figure 119: Presence of product obtained from the NIR probe at the four different lactose monohydrate particle size (150M, 200M, 450M and microfine. The black dotted line shows the end of the filling time and the start of the drying time. All other parameters during granulation and drying kept fixed throughout i.e., water as a liquid binder, L/S of 0.1, 2 kneading zones, screw speed of 250rpm and drying air temperature, flow rates and drying time of 50°C,400 m <sup>3</sup> /hr and 800 seconds respectively. _____	189
Figure 120: Slopes of the drying curve between time 300 seconds and 380 seconds at the dryer cell at different primary particle size of lactose. _____	190
Figure 121: Residual moisture content at the dryer cell 5 as a function of primary particle size (150M, 200M, 450M and microfine) extracted from the moisture content profiles. All other parameters during granulation and drying kept fixed throughout i.e., water as a liquid binder, L/S of 0.1, 2 kneading zones, screw speed of 250rpm and drying air temperature, flow rates and drying time of 50°C,400 m <sup>3</sup> /hr and 800 seconds respectively. _____	191
Figure 122: Breaking force variation for 100 tablets of each condition made of different lactose primary particle size (150M, 200M, 450M and microfine). All other parameters during granulation and drying kept fixed throughout i.e., water as a liquid binder, L/S of 0.1, 2 kneading zones, screw speed of 250rpm and drying air temperature, flow rates and drying time of 50°C,400 m <sup>3</sup> /hr and 800 seconds respectively. The compression force used for tableting was 5kN for all experiment. _____	192

Figure 123: Average breaking force for 100 tablets produced at different primary particle sizes of lactose monohydrate; 150M,200M,450M and microfine) with other parameters kept fixed i.e., water as a liquid binder, L/S of 0.1,2 kneading zones and screw speed of 250rpm. The compression force used during tableting was 5kN for all the four experiments. _____	193
Figure 124: Tensile strength of 100 tablets of each condition (four different lactose primary particle size (150M,200M,450M and microfine) as calculated by the equation developed by Pitt and Newton (1988). All other parameters during granulation and drying kept fixed throughout i.e., water as a liquid binder, L/S of 0.1, 2 kneading zones, screw speed of 250rpm and drying air temperature, flow rates and drying time of 50°C,400 m <sup>3</sup> /hr and 800 seconds respectively. The compression force used for tableting was 5kN for all experiment. _____	194
Figure 125:Average tensile strength for the 100 tablets made of different particle sizes of lactose (150M,200M,450M and microfine) with other parameters kept fixed i.e., water as a liquid binder, L/S of 0.1,2 kneading zones and screw speed of 250rpm. The compression force used during tableting was 5kN for all the four experiments. _____	194
Figure 126: Dissolution profiles of tablet produced with different lactose primary particle size (200M,450M and microfine) with other parameters kept fixed during granulation i.e., screw configuration of 2 kneading zones, L/S of 0.1 and screw speed of 250rpm. Dissolution measurements were repeated 10 times for each of the condition with distilled water was being used as the dissolution medium with temperature of 37 °C and motor speed of 700 rpm. _____	196
Figure 127: Schematic of the near infrared chemical imaging equipment used in this study _____	199
Figure 128: Experimentation set up for the study of near infrared chemical imaging penetration depth. The thickness of each plastic layer is measure with the Keyence microscope to be 300µm and the thickness of the tablet was measured to be 3.8mm. _____	203
Figure 129: The 2 <sup>nd</sup> derivative spectral data for the lactose tablet with 0-5 layers of plastic layers placed on it at the wavelength region between 1905-1969nm. This highlighted region (yellow shade) represent the water peak. ____	204
Figure 130: The 2 <sup>nd</sup> derivative spectral data for the lactose tablet with 0- 5 layers of plastic placed on it. This peak for the wavelength region between 1905-1969nm in which this region represents the water peaks as well as is the region where the fingerprint of lactose is presented. _____	205
Figure 131: Raw images of plastic micro ruler obtained with Near infrared chemical imaging instrument at different distance to the spectrometer detector to determine the DoF of the lens. _____	209
Figure 132: Example of surface roughness profile of the granule obtained from the digital Keyence microscope (granules with diameter between 1.5-2.5mm). _____	210
Figure 133: Surface profile of granule (diameter between 1.5-2.5mm) with determination of the centreline which was obtained as the arithmetic mean of all the height points of the profile. Surface profile measurement was performed with the use of Keyence microscope. _____	211
Figure 134 : Roughness (Ra values) for all the granules produced at different fluidized bed drying times calculated using equation 5 above. The measurement was repeated ten times for each drying time. _____	211
Figure 135: Raw NIR spectrum of lactose granules at different moisture contents (0%,5%,10%,15%,20%) with the two water peaks highlighted at 1450nm and 1950nm. The spectral colour representation of each component is that red colour represents dry granules, green represents 5% moisture content, purple represents 10% moisture content, orange represents 15% moisture content, blue represents 20% moisture content and black represents ceramic background which has no spectra. _____	213
Figure 136: Calibration curves show a correlation between the moisture content and the intensity of reflected light at the two water peaks (1450nm, and 1940nm). This Figure plotted to give an indication on how good the model prediction in determining moisture content. _____	214
Figure 137: Predicted NIR-CI moisture content vs. nominal moisture content of granules for calibration curve validation. This was performed using four set of validations with granules of known moisture content. _____	214
Figure 138: QCI images of the calibration curve including the different five moisture content components 0% 5%,10%,15%, 20% in which (a) RGB (b) Grey obtained by the Partial least square quantitative model. _____	215
Figure 139: Calibration curve generated using QCI shows a correlation between the grey value and the moisture content. This plot is particularly useful to analyse moisture content distribution within every single granule. ____	216
Figure 140: Example to illustrate the computation of moisture content distribution in single granule in MATLAB. This was computed in every single granule in which computation was performed at a pixel wise step, however for less	

complexity, only 20 circles were drawn. A total of 10 granules of each condition were analysed and the average distribution of the 10 granules was plotted. \_\_\_\_\_ 217

Figure 141: Drying curve of lactose granules at different fluidized bed drying times using loss on drying (LOD) and NIR chemical imaging methods. \_\_\_\_\_ 218

Figure 142: Prediction map of moisture distribution content in single granules at different fluidized bed drying times including fresh granules prior to drying (a) fresh granules (b) 20 seconds FB-dried granules (c) 40 seconds FB-dried granules (d) 60 seconds FB- dried granules (e) 120 seconds FB- dried granules (f) 180 seconds FB-dried granules. The figure present 10 granules from each condition. \_\_\_\_\_ 222

Figure 143: Moisture content distribution across the radial distance of single fluidized bed dried granule as a function of FB drying time, this also includes fresh granules prior to drying. This plot obtained with using MATLAB/imaging processing tools. \_\_\_\_\_ 223

Figure 144: Schematic diagram of the proposed future work \_\_\_\_\_ 230

# 1.0 Introduction and Literature Review

---

## 1.1 Introduction

Pharmaceutical processing is typically conducted in either “batch” system or “continuous “system. Batch system consists of a step-by-step process for manufacturing products. The raw materials are input at the start of the process into the system, and the product is collected at the end of the process. There are no materials added cross the system between the time the raw material is input and the time when product is existing (Figure 1a). In the continuous process, the materials and products are continuously loaded into unloaded from the system, respectively, throughout the duration of the process, (Figure 1b) (Lee, S.L., et al 2015). In this research project, both processes will be used and so more details will be covered in the coming sections.

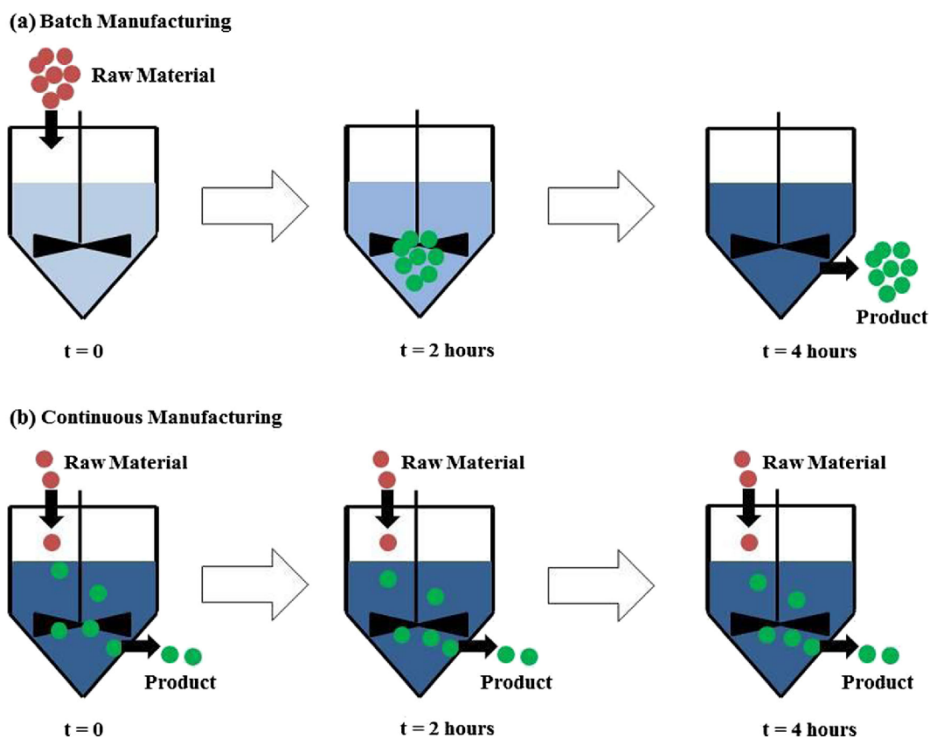
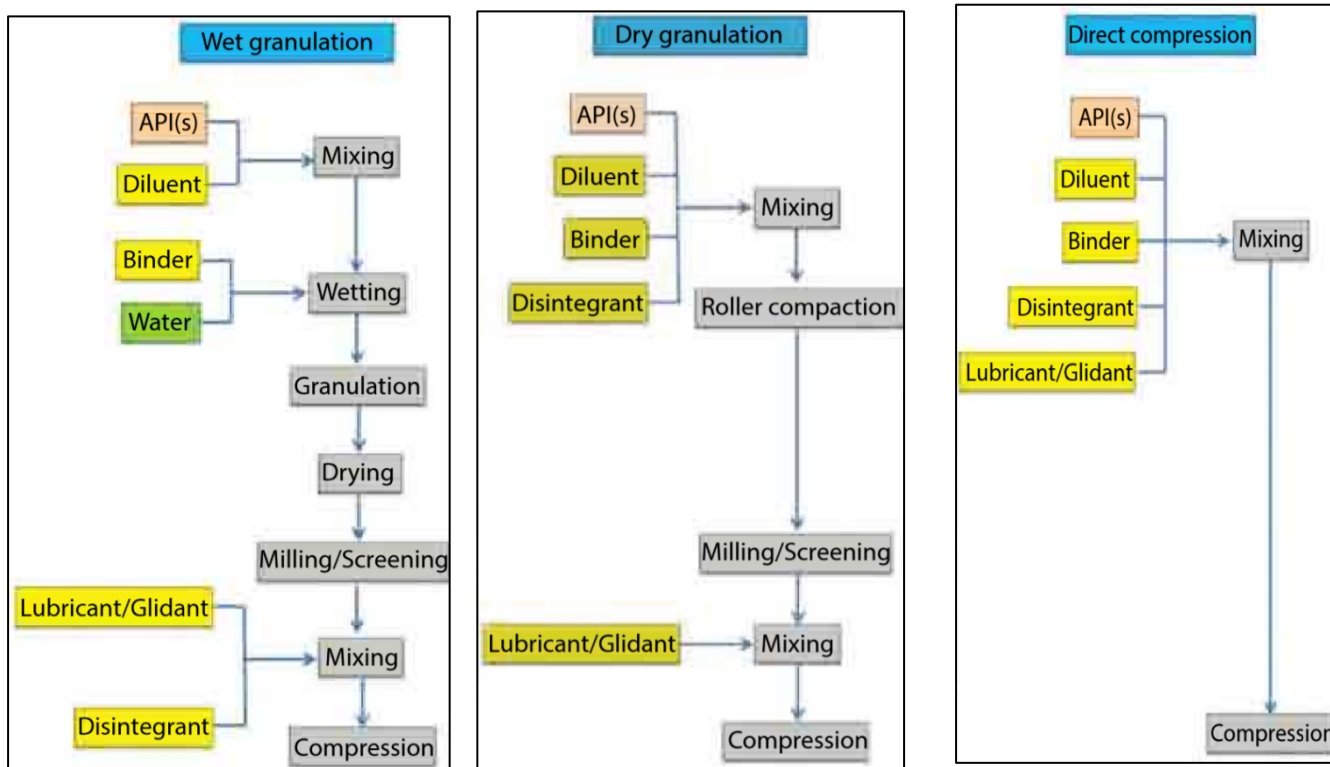


Figure 1: A simple depiction of two types of manufacturing. (a) Batch manufacturing (b) continuous manufacturing (Lee, S.L., et al 2015).

Solids such as granules, capsules, tablets and pills are the most popular pharmaceutical products when compared to liquids, ointments and sprays. Tablets are the most commonly used in the pharmaceutical industry, accounting for more than 80% of all the administered dosage forms (Fonteyne et al., 2014). The convenience of administration and patient preference, high-precision dosing, stability and cost effectiveness are the main reasons for the continued popularity of the tablet (Mangal, et al., 2015). The typical way to manufacture tablets is by applying stress to the APIs and excipients powder blends contained in a die using a punch, resulting in powder compression into a coherent compact. During the compression, bonds are formed between the particles, therefore giving a particular mechanical strength to the compact (Mortier et al., 2011). Good flow and high compactability of formulation enable the transformation of an active pharmaceutical ingredient into a satisfactory quality tablet that gives a desired pharmacological response. Good formulation flow is very crucial to achieve fast and reproducible filling of powder into the die to reduce variation in the weight, at the same time, high compatibility is needed to ensure that the produced tablets are adequately strong to tolerate handling during both manufacturing and transportation (Shang et al., 2013). Most of the active pharmaceutical ingredients require the necessary flow and compactability for direct tablet manufacturing. Consequently, the flow and compactability of the active pharmaceutical ingredients should be improved to enable the production of high-quality tablets (Mortier et al., 2011). The typical process used to improve the flow and compactability of tablets formulation is known as granulation (wet or dry granulation), it is a step in which the particles of active pharmaceutical ingredients and excipients are agglomerated together into larger particulate structures called granules (Iveson et al., 2001). Wet granulation includes addition of a liquid binder to form granules, while in dry granulation no liquid binder is added. Generally, wet granulation process is employed in different industries to improve flow properties, processability, uniformity, permeability etc. of the raw materials, reduce dust formation and caking and control dispersion and solubility (Vercruyssen et al., 2012). A typical schematic diagram of the manufacturing process of a pharmaceutical product is shown in Figure 2.



**Figure 2: The tablet manufacturing processes including wet granulation, dry granulation and direct compression (Mangal, S., et al 2015).**

It can be seen from the Figure 2 that after performing wet granulation, a subsequent drying is required, which is important to remove the granulation liquid from the wet materials. The procedure for drying the wet granules may influence the properties of the granules and, hence, the further downstream processing. After drying, the granules (dry) may undergo a milling step and/or a post-blending step, after which the tableting step is performed (Mortier et al., 2013, Osborne et al., 2013, Nieuwmeyer et al. 2007, (Nieuwmeyer, van der Voort Maarschalk and Vromans, 2008) and Farber et al., 2003. The tableting is the main final process and therefore it is important to investigate the parameters that affect it.

A wide variety of equipment can be used for wet granulation; the preferred route for continuous wet granulation is the twin-screw granulator. In twin screw granulation the material is fed into a barrel where the liquid is added and two co-rotating screws both push the material forward and apply stress to form granules. Twin screw wet granulation has received a lot of attention due to its advantages as a continuous process. In addition, the twin-screw wet granulation technique involves less scale up steps, has a higher throughput and requires fewer materials to run the process, which makes it cost effective.

Although this technique is well established in the polymer, food, and detergent industries, in the pharmaceutical industry, there is a lack of understanding of how the resulting granular properties are affected by the drying process and downstream tableting process. This aspect forms the basis of the current work.

### **1.1.1 Why Drying of a Granule is Significant?**

The drying process simply involves the removal of a liquid from a wet material. It is considered as a very important unit operation that is mostly used in all industry producing solid product ranging from food to pharmaceutical industry. The removal of moisture from granules using the drying process is necessary to keep the residual moisture content low enough make them easier to handle, reduce the product caking, preserve and prevent the product deterioration, and corrosion. Generally, the drying process requires a very high input of energy due to the water latent heat of evaporation (Syahrul et al., 2002). Drying is a very fundamental stage before the tableting step in the pharmaceutical industry when wet granulation process is used. The kinetics of drying has a significant effect on the resultant granule properties. Understanding the drying mechanisms will enable the optimization and better control of the resultant granule and tableting properties.

Fluidized bed drying is the most popular process to dry a wet material particularly in the pharmaceutical industry and considered to be the best and quickest drying system for the wet granules (Hegedus et al., 2007). The drying process is carried out in a bed fluidized by a drying medium and it may be carried out as a batch or continuous process, both processes were implemented in this research project. The FB dryer in batch drying is inputted with wet materials, the air starts to flow, and the materials are removed out of the dryer when they are adequately dried. In batch drying, the conditions of the process are readily selected, and the product tends to be of uniform quality due to the bed homogeneity during equipment operation. In continuous drying, the materials to be dried go into the FB dryer as a continuous stream and leaves the drier also in a continuous manner. Even though that this operation is of a steady state, the wet materials quality may find to be non-uniform because of the high mixing of solids and the different time of residence in the dryer for the individual particles (Mortier et al., 2011). There are many advantages associated with fluidized bed drying of granules; it



offers enormous transfer area between the solid and the drying medium. Improves the transfer of mass and heat between the phases. Provides high degree of mixing for the materials with high transfer coefficients of heat and moisture between the solid and gas. It eases the transportation and the handling of the fluidized materials and it suits large-scale operation.

### 1.1.2 Principle of Fluidized Bed Drying

Principally, the drying is a simultaneous heat and mass transfer process. The heat is crucial for evaporation of excess moisture or liquid. When the granule is brought to heat, the moisture is then removed into the drying medium from the material. Figure 3 shows the representation of the transfer of heat and mass in the drying of particle. The surroundings heat (C) is transferred to the surfaces of the granule (B) by convection and from there further into the granule (A) by conduction (Syahrul et al., 2002).

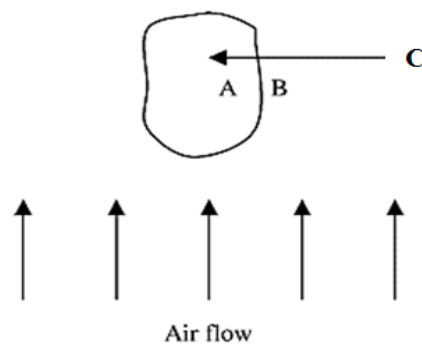


**Figure 3: Representation of the transfer of heat and mass in the drying of a particle (Syahrul, Hamdullahpur and Dincer, 2002).**

The drying process in the fluidized bed is performed by placing the granules in a perforated screen or sieve device where air is entering through at sufficient rate to lift and discrete the granules that are in motion and take on a fluidized state. The drying therefore happens due to the resultant intensive interaction between the medium of the drying (air) and the granules. Figure 4 outlines the drying curve of wet granules throughout the process of drying (Mezhericher, 2014). This Figure shows the relation between the moisture content of the granules and the drying time with indication to the three

drying stages (surface evaporation, internal evaporation and final sensible heating that result in dry granule).

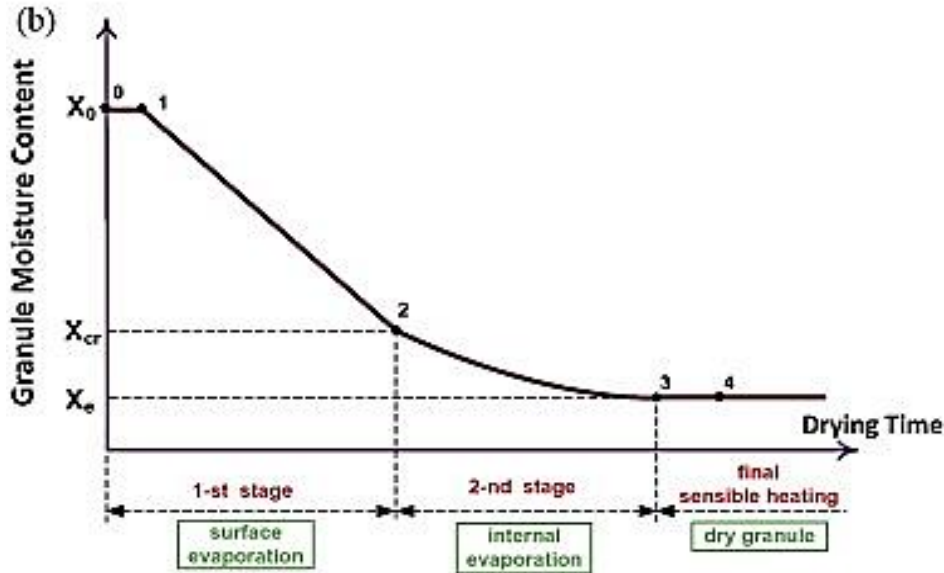


**Figure 4: Drying curve of wet granule,  $X_0$  is the initial moisture content,  $X_{cr}$  is the critical moisture content and  $X_e$  is equilibrium moisture content] (Mezhericher, 2014).**

Figure 5 shows a schematic diagram indicating the phenomena of liquid transport at both the 1<sup>st</sup> and 2<sup>nd</sup> drying stages (Mezhericher, 2014). For a wet granule including liquid and solid, the drying kinetics is typically split to two drying stages as illustrated in Figure 5. At the first stage of drying, the wet granule is exposed to a drying air; this leads the wet granule to gain sensible heat. This then causes the vaporization of liquid to begin on the whole wet granule surface. Ultimately, the wet granule surface entirely dries out to become concealed with a dry layer, which is porous, known as crust. Since then, the evaporation of liquid front transfers below the crust layer, moving to the interior of the wet granule, and hence the 2<sup>nd</sup> stage of drying initiates. In this stage, the surrounding crust layer hinders the drying of interior of the wet granule. In general, at the 1<sup>st</sup> stage of drying, the wet granule temperature is not uniform alongside the radius of the droplet. At the start of the 2<sup>nd</sup> stage of drying, two concentric regions are formed as seen in Figure 5 (b); the exterior, which is the dry crust and the interior, which is the wet core. The crust region is described as a spherical dry layer perforated by number of identically cylindrical pores. The wet core is deemed as circular in shape including both

components, liquid as well as solid. From Figure 5(b), it can be seen that the pores in the crust can work as routes to allow the passage of the vapour from the wet core of granule into the outside. This 2<sup>nd</sup> drying stage proceeds pending for the granules moisture content to reaches an equilibrium with the medium of the drying. Subsequently, the drying ends and the dry granule is then heated to reach a balance with the drying medium.

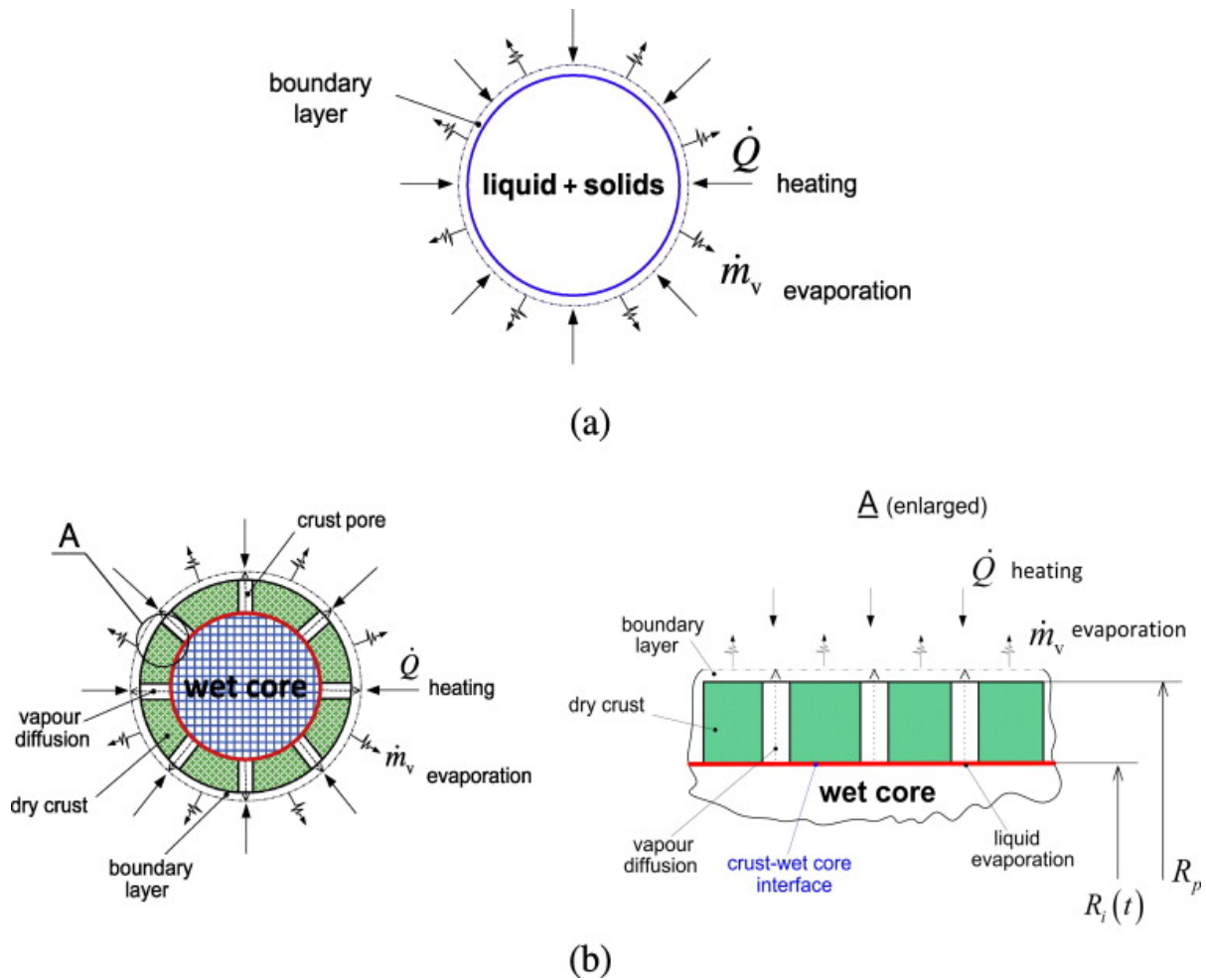


Figure 5: Transport phenomena in wet granule at (a) the 1<sup>st</sup> stage of drying (b) the 2<sup>nd</sup> stage of drying (Mezhericher, 2014).

### **1.1.3 Consideration of the scales and the potential challenges of using the two-unit operations (TSG and FBD) in tandem alongside with the NIR chemical imaging challenges.**

Given that this project utilizes both small laboratory scale and pilot plant industrial scale equipment it is of a paramount importance to highlight/ define the scales considered in this research project quantitatively. The laboratory scale TSG (16 mm Prism Euro lab TSG, Thermo Fisher Scientific, Karlsruhe, 49 Germany) has a barrel length of 400 mm and a diameter of 16 mm (length to diameter ratio (L/D) of 25:1) and is capable of producing a maximum of 1000 rpm for the screw speed and 12Nm of torque and can give a powder feed rate up to 25 kg/h. The pilot plant industrial scale equipment (ConsiGma-25, Powder to tablet line (GEA Pharma Systems) is a full-scale production line with a rate of production of up to 25 kg/hr. There are respective challenges when considering the two-unit operations (TSG and FBD) in tandem, especially for the novice researcher. One major problem is that there are only existing studies on the two-unit operations when dealt with individually, but there is little written in the literature regarding combining the two different unit operations, if any information on the integration of the two units is available, it will help to make the tandem operations a more viable proposition. Furthermore, other key challenges could be faced when one works with model formulations, many APIs have a poor compressibility, which has an impact on tablet quality, especially when high API content tablets are required. Low API content tablets production, on the other hand, is also a challenge due to the difficulty of accurately blending a tiny amount of API in a big amount of excipient to obtain the requisite uniformity and homogeneity. Segregation of the various components, for example, can occur during tableting. Weight variation and content homogeneity will be a concern as a result of this. Particle size variations between the API and excipients or between different excipients are the main cause of segregation. In most circumstances, the API particle size is substantially smaller than the excipients' particle size. Indeed, there is a greater risk of segregation, in which smaller API particles slip through larger excipient particles. If a powder formulation has issues with flowability, compressibility, segregation, or dustability, it may be necessary to wet granulate it before tableting. The granulation procedure overall reduces segregation by narrowing the particle size distribution of a tablet powder composition. This reveals improved

compressibility and allows for the production of tablets with larger API concentrations and better homogeneity. Several labour-intensive tests (such as hardness, dissolution, disintegration, friability, and uniformity) must be undertaken in order to establish the quality of tablets and must meet certain parameters. The pharmaceutical industry spends a lot of time and money developing and validating these tests to ensure that the final tablet product is of high quality. Other challenge could be faced when working with powder material that is heat or chemically/ physically moisture sensitive drugs. Because drying at high operating temperatures might result in thermal decomposition of the API and some certain excipients, conversely, low temperature drying might fail to meet the established limit with reasonable drying time. So, to avoid the impact of material sensitivity, one should carefully choose the proper materials to work with or build up an experimental strategy in terms of process and formulation to reach optimum conditions that are safe to be used with the sensitive materials. Moreover, the drying of wet granules often encompasses undesirable and uncontrolled size reduction or growth during the process of drying in fluidized bed. Furthermore, the moisture content of the final granules is not the same due to the difference in the size of the granules as they are produced from the TSG. Small granules dry faster compared to the larger granules. This led to over drying of some granules. The initial properties and qualities of granules as a result of the formulation or process parameter settings utilised during TSG granulation could account for much of this. Because any changes to the twin-screw granulation process will have a direct impact on the drying process and final granule and tablet quality attributes. Therefore, there is little information in the literature about the relationship between the initial granule characteristics produced by TSG and Fluidized bed drying; thus, this research aims to bridge that gap and connect the two-unit operations together.

Furthermore, determination of moisture content is important for many industrial sectors. It is used to ensure achieving the required quality of the final product. This project aims at investigating the validity of using a non-destructive near infrared (NIR) chemical imaging (CI) technique as a tool to determine the moisture content of pharmaceutical granules. This technique enables visualizing the distribution of moisture content, as well as providing a quantitative information of the granule's moisture content. Although, this method enables fast assessment of moisture content, it is associated with some challenges, which should be addressed when utilising this technique for this purpose.

When working with NIR chemical imaging in general, it is very important to make sure that the signal being measured is not impacted by other sources of variance. As a result, only the spectral information associated with the component of interest should be correlated with the component's information. If other sources of variance contribute to the signal, the results will be biased, and detecting possible inaccurate results may be challenging. Also, when working with samples containing many ingredients, the NIR spectra are made up of broad, and highly overlapped bands, making it more difficult to locate distinct and selective absorption bands for each ingredient within the sample. These limitations could be overcome by using a multivariate data analysis approach (e.g., PCA), which extract meaningful information from the full data set by using the entire spectral profile. One of the key challenges addressed in this project is sample surface topography/surface roughness. In the literature, NIR-CI has received a lot of attention because it is a chemical-free, rapid, non-destructive, and non-invasive approach, without taking into account that it has some drawbacks/challenges. A hurdle addressed in this project was a lack of information regarding the effect of surface roughness of the material being studied with NIR-CI technology on the reliability of the acquired result. The effect of surface roughness on the NIR-CI result's dependability was thus studied.

## 1.2 Literature Review

---

### 1.2.1 Conventional Batch Fluidized Bed Drying

To assess the effect of the fluidized bed drying on the quality attributes of granules, a batch drying is considered in this project, in other word, conventional fluidized bed dryer (laboratory scale) is used. A separated twin screw granulator unit (laboratory scale) is used to produce the wet granules. Therefore, this section of literature will review the studies conducted on the conventional batch fluidized bed dryer. Different formulation and process variables in the fluidized bed can lead to different levels of moisture content; therefore, this might affect the properties of granule and tablet. Previous studies showed that different process parameters such as drying temperature, velocity and drying time could lead to different moisture content. These will be explored in this section.

Taghavivand et al. (2016), performed a study to investigate the performance of drying for pharmaceutical granules by varying the air temperature and velocity in a conical fluidized bed dryer. Their findings showed that increasing both drying air temperature and air velocity caused a decrease in the time of drying. Also, the rate of drying was found to be low at lower drying temperatures. Similarly, Syahrul et al. 2002 studied the influence of the inlet air temperature, velocity and the material initial moisture content on the performance of drying process and drying rate. Their outcomes showed that the thermal efficiencies of the fluidized bed during the drying process was severely decreased as moisture content of the corn was decreasing, consequently increasing the time of drying and the efficiency become very low at the end of the process of drying. These results suggest that the transfer of moisture from the material strongly rely on the temperature of the air, velocity of the air, and the moisture content of the material. Watano et al. (1998), investigated the drying process of wet granules in an agitation-fluidized bed. In their study, they investigated the impact of air temperature and air velocity.

Moreover, it was found that as the air velocity increases, the drying time required to dry the wet granules decreases. This was due to the increase in thermal energy. Briens & Bojarra (2010), investigated the effect of different superficial gas velocities in fluidized bed drying with granules

contain lactose monohydrate, corn-starch, and polyvinylpyrrolidone. In the study conducted by Briens & Bojarra 2010, the moisture content of granule, bed temperature, air outlet temperature and air outlet humidity as a function of time at various air velocities was determined as shown in Figure 6. The moisture content of the granule was determined by sampling and loss on drying measurements Figure 6 (a). The initial moisture content of the granule was just below 20 wt.%, and then dropped considerably to reach a plateau of moisture content of around 1 wt.%. End point for dry granule was specified to be less than 2 wt.%. The time of drying based on this criterion was decreased with gas velocity from 82 minutes at a velocity of 0.8m/s to 33 minutes at a velocity of 1.6 m/s. Figure 6 (b) shows the measured temperature of the bed throughout the drying process of the granules. From this figure, it can be observed that when granules are very wet, the temperature of the bed was roughly between 7 to 10°C. The temperature of the bed then remained constant until the granules were surface dried at a moisture content of around 5 wt.%. The transition of this surface dry was determined by both visual observations and flow measurements of the bed fluidization behaviour. The temperature of the bed started to increase when the granules were surface dry, and temperature of the bed started to approach the temperature of the inlet air. Briens & Bojarra 2010 studied the temperature of the outlet air throughout the process of drying as seen in Figure 6 (c). This Figure show that the outlet temperature of air decreased initially then remained almost constant and then starts to increase when the granules were surface dried. The initial decrease of the outlet air temperature occurred until the moisture content of the granule reached around 17 wt. %. Figure 6 (d) shows the humidity of the outlet air versus the granule moisture content at various velocities. From this figure it can be seen that the humidity of the outlet air was initially high and then reduced once the granules were surface dried. Significant scatter and lower values of outlet humidity at 0.8 and 1 m/s were initially observed. This reflects the poor initial fluidization conditions with very wet granules particularly at the lower fluidizing velocities.



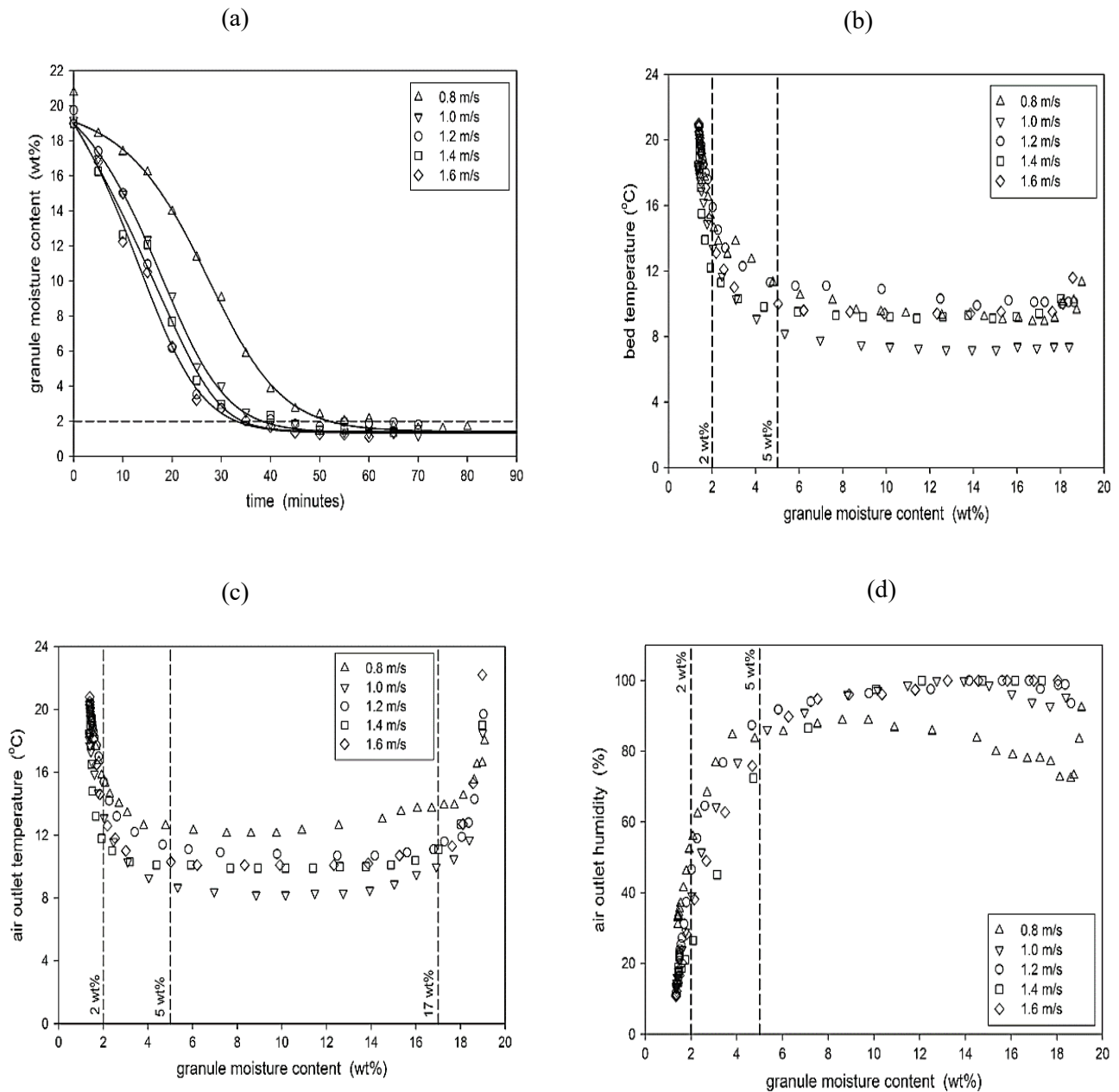


**Figure 6: (a) Granule moisture content vs. time for different air velocities (b) bed temperature vs. granule moisture content (c) Air outlet temperature vs. granule moisture content (d) Air outlet temperature as a function of granule moisture content at various velocities (Briens and Bojarra, 2010).**

Srinivas & Setty (2013), conducted a study to investigate the drying behaviour of uniformly sized particle (1.2 to 3.1 mm) using a fluidized bed dryer at different parameters (air velocity, particle size, temperature, and initial moisture). The results showed that the drying rate for the uniformly sized

particles were found to increase as the air temperature and air velocity increase. They have also found that the drying rate decreases when the size and moisture content of particle has increased as shown in Figure 8. Figure 7(a) presents the results of varying the air velocities of 10 % binary mixture in the range between 2.13 and 2.98 m/s. This experiment was performed at an air temperature of 40°C and an initial moisture content of 5%. It can be observed that as the air velocity increases, the drying rate increases. They suggested that increasing the air velocity has increased the convective mass transfer of moisture from particles into the air leading to an increase in the rate of drying. Figure 7 (b) presents the result of varying the air temperatures of 20 % binary mixture in the range between 40 and 70°C, an initial moisture content of 5 % and an air velocity of 2.13 m/s. Similarly, increasing the air temperatures resulted in an increase in the rate of drying. This was explained by the increase in heat input as temperatures increases and therefore the evaporation rate of moisture from the moist particles increased. Figure 7 (c) presents the result of varying the size of particles at an air temperature of 40°C, an air velocity of 2.13m/s and an initial moisture content of 5%. It can be clearly seen that as the size of particle increases, the rate of drying decreases. They indicated that this decrease in the drying is because increasing the diameter of the particle reduces the surface area available and therefore lowering the rate of drying for particles that are coarse and increasing the drying rate for particle that are fine in size. Figure 7 (d) presents the results of varying the initial moisture content of 30% binary mixture at a temperature of 40°C and air velocity of 2.13m/s. From Figure 6, it can be observed that increasing the initial moisture content has reduced the rate of drying. As moisture content of the particles increases, the bound moisture with particles increases and therefore the required time to achieve specific moisture content in the product increases.

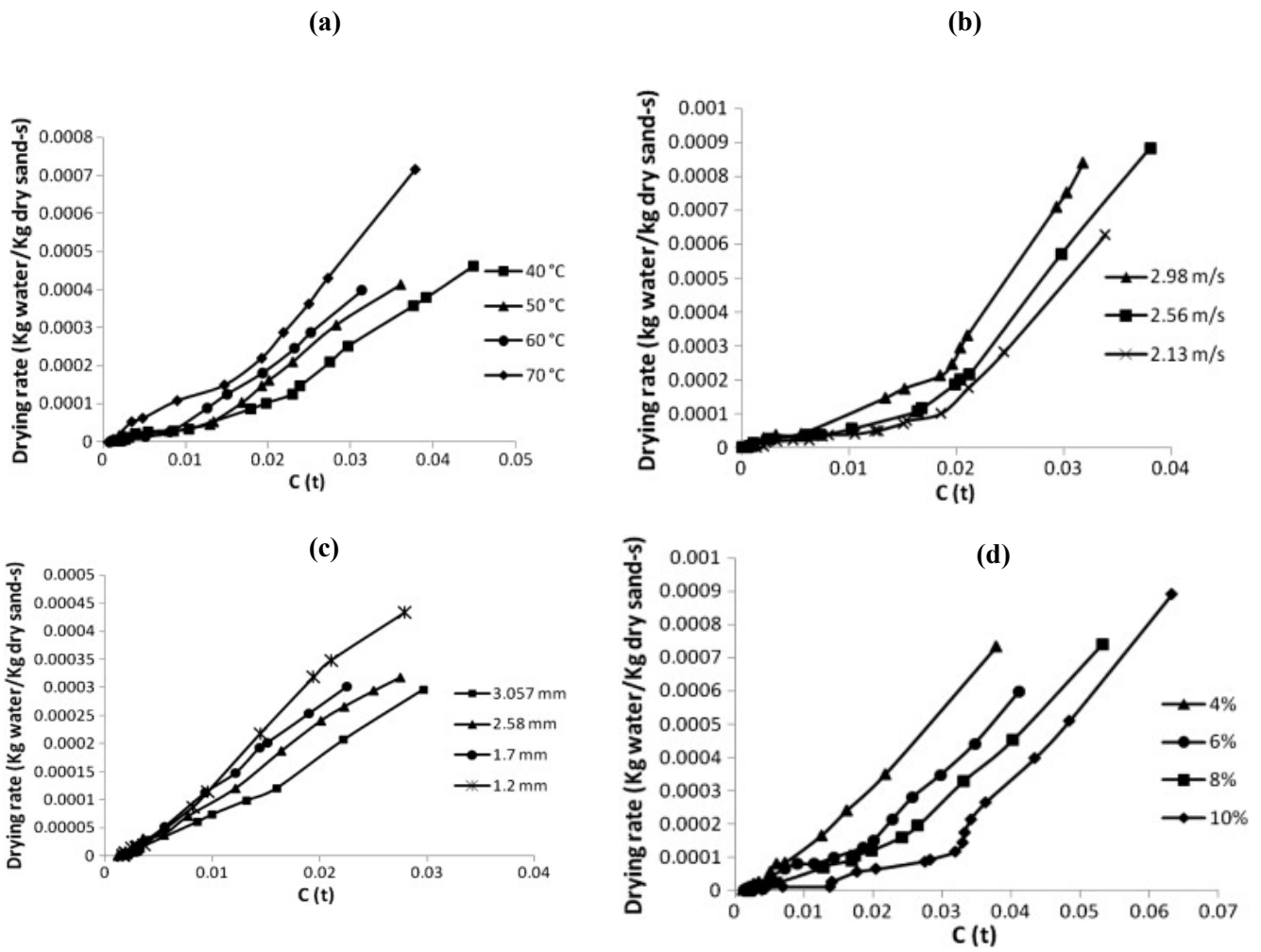


Figure 7: Effect of (a) air temperature (b) air velocity (c) particle size (d) initial moisture content on the drying rate. [“ $C(t)$  is the moisture content with respect to time (kg water/ kg dry sand”)] (Srinivas and Pydi Setty, 2013).

## 1.2.1.2 Fluidized Bed Drying Challenges

The main challenges of fluidized bed drying are:

- The drying of wet granules often encompasses undesirable and uncontrolled size reduction or growth during the process of drying in fluidized bed.
- The moisture content of the final granules is not the same due to the difference in the size of the granules. Small granules dry faster compared to the larger granules. This led to over drying of some granules.

Wet granules drying can involve an unwanted and uncontrolled size increment (growth) or size reduction (breakage). In literature, researchers showed that during the granules drying process in fluidized bed, there is a possibility for these two phenomena to take place (Nieuwmeyer et al. 2007). Growth can mainly occur as a result of particles collision together, particularly once being wet so when two granules or more stick to each other, a large granule will be obtained. Growth can also occur as result of the possibility of granulation continuation, which apparently cause size increase or growth (MacKaplou et al., 2000).

### 1.2.1.2.1 Attrition and Breakage of Granules in Fluidized Bed

The breakage scenario can occur when the granules collide together or with the vessel wall, which will lead to fine formation, and this as a result can reduce the product quality. MacKaplou et al. 2000, reported that the size of the dry granules depends on the process of drying and size measuring method. The methods of sizing such as sieving might also decrease the size of the granule, depending on the stresses experienced by the granules. The drying process influences major granules properties such as granules size distribution, granules bulk and tapped density and porosity and migration of solute materials. It was found that fluidized bed drying process can cause high attrition (fines) and higher porosity with high intragranular migration (MacKaplou, et al. 2000). Both cases of breakage and growth are unwanted since the primary aim of drying is to dry the granules and not to have a change in size.

The breakage of the granules could be influenced by various properties; these are split into two categories:

- The properties of the granules such as shape, size, surface roughness, strength and binder viscosity (Ayazi et al., 1990).
- The properties of the surrounding environment such as air flow, height of the bed, pressure, temperature and humidity (Ayazi et al., 1990).

Particulate materials breakage or attrition is well known in many different fields with several particle types. The breakage and attrition were defined in a number of ways. Bemrose & Bridgwater, (1987), considered the attrition as unwanted reduction of size regardless the cause. In recent times, focus was given to the fluidized bed coal combustor and gasifier (Verkoeijen et al., 2002). The occurrence of attrition maybe because of several factors; these are mechanical forces (in the bulk of materials or at walls of the container), thermal forces (because of the change in the volume of the solid or the liquid vaporization), chemical stress (due to change in phase or chemical reaction) or changes in pressure between the inside and the outside of the particles. Furthermore, particle attrition can be also resulting from the motion of the particle in the equipment. The forces which cause breakage or abrasion maybe because of the collisions between particles that are moving fast when the kinetic energy is absorbed during the collisions. Otherwise, the forces may be transmitted through a matrix of particles that are moving slow. There are some important variables that determine the breakage nature; these are the shapes, the relative velocities, and the contact direction between the particles, contact stresses and masses. Moreover, possibility of breaking of particle can be also affected by the presence of the one crack or more (Bemrose and Bridgwater, 1987). Verkoeijen et al., (2002), described the mechanisms of breakage as a function of both the direction and magnitude of force. Figure 9 shows a schematic illustration of the described mechanism by Verkoeijen et al., 2002. The removal of sharp edges in which fine dust is formed reflects attrition (Figure 9a). Upon attrition, the shape of granule becomes more spherical. The removal of crumbly material from the granule surface indicates abrasion (Figure 9b), in which the shape of the granule also becomes rounder and smoother with formation of fine dust (Verkoeijen et al., 2002). Fines formation by attrition or abrasion is a significant parameter due to its

effect on the granule mass flowability. Fragmentation as illustrated in Figure 8(c) occurs as a result of the high normal forces, for instance, head-on impact in which the original granule is divided into a number of fragments. Figure 8(d) illustrates the Chipping of the granule which occurs as a result of high tangential forces in which bits and pieces are carved from the original granule. The pieces are smaller than those formed by fragmentation, thus resulting in coarser and less spherical granule.

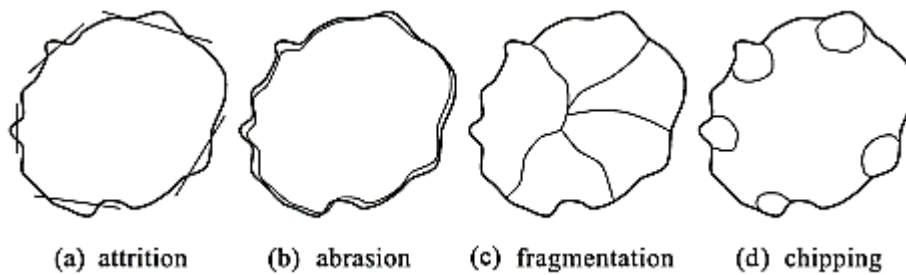


**Figure 8: Schematic illustration of the described mechanism (Verkoeijen et al., 2002)**

Verkoeijen et al. (2002), granulated lactose using a high shear mixer and dried the produced granules in fluidized bed at various conditions. In their study, they used water content and size analysis to characterize the granules. It was found that the process of drying is dynamic with respects to the phenomena of growth and breakage. The heterogeneity of granule size, water content and composition determine the behaviour of granular upon drying. Granules that are large are made up of primary particles, which are small and therefore hold more water than the granules that are small, which is made up of primary particles that are large. This distinguishes the rate of drying and the extent of size decrease of different size classes of granule. The process of drying can involve often a reduction in size, which is deemed to be undesirable and uncontrolled. Attrition effect was described on the powder masses flowability (Aulton, 2002) or in the active substance homogeneity in the granules within the pharmaceutical process (Van Den Dries et al., 2003). In the industry of oil, undesirable breakage to the particles of catalyst was investigated by Kelkar and Ng, (2002), however, in the detergent industry, the granules breakage of detergent enzyme was investigated by (JØrgensen et al. 2005). Although the unwanted reduction in the pharmaceutical granules size during granulation and drying in fluidized bed (Niskanen and Yliruusu, 1994) or in granulation in high shear granulator (Van

Den Dries et al., 2003) were reported, a relatively small attention was given towards attrition. Nieuwmeyer et al. 2007, investigated the factors that affect the level of breakage during the processes of drying. In this study, also tried to understand the phenomenon of breakage related to drying with the aim of controlling this phenomenon. Their work indicated a three-phase system (growth, plateau, breakage) in which the change in the granules size follow. It was found that the extent of granules breakage, growth and fines formation are a function of size, composition and content of water with realizing that the granules strength is dependent on the water content, which becomes obvious by the three different phases (growth, plateau, breakage) in the process of drying. However, the existence of very little water amount or the development of solid bridges cannot stop the abundant reduction in size. In another work, Nieuwmeyer et al. 2008, did a study with lactose granules produced in a high shear granulator and dried in a fluid bed dryer at different conditions. Water content and size analysis are the characteristics of the granules that were used in his study. The study revealed that the process of drying is very dynamic in terms of both breakage and growth phenomena. And that the heterogeneity of granular size, water content and the composition determine the behaviour of granule upon drying.

## **1.2.2 Continuous Manufacturing Process**

Continuous manufacturing is described as a process without disruption over a continuous period. This implies linking all the unit operations throughout into one production line. This is to increase total capacity, capital utilization and product yield and quality while lessening inventory and product time to-market (Vercruyssen et al. 2013). The regulatory agencies require the pharmaceutical industry to continuously assess and assure the quality and safety of the drug at any time. One of the main reasons of why the pharmaceutical industries have not been driven to take initiative to transfer from batch to continuous production is the uncertainty of approval by the regulatory agencies. However, lately, continuous manufacturing has gained importance in the pharmaceutical industry. Therefore, to improve the pharmaceutical production quality, the regulatory agencies have shown strong desire to move towards the continuous manufacturing. Additionally, guidelines to encourage the pharmaceutical industry to implement state of art scientific approaches such as Quality by Design (QbD) and Process Analytical Technologies (PAT) was outlined by the US Food and Drug Administration (FDA) and International Conference for Harmonization (ICH). Applying these approaches will enhance and optimize product quality and pharmaceutical development, thus making it easier to switch from batch production to continuous production. Table 1 shows summarized features and potential benefits of continuous manufacturing (Lee, S.L., et al 2015).



**Table 1:** Features and potential benefits of continuous manufacturing (Lee, S.L., et al 2015)

Features of continuous manufacturing	Benefits
<b>Small equipment and space required</b>	Efficient, increased throughput per unit volume and time lower hazards
<b>Short supply chains</b>	No storage/shipping costs for intermediates Rapid response to the shortage of market lower degradation for sensitive intermediates
<b>All key characteristics should be roughly constant at any time</b>	Lower batch-to-batch variations easy to develop monitoring systems for the process and control strategies Potential removals of some downstream corrective steps
<b>Non-stop continuous transport of materials (no batch handling)</b> Less operators on site	<b>from unit to unit</b>  high operator safety
<b>Continuous flow production</b>	Easy scale-up Possibility for diminishing reaction Facilitation of new synthetic routes (i.e. microwave, photochemistry, ultra-high or low temperature) Safe operation when dealing with highly exothermic reactions

### **1.2.2.1 Continuous Powder to Tablet Line ConsiGma-25**

In this research project, continuous powder to tablet line ConsiGma 25 (GEA) was also used. This is a full-scale production line with a rate of production of up to 25 kg/hr. The line composed of multiple connected units as illustrated in the schematic diagram in Figure 9. Nearly all-pharmaceutical continuous wet granulation processes are equipped with a twin-screw granulator to produce granules, the wet granules need to be dried to remove the moisture and form granules acceptable for further processing. The continuous powder to tablet line Consigma-25 used in this study has a twin-screw granulator therefore needing a dryer. The dryer fitted in the line is a segmented fluidized bed dryer and is divided into 6 cells as shown in Figure 9. The wet granules from the granulator are moved to a cell via a valve positioned at the top of the fluidized bed, the cell is then filled for a finite amount of time defined as the filling time. When the filling time for one cell has been reached the valve turns and the next cell is loaded. All the six cells of the fluidized bed dryer share a main gas input and output. After the granules have been in a cell for a specified drying time (which includes the filling time) or when they reach a target temperature the cell is unloaded via a rotary valve at the bottom of the fluidized bed dryer and a pneumatic conveying system. The process can continue indefinitely, as the cells are loaded and unloaded sequentially. Each cell of the fluidized bed dryer is equipped with a temperature probe situated just above the air distributing plate. Given its location, the probe measures a combination of the air and product temperature depending on its coverage. The dried granules go to the milling unit in which it composes of impeller blade and mill screen to control the final granule size distribution. Having the milling completed, the milled granules flow to the blending units for further addition of further excipients. This step is usually to add materials that are sensitive to moisture or temperature because they would be subjected to degradation if processed in the previous steps. The material that was blended then goes to another blender unit just above the tableting press in which a solid lubricant is added to it. The lubrication of the blend prior to tableting is very important to ensure easy exit of tablets from the die. The lubricated blend then finally goes to a rotary tablet compression module (Modulp, GEA) in which the final product (tablets) is produced.

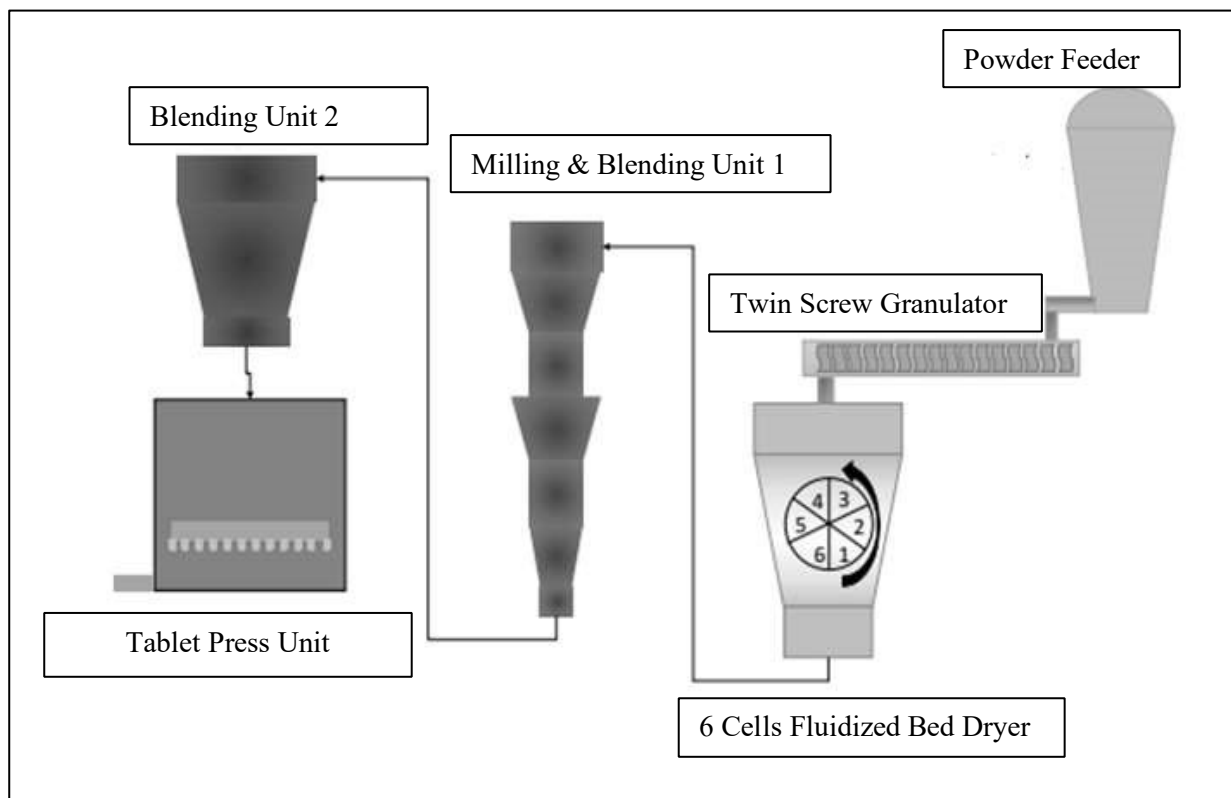


**Figure 9: Schematic diagram illustrating the ConsiGma- 25 pilot plant utilized in this project (drawn not to scale).**

Consigma 25 continuous manufacturing system has been attaining attractiveness in the past few years and so pharmaceutical research has begun to pay more attention to the continuous production with Consigma being the most researched continuous wet granulation process. Most of the research has been paying attention on how different parameters influence the final attributes of tablet particularly focusing separately on the two processes of twin-screw granulation and fluidized bed drying. However, there are still some identified gaps in literature, which needs to be investigated further using this continuous line. In this section, the studies that used both the twin-screw granulator and the fluidized bed dryer are reviewed.

### 1.2.2.2 Stability and Repeatability of the ConsiGma 25 Line System

Stability and repeatability are vitally important aspects to ensure in continuous manufacturing processes especially when it is needed to run uninterruptedly for several hours or days. Vercruyse et al. 2013 has continuously ran the innovative operating ConsiGma™-25 system three successive 5 hours that allows the production of powder to tablet. Twin screw granulation was considered as an intermediate step in this process to determine the quality of the granules and tablets as a function of the repeatability, stability, and process time during continuous production runs. Figure 10 shows process variables stability with time in which torque and jacket temperature of the twin-screw granulator, pressure difference over the filters of the dryer and mill screen temperature remained clearly stable after the first period of stabilization for the entire 5 hours run.

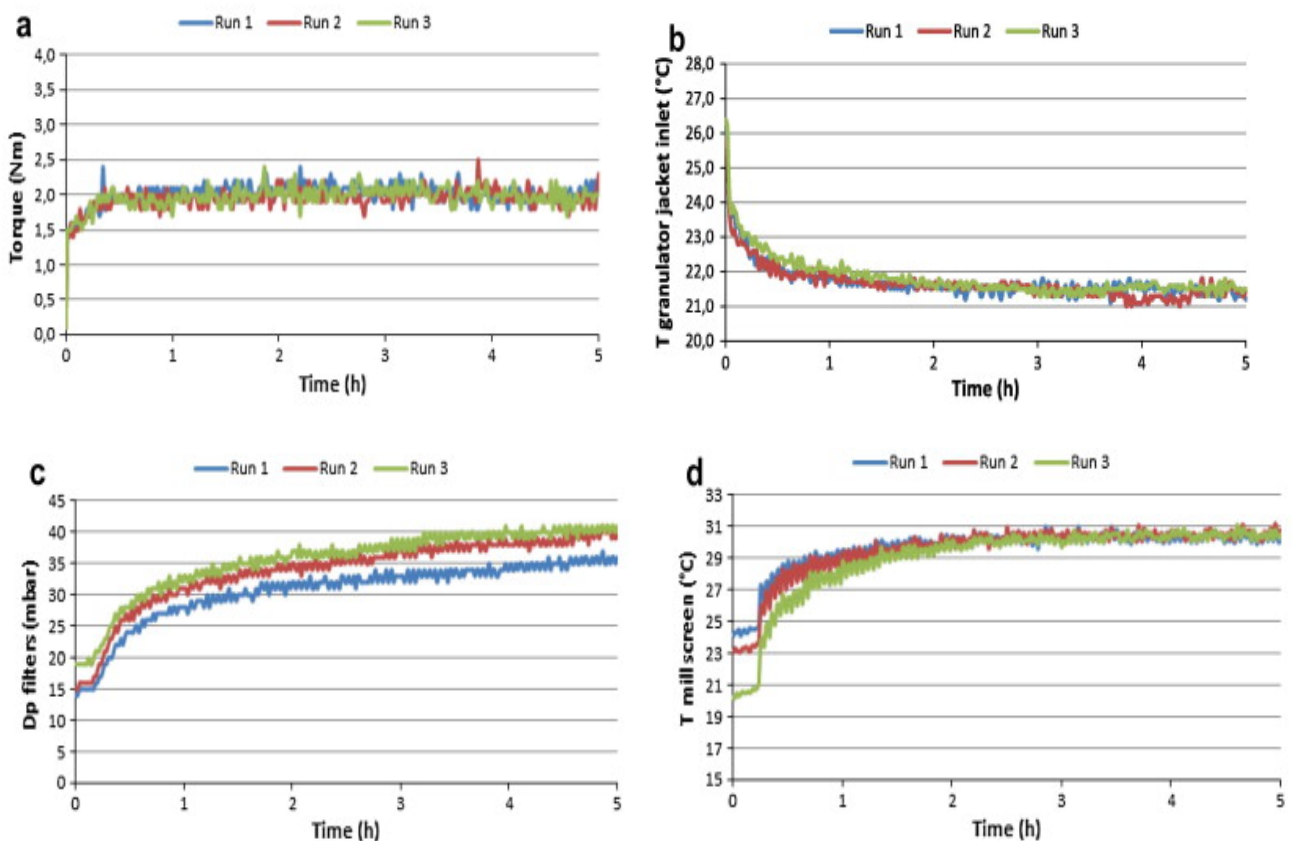


**Figure 10: Process variables stability with time (a) twin screw granulator torque, (b) jacket temperature of the twin-screw granulator, (c) difference in pressure over the filters of the dryer, and (d) temperature of mill screen (Vercruyse et al. 2013).**

Quality attributes of tablet such as weight and hardness were also analysed. Figure 11 shows an overview of weight uniformity and hardness of tablets results in which more deviations can be observed, this particularly was more visible in the tablet hardness, the mean values of hardness ranged from 78.2 to 94.4 N and hence these were in compliance with the actual given batch process specifications (i.e., 70–110 N). Generally, this result deemed to be a stable especially for the tablet weight.

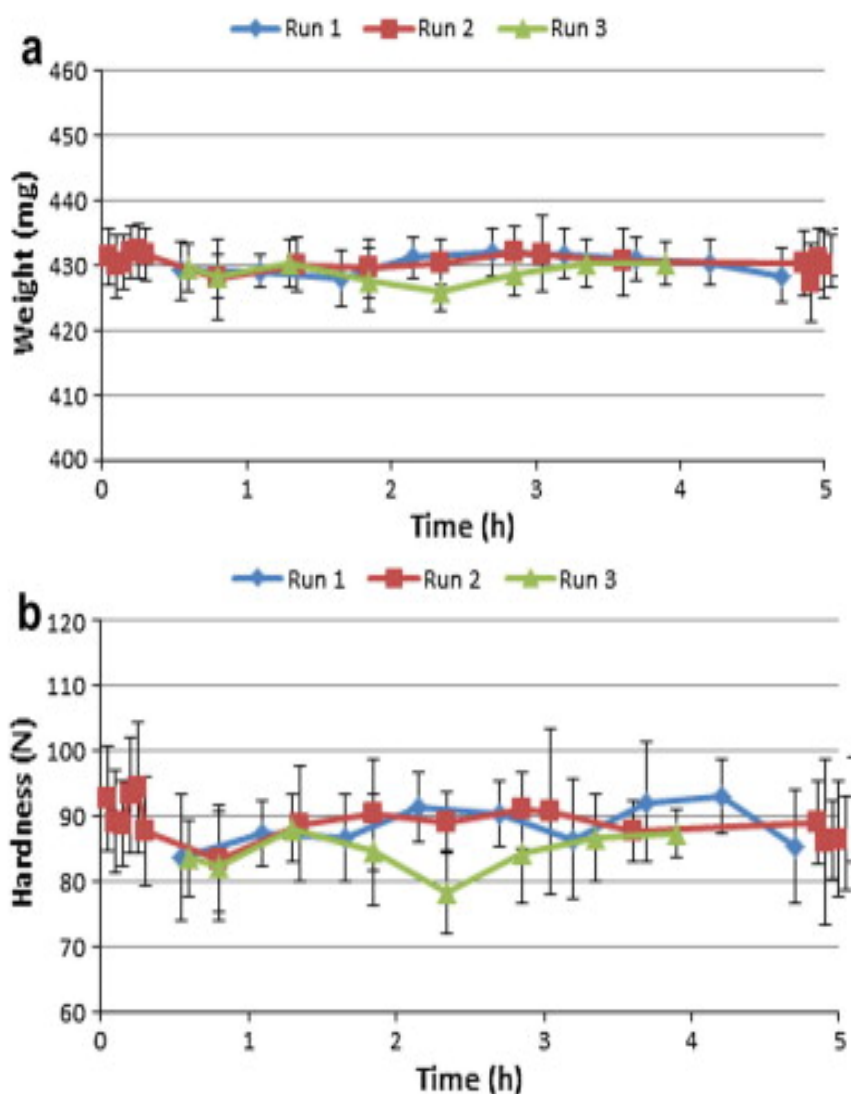


**Figure 11: Tablet attributes stability and repeatability over time (a) tablet weight (b) tablet hardness (Vercruysse et al. 2013).**

Vercruyssen et al. 2015, conducted another study using a “ConsiGma™-1 mobile laboratory (1 segment) and ConsiGma™-25 (six-segmented fluid bed dryer)” to determine if the manufactured material using a single cell of the ConsiGma™25 system is predictive of the granule and tablet quality during full scale production (when filling all the drying cells). Also evaluated and compare the ConsiGma™-1 system performance to the ConsiGma™25 system. Figure 12 shows a good stability and repeatability of the profiles of temperature and moisture content for the materials processed during the 1-hour continuous run and with the average temperature and moisture content of the single cell runs performed with the C25 and the C1 system. It can be clearly seen from Figure 12(a) that the profiles of temperature obtained during the 1 h run and the C1 runs were actually comparable. However, for the granules processed in the single cell runs with the C25 system appeared to dry a bit faster resulting in a higher product temperature at the cell discharge (37.8 °C compared to 35 °C). This could be due to the design of the C25 dryer. Figure 12 (b) presents the result of the LOD for the milled granules that were tested immediately after drying. It can be seen that for the 1 h continuous run, there is no deviant in the values of the LOD during the phase of the start-up or shutdown nor trends in function of process time. Thus, indicate a stable and reliable process of drying. Zomer et al., 2018 monitored the stability of the operations within the line by designing models that were able to identify any an undesirable event or performance deterioration throughout the continuous manufacturing process. For instance, this covered the detection of lengthy offsets in the feeding of material in granulation stage, inconstant conditions of inlet air and blocking of filters in the dryer, resulting in an uneven material discharge for the downstream process. This eventually allow the operator in performing a real time check on the line and therefore taking a specific action for improvement such as, cleaning, adjusting or exchanging a component. The aforementioned studies show the potential of running the entire line for long hours with maintaining a control on the process as well as the flexibility of using single experiments for the purpose of process optimization.

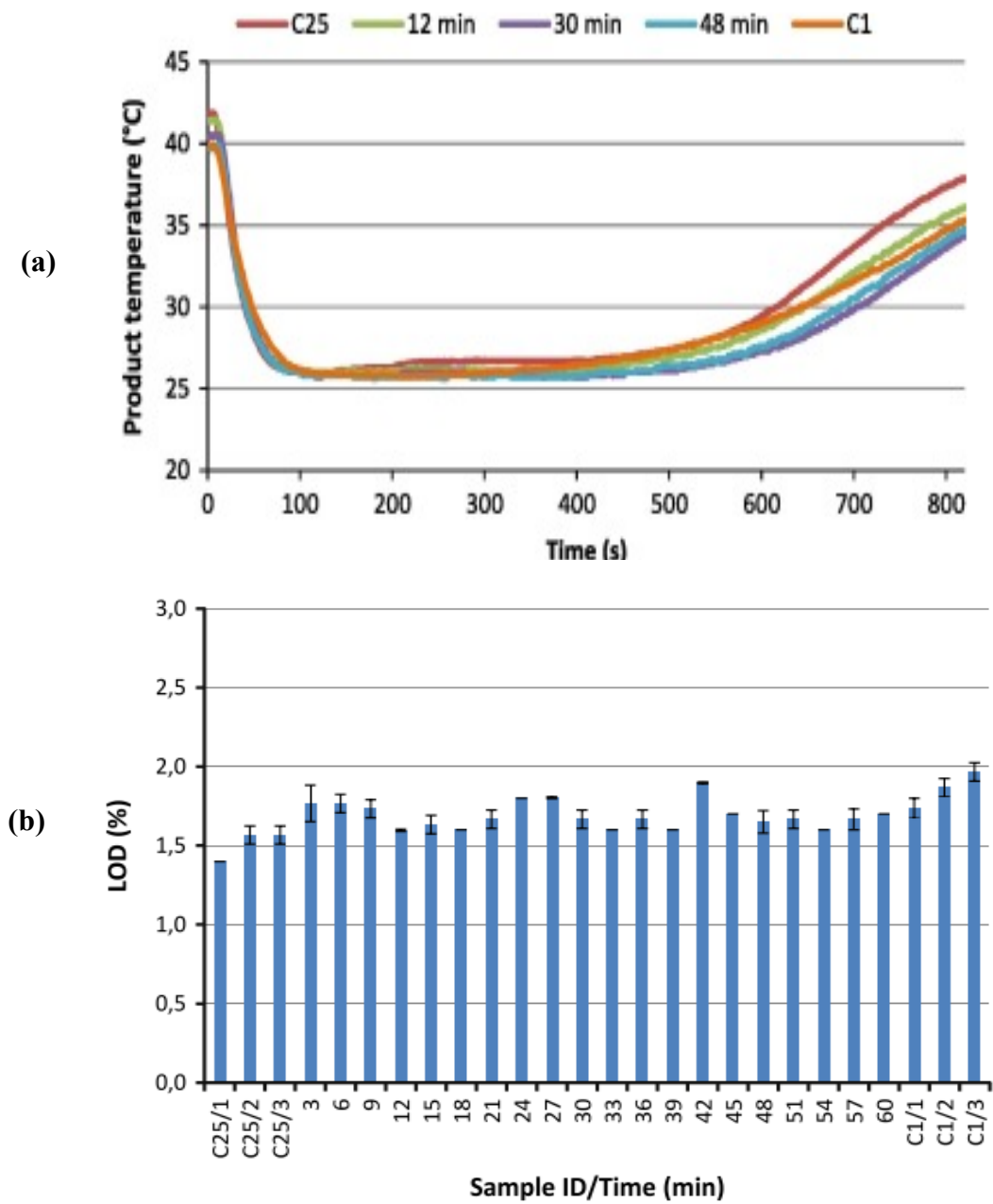
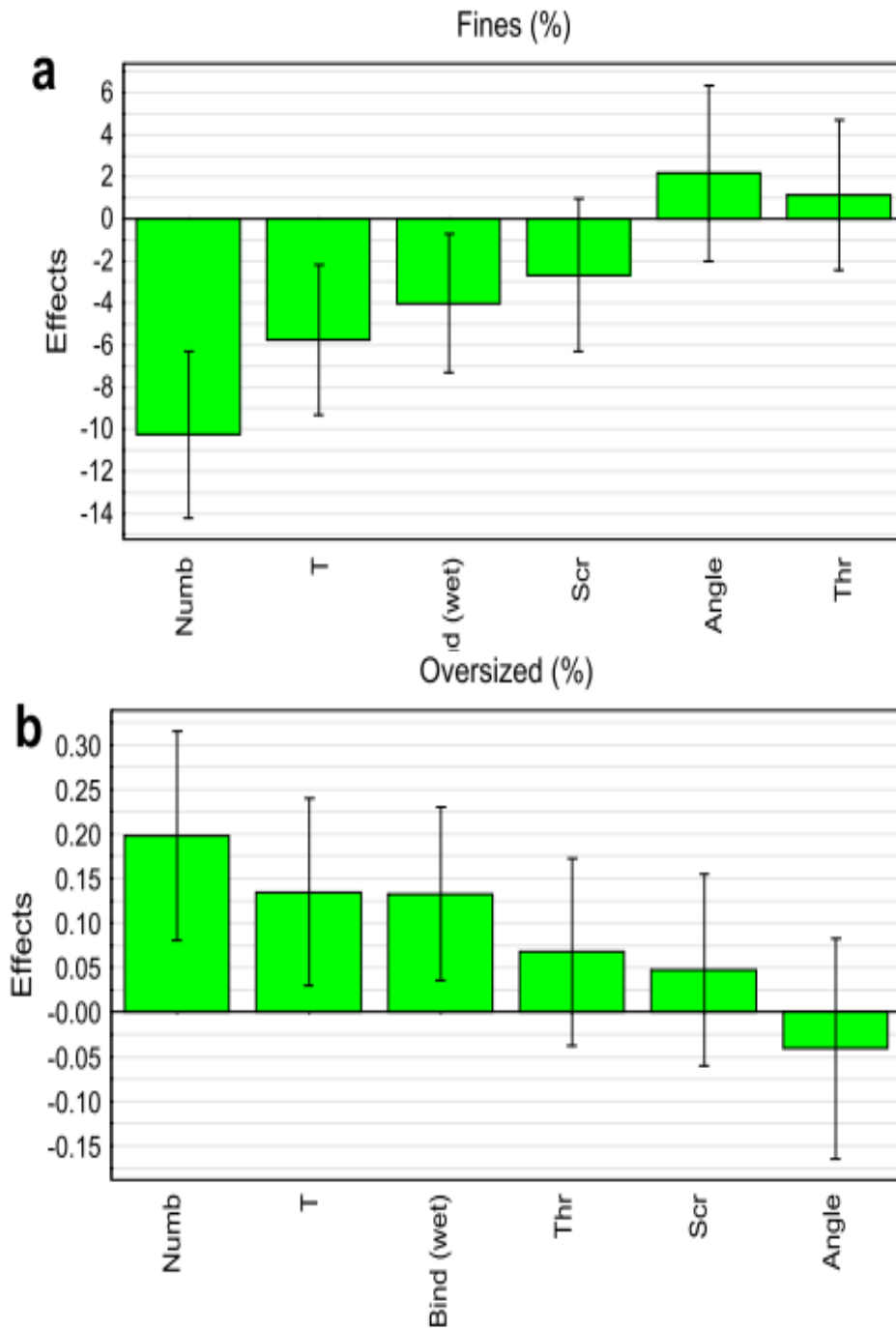


Figure 12: Measurements of (a)temperature profiles (b) Loss on drying for materials processed during the 1 h continuous run and the single cell runs conducted with the C25 and the C1 system (Vercruyse et al. 2015).

### **1.2.2.3 Twin Screw Granulation in ConsiGma 25 System**

Yet, twin screw granulator is the most unit studied in literature out of all the units exist in the ConsiGma 25 line. This is might be due to the existence of the laboratory scale ConsiGma 1 equipment which consists of the same twin-screw granulator presents in the large scale ConsiGma™-25 system. Different process and formulation parameters such as speed of the screw, powder feed rate, liquid to solid ratio and configuration of the screw were varied together with some studies concentrating on the utilized materials in the process of granulation. Limited number of studies has determined the impact of the screw configuration on the attributes of granules and tablet. Vercruyse et al., 2012, studied the effect of different process parameters in the Consigma-25 twin screw granulation unit on the properties of granules and tablets. The parameters varied were powder throughput, screw speed, number of kneading elements used, the angle at which the kneading elements are placed, temperature of the barrel and the method of adding the binder (dry vs wet). Figure 13 shows the impact on the percentage of fines and oversized granules. Kneading elements number had a great impact on the percentage of both fines and oversized granules, unlike the angle of kneading elements which did not have an impact on both the fines and oversized amount. The same study has reported an effect of number of kneading elements and their stagger angle on the tablet dissolution properties which is due to the effect of granules density. In another study conducted by Beer et al., 2014, the effect of number of kneading elements was reported to affect the release of tablets in which an increase in the number of kneading elements resulted in a continued decrease in the performance of tablet dissolution.





**Figure 13: Impact of different twin screw granulator parameters on percentage of (a) fines (b) oversized [Numb: number of kneading elements: temperature of granulator barrel, Bind(wet): wet binder addition, Scr: speed of the screw, Angle: kneading elements angle and Thr: powder throughput] (Vercruyse et al., 2012).**

A Comparable result was obtained in the study conducted by Vercruyse et al., 2014 with respect to the effect of number of kneading elements on the granule size distribution. Figure 14 presents the effect on

the granule size distribution, it can be seen from this figure that increasing the number of kneading elements lead to lower amounts of fines and a higher number of agglomerates, due to more intensive mixing of powder and liquid. Another similar result was reported by Kumar et al., 2016 in which a better mixing of the powder and the liquid was achieved as the number of kneading zones increases, this led to reduce the number of fines and bigger granules. Moreover, Kumar et al., 2014 conducted a study which varied the rotation speed of the screw, powder throughput, number of kneading elements and kneading elements angle. It was found that these parameters not only had a direct influence on the material feed residence time but also on the axial mixing during granulation using TSG in a ConsiGma- 25.

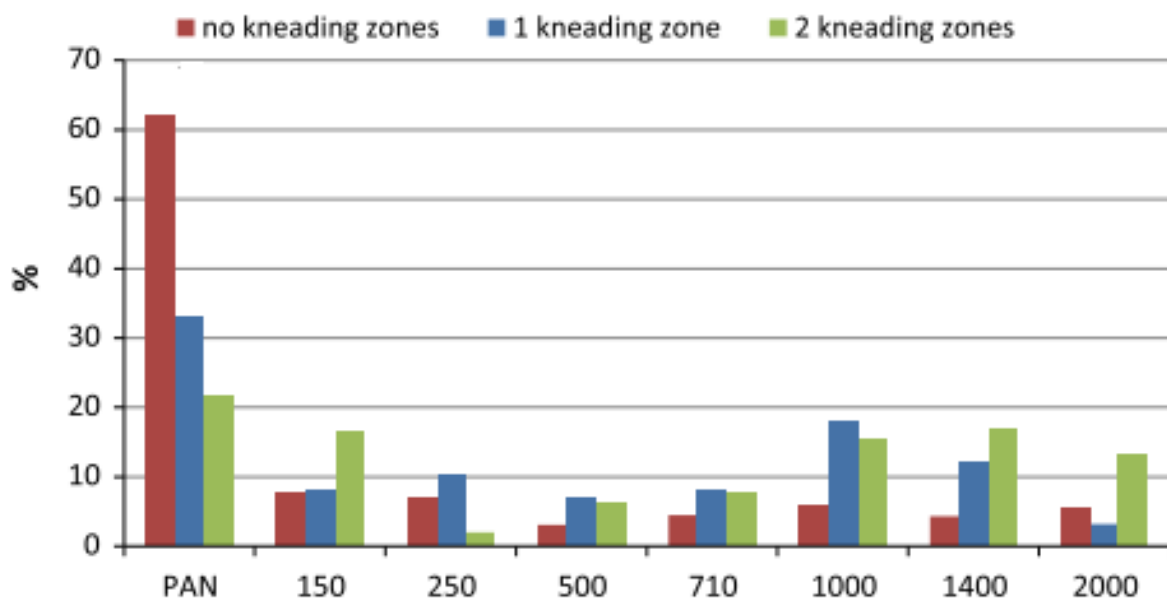


**Figure 14: Impact of number of kneading elements on the granule size distribution (Vercruyssen et al., 2014).**

The parameter liquid to solid ratio (L/S) in TSG which is defined as the measure to the amount of liquid binder added to a given amount of powder material has also had an enormous attention in several studies utilizing both lab scale TSG and ConsiGma 25 system. Hwang et al., 2019, investigated the effect of liquid to solid ratio on the granule size distribution for two different powder materials and the outcome of the investigation is shown in Figure 15. All the experiments in this study were performed using standard screw configurations in which each screw consisted of two kneading

zones separated by a conveying element with each zone contain six kneading elements placed at a 60° angle. It was found that increasing the liquid to solid ratio has led to a decrease in the percentage of fines and an increase in the percentage of the oversized granules, this was observed for the two different materials (lactose and MCC) as seen in Figure 16.

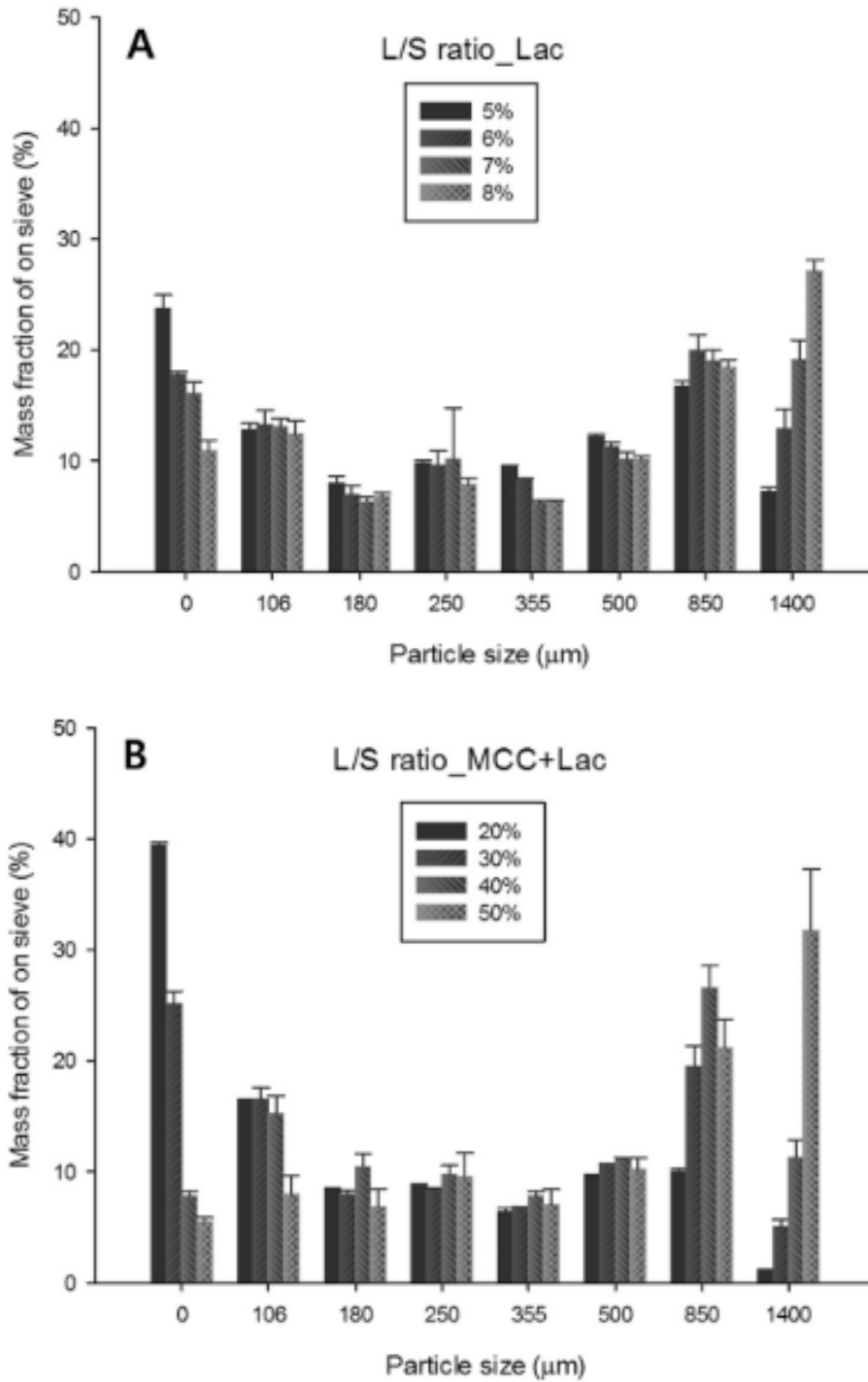
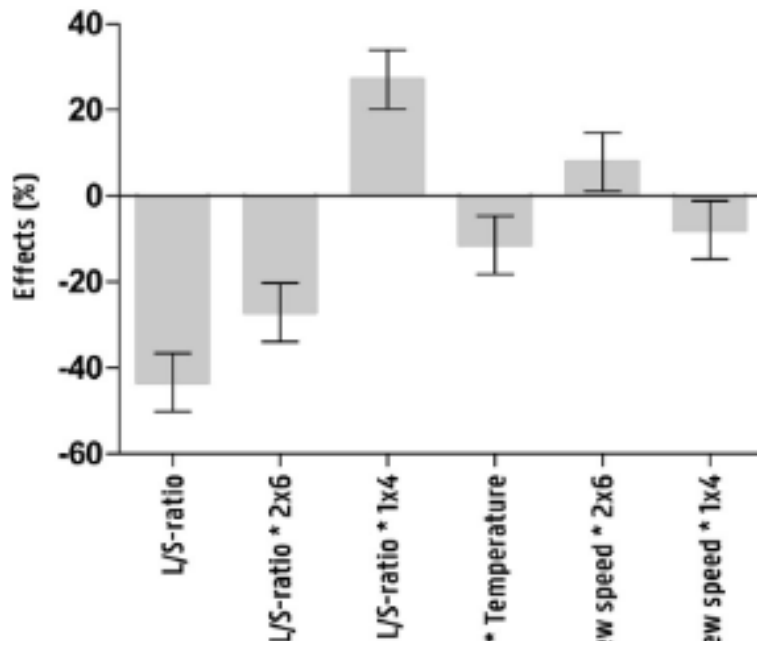


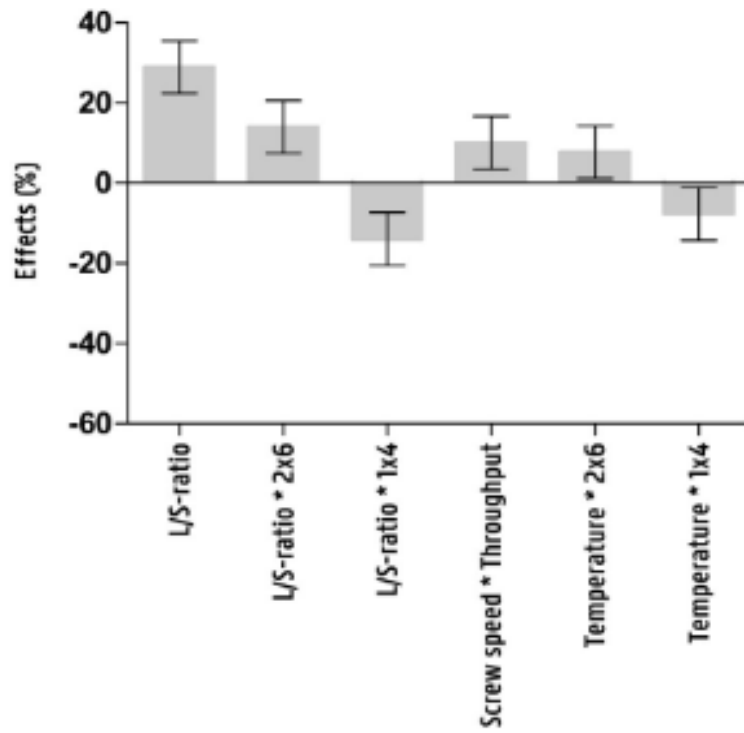
**Figure 15: Impact of liquid to solid ratio on the particle size for two different powder materials (a) Lactose (b) MCC. (Hwang et al., 2019).**

Vandevivere et al., 2019, reported a similar outcome in their study in which a continuous twin screw wet granulation (ConsiGma line) was used to investigate the effect of different granulation parameters on the fines, oversized fractions and the  $d_{50}$  of granules as shown in Figure 16. The investigated parameters included the effect of varying the screw configuration besides the liquid to solid ratio, temperature of the barrel and screw speed. Increasing liquid to solid ratio allowed more densification and granule growth, therefore, the interaction between the screw configurations and the liquid to solid ratio affected the  $d_{50}$  fines fractions and oversized fractions. When high number of kneading elements was used along with low liquid to solid ratio, a higher fines fraction was obtained because of inadequate liquid binder was available to sufficiently wet the particles but then again when higher liquid to solid ratio was used along with lower kneading elements, opposite effect was obtained as more fines fraction was produced when lower kneading elements was used. Verstraeten et al., 2017, analysed in depth the pharmaceutical twin-screw wet granulation ConsiGma<sup>TM</sup>-25 system in view of detailed process understanding using hydrophilic and hydrophobic formulations. Different process settings were altered in their study, such as L/S, mass throughput and speed of the screw, and their impact on the formation of granules were determined. Figure 17 shows how the PSD increases in both formulations (hydrophilic and hydrophobic) as the liquid to solid ratio increases. Overall, the two formulations behave in similar way, when low liquid to solid ratio was used, bimodal distribution was observed, and increasing the liquid to solid ratio led to have a monomodal distribution in which bigger granules were obtained. The study has also looked at the impact of screw speed on the granules formation, although it exists that the speed of the screw predominantly affects the material residence time and the energy input into the system, there was not seemed to be a significant impact for it on the granules attributes in particular when it is compared to the impact of the screw configurations and liquid to solid ratio as presented in the earlier figures.

(a) Fines Fraction



(b) Oversized Fraction



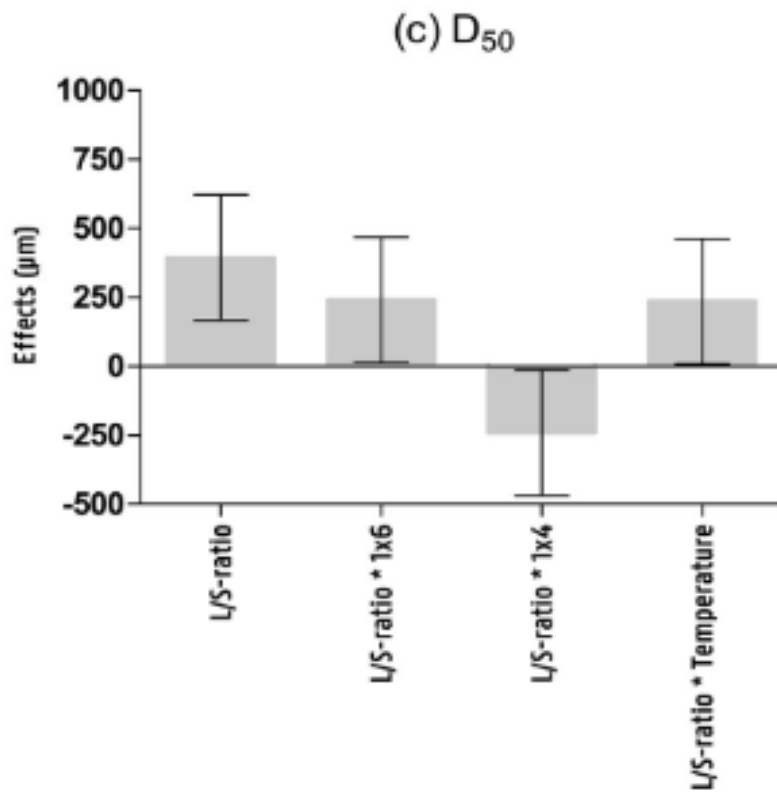
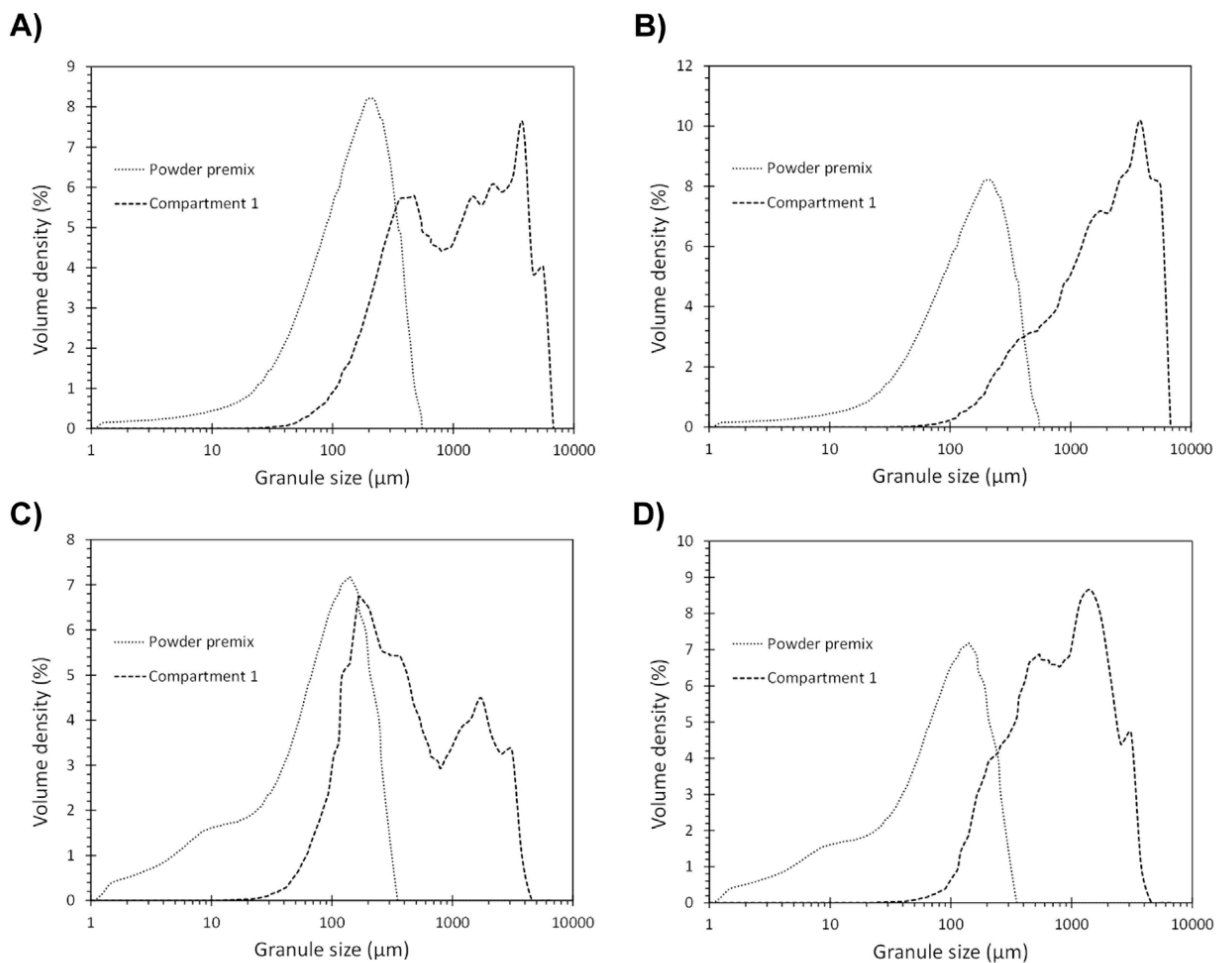


Figure 16: Effect of varying different granulation parameters on (a) fines fraction (b) oversized fractions and (c)  $d_{50}$  of granules (Vandevivere et al., 2019).



**Figure 17: Particle size distribution before and after wetting (a) hydrophilic blend at low L/S (b) hydrophilic blend at high L/S (c) hydrophobic blend at low L/S (d) hydrophobic blend at high L/S (Verstraeten et al., 2017).**

The impact of utilizing different materials in term of binders and powders at the granulation stage were studied using the ConsiGma 25 system. Vanhoorne et al., 2016, used different concentrations and grades of HPMC to determine their effects on the attributes of both granules and tablets. The binder concentration in the solution were varied from 20 to 40% HPMC to increase viscosity of the liquid binder. One of the finding of this study was that the degree of substitution of HPMC had a significant impact on the size of the granules and this is because of the variation of the wetting capacity of the different HPMC grades. It was found that the amounts of fines increase as the liquid binder viscosity increases. Figure 18 presents the effect of using different concentration of HPMC on the granules size distribution. Inclusion of HPMC of higher concentration in the formulations required

the addition of more liquid to produce granules with similar size distribution as in the formulation which contains lower HPMC concentration.

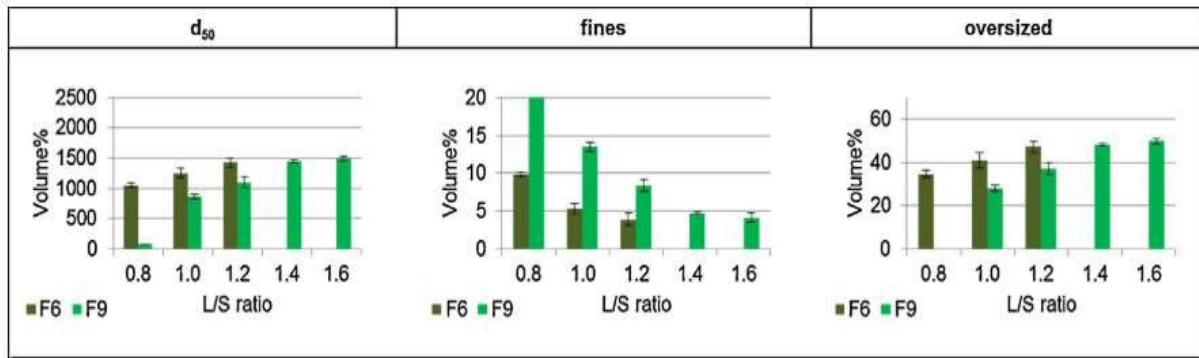


**Figure 18: Effect of the concentration of HPMC on the size distribution of granule [ F6 formulation contains 20% HPMC and F9 40%HPMC] (Vanhoorne et al., 2016)**

The binder viscosity had shown an impact on the tablet attributes as illustrated in Figure 19. In particular, when higher HPMC concentration was used i.e., 40% this is because of higher plastic deformation capacity.

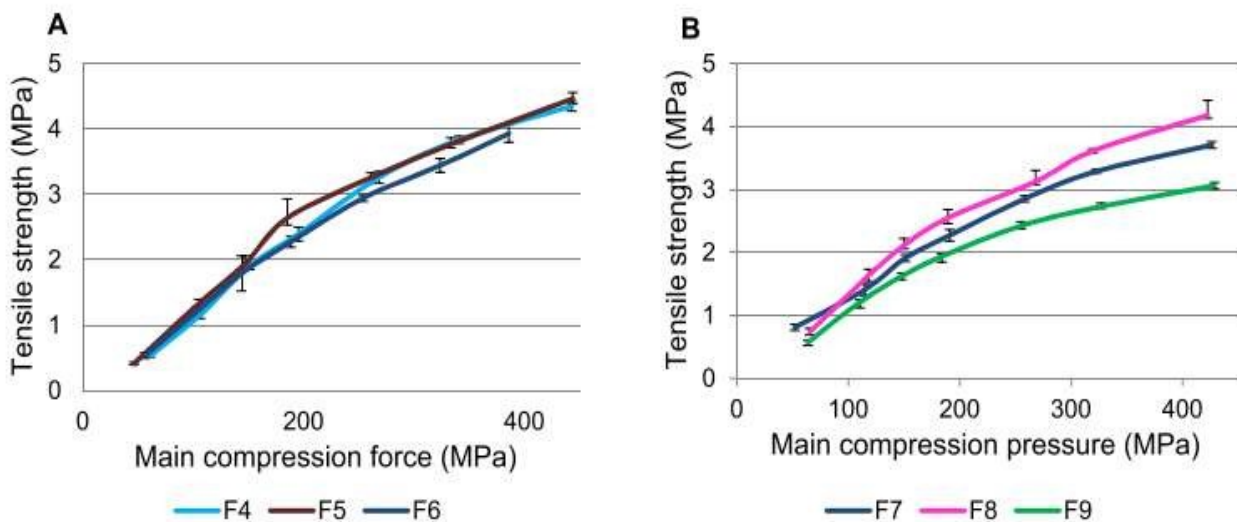


**Figure 19: Tableability of (A) 20% HPMC concentration and 20% powdered theophylline (B) 40% HPMC concentration and 20% powdered theophylline (Vanhoorne et al., 2016).**

Keleb et al., 2002 and Dhenge et al., 2012 found that the granules size is proportional to the binder viscosity. Moreover, they found that the granules size increases as the binder viscosity increases when they used PVP as a binder and that the granules required less liquid to be produced. However, these findings were obtained when conveying and kneading elements were implemented. In the case of



using conveying elements, the outcomes were opposite due to the fact that conveying elements provides less shear to the materials being granulated and therefore less dispersion time of the liquid into the material with difficulty in penetration of the highly viscous liquid binder into the powder within the conveying elements screws (Dhenge et al., 2012). The primary particles size of the starting materials was also considered in the continuous twin screw granulation using ConsiGma system, Hwang et al., 2019 found that as the primary particle size increases, the amounts of fines and oversized granules decreases. This is attributed to the effect of the surface area available to contact with the liquid. In other words, larger particle size of powder has smaller surface area that makes contact with the liquid binder during granulation, so the oversized and fines fraction of the granules is then reduced.

Huang, et al. 2013 conducted a study in which four different commercial grades of lactose powder (spray-dried, sieved, milled monohydrate and anhydrous lactose powder) were compared in term of their suitability for a low dose oral formulation of pentyloxyl paliperidone derivative using a batch high shear granulator. The influence on the size, flowability and other attributes of the granules formed were investigated in their study. They observed that as the powder primary particle size increases, the granules size increases. It was also noticed that the lactose powder of the spray-dried grade produces granules with better flowability and narrow PSD and tablets of good hardness. In comparison with batch high-shear wet granulation, the impact of using different primary particle size (i.e., lactose) on the behaviour of granulation, granules and tablets properties has received limited attention in the continuous twin screw wet granulation. Overall, in almost all the literatures performed on the lab scale twin screw granulation and the continuous manufacturing utilizing the ConsiGma, increasing the liquid to solid ratio tend to always increase the  $d_{50}$  of the granules with having a monomodal distribution rather than bimodal. Moreover, screw configurations tend to produce also similar result with respect to adding more kneading elements. None of the aforementioned studies has paid attention to determine the effect of these parameters to the drying process, therefore the focus of this project to determine the impact of screw configuration, and the primary particle size of the starting materials on the drying of the granules and on the downstream processes i.e., tableting.

### 1.2.2.4 Six-Segmented Fluidized Bed Dryer in the ConsiGma 25 System

In the previous years, the six segmented fluidized bed dryers of the ConsiGma 25 system have received an attention in a small number of studies. Since the fluidized bed drying is not an intrinsically continuous operation, the fluidized bed dryer within the ConsiGma 25 system composed of six segmented cells, in which they are successively fed by the twin-screw granulator with wet granules. Figure 20 illustrates the filling cycle in the six segmented fluidized bed dryers in the ConsiGma 25 line (De Leersnyder et al., 2018). After a dryer cell filled with granules for a chosen filling time, wet granules are then fed to the adjacent cell, while the drying cycle completes by the previous cells. Based on the chosen times of filling and drying, cells 2 to 6 can contain granules at the same time. The continuous action of the six segmented fluidized bed dryer makes it unconventional, however, the fundamental of the drying process in this continuous dryer is the same, this suggests that the outcomes of the literature with regards to the drying process performed in a conventional batch dryer could be still applicable in the continuous dryer

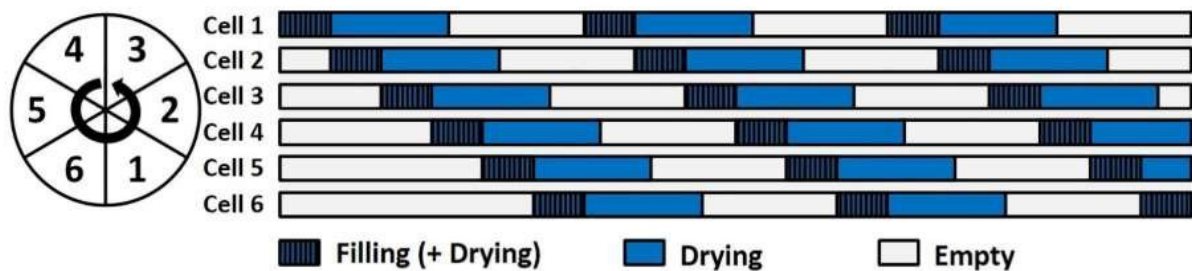


**Figure 20:** Visual illustration to show the filling cycle in the segmented fluidized bed dryer of the ConsiGma 25 system (De Leersnyder et al., 2018).

The fundamentals of the drying process in the fluidized bed dryer have been extensively studied in several industries and all the findings showed a good agreement irrespective of the materials or the equipment used. The main findings were that increasing the air flow rates, increases the heat and mass transfer and hence higher rate of drying is achieved. As well, increasing the drying air velocity and air temperature, has led to increase in the drying rate since more available energy for drying. Additionally, the drying of the materials with smaller primary particle size tends to result in faster

drying due to the fact that they have more available surface area per unit mass for heat and mass transfer to occur.

Moreover, some other studies focused on comparing the effect of equipment design on granules attributes, Vercruyssen et al. 2015 found that the equipment design could affect the granules attributes in particular, the granule size distribution as seen in Figure 21. For C1 system, the granules were conveyed from the twin-screw granulator outlet by gravity to the fluidized bed dryer. For C25, the granules were transferred pneumatically from granulator outlet through to the top of the six segmented fluid bed dryers. Consequently, the granules dried in the C25 system were exposed to more breakage during the transport process of wet granules. This was explained to be attributed to the collision, which was taking place between the granules and the transfer line wall and the granules and the dryer vessel wall.

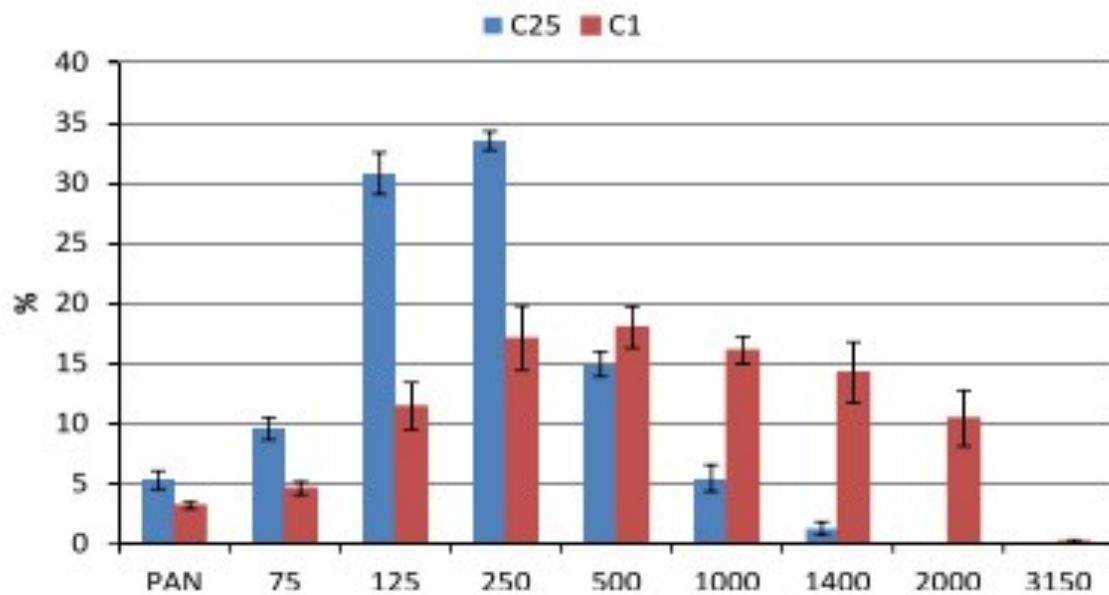


**Figure 21: Granules size distribution derived from C25 and C1 single cell runs after drying process in the fluidized bed (Vercruyssen et al. 2015).**

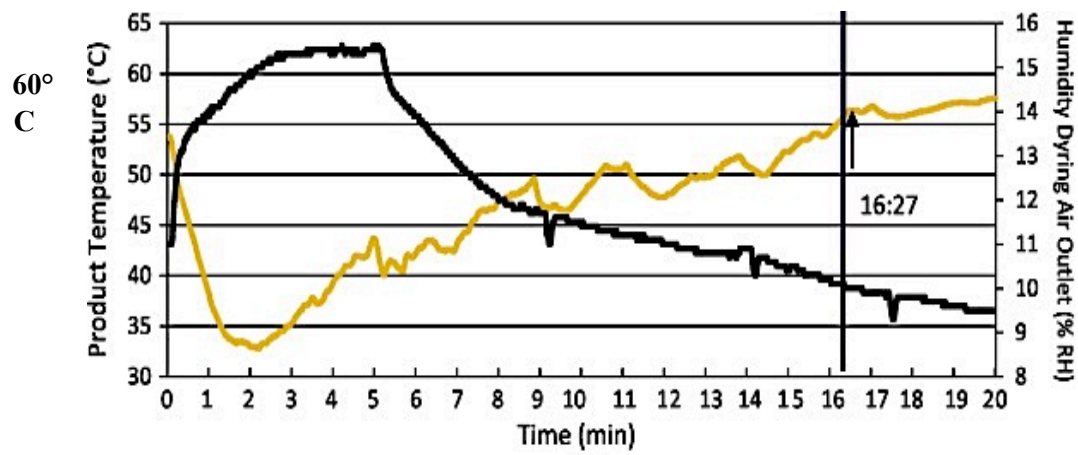
Similar study conducted by De Leersnyder et al., 2018, which mainly studied the phenomena of granules breakage and attrition during drying in fluidized bed after the continuous twin screw granulation. As seen in Figure 22, De Leersnyder et al., 2018 used two different ConsiGma 25 system

and compared their results, it was found that the granules breakage and attrition occurred more when the horizontal ConsiGma 25 system was used and that was mostly attributed to the wet granules pneumatic transfer between the twin-screw granulator and the fluidized bed dryer. Less granules breakage and attrition were observed when the vertical ConsiGma 25 system was used as the wet granules were not susceptible to pneumatic transfer when transferred from the granulator to the dryer. The impact was especially major when the granules were transferred when they are still not fully dried. They found that shorter drying times led to a higher extent of breakage and attrition. When short drying times were applied, granules were still wet when entered the dry transfer line leading to breakage in that line because of the pneumatic transport. The study also looked at the effect of drying time, air flow rate and air temperature on the moisture content of granules during drying in the segmented fluidized bed dryer, it was found that increasing these parameters led to a decrease in the moisture content of granules.

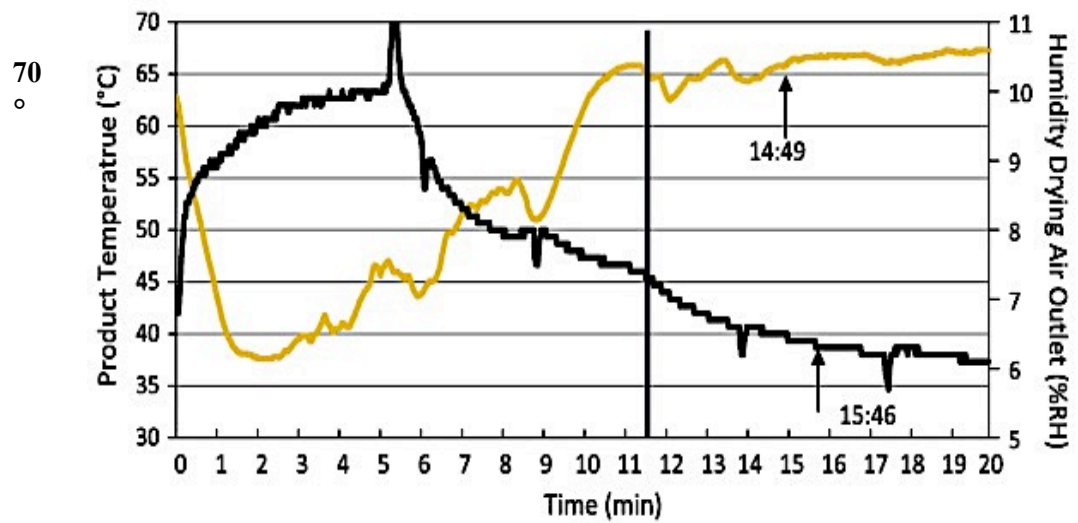


**Figure 22: Illustration of the two ConsiGma™-25 (left) Horizontal set-up and (right) vertical setup with the red line represents the wet transfer line (only in horizontal set-up) and the green represents the dry transfer line.**

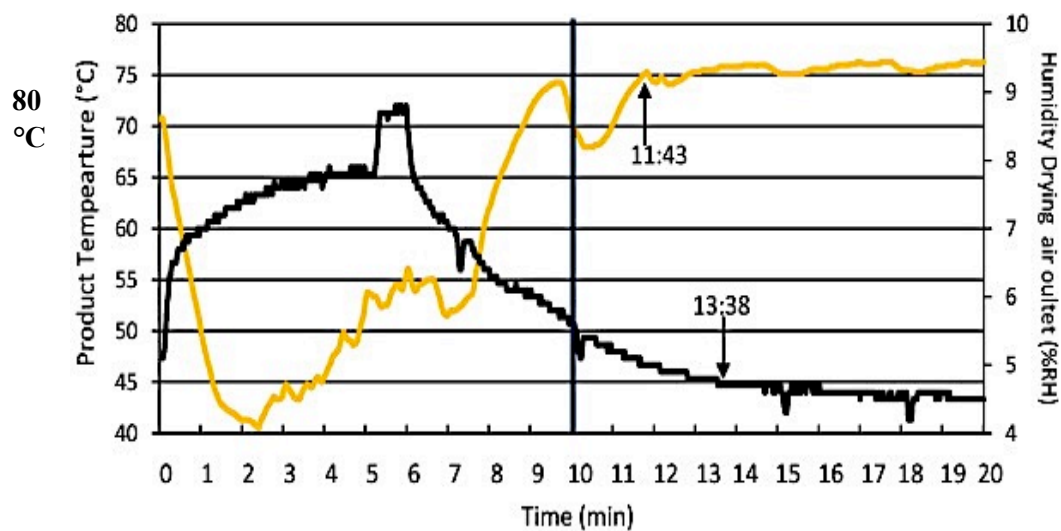
Mezhericher 2014, investigated the impact of fluidized bed drying temperature on the resultant granular product. The study showed that faster drying as a result of increasing drying air temperature cause damage to the granule microstructure resulting in granule breakage and consequently reducing the size and strength of the granules. However, others argue that depending on the formulation used, there is a specific limit in which the increase in temperature significantly affects the original granular properties. Fonteyne et al. 2014, studied the detection of the drying end point in fluid bed drying of ConsiGma-25 system. They used classical indirect methods such as temperature of product or outlet air humidity to detect the drying end point. They also compared the classical methods with in-line moisture determination using different approach namely, NIR spectroscopy, Raman and a mass balance. The study used an anhydrous theophylline as a model drug, this drug was mixed together with lactose monohydrate 200M and polyvinylpyrrolidone (PVP) and granulated using distilled water (Fonteyne *et al.*, 2014). Figure 23 shows the results of three test experiments performed at different temperature namely at 60, 70 and 80°C. Regarding the outlet air humidity for the experiment performed at a drying temperature of 60°C there was no observation for a steady state. Steady state was reached for test experiments performed at a temperature of at 70°C and 80°C, however, this was at late time compared to end point of drying as shown by the NIR determination method of moisture. They concluded that the temperature of the product is a very reliable parameter that worked well to determine the end point of drying for all the six-segmented fluid bed dryer due to the fact that each dryer cell by its own has an installed temperature sensor where this sensor is actually embedded in the product. Figure 25 also indicates the steady state for the determined temperature of the product.



(a)



(b)



(c)

Figure 23: Temperature of the granules (yellow line) and outlet humidity of air (black line) for the experiments performed at a temperature of (a) 60°C (b) 70°C and (c) 80°C (Fonteyne et al., 2014).

Fonteyne et al. 2014, also studied the influence of temperature and granules size on the moisture content as seen in Figure 24. This Figure shows 19 experiments of the granule's residual moisture content. The granules were split into three groups; the first group is the granules with a moisture content of 4% or less "(experiments 1, 2, 6, 13, 16, 18 and 19)". The second group represents the granules with residual moisture content of above 5% and these are "experiments 3, 4, 7, 9, 11, 14, 15 and 17". The third group is the granules, which have residual moisture content between 4 and 5 % and these, are experiments 5 and 10. The group of the granules with the moisture contents of above 5 % were dried at a temperature of 35°C, whereas the group which had a moisture content of less than 4 % were dried at a temperature of 75°C. This group does not show big variances in the moisture content between the different size fractions; oversized, yield and the fines. For the group of the granules that dried at temperatures of 55°C and 35°C, the residual moisture content seen to increase with increasing the size of granules. The fraction of fines has lower moisture content when compared to the fraction of yield and oversized. This is mainly because fines particles can dry much quicker as they have higher ratio of surface to volume. The water in the granule core therefore reaches the granule surface faster in the granules that are small compared to the granules that are large. It can be also notice from the figure that as the temperature increase, the granule moisture content decreased.

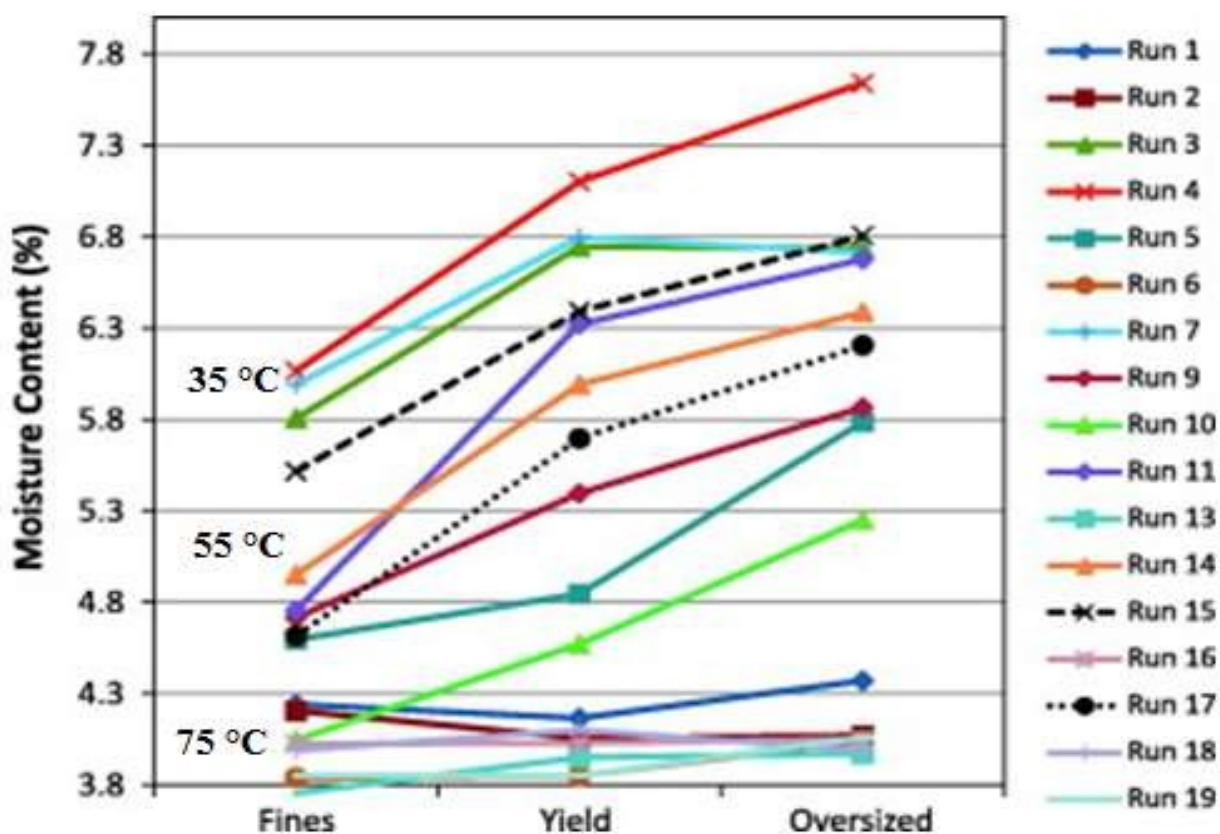


Figure 24: Moisture content of granules at different size fractions and drying air temperature as measured by means of Karl Fischer (Fonteyne et al., 2014).

### 1.2.3. Combination of the two units (TSG and FBD) and the unique feature of this research

To date, the TSG and FBD units have been studied in isolation, in the last 15 years, continuous twin-screw wet granulation has gained an increased interest within the pharmaceutical industry (Verstraeten et al., 2017), (Portier, Pandelaere, Delaet, Vigh, Di Pretoro, et al., 2020). Many investigations have already been performed on continuous twin-screw wet granulation as unit operation, the number of studies and publications on Twin-Screw Wet Granulation have increased exponentially (Keleb et al., 2004; Ito and Klei- nebudde, 2019; Dhenge et al., 2010; Meier et al., 2015; Arndt et al., 2018; Osorio et al., 2017; AlAlaween et al., 2020). The impact of specific process factors such as Liquid-to-Solid ratio (L/S) (Nicola et al., 2018), screw arrangement (Djuric and Kleinebudde, 2008; Li et al., 2014), barrel fill level (Lute et al., 2018), and overall process settings



(Portier et al., 2020; Portier et al., 2020) were mostly evaluated in these publications. Apart from these technological settings, the importance of granulating liquid distribution (El Hagrasy et al., 2013; Dhenge et al., 2012) and the potential implementation of Process Analytical Technology (PAT) tools coupled with real-time process control have also been studied (Madarasz et al., 2018; Harting and Kleinebudde, 2018). Some research has focused on the impact of process factors (Portier, Pandelaere, Delaet, Vigh, Di Pretoro, et al., 2020), (Vanhoorne et al., 2016), (Vercruysse et al., 2012), (Dhenge et al., 2011) and formulation properties (Fonteyne, Wickström, et al., 2014), (Fonteyne et al., 2015), (Willecke et al., 2018), (Willecke et al., 2017), (Lute et al., 2018), (Yu et al., 2014), (Portier, Pandelaere, Delaet, Vigh, Kumar, et al., 2020), (Vandevivere et al., 2020) on the quality attributes of granule. Other studies conducted by these authors (Verstraeten et al., 2017), (Vanhoorne et al., 2016), (Fanny Stauffer et al., 2019), (Dhenge et al., 2012), (Lute et al., 2016), (Qiao et al., 2012), (Dhenge et al., 2012), (Dhenge et al., 2012), (Dhenge et al (Van Hauwermeiren et al., 2019) has targeted a more fundamental understanding of the twin-screw granulation mechanism. The ConsiGma system (GEA Pharma systems, Wommelgem, Belgium), which uses a continuous powder-to-tablet line, was employed in many of these studies (Verstraeten et al., 2017), (Vanhoorne et al., 2016), (Portier, Pandelaere, Delaet, Vigh, Kumar, et al., 2020), (Fonteyne, Wickström, et al., 2014), (Fonteyne et al., 2015), (Willecke et al., 2018), (Willecke et al., 2017), (Fanny Stauffer et al., 2019). In the consecutive step of an integrated continuous manufacturing line, the wet granules are processed in an appropriate drying equipment, most typically a Continuous Fluid Bed Dryer. The deployment of segmented Fluid Bed Dryers (FBD; GEA Group), which operate in a semi-batch mode by containing 6 independent drying chambers, is now the most extensively utilised technological solution for drying constantly produced granules. The semi-batch size is determined by the filling time and the actual mass flow rate of the wet granules as they are directed to their respective chambers. The system's capabilities and limitations are extensively studied in the literature (Vercruysse et al., 2013; Vercruysse et al., 2015).

Although the drying process is critical to ensuring a satisfactory final product, the six-segmented fluid bed drying following the granulation unit of the ConsiGma system has been researched to a lesser extent. Vercruyssen et al. tested the stability and reproducibility of a single formulation for the twin-screw granulation and six-segmented drying unit throughout a 5-hour production run (Vercruyssen et al., 2013). The investigation found that the residual moisture content after drying remained constant throughout the whole run, indicating that the drying procedure for the formulation in question was reliable. Vercruyssen et al. (Vercruyssen et al., 2015) also tested whether the product quality (i.e., residual moisture content, particle size distribution, bulk and tapped density, and friability) obtained by using only a single cell of the segmented dryer unit of the ConsiGma-25 system (C25) was comparable to the granule quality of granules collected during full-scale manufacturing when all dry cells were used. Because the granule quality was identical, using a single cell during formulation and process development could be advantageous. The study, however, did not look into the consequences of changing the drying parameters. Furthermore, the granule quality acquired during full-scale manufacture with the ConsiGma-25 system was compared to the quality obtained during an identical drying experiment (i.e., identical drying conditions) performed with a mobile ConsiGma-1 system (built for R&D investigations). The ConsiGma-1 (C1) system was not predictive for granule quality in steady state during full-scale manufacturing, as seen by deviating granule quality. Other investigations used the ConsiGma-25 dryer to determine granule moisture content using in-line near infrared (NIR) measurements (Chablani et al., 2011), (Fonteyne, Gildemyn, et al., 2014). Recently, Stauffer et al. (F. Stauffer et al., 2019) highlighted the impact of wet granule properties on the stability of the drying (i.e., air flow deviations). The relevance of granule characteristics prior to drying was highlighted in their investigation, as an excess of fine particles accumulating on the drying filter's surface resulted in an unstable drying process. De Leersnyder et al. also conducted a thorough examination of the effects of drying process parameters on granule quality attributes and breaking behaviour (De Leersnyder et al., 2018). The ConsiGma-25 was used in this investigation in both a horizontal and vertical configuration. In a horizontal set-up, the granulator is next to the dryer with a pneumatic granule transfer via a wet transfer line, whereas in a vertical set-up, the granulator is above the dryer with a gravimetric transfer of wet granules to the dryer. The drying unit, whether performed in batch or in a

continuous from-powder-to-tablet manufacturing line with a twin-screw granulation (TSG), is an important intermediate process step in achieving the appropriate tablet quality. Hence, understanding this step and determining the possible TSG parameters that could affect it is of a paramount importance, this research project, therefore, was designed to fundamentally understand the impact of twin-screw process and formulation parameters on the drying behaviour of granules in fluidized bed. This research will also be critical in designing a future generic flowsheet model as well as a general drying model for the ConsiGma-25 line's drying unit. The author is unaware of any research that has been done to investigate the impact of the twin-screw granulation on granule drying in fluidized beds and other downstream processes such as tableting. Furthermore, this research will be unique in that it examines linking both TSG and FB, which has not been explored in the literature during twin-screw granulation and fluidized bed drying studies, thus, its outcome is still unknown. To the author's knowledge, there are two publications on the topic of twin-screw wet granulation process scaling (Djuric et al., 2009; Osorio et al., 2017), as well as one publication comparing two different equipment scales of a continuous granulation and drying line, namely the GEA Consigma systems (Vercruysse et al., 2015). Vercruysse et al. (2015) and Osorio et al. (2017) utilised formulations including cellulose in their work. Other studies looked into the impact of different cellulose grades on the twin screw wet granulation method. Other studies looked into the impact of different cellulose grades on the twin screw wet granulation process (Fonteyne et al., 2015; Hwang et al., 2019). The Influence of equipment design and process factors on granule breakage in a Semi-Continuous fluid bed dryer following Continuous Twin-Screw Wet Granulation was recently elucidated (Ryckaert et al., 2021). Overall, this research contributed to a better knowledge of fluid bed drying breakage behaviour. The feeder, twin-screw granulator, and dryer were all merged into one operation in the recently released Bohle granulation line (Meier, 2018). However, to the best of the authors' knowledge, no scientific articles on analysing the effect of key process parameters on drying process using an integrated real continuous pharmaceutical granule process have been published. Furthermore, only a few articles (Demuth et al., 2020) investigate the development of low-dose tablet formulations based on twin screw wet granulation, and none of them combine it with continuous drying. How the granules behave in the fluidized bed dryer during the continuous loading of dryer cell

was mostly missing in the literature of the continuous manufacture using Consigma-25 system. This project aimed at filling these missing gaps which were either poorly researched or not even exists in literature. As a result, the focus of this research project is on bridging the gap between twin-screw granulation and the wet granules' fluidized bed drying process. These two primary units (Twin screw g) are the most important ones.

### **1.3 Effect of Moisture on Tablet Properties**

Obtaining a good quality pharmaceutical tablet depends on the behaviour and properties of powder. Moisture is one of the keys and critical properties of powder, which needs to be considered during the manufacturing of the tablets. Plastic properties of particles are directly affected by moisture. Excess moisture on the surface of particles increases the distance between them and thus less friction between close particles. This results in increasing the fluidity of powders. Absorbed water also led to a reduction in the surface energy of crystals and increment in tablets adhesion to the matrix and die surfaces and thus reduces their tensile strength (Zhuikova et al., 2009).

Takasaki et al. 2016, studied the effect of changing the amount of water added to produce the granules on the properties of tablet produced by moisture activated dry granulation (MADG). In this study, they produced MADG tablets with various amount of water (0, 1, 1.5, 2, 2.5, 3, and 5%. w/w). Moreover, the influence of moisture content on tablet characteristics was studied by determining the water activity. It was found that the tensile strength of the MADG tablet increased as the water activity increased. This is when the added amount of water was between 0 to 2.5 %. This can be seen in Figure 25, however, further increase in the amount of water added (2.5% and 5%) caused a significant reduction in MADG tablet tensile strength. And increasing the quantity of water added to above 2.5% (which is equal to a water activity of 0.61), reduced the strength of the tablets considerably between 2.5% and 5.0%, (5% of the water added is equal to 0.78 of water activity). This is in agreement with the study conducted by Çelik (1992).

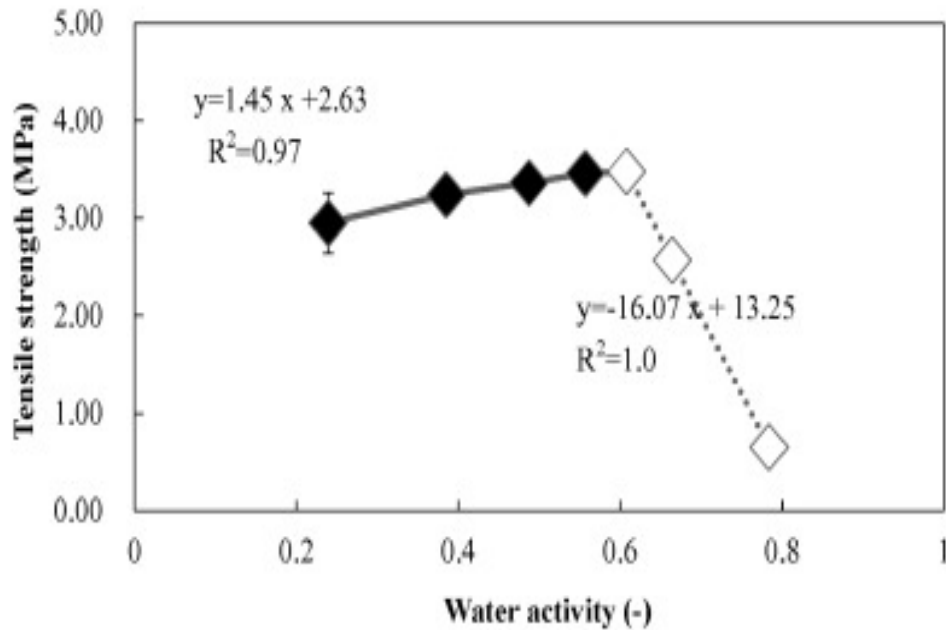


**Figure 25: Effect of water activity on the strength of tablets (MADG) at a compression force of 10 kN “◆; Amount of added water: 0.0%, 1.0%, 1.5%, 2.0% ◇; Amount of added water: 2.5%, 3.0% and 5.0% “(Takasaki et al., 2016).**

Çelik (1992) studied the tablet compactibility of paracetamol powder and his findings revealed that mean yield pressure was reduced as moisture increases. However, another study done by Malamataris et al., 1991, found that tablet strength reached peak and then began to reduce when moisture amount was roughly doubled. Nokhodchi 2005, suggested that increasing or decreasing moisture content could increase or decrease tablet strength, with the change being dependent on the powder’s moisture content. Nokhodchi et al. 1995a, investigated the impact of moisture content on the crushing strengths of ibuprofen tablet produced at different compression speeds (15-240 mm/s) with changing the moisture content. In their study, they found that increasing the moisture to approximately 2.5% gradually increased the strength of the compacts. They explained this by the effect of “hydrodynamic lubrication of moisture in which it promotes an optimum transmission, utilization of compaction force and the formation of a moisture film around the drug”. However, they found that higher moisture content to above 3.5% w/w caused a decrease in the strength of the tablet. They justified this decrease to be attributed to hydrostatic resistance of the moisture existing in the void gaps, which produced a “force transmission which led to a decrease in the particle-particle contact areas, surface energy and adhesive forces”. Moreover, their results showed that the level of moisture significantly determined

the compressibility of their powder during the consolidation. Nokhodchi et al. 1996, performed another study to investigate the impact of moisture content on the paracetamol consolidation and compaction characteristics. In their study, they particularly investigated the tablet strength. According to their study, they found that increasing the moisture content in the paracetamol powder to about 6% w/w has increased the strength of the compacts; this is because of the moisture plasticizing effect of on the powder. However, higher moisture of up to 8% has reduced the strength of the compact considerably. Wade et al. 2013, studied the impact of moisture on the attributes of hydroxyapatite (HA) compaction. The moisture content used in this study are 2.12, 4.02, 4.56, 4.97 and 5.26%. Compressibility, compatibility and elastic recovery were studied with respect to moisture content. They found that increasing the moisture has increased compressibility of hydroxyapatite compacts and facilitated the reduction in volume. Though, increased moisture content decreased the bonding of HA particles, consequently this led to a reduction in the strength of the tablet. This can be seen in Figure 26, which presents the tensile strength of the tablet as a function of the solid fraction of the tablet at different moisture content. They also found that elastic recovery increased with when moisture content increases, this contributed toward the reduction in the strength of the tablet.

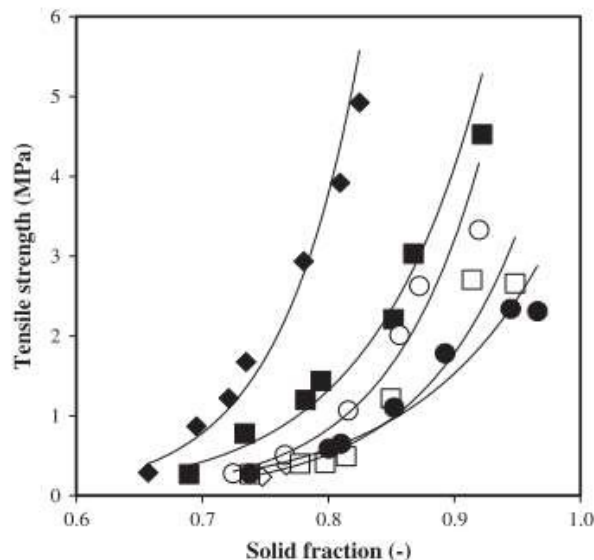


**Figure 26: Strength of tablet as a function of solid fraction of different moisture content; “◆ 2.12% moisture, ■ 4.02% moisture, ○ 4.56% moisture, □ 4.97% moisture, ● 5.26% moisture” (Wade, Martin and Long, 2013).**

Gabbott et al. 2016, performed an experiment to determine the influence of wet granulation process parameters together with the residual moisture content remained after the drying on the quality attributes of granule and tablet. The findings of this study showed that the residual moisture content remained after drying of the granule had a considerable influence on the crushing strength of the tablet. The influence of moisture on the tensile strength of the tablet has been previously reported by Wade, Martin and Long, 2013 and (Takasaki et al., 2016), however, this was not done in combination with granulation parameters and properties of granules. Understanding both the impact of granulation and drying process parameters on the properties of granule and tablet gives a basis for process optimization and scaling process. It was found that the tablet hardness was mainly affected by the moisture content of the granules; in other words, higher granules moisture content resulted in harder tablets with lower tablet porosity. The results indicated that the granules residual moisture content as well as the time of granulation and the interaction between these two parameters are the only reasons behind the significant influence in the tablet hardness. The same influence has been previously reported by Wade et al. 2013, but that was for powders not granules. The influence of moisture is attributed to its plasticizing effect on the granules, which decreases the resistance of particle to compression and improves the deformation of particles. The conclusion from these reviewed papers is that there are many studies performed to determine the impact of moisture content on tablet tensile strength. However, this was for primary powder compressed directly into a tablet without the granulation and drying stages. Nevertheless, this still can be beneficial to be reviewed to have an overall insight about the impact of moisture on the tablet. The project therefore will cover this since the aims to determine the effect of moisture content on the tablet made from the granules dried by fluidized bed at different conditions. This was found to be mostly missing in the literature and it will be therefore investigated.

## **1.4 Conclusion on the Fluidized Bed Drying of Granules**

The drying of moist particles can be of a complex process involving simultaneous, heat and mass transfer, especially under changeable condition. Understanding the heat and mass transfer in the material being dried will enhance the parameters of drying process and therefore product final quality. Despite the good number of the studies conducted to investigate the fluidized bed drying of granules, there are limited research that link the twin-screw granulation with the fluidized bed drying process. In other words, there is a lack of connection between granules properties of twin screw and fluidized bed dryer and subsequent tableting properties. Still, most of the work that has been conducted in the literature utilizing the ConsiGma 25 line has been focusing mainly on the stability of the line and on individual unit separately. The focus of this research project is to link/ connect between the twin-screw granulation parameters and the drying process of the wet granules in the fluidized bed dryer. These two main units (Twin screw granulator and fluidized bed dryer) are highly interconnected since the FB dryer is used to remove the liquid that was used as a binder during the twin-screw granulation stage, hence, alteration in the twin-screw granulation process will directly have an impact on the drying process and final quality attributes of granules and tablets.



## 1.5 Near Infrared Chemical Imaging in Pharmaceutical Industry

This project highlights the use of near infrared (NIR) chemical imaging technique to determine the moisture content within the single granules at different fluidized bed drying times as well the distribution of the water within the surface of the granules. This distribution is important to ensure greater control of the properties of the dried materials and the subsequent tableting step.

### 1.5.1 Introduction to Near Infrared

NIR was discovered in 1800 by Frederick William Herschel, a professional musician and an astronomer. The NIR region was, however, not considered significant until 150 years later (Manley, 2014). Before then, there were analytical techniques, which were favoured over the NIR due to its unambiguous results and explanation of molecular structures (e.g., mid-infrared spectroscopy, MIR). At that time, the principles of the gravimetric method to determine the moisture by oven drying or the chemical methods to determine protein by Kjeldahl were more clearly understood. Since 1949, Karl Norris, have documented the succeeding recovery and development of the NIR technology. Early 1970 was the greatest progression when Phil Williams begins to use NIR spectroscopy to measure the moisture content and protein as a source for wheat trading. It is therefore implemented as a tool in the process analytical technology (PAT) and quality control (QC) as the method of choice in several fields such as agriculture industry, food, pharmaceuticals, petrochemicals, textiles, cosmetics, medical applications and chemicals such as polymers (Manley, 2014a) and (Amigo et al., 2008). In the region of the infrared (NIR), the absorptions are mainly caused by overtones and combinations of vibrations of fundamental molecular from the mid region of NIR between X-H bonds ( $X = O, N, C, S$ ). The near infrared covers a spectral range in the visible region of (800–2500nm) and spectral range of (12821–4000  $\text{cm}^{-1}$ ) in the mid-infrared region (M Blanco et al., 1998) and (Manley, 2014a). There are three different measurement modes at which the near infrared spectra can be obtained, these are transmission (for clean liquids), reflection (for solids, powders, granulate), transflection (for slurries, semi-solids, liquids, films and emulsions). Reflection was the only measurement mode that have been used in this

project and that was conducted on solids samples and therefore a brief summary about reflection is given. The detector measures the light amount that is reflected from the surface of the sample, which have a diffuse and a specular component. The specular component represents the light that is just reflected from the surface of the sample and not absorbed and therefore this component has small or no information about the sample. The diffuse component represents the reflected light after interacting with the sample and this component has an information about the sample materials at several depths and locations in the sample (M Blanco et al., 1998). Thus, the diffuse component is only of interest due to the aforementioned reason and not the specular component. An appropriate pre-processing is often performed on the collected spectra to minimise the specular component (Clarke et al., 2002).

### **1.5.2 Near Infrared Chemical Imaging**

Imaging spectroscopies integrate two well-known methodologies, that is spectroscopy and imaging, to offer a new advantageous tool (Elmasry and Jens Peter Wold, 2008), (Manley, 2014a). It is a comparatively new technique, and its full potential has thus far to be exploited. The spectral information allows the detection and the ability to distinguish amongst several different objects, even though have a similar colour externally. The key benefit is that the spatial distribution of chemical composition in the product can be acquired, not just the bulk composition (Elmasry and Jens Peter Wold, 2008). The development of near infrared chemical imaging (NIR-CI), which combines spectroscopy of the NIR with digital imaging, enables both spatial (localisation) and spectral (identification) information to be obtained simultaneously. This information will be stored as a three-dimensional dataset (3D) or hyperspectral data cube in which the x and y axis represents the pixel or spatial information while z axis represents the wavelength in the spectral measurement (Ravn, Skibsted and Bro, 2008) and (Amigo et al., 2008) and (Amigo, 2010). Figure 27 (a) illustrate a schematic diagram of the hyperspectral data cube unfolding for the approaches of processing data. Before processing the data, it is essential to unfolding the three- dimension (3D) hyperspectral data cube to two-dimensional (2D) data matrix, where each row is a spectrum associated to one of the pixels (see Figure 27 b). The matrix of the two-dimension data is processed and refolded to the three-dimension (3D) hyperspectral data cube by the desired chemometric model (see Figure 27 c) in which

physical or chemical images can be acquired (Figure 27 d). These images give distribution information from the surface of the sample.

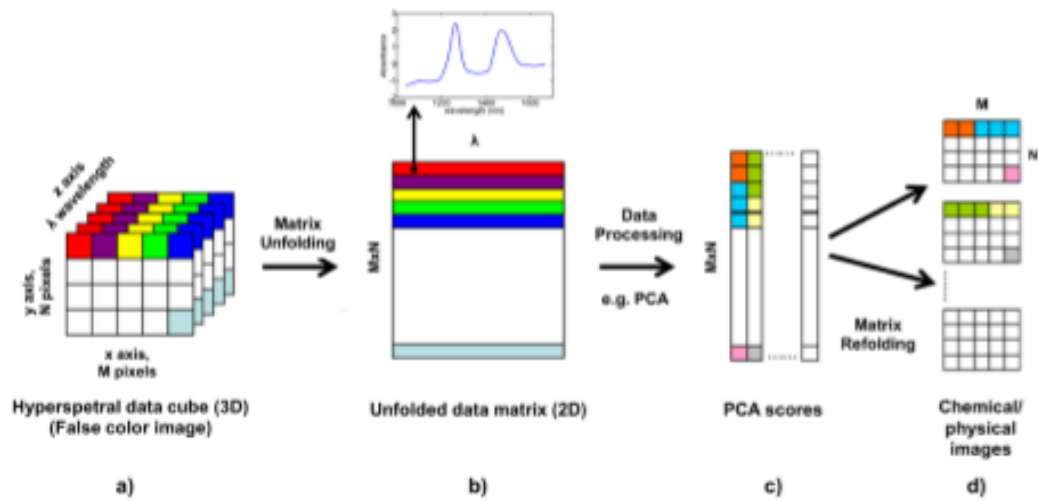


**Figure 27: 3D hyperspectral data cube unfolding for the approaches of processing data.**

Mainly, the near infrared chemical imaging has two types of systems; these are the line mapping system and global imaging system. In this project, the line mapping system was the type used in near infrared chemical imaging and so only this type will be discussed here. This system defines both the area of the sample and the pixel resolutions, in this case, the number of pixels recorded will be determined. For every acquisition, reflectance spectra from a line of 320 pixels are collected. The sample then is moved with a very accurate moving stage where another line of 320 pixels is recorded and hence another reflectance spectra are collected from this line. In this manner, the generated lines of spectra are used to build up spectral information from all the pixels in each line within the defined area of the sample. This would create cube of a hyperspectral data as seen in Figure 29 above. Before the analysis of the multivariate data, the raw reflectance (R) data are transformed into absorbance (A) using equation 1.

$$A = -\log_{10}R = \log_{10}(1/R). \quad (\text{Eq. 1}).$$

On average the length of the path ( $\ell$ ) is assumed to be constant for the measurement of the near infrared (NIR) and by using the law of the Beer Lamberts, a linear relationship between the absorbance (A) and concentration of the analyt (c) can be obtained, equation 2.

$$A = \log_{10}(1/R) = \varepsilon \times \ell \times c \quad (\text{Eq. 2}).$$

where  $\varepsilon$  is the molar absorptivity that is a measure of how powerfully a substance/material can absorb light at a certain wavelength.

### 1.5.2.1 Multivariate Data Analysis

The collected NIR spectra of the measured sample contain both physical and chemical information. So, the desired information (either physical or chemical) can be then extracted using an appropriate pre-processing and multivariate analysis of data. Principal component analysis (PCA) is a statistical procedure that is one of the most qualitative methods applied for the reduction of dimension and recognition of pattern in spectral data sets. Partial Least Squares (PLS) regression is a quantitative method used in analysing multivariate data. Its built and used to determine desired characteristics ( $y$ ) from a measured spectrum ( $x$ ). Partial least square is a regression of two block method depending on estimated latent variables (LV) which requires an  $x$ -block and a  $y$ -data (Wold and Sjostrom, 2001). It is desired to reduce the model complexity, by using as few latent variables as possible. The minimum point in the curve of RMSECV can be used to decide upon the optimum number of latent variables that is good for the partial least square model. Adding too many latent variables will lead to poor performance of the overall model as a result of the noise and over fitting caused by adding more LVs (Wold and Sjostrom, 2001) (Varmuza & Filzmoser 2009). Another way of validating the partial least square model is by performing a validation test where an independent sample with known/ measured  $y$  -values is included in the model. The PLS model will then predict the values of the included sample and a comparison between the predicted and the measured values can be done. The parameters which lead to the lowest root mean square of prediction (RMSEP) is the chosen ones for the partial least square model. The root mean square of prediction (RMSEP) is determined in similar way as the root mean square error of cross validation (RMSECV). The RMSECV require less labour than the test validation even though it tend to suggest adding more latent variables for building the model with optimal results compared to the test validation (Wold and Sjostrom, 2001).

### 1.5.2.2 Studies on Near Infrared Chemical Imaging

The NIR chemical imaging have the potential of describing distribution of components within a sample. It has been and is still being studied increasingly to determine the quality and safety aspects of food and agricultural products. NIR chemical imaging also applied in other fields and research areas include pharmaceuticals, medical archaeology etc. applications. This project will focus on NIR chemical imaging analysis of pharmaceutical materials (determination of moisture content). NIR-CI is therefore a powerful technique for enabling a great deal of information on pharmaceutical samples, and this because NIR spectrum can be measured for every pixel of the image over a wide range of wavelengths (Amigo et al., 2008). It has been applied in a number of different pharmaceuticals fields (e.g., drug release in the dissolution of the tablets (Hernandez et al., 2016), uniformity of contents (Koide et al., 2015), (Ravn, Skibsted and Bro, 2008) or the study of granulation process. (Amigo et al., 2008), (Vercruysse et al., 2014), and (Kumar et al., 2014). Further details can be found in the review conducted recently by (Manley, 2014a). This review covers general aspects of chemical imaging, including the monitoring of pharmaceutical process. A study conducted by (Koide et al., 2015) to analyse the ingredients distribution within the clarithromycin tablets using NIR-CI. Another study by (Elkhider, Chan and Kazarian, 2007) has looked at the impact of moisture content and pressure on the compaction and distribution of components within an ibuprofen and Hydroxypropyl methylcellulose tablet with using Fourier-transform infrared spectroscopy (FTIR). They used this technique to study the distribution of tablet components. Vercruysse et al., 2014, have used NIR chemical imaging to get an understanding of how the granulation liquid (distilled water) is mixed and distributed with  $\alpha$ -Lactose monohydrate 200 M using continuous twin-screw granulation. The study reported that NIR chemical imaging has been demonstrated to be a fast and adequate measurement tool for enabling process visualization and therefore better understanding of a continuous twin-screw granulation system (Vercruysse et al., 2014). Moreover (Ravn et al., 2008) has compared common calibration approaches to study NIR-CI on the pharmaceutical dosage forms. The work focused on using different calibration method to process NIR-CI of tablets made of different powder mixed with API. The methods were compared to see which one would give the right chemical image contrast and

so it was confirmed that partial least square (PLS) was found to be the best calibration method in their work. Christopher et al.,2008, conducted a study to measure the density distribution and tableting force distribution in pharmaceutical tablets by using Near infrared chemical imaging. They examined lactose tablets blended with different percentages of lubrication (Magnesium Stearate) and so they scanned the tablets in three ways; the 1<sup>st</sup> is that the top of the tablet is scanned, the 2<sup>nd</sup> is when the bottom of the tablet is scanned, and the 3<sup>rd</sup> is when the edge of the tablet is scanned (see Figure 28).

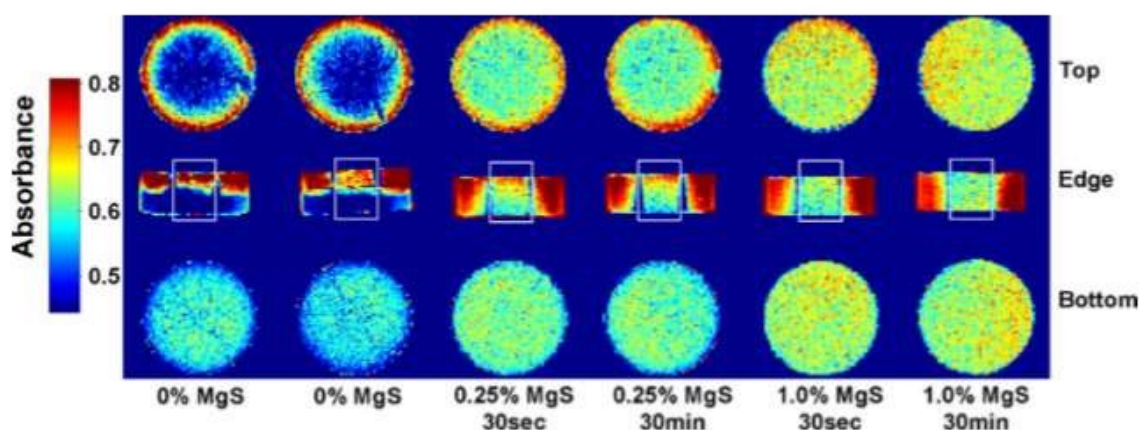


**Figure 28: Absorbance profiles of tablet scanned from top, edge and bottom. The images are displayed in the same scale, based on absorbance at 2120 nm. (Christopher et al.,2008).**

The aim of scanning the edge of the tablet as its positioned vertically was to identify the critical angle at which a high reflectance region occurs since the edge of the tablet is not a flat area, so there are regions out of focus as the round tablet curves away from the horizontal, so this reduced the image quality. The absorbance profile for one of the edges of the tablet is illustrated clearly in Figure 29. Therefore, this study only considered the central region of the edge images for further analysis and excluded the regions that are out of the field of focus as shown in Figure 29.

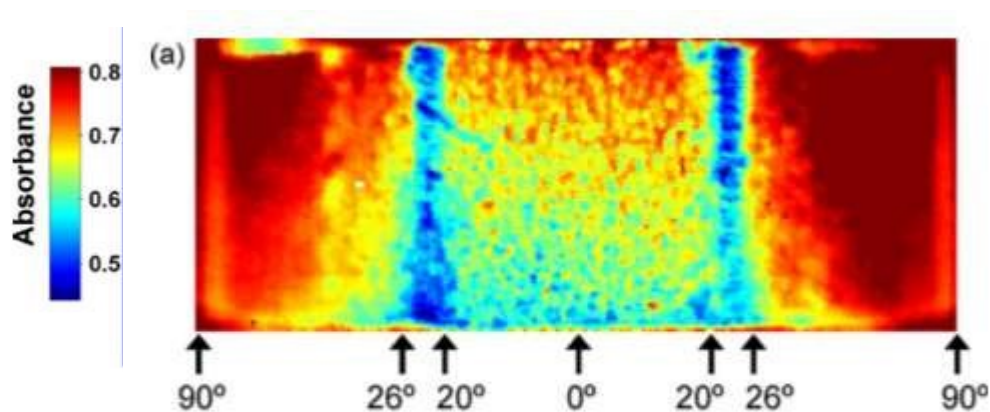


**Figure 29: Profile of absorbance for a lactose tablet edge blended with 0.25% MgS (Christopher et al., 2008).**

Thus, in all of the above-mentioned literatures, huge attention was given to NIR-CI as it is being chemical free, fast, non-destructive and non-invasive technique and not considering that there are some limitations associated with the NIR-CI. In other words, there is a lack of information about the effect of surface roughness (depth of field) of the material being examined with NIR-CI technique on the reliability of the result. This project therefore will attempt to highlight such limitation of NIR-CI technique.

### 1.5.2.2.1 Penetration Depth of NIR-CI

Clarke et al. 2002, used the reflectance NIR microscopy to investigate the penetration depth of the NIR radiation into a sample of 3 mm substrate (Meclizine hydrochloride) which was chosen as a representative for a drug substance with layers of material stacking on top of the substrate as seen in Figure 30. The layer material used in this study was a cellulose (paper), however, this was prepared as a slurry in which applied to the substrate surface thinly. The key finding of this study was that the penetration depth of the NIR into a sample depends on the wavelength of the light, that is the longer the wavelength of the light, the lower the depth of penetration. Moreover, an exponential relationship between the NIR penetration depth of light into the sample and the wavenumber was found. It was also found that the depth of penetration (sample depth contributing to the reflected radiation measured) increased exponentially from  $\mu\text{m}$  109 - 777  $\mu\text{m}$  as the wavelength increases from 1100 to

2500 nm. Another highlight of this work was that an exponential relationship between the absorbance and the paper thickness such that increasing the thickness paper would result in lower penetration. Though, this study has also determined that half of the reflectance spectrum obtained is coming from the top surface of the sample in the range between 25  $\mu\text{m}$  to 180  $\mu\text{m}$  at a spectral range between 1100 to 2500 nm). Similar approach to Clarke et al., 2002 was implemented in this PhD research project to determine the penetration depth of the NIR-CI instrument. This was done by using lactose tablet as the pharmaceutical material and base of a plastic weighing boat in different thickness placed on the top of the tablet to detect for the lactose spectra as the thickness of the weighing boat increases.

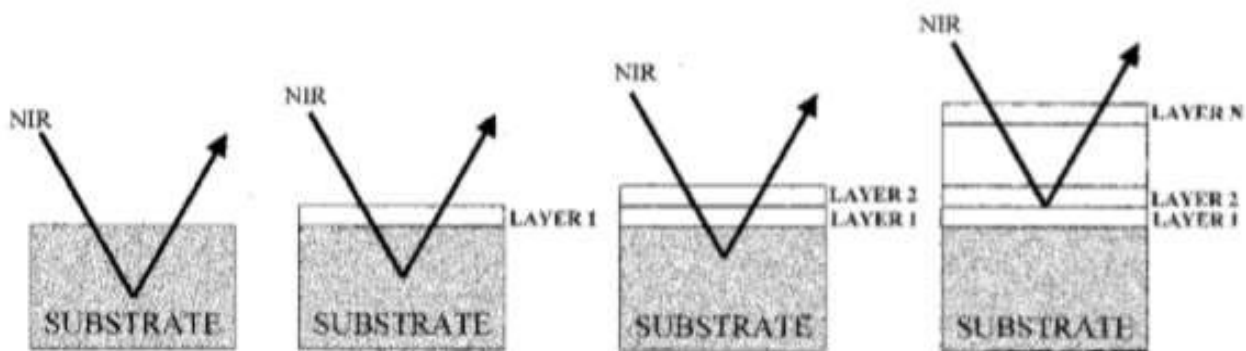


**Figure 30: Schematic illustration of the experimental model (established by (Clarke et al., 2002) to determine the information depth for the pharmaceutical materials (3mm substrate) using reflectance of NIR microscopy.**

Another work conducted by (Huang et al., 2016) to study the depth of penetration of the NIR light (937.5– 1653.7 nm) into five different depths (1-5 mm) of milk powders placed on melamine holder as seen in Figure 31). To investigate the depth of the penetration of NIR light, the five different depths of milk powder were scanned by the NIR hyperspectral imaging separately to detect for the melamine underneath the milk powder as the depth of milk powder increases. Performing this study ended up with establishing a relationship between the near infrared reflectance spectra in the range (937.5– 1653.7 nm) and the penetration depth, this was investigated by means of PLS- discriminant analysis which was used to develop classification models for all samples used. Thus, this study found that the accuracy of the classification model decreased as the milk powder depth increases. Eventually, they concluded that the model of the 2mm milk powder depth was the optimum one due to the accuracies of its classification model which was reported to be higher than 95% for both samples milk and milk-



melamine. Therefore, this study came up with a conclusion that the use of 2mm depth for the milk powder is recommended to detect for any contaminants that could be in the milk powder when using Near infrared hyperspectral imaging.

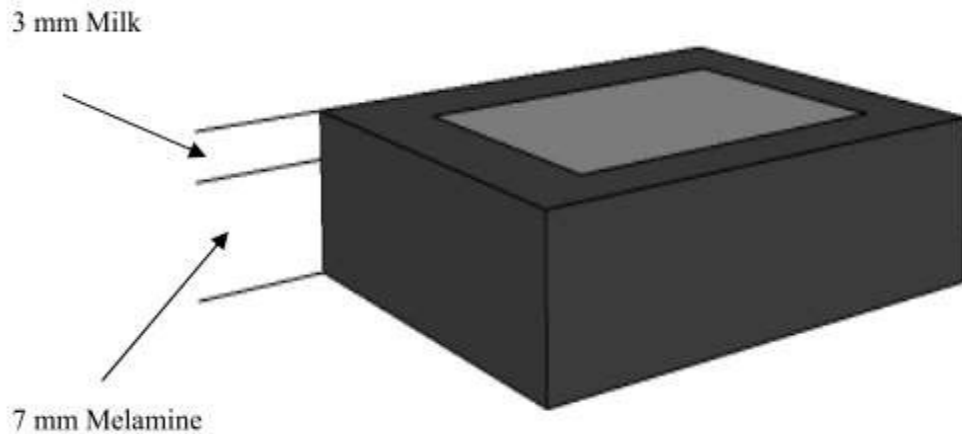


**Figure 31: Illustration of the 7 mm melamine holder with milk powder of 3mm depth placed on the top of it. The area with light grey shows the surface of the sample (30 mm x30 mm) (Huang et al., 2016).**

The previous studies reveal that there are different values of penetration depth of the NIR radiation into the pharmaceutical materials. Clarke et al. 2002, stated in his study that Hammond et al. conducted a work on pharmaceutical powders which had a density of  $0.5 \text{ g cm}^{-3}$  and the result for the penetration depth of the NIR light into these pharmaceutical powders was approximately  $500 \text{ }\mu\text{m}$ . Moreover, in the NIR reflectance probe studies performed by Hammond et al. which were based on lactose monohydrate of bulk density of  $0.575 \text{ g cm}^{-3}$  and mass of  $4 \text{ mg}$  were found to shows a penetration depth of no greater than  $500 \text{ }\mu\text{m}$ . Another study performed by Berntsson et al. 1998 using reflectance NIR spectroscopy, discussed the effective size of samples and penetration depth issues associated with pharmaceutical materials. Their study involved the use of film coated pellets with different thicknesses of powder as well as microcrystalline cellulose (MCC) samples. Using MCC, the effective size of the sample was determined to be  $20 \text{ mg/cm}^2$  and the depth of penetration was determined to be  $670 \text{ }\mu\text{m}$  at  $1500 \text{ nm}$ . However, using the film coated pellets, the effective size of the sample was determined to be about  $70 \text{ mg/cm}^2$  and the depth of penetration was found to be  $1\text{mm}$  at a wavelength of above  $1500 \text{ nm}$ . Thus, the penetration depth of the NIR radiation into the sample has

been discussed by number of authors in literature and to date, the studies have shown variation in the actual penetration depth value. These studies have also found that the penetration depth of the near infrared radiation depends on several factors such as light wavelength, density and size of particle and absorptivity of the examined materials. Therefore, the literature review shows that there is no decided value for the penetration depth in the Near infrared spectroscopy. Hence, it is crucial to know the penetration depth of the light prior to performing the main experiment using the NIR spectroscopy, so for example to get an insight if the light is penetrating just immediate particle like the 1<sup>st</sup> 10 µm layer or it is penetrating a number of layers underneath the outside surface like 200 µm. Therefore, the first step of this project is to investigate the penetration depth of the NIR-CI.

#### **1.5.2.2.2 Near Infrared Chemical Imaging in Drying**

NIR spectroscopy technique has been used for monitoring and determining the moisture content of pharmaceutical products during the processes of fluid bed drying and spray drying. Fonteyne et al. (2014) have used NIR spectroscopy in a fluid bed drying process to monitor and predict the end of drying process and moisture content of lactose granules. Their work focused on the validation of an inline NIR to quantify the moisture content in the six-segmented fluid bed dryer of a continuous from powder-to-tablet manufacturing line using ConsiGma 25 system. Most of the work in the literature based upon theoretical work to explain the drying mechanism of wet granules, however, this project describes the mechanism of drying of wet granules with the aid of supportive visualization chemical images. Solids drying process is generally subdivided into two main stages according to the rates of drying. These stages are the constant rate period and the falling rate period (Poutiainen et al., 2012). The first drying stage involves the evaporation of liquid from the surface of the wet granule, whereas the second drying stage involves the evaporation of liquid from the inside of the granule. The final sensible heating involves no evaporation in which a dry granule is obtained (Mezhericher, 2014). Quantitative Chemical Imaging will enable visualization of the different drying stages taking place. Water contents distribution is a key quality parameter of pharmaceutical granules. A previous work was conducted by (Mortier et al., 2012), in which a model for describing the drying behaviour of

single pharmaceutical granule was established. In their work, the model was based on the model described by (Mezhericher et al., 2007), which considered the drying of a single droplet in a spray dryer. However, the work was missing the distribution of the moisture content within the single granules dried by fluidized bed. Therefore, this project highlights the development of a robust quantitative technique to quantify and track the distribution and movement of liquid during drying process at single granular level as a function of time.

### **1.5.3 Conclusion of the Literature Review on NIR-CI**

Despite the fact that the NIR spectroscopy is a secondary method implying the requirement for the development of a calibration model (reference values), it is now deemed to be equal with the other significant analytical technologies. In contrast to other analytical methods such as Gas and high-performance liquid chromatography and conventional chemical methods (Kjeldahl and Soxhlet), NIR is fast, chemical free, easy to use once calibrations model have been established and it is non-destructive. Most of the work that has been conducted in the literature utilizing the NIR chemical imaging has been mainly focusing on proving that the NIR-CI is fast, chemical free, easy to use and is non-destructive technique. Therefore, this project attempted to highlight the use of NIR-CI as a technique in determination of moisture content during drying of pharmaceutical granules with tracking the distribution of liquid across the radial distance of the single FB-dried granules. Thus, a tool to predict the drying stages of granules at any point of time. Even though the NIR accuracy rely on the precision and accuracy of the calibration model, the reproducibility of the NIR predictions is very high.

## Aim of the Research

---

To date, there is no well-established connection between twin-screw granulation and fluidized bed drying process in this research field (including small laboratory scale TSG equipment and industrial scale pilot plant i.e., ConsiGma 25). Understanding how parameters in twin screw have subsequent effect on the drying process of granules in fluidized bed and on the final product will therefore contribute to bridging this knowledge gap.

**This research project therefore is aiming to investigate the following points:**

- Investigate the effect of varying the formulation parameters in the twin-screw granulator (i.e., liquid to solid ratio and binder viscosity) on the granule's formation and hence on the subsequent transformation of those granules during fluidized bed drying process.
- Investigate the effect of changing the process parameter (i.e., screw configuration) on the attributes of granules during twin screw granulation and consequently on the consecutive fluidized bed drying process of those granules.
- Study the formation and drying behaviour of granules and the subsequent production of tablets produced at different screw configurations and lactose powder of different primary particle size in a unique and first of its kind industrial-scale pilot plant ConsiGma 25 (powder to tablet line, GEA Pharma Systems). The system uses an inline real-time near infrared (NIR) probe to measure the moisture content of granules and inbuilt temperature sensors.
- Developing a novel quantitative analytical method by utilizing NIR-CI to determine the moisture content and quantify/track the distribution and movement of liquid at single granular level as a function of fluidized bed drying time. Obtaining the

moisture distribution across the radial distance of single granules can potentially contribute to the understanding and hence optimization and better control of the resultant granule attributes and downstream process post drying.

## Thesis Overview

This thesis could be outlined as in the following chapters:

**Chapter 1:** Presents the introduction, the literature review and finally the aims of the research project. This includes the literature which covers different subjects including variables (air temperature and air velocity) affecting drying process in conventional batch fluidized bed dryer and the main fluidized bed drying challenges. Furthermore, it also includes about the use of continuous pharmaceutical manufacturing (Consigma 25 powder to tablet line), paying more attention to the drying process in the six segmented fluidized bed dryers. Finally, this chapter presents the literature about using near infrared chemical imaging in drying.

**Chapter 2:** Presents the materials and Methods used in this project.

**Chapter 3:** Presents and discusses the results obtained from investigating the effect of batch fluidized drying process parameters on granules and tablet properties. This covers the powder behaviour before granulation, twin screw granulation (size distribution, moisture content and drying of granules in humidity chamber), and the effect of fluidized bed drying on granules size, moisture content, sphericity and porosity and lastly it includes the effect of moisture content on tablet tensile strength.

**Chapter 4:** Presents and discusses the results obtained from linking the effect of twin-screw formulation parameters on the granules attributes and consequently on the fluidized bed drying. This covers the effect of changing liquid to solid ratio and the viscosity of the liquid binder on granules at the twin-screw granulation (moisture content, size distribution, porosity, surface topology) and fluidized bed drying of granules (moisture content and size distribution).

**Chapter 5:** Presents and discusses the results obtained from determining the impact of changing the screw configurations on the granules attributes (moisture content, size distribution, porosity, surface topology) and consequently on the fluidized bed drying (moisture content, size distribution, porosity, surface topology).

**Chapter 6 and 7:** These chapters present and discuss the use of continuous powder to tablet line (Consigna 25, DiPP) to determine the effect of varying the screw configuration and primary lactose powder particle size on the granule's formation, drying and tableability. The system uses an inline-real time near infrared (NIR) probe to measure the moisture content of granules as well as uses inbuilt temperature sensors to measure the temperature profile inside the dryer cell.

**Chapter 8:** Presents an investigation of the penetration depth of the NIR radiation light into a material and the depth of field of the NIR-CI equipment. It also discusses the results obtained from using NIR chemical imaging as a technique to determine the moisture content and the spatial distribution of moisture content in single FB- dried granules as a function of drying time.

**Chapter 9:** Presents the main conclusion, future work, references and appendix.

## 2.0 Materials and Methods

---

### 2.1 Materials and Method used in the lab- scale TSG and FBD

#### 2.1.1 $\alpha$ - Lactose Monohydrate

The material used in this project is  $\alpha$ - lactose monohydrate (150M Lactopure®, FrieslandCampina Domo, Netherland). Overall lactose is a disaccharide, which has the molecular formula of  $C_{12}H_{22}O_{11}$ . Its naturally exists in two solid forms:  $\alpha$ - lactose and  $\beta$ -lactose anomer. Figure 32 shows the structure of the  $\alpha$ - Lactose monohydrate.  $\alpha$ - Lactose monohydrate consists of two-sugar galactose and glucose. Lactose is considered the main source of carbohydrate in milk. The lactopure lactose is produced from the nutrition of infant -quality demineralized cheese whey with a slightly yellowish colour. The yellowish colour is caused by the riboflavin (vitamin B<sub>2</sub>), which is naturally present in it.

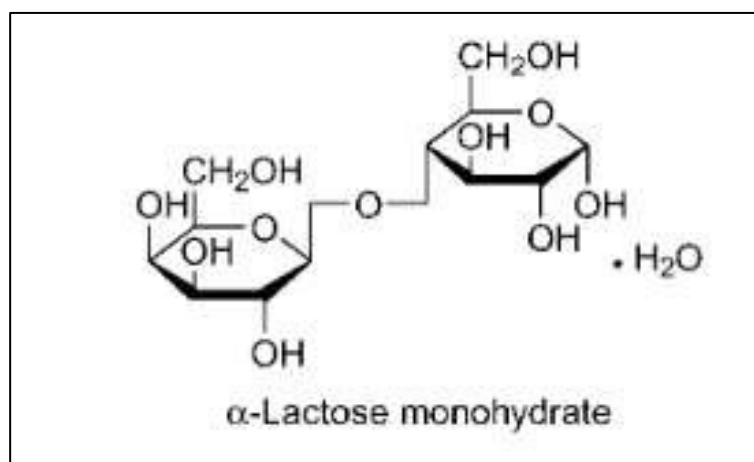


**Figure 32: Structure formula of  $\alpha$ - Lactose Monohydrate (Rowe et al. 2006).**

Lactose is widely used in industries such as food, pharmaceuticals, confectionary. In the industry of pharmaceuticals, lactose is used as a diluent, filler and binder in tablet production (Rowe et al. 2006). Lactose is a soluble in water material. There are some physicals properties, which are very important to be studied about this material such as the moisture stability, sorption and hygroscopicity. The best way to study these properties is by determining the moisture sorption isotherm of this material. Figure 33 presents curve of for crystalline  $\alpha$ - lactose monohydrate sorption isotherm at different temperatures



(12 to 40°C). It explains the relationship between the water activity of the product and the moisture content in percentage. It can be clearly seen that  $\alpha$ - lactose monohydrate powder adsorbs tiny amounts of moisture at small water activity between 0–0.85 for the temperature range studied (12–40°C), and therefore this material has a very low attraction to humid air at the low water activity values (0 to 0.85). However, above the point 0.85 of water activity, the lactose powder starts to dissolve. The moisture content increases exponentially over 0.85 and reaches asymptote at water activity of 1 (Bronlund and Paterson, 2004).

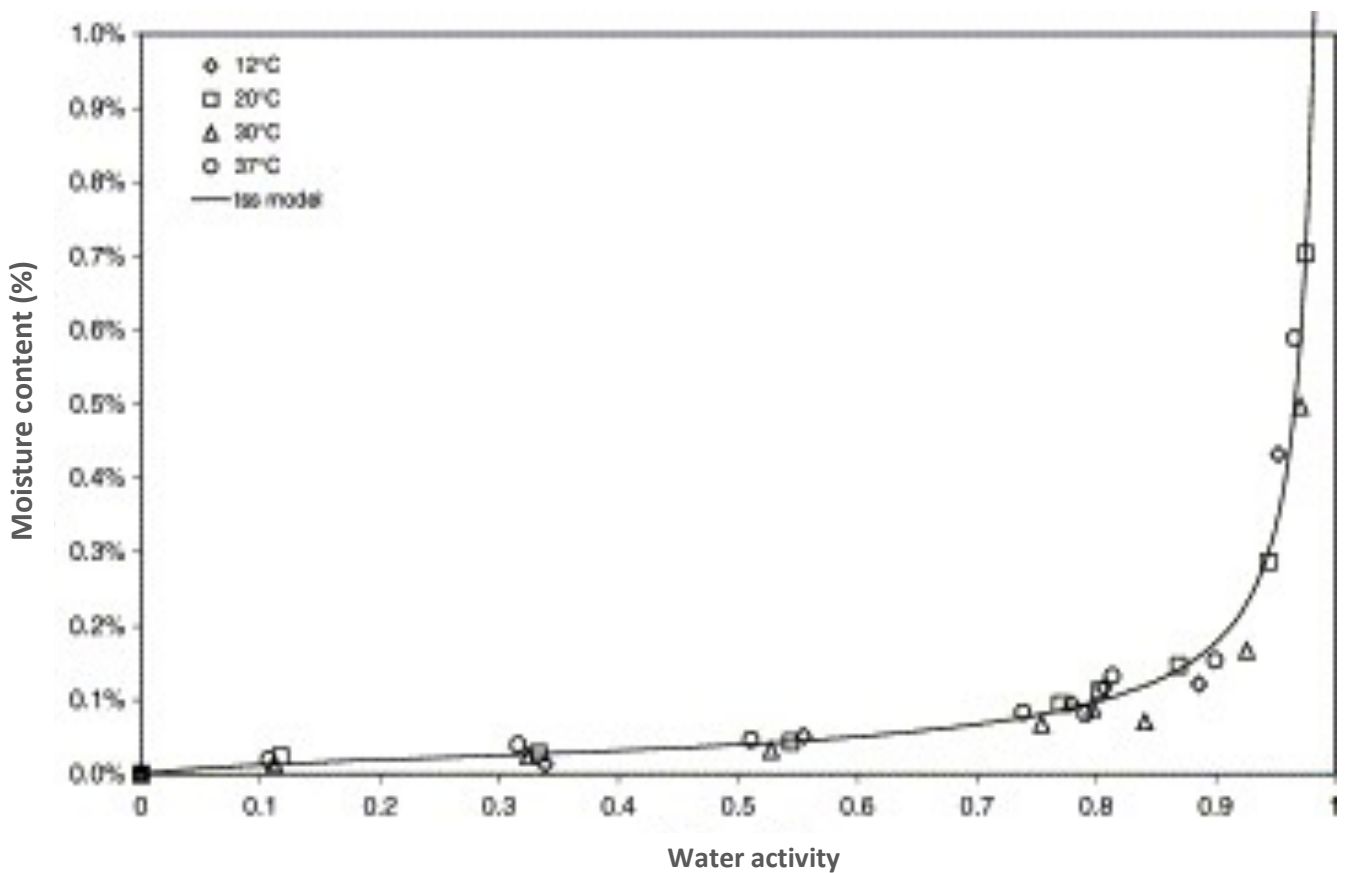


**Figure 33: Sorption isotherm curve of crystalline  $\alpha$ - lactose monohydrate at different temperatures (Bronlund and Paterson, 2004).**

### 2.1.1.1 Lactose Powder Characterization

The lactose powder material was subjected to some key characterizations such as primary particle size, morphology, flowability, and thermal profile measurement.

### 2.1.1.2 Particle Size Distribution

The measurement of lactose primary particle size distribution (PSD) in this study was measured using Camsizer XT (Retsch Technology GmbH, Germany). The Camsizer XT analyzes the particles shadow projections by using dynamic image technique. This technique is able to detect particles size between the ranges of 1  $\mu\text{m}$  to 3 mm. Figure 34 shows the lactose particle size distribution in volume basis.

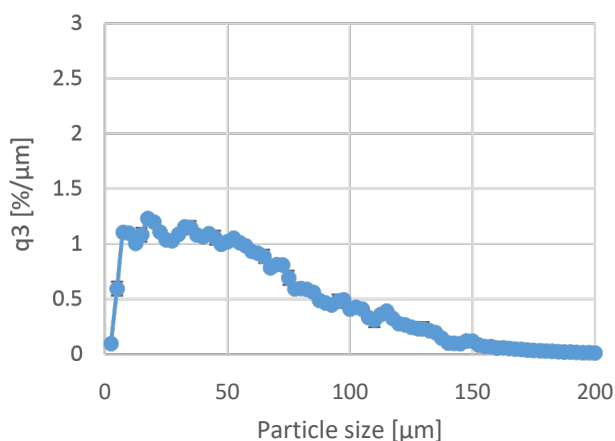


**Figure 34: Volume based particle size distribution of lactose primary powder.**

The particle size parameters  $d_{10}$ ,  $d_{50}$  and  $d_{90}$  of this lactose powder measured to be 12.8, 50 and 111.9  $\mu\text{m}$  respectively.

### 2.1.1.3 Powder Morphology

The powder shape and surface were examined using scanning electron microscopy (SEM). The lactose particles were nonconductive, hence, coated (for 36 seconds) with thin layer of gold using coating machine (Leica EM ACE200, Leica Microsystems, UK). Figure 35 shows the particle morphology of lactose monohydrate using SEM (JEOL IT100, JEOL, Japan). It can be seen that lactose primary particles tend to be taumahauk in shape.

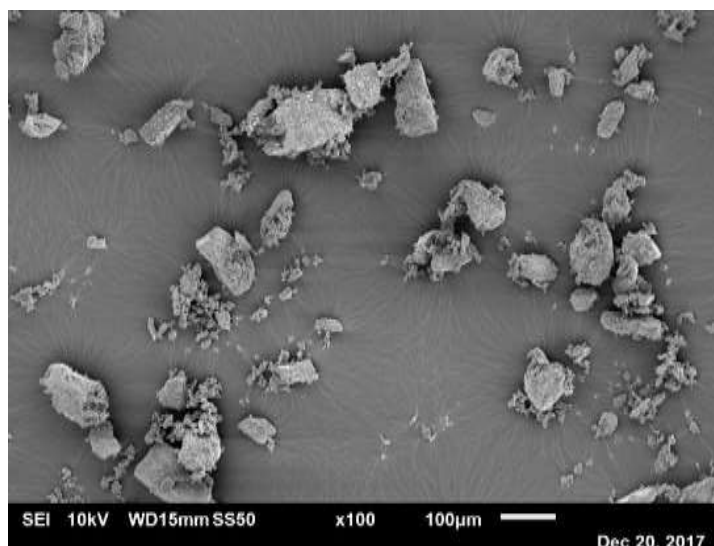


**Figure 35: SEM of the primary particles of lactose monohydrates (150M lactopure).**

#### **2.1.1.4 Flowability Test**

The flow function coefficient (ffc) was measured by the ring shear tester RST-XS (Dietmar Schulze, Germany). The flow function coefficient for this material was found to be 3.9 with error of  $\pm 0.20$ . The powder is considered free flowing due to its FCC value.

#### **2.1.1.5 Differential Scanning Calorimetry (DSC)**

The thermal profile of lactopure lactose monohydrate was determined by differential scanning calorimetry (DSC, METTLER TOLEDO, Switzerland) using 7.7 mg of sample in an aluminium pan and a heated at a rate of 10°C per minutes. The purpose of this analysis was to check the stability of this material to drying temperature when dry in fluidized bed and to see if the material decomposes or deteriorates, as a result of the high temperature applied in FB, also to confirm the nature and impurities of this material (lactose 150M). Differential scanning calorimetry is the most commonly thermal technique used, which gives a quick and easy way to obtain information about material. It is used to measure the changes in energy that occurred as the sample is heated up, cooled down or isothermally held, as well as temperature at which these changes could quantitatively occur. The obtained DSC thermal curve for  $\alpha$ -lactose monohydrate is shown in Figure 36. The 1<sup>st</sup> peak of the curve represents water of crystalline (150°C) and confirms that this lactose is  $\alpha$ -monohydrates. This is

followed by the melting of lactose near 220°C, as seen in the 2<sup>nd</sup> peak of the curve. Generally, lactose has no significant tendency to react with the drug or with the formulation components. Crystalline lactose has a low hygroscopicity and this is supporting its virtual chemical inertness. The water of crystallization in  $\alpha$ - lactose monohydrate is gradually lost at a temperature above 100°C. At a temperature of about 150°C the loss of this water is completed. This loss of water is accompanied by a change in the lactose crystalline structure and therefore the lactose monohydrates changed to become anhydrous. Heating the lactose further to higher temperatures causes decomposition in the lactose this what so called pyrolysis process. The products of the primary reactions in pyrolysis tend to polymerize producing black and brown coloured macromolecules and consequently continuing heating lactose becomes black in colour

(Gombás et al., 2002).

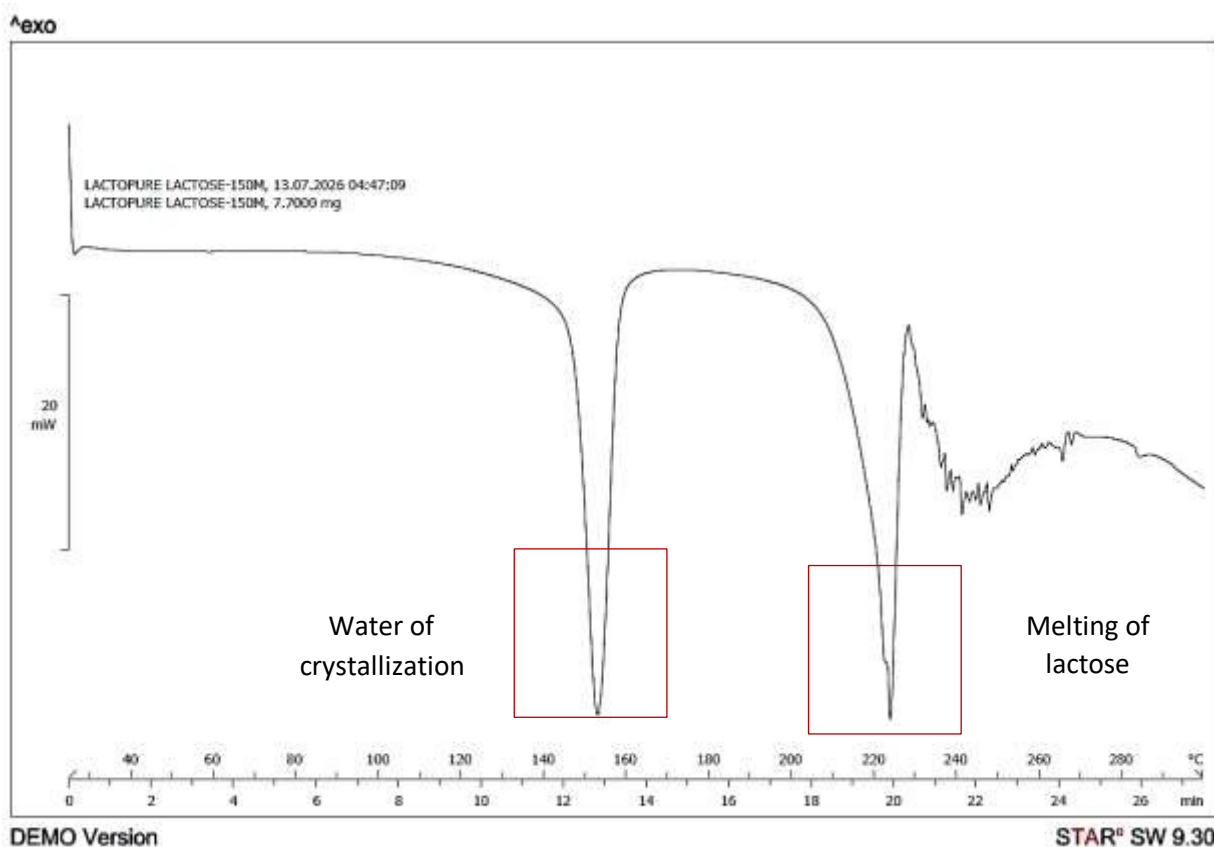


**Figure 36: Thermal DSC curve for  $\alpha$ - lactose monohydrate powder in which the 1<sup>st</sup> peak of the curve represents water of crystalline (150°C) and confirms that this lactose is  $\alpha$ -monohydrates, and the 2<sup>nd</sup> peak represents the melting of lactose (220°C).**

### 2.1.1.6 Powder Humidity Conditioning

Before each experiment, the lactose powder was conditioned in a humidity chamber (Binder KMF 240 climatic chamber, Binder, UK) for approximately 3 days at a relative humidity of 40% and a temperature of 20°C. This was to eliminate the difference in the temperature and humidity of primary powder.

### 2.1.2 Hydroxypropyl Cellulose (binder)

Hydroxypropylcellulose (HPC) is a derivative of cellulose ether in which some of the hydroxyl groups on the backbone of the cellulose have been hydroxypropylated. Figure 37 shows the structure formula of hydroxypropyl cellulose. Hydroxypropylcellulose is a white to slightly- coloured, odourless and tasteless powder. It is made by reacting propylene oxide with alkali cellulose at high pressure and temperature to produce a highly substituted cellulose ether. HPC considered being more plastic and impartially hydrophobic when compared to other cellulose ethers that are water-soluble. This is due to its high hydroxypropylation level, which is about 70%. HPC is fully soluble in both water and organic solvents such as acetone, ethanol, methanol and isopropyl alcohol. Moreover, HPC solubility in water depends on temperature.

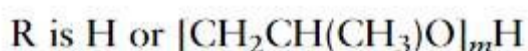
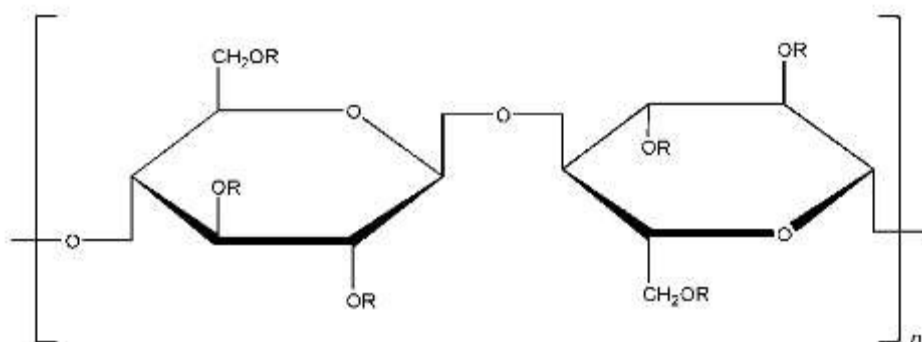
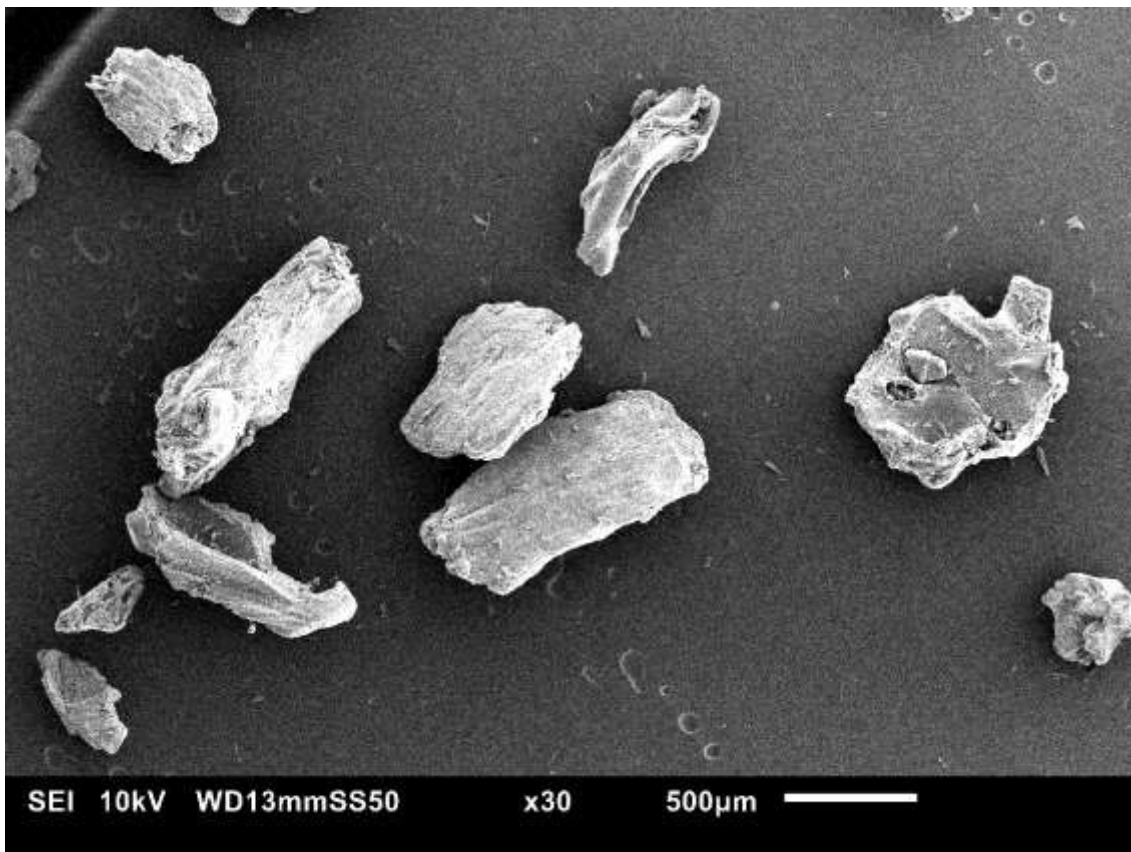


Figure 37: Structure formula of Hydroxypropyl Cellulose (Rowe, Sheskey and Owen, 2006).

Figure 38 shows the scanning electron microscopy of the HPC particles. From this figure, it can be seen that the HPC particles tend to be more irregular and elongated in shape. Overall, HPC can be used as a coating agent; tablet binder; thickening agent and viscosity-increasing agent. In the pharmaceutical industry, HPC is commonly used in oral and topical pharmaceutical formulations. HPC in oral products is mainly used in tableting as a binder, film coating and controlled release matrix. HPC concentrations in the range of 2-6% w/w may be used as a binder in either wet or dry granulation, direct processes of tablet compression. HPC concentrations in the range of 15-35% w/w can be used to produce tablets with an extended drug release. The drug release rate increases as the viscosity of HPC decreases (Rowe et al. 2006).



**Figure 38: Scanning electron microscopy of the Hydroxypropyl Cellulose (HPC) particles.**

## **2.2 Twin screw Granulation and Granules Production**

### **2.2.1 Liquid Binder Preparation**

There are only two liquid binders used in this project; these are distilled water and HPC of different concentrations (2%, 5%, 10% and 15%). For the experiments conducted with distilled water as a liquid binder, no preparation was needed apart from preparing a pump calibration for the distilled water. However, for the experiments conducted with HPC being the liquid binder, a preparation of this binder was needed. The liquid HPC binder was prepared at the laboratory by dissolving HPC powder of a known amount (depending on the desired concentrations) in hot water slowly at a temperature of 60°C with continuous stirring to avoid formation of lumps. In this project, HPC was used as a liquid binder in one of the project chapters and that's was to determine its different viscosity impact on the granule's properties in twin screw and consequently on the drying process. Therefore, solutions of different HPC concentration (2%, 5%, 10%, and 15%) were made as described above. Having made the HPC solutions, their dynamic viscosities were measured with a rheometer (Kinexus, Malvern Instruments, UK). This was using a cone and plate geometry of 1°/50mm with a shear rate and a temperature of 1 s<sup>-1</sup> and 25°C respectively.

#### **2.2.1.1 Peristaltic Pump Calibration**

A pump calibration for the two liquid binders (distilled water and HPC solutions) before the actual twin screw granulation experiment was done. A peristaltic pump (Watson Marlow, UK) was used to pump liquid binder into the twin-screw system. Therefore, the pump was calibrated by measuring the liquid flow rate in grams per minutes at step of one rpm. A measuring cylinder was used to collect the liquid binder conveyed through the tube for one minute and then weighed in a gram unit scale. Figure 39 shows the pump calibration for water as a binder. So, for example, interpolation between two points will be needed if the pump rotator speed has to be changed. Similar procedures were done with the HPC liquid binder calibration and Figure 40 shows the pump calibration curve for HPC liquid binder.

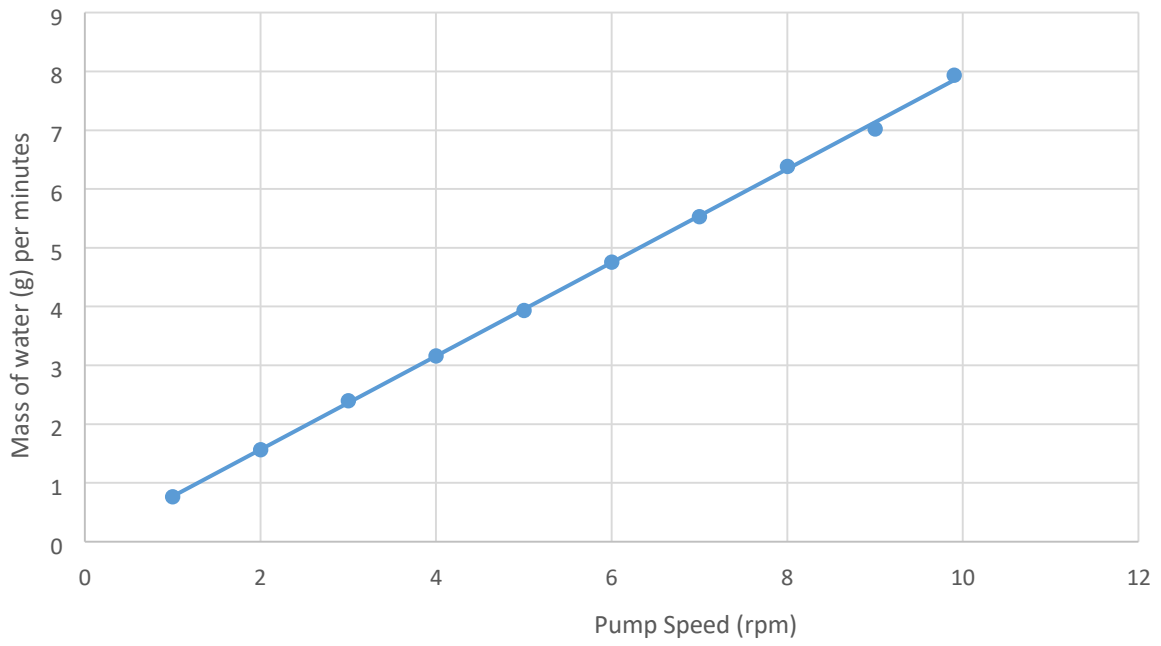


**Figure 39: Pump calibration for water liquid binder**

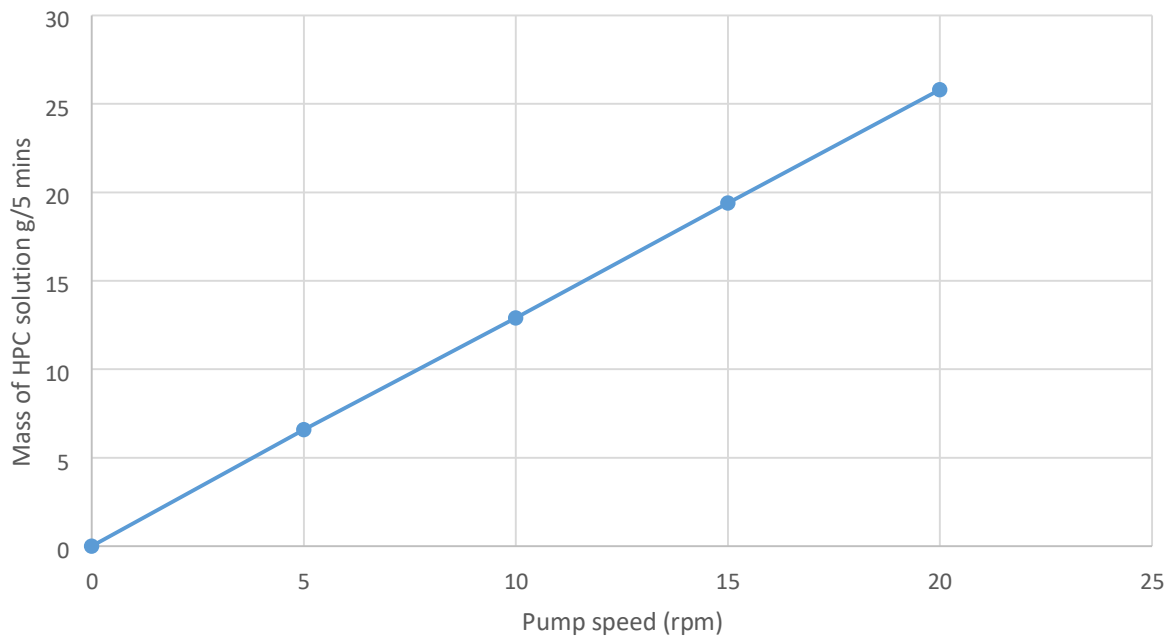


**Figure 40: Pump calibration for HPC liquid binder.**



## 2.2.2 Granulation Equipment

### 2.2.2.1 Twin Screw Granulator

Twin screw granulator (Euro lab16 TSG, (D/L of 25/1), Prism, Thermo Fisher Scientific, Karlsruhe, Germany) with co-rotating screws was used to produce the granules in this project. Figure 41 shows a photograph diagram of the twin-screw granulator labelling all its components. The twin-screw granulator contains the feeding hopper, feeding funnel, liquid nozzle, barrel that contains the two screws and cooling system as seen in Figure 41. The powder is fed into the granulator using gravimetric, loss-in-weight twin screw powder feeder (K-PH-CL- 24-KT20, K-Tron Soder, Niederlenz, Switzerland). The granulation liquid was injected into the granulator using a peristaltic pump (101U, Watson Marlow, Cornwall, UK). The barrel of the extruder was cooled, and the temperature adjusted to 25 °C.

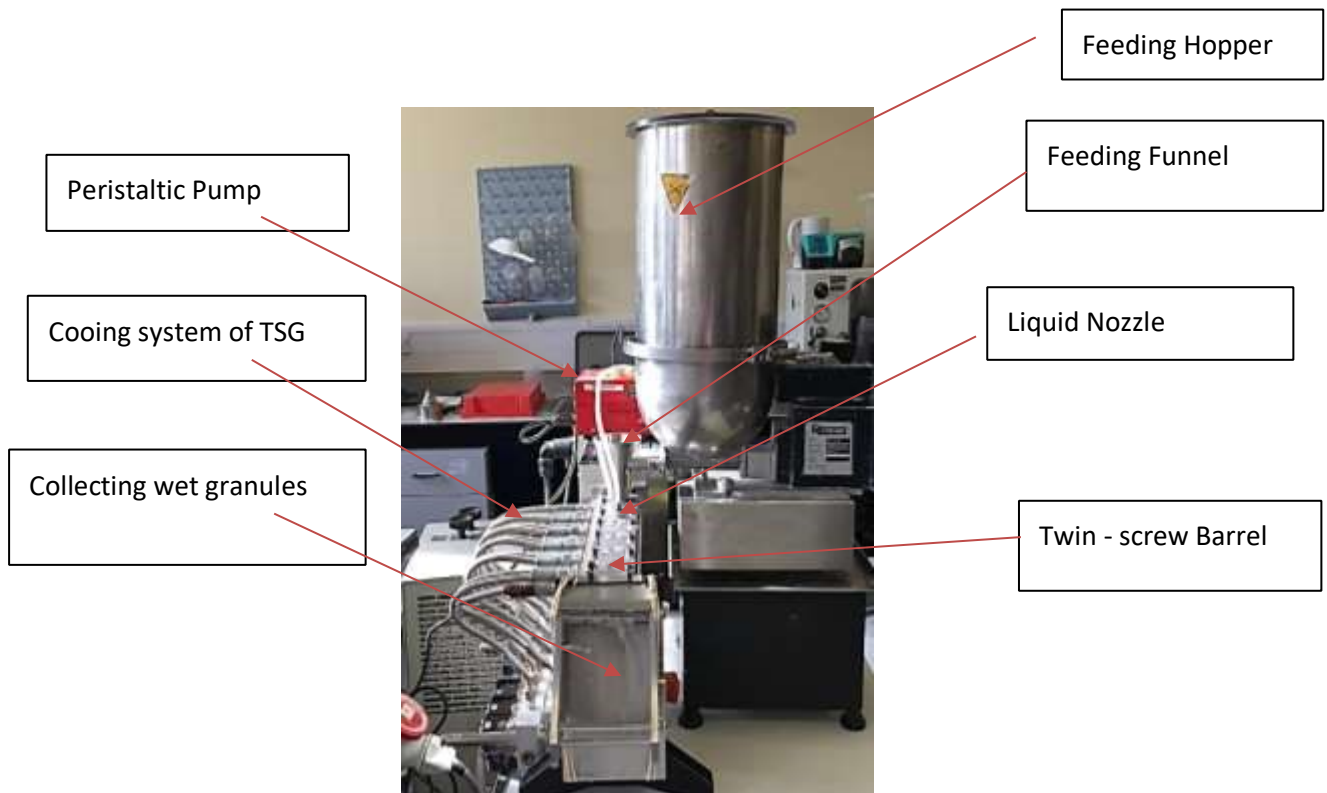


**Figure 41: Image of the twin-screw granulator.**

### 2.2.3 Granules Production in TSG

As a part of acclimatizing with the equipment and process flow, preliminary experiments on twin screw granulation have been carried out in order to determine the effects of the rate of powder feed, liquid to solid ratio and speed of the screw on the granules size distribution and moisture content (loss on drying method using oven and moisture analyser). The granulation conditions that were used in the twin-screw granulation are powder feed rate of 2 kg/h, L/S of 0.1, screw speed of 250 rpm and the temperature of the barrel was kept at a 25°C. These conditions were kept fixed throughout all the experiments. However, for some chapters, some formulation and process parameters were varied to investigate their effect on the granulation and consequently on the drying. In this case, the conditions used will be explained in each chapter and otherwise some chapter uses these fixed conditions. The obtained wet granule batches (500g batch size) were collected starting after 60 seconds, when steady-state conditions were reached. The granulation was carried out using full length of the granulator with a screw configuration that involves both conveying and kneading elements. Figure 42 illustrate the screw configuration used in this chapter. The screw configuration used in this work was 16 kneading elements in each screw, which makes a total of 32 kneading elements for both screws and 2 long pitch-conveying elements with the remaining short pitch conveying elements.

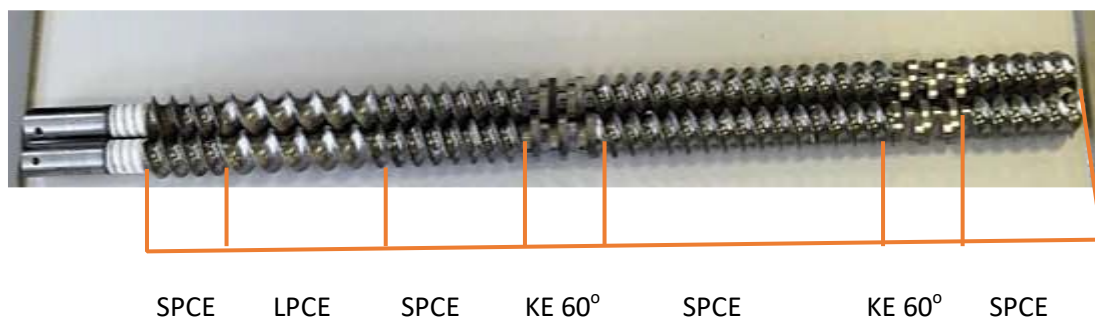





**Figure 42: Image of the Screw configuration used in this in this project (16 KE in each screw).**

Table 2 illustrates a brief description of the screw element types used in the twin-screw granulation process, these are the long pitch conveying element (LPCE), the short pitch conveying element (SPCE) and the kneading elements. The twin-screw granulator was then turned on and set to the aforementioned conditioned. To start collecting the granules, the temperature has to stabilize at 25°C

first, and a metal tray was used to collect the wet granules. The granules obtained from the TSG were then immediately transferred to the FB- for drying.

**Table 2:** Type of Screw elements used in the twin-screw granulation

Type 1 <b>Long Pitch Conveying Element (LPCE)</b>	Type 2 <b>Short Pitch Conveying Element (SPCE)</b>	Type 3 <b>Kneading Disc (60° Pitch)</b>
		
$L=2D$	$L=D$	$L=D/4$

## 2.3 Drying Equipment

### 2.3.1 Fluidized Bed Dryer

A vertical Fluidized bed (Glatt WSG-3 AG Schweiz, Germany) was used to dry the granules produced by the twin-screw granulator. This fluidized bed comprises of three sections as illustrated in the photograph diagram in Figure 43; these are, the bottom conical section (lower bowl) which is the section at which wet granules are placed at, the middle cylindrical sections and the upper cylindrical conical section. Figure 44 shows a schematic diagram of the fluidized bed dryer used with dimensions.

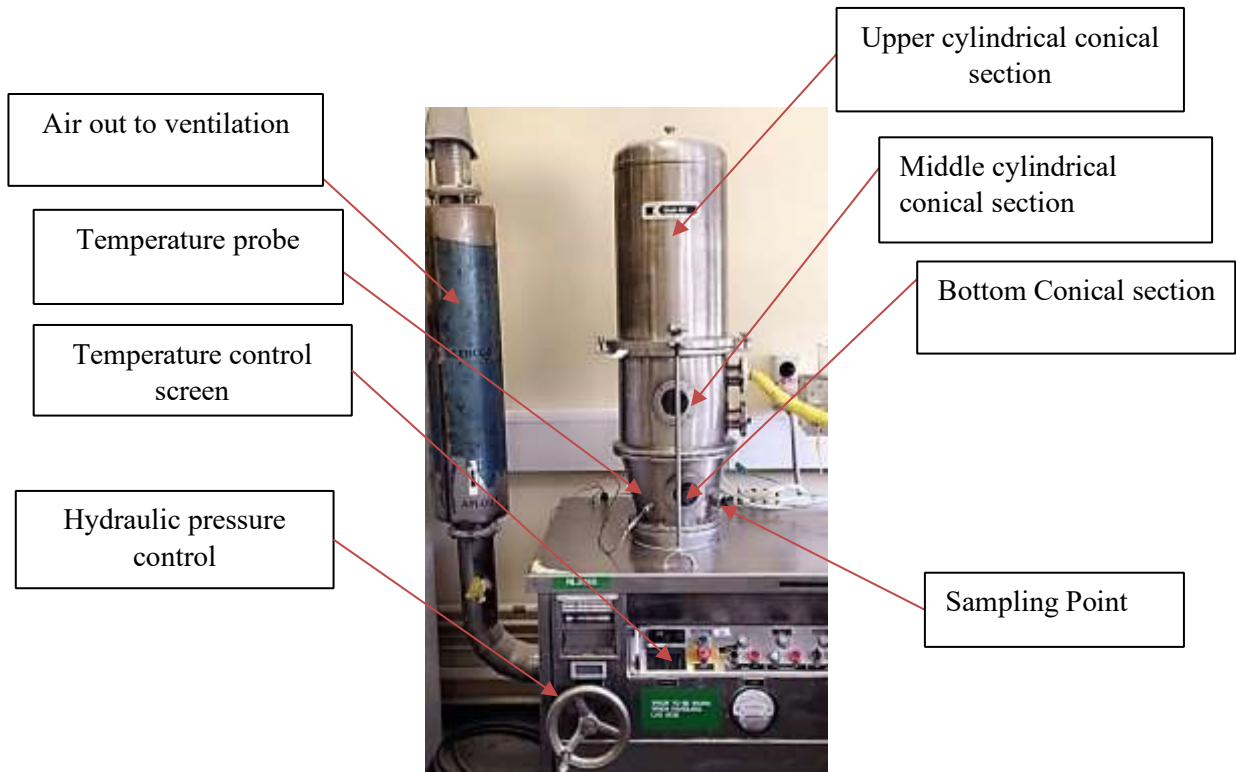


**Figure 43: A photograph diagram of the fluidized bed used for drying of the granules.**

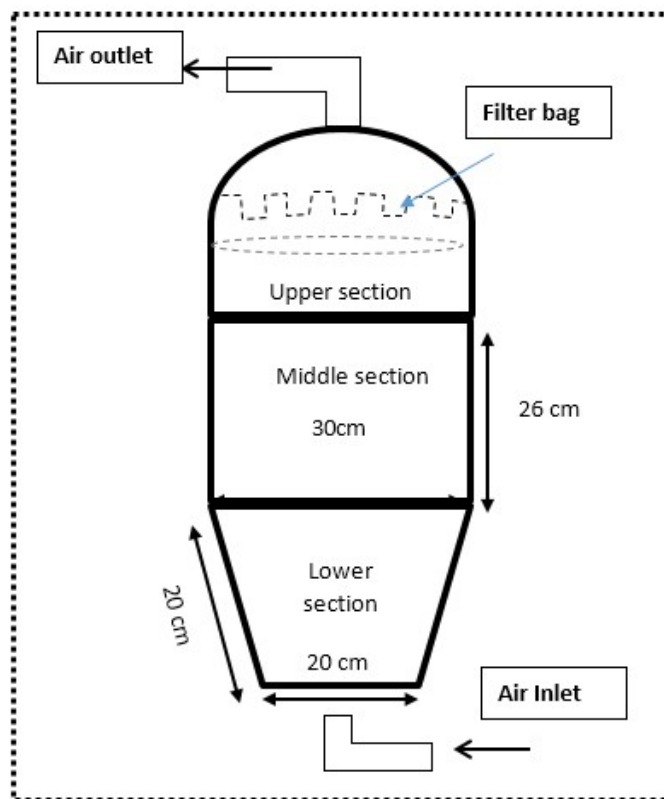


**Figure 44: Schematic diagram of the Fluidized bed dryer with dimensions.**

### **2.3.2 Fluidized Bed Drying of Granules**

Post granulation, the wet granules from TSG were subjected to the fluidized bed drying. Approximately 500 g of wet lactose granules (collected in a tray from TSG) and then placed in the bottom conical section. The granules were dried at different velocities of air (2, 2.6 and 3.4 m/s) and temperatures of 25, 50 and 75°C. When investigating the process and formulation parameters in the twin-screw granulation, the fluidized bed conditions were kept fixed at an air temperature of 50°C and air velocity of 2m/s. Air velocity measurement was performed using an air velocity meter (TSI Model 9545/9545- A, USA). The fluidized bed was heated up for 30 minutes before starting the drying experiment; this is to allow the heat distribution in the equipment and to obtain a stable temperature. A representative sample of 10 g at different drying time was taken by opening the fluidized bed. The granules moisture content was then measured for each sample as explained in product characterization section later in this chapter

### **2.3.3 Tablet Production**

The universal testing machine (Instron 3367, Germany) was used to compress the dried granules into tablets. The dried granules were made at different fluidized bed process conditions such as air temperatures and air velocities. The die diameter used to make the tablet throughout all experiment was 12 mm and a height of 13.9 mm. An electronic scale of 4 digits was used to weigh approximately 0.55 g of granules for making one tablet each time and manually filling the granules into a cylindrical steel die. Following this, the volume of each tablet was measured. The tablets then were stored in a humidity chamber at temperature of 25°C and 40 RH% to be tested for their tensile strength. Figure 45 summarizes the project methodology processes.

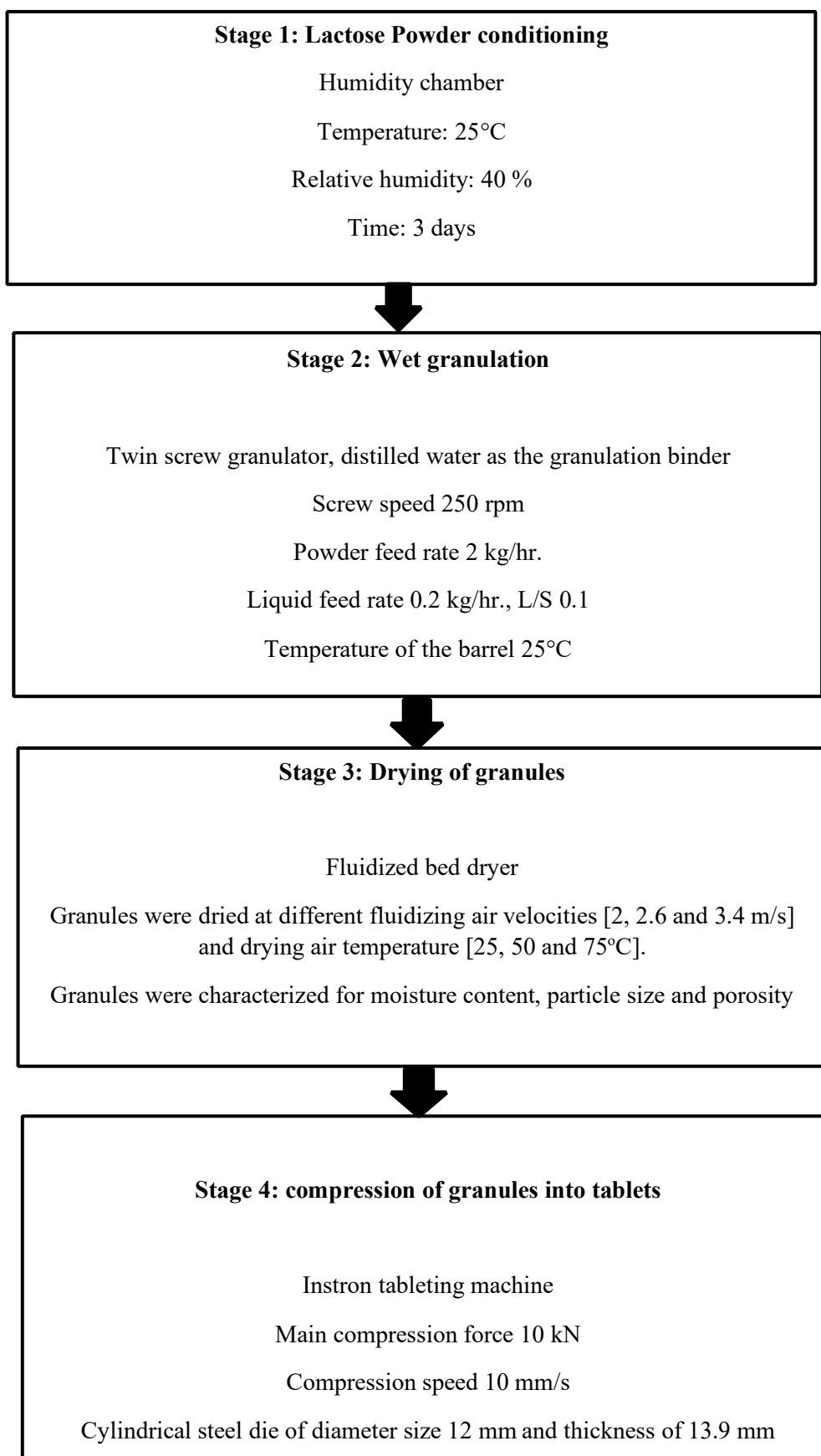


**Figure 45: Flow diagram summarizing the project methodology process used for this chapter.**

## **2.4. Product characterization**

### **2.4.1 Granules Moisture Content**

Sartorius infrared moisture analyser (Sartorius, MA 37, Germany) was used to measure the moisture content of the granules. A sample of 2 g of granules was used in each moisture content measurement. The temperature of the moisture analyser was set to 105°C with fully automatic mode, which means that the reading is given once the moisture analyser detects no change in moisture value. The moisture content measurement was carried out every 20 minutes during the drying process at room temperature. For the moisture content of the granules dried in the fluidized bed, the measurement was carried out every minute. This is due to the short drying time in the fluidized bed.

### **2.4.2 Analysis of Granule Size Distribution**

Once granules drying finish, the GSD of each experiment was measured using a Retsch Camsizer (Retch GmbH and Germany). The camsizer consists of two types of camera; these are the basic and zoom cameras. They are set with reproduction scales to take images of the falling granules in the measurement zone. The basic one takes an image to the particles in an actual size. The zoom one gives a zoomed image of the particle or the granule. The software interprets these images into data about the size of the particles being tested. In this project, representative samples of approximately 10 g of granules were used for this measurement.

### **2.4.3 Granules Porosity by X-Ray**

The determination of the granule's porosity was done using MicroCT 35 (Scanco medical AG, Switzerland). The X-ray experiments were performed using a voltage, current and a power of 45 kV, 177  $\mu$ A and 8 Watt respectively. The size of the voxel used was 3.5 $\mu$ m. ImageJ software was used to analysis the x-ray images by using the black colour in the sample to represents the air and the white colour to represents the solid material. The level of the grey scale (16-bit) is ranged from 0 to 65,535. The 0 is being the complete black and 65,535 is being the complete white. The colour becomes whiter as the number increases. A calibration step is required before calculating the porosity. This is

applicable for any sample to define the black area (air). The grey scale then can be determined for the black area that is near the sample. A total of 240 slices were obtained for each sample, thus, when determining the porosity of the sample, a consideration for all the 240 slices should be taken into account. Therefore, the porosity was determined and an average porosity value for all the 240 slices was obtained. Dividing the value of the black pixel (which indicates the air in the sample) by the total value of the air and solid pixel should give the porosity of the sample.

## 2.4.4 Tablet

### 2.4.4.1 Tablet Tensile Strength

The strength is a very crucial characteristic especially for the pharmaceutical tablet. It is a measure of how strong the tablet is to endure a force, which have the tendency to break the tablet apart. The tablet structure can be affected by several activities such as packing, shipping procedure; therefore, it is very important for the tablet to have adequate vigour to withstand breakage. Moreover, dissolution rate of the tablet is significantly connected with the tensile strength (Augsburger and Hoag, 2008). The dissolution rate of the tablet is likely to reduce with a high strength tablet. Consequently, if the strength of the tablet is too high, tablet might have a slow rate of dissolution. Therefore, it is very necessary to optimize the strength of the tablet so that it is not negatively affect the dissolution rate of the tablet. In this study, a Z 0.5 strength machine (Zwick Roell, LTD, Germany) was used to determine the tablet tensile strength. Ten tablets were used for each test. The tablet strength was done by diametrically compressing the tablet between two platens. So, the tablet is placed on the platform at a vertical position beneath the compression punch, in which the arm then moves down at constant velocity (the compression speed that was used throughout all experiment was 1 mm/min) downward until a sudden decrease in the compression force is observed. The strength of the tablet is taken at the maximum force ( $F_{\max}$ ) just before the sudden force reduction. The tablet tensile strength was determined using equation 3.  $F_{\max}$  is the maximum force in N, h is the thickness of the tablet in mm and d is the diameter of the tablet in mm.

$$\text{Tensile strength} = \frac{2F_{\max}}{\pi x h x d}$$

Eq.3



Figure 46 illustrate the schematic diagram of the project process in addition to the characterization that carried out during different process stages.

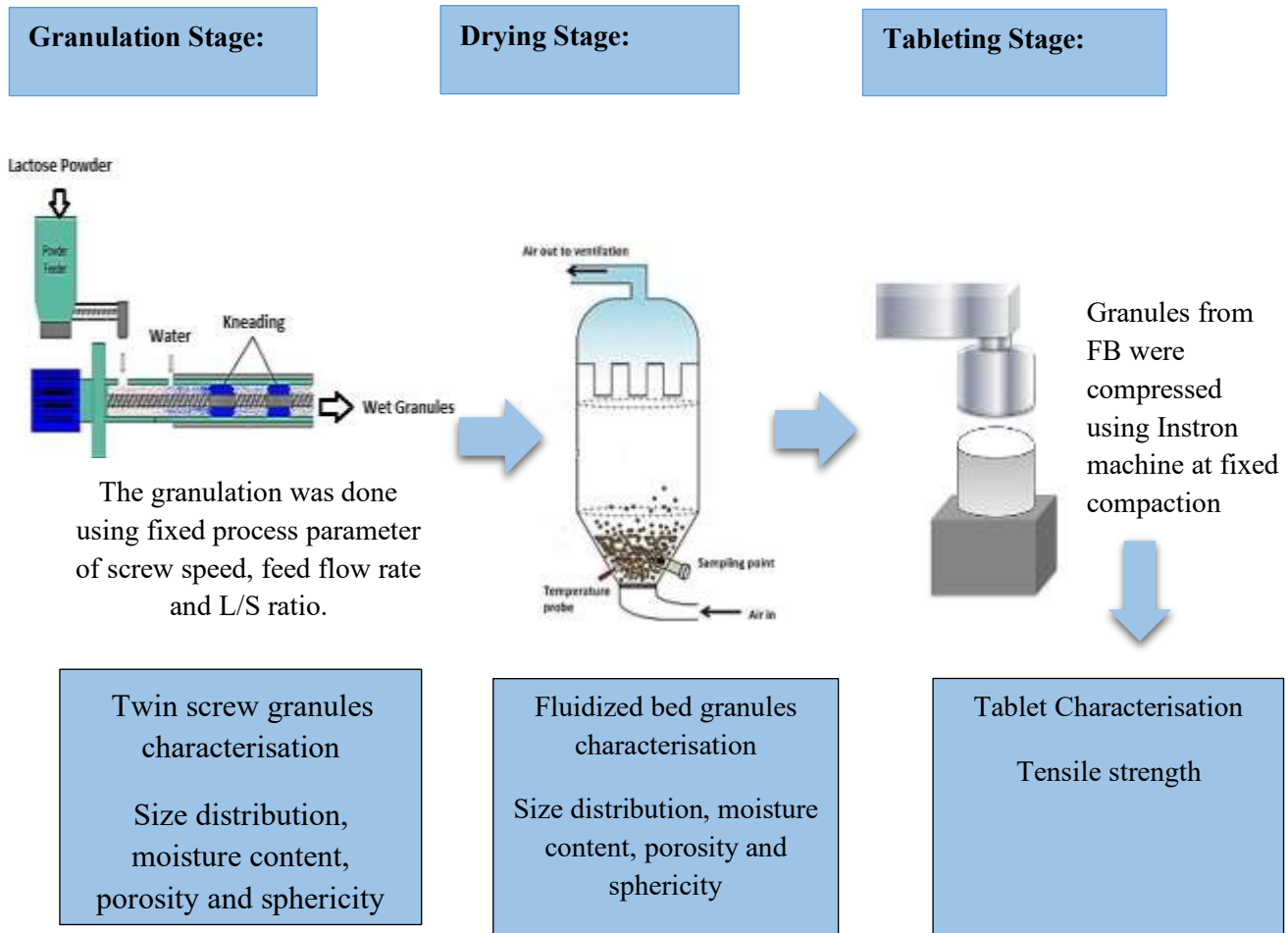


Figure 46: Illustration of Project process diagram.

## 2.5 Experimental work in the Continuous ConsiGma-25 line

The experiments of granulation, drying and tableting were all conducted on the ConsiGma-25, Powder to tablet line (GEA Pharma Systems). This line as shown in Figure 47, contains control screen of the process and formulation parameters for twin screw and fluidized bed (1), hopper for loading the powder (2) an integrated co-rotating twin screw granulator (3), Six -segmented Fluidised Bed Dryer (4). Milling unit (5). Formulation modification unit (6). Tableting unit (7). Control screen for tablet press (8)



**Figure 47: ConsiGma-25 Powder to Tablet line used in this project containing an integrated co-rotating twin screw granulator, six- segmented fluidized bed dryer, milling, formulation and tableting units.**

Twin screw granulator is connected directly to a six- segmented fluidized bed dryer with a removable connector. There are two liquid binder inlets, and these are located at different positions, however, only one liquid inlet was used to deliver the binder and that was through a tube of silicon. For feeding the powder into the system, the twin-screw granulator has only one feeding point and that is allocated at the top of the twin screw. The process and formulation parameters can be flexibly controlled

through an attached computer screen. The six- segmented fluidized bed as the name implies, consists of six cells.

These cells are filled in an anticlockwise direction with wet granules coming from twin screw granulator as illustrated in Figure 48.

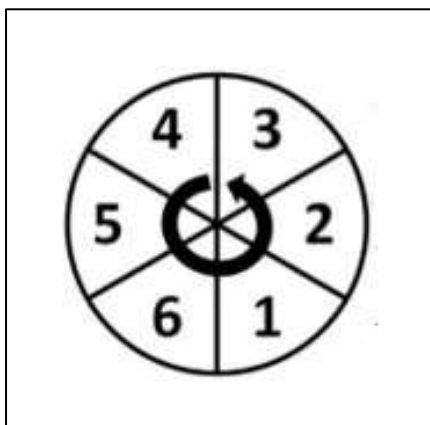


**Figure 48: Illustration of the filling cycle (anticlockwise direction) in the six segmented fluidized bed dryers of the Consigma-25 line.**

The granule flow is controlled at the dryer by opening the valves, which in turn permits the flow into the exact cell. So, for example, the drying time for this study was fixed at (800 seconds) this includes the cell filling time 5 minutes (300 seconds), the granules flow to the next cell happens after 300 seconds, resulting in a cell loaded with 0.83kg of wet granules. The granules are dried at a fixed drying air inlet temperature of 50 °C and drying flowrate of 400m<sup>3</sup>/hr. After the drying process in the fluidized bed process is completed, the dried granules go to the milling unit (Quadro comil U10, Quadro Engineering, Ontario, Canada) in which the final granule size distribution is controlled (the mill size is 1596µm). Once the milling is completed, the milled granules flow to the blending units just above the tableting press for addition of further excipients. In this study, the milled granules were blended with 10g of magnesium stearate for lubrication purposes prior to tableting. The rate of tablet production by the at the tablet press is 12000 tablets per hour. In this unit, there is also a control screen where the punch displacement, compression force and tort speed can be set. The punch displacement is used to control the tablets thickness. In this study, the compression force was kept constant at 5kN throughout all the experiments. The produced tablets were then undergoing hardness,

thickness and diameter measurements using hardness tester (Pharmatron, AG-Multitest 50 G2, Switzerland).

### 2.5.1 Twin Screw Granulation and Drying

Before the actual experiment, an NIR probe was calibrated for moisture content. To calibrate the NIR probe, lactose powder was mixed with different amount of water manually (0,2,4,6,8,10,12%). The samples of different moisture content were divided into two parts. Immediately one sample goes to the loss on drying measurement by moisture analyser. The other sample was analysed using the NIR probe, where the probe was inserted into the powder bed and then the reading was completed and recorded. Then Figure 92 shows the NIR probe calibration curve which correlates the online NIR probe measurement for the moisture and the loss on drying measurement for the moisture content.

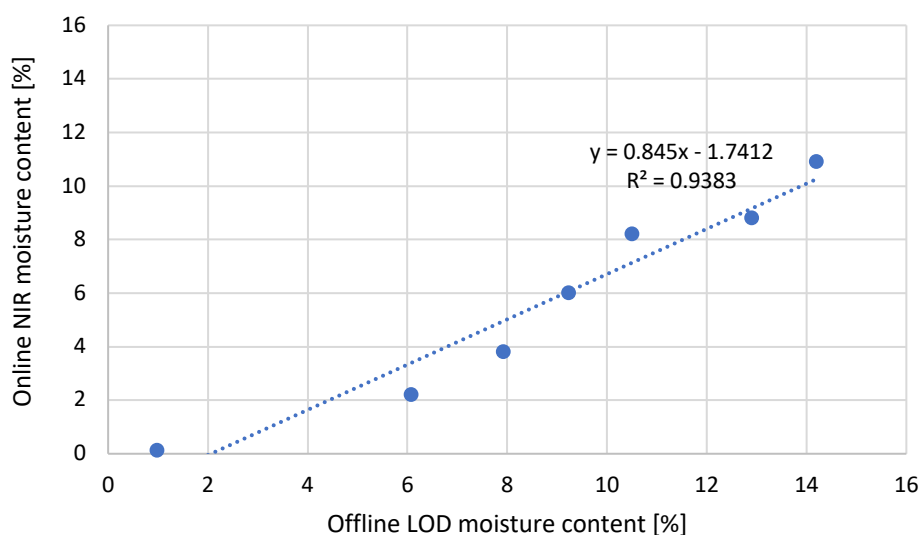


**Figure 49: Near infrared probe calibration curve for different moisture contents of lactose powder mixed with water manually (samples were analysed using both near infrared probe and loss on drying by moisture analyser).**

## 2.5.2 Tablet Dissolution Measurement

The tablet dissolution measurement was conducted using the setup shown in Figure 50. This set up contains a microprocessor conductivity meter connected with a probe (Jenway, Model 4510, UK). The conductivity meter is connected with a probe to be inserted in the solution media. The probe measures both the conductivity and the temperature of the solution media contained the tablet. The setup also contained a hot plate in which can be used to control the temperature of the solution media during the experiment. A temperature of  $37^{\circ}\text{C} \pm 0.5$  was used in this study; mimicking human body temperature based on the USP I. All the tablet dissolution measurements were performed in a beaker of distilled water with a volume of (200 ml). A magnetic stirrer bar was used to stir the water at a stirrer speed of 700 rpm, this is to ensure a uniform distribution of the ions within the solution. Moreover, act in accordance with USP I, a meshed basket was positioned in the solution to carry the tablet during the measurement, using the basket will make sure that the tablet does not obstruct with the magnetic stirrer bar. To commence with the measurement, a beaker filled with distilled water with the aforementioned volume was positioned on the hot plate and the speed of the motor stirring and temperature were set to 700rpm and  $37^{\circ}\text{C}$  respectively. The measurement was started before the tablet is placed in the solution, so that a conductivity of zero was recorded for the distilled water, the tablet was then put in the basket in the solution. The reading of the conductivity was taken at a step of 5 seconds. The conductivity reading of the solution increased as the tablet dissolves in the water. When the solution reads constant values of conductivity, the tablet deemed to be fully dissolved. A sample of 10 tablets was done for each of different experimental conditions. Figure 50 shows a simple diagrammatic representation for the dissolution apparatus used in this project.

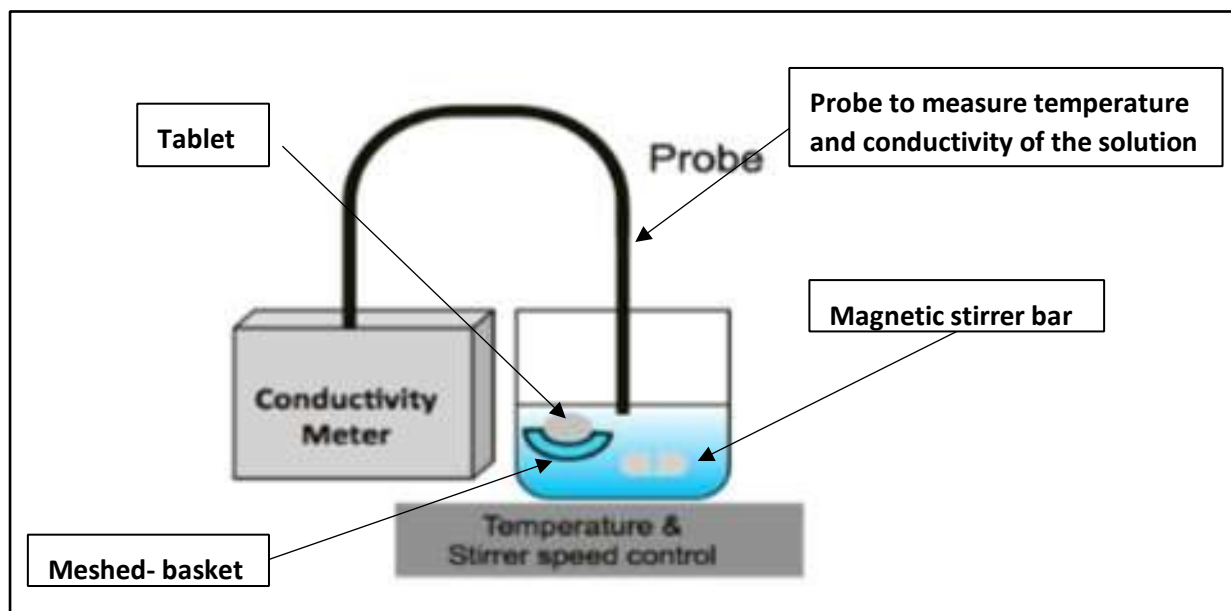


**Figure 50: Schematic illustration of the dissolution testing set up and the parameters used in this study was based on using the USP apparatus I (with temperature of  $37^{\circ}\text{C} \pm 0.5$ , a water of volume of 200 ml and a motor stirring speed of 700rpm).**

## **Chapter 3: Drying in a Batch Laboratory Scale Fluidized Bed Dryer: Effect of Fluidized Bed Process Parameters**

---

### **3.0 Introduction**

It is not possible to study the attributes of granules during drying in the continuous six segmented fluidized bed dryers of the ConsiGma 25 system which is used later in this work. Therefore, the aim of this chapter was to study the resultant granules attributes in the drying process performed in laboratory scale fluidized bed dryer compared to the granules produced in a twin-screw granulator. This should enable process optimization and product development for the granulation, drying and downstream processes. Thus, this chapter is divided into three main sections: the first section presents the primary lactose powder behaviour. The second section presents the twin-screw granulation result which includes the characterization of moisture content of granules produced directly from the twin-screw granulator

(wet fresh granules), granule size distribution, In addition to the shape (Sphericity) and structure (Porosity) of the granules. The third section presents the result of the effect of fluidized bed drying process parameters on granule properties. This covers the granule size distribution, moisture content, sphericity and porosity of the granules and the effect of the fluidized bed drying process parameters on tablet tensile strength.

### **3.1 Powder Behaviour Before Granulation**

The aim of the study in this section is to understand how the moisture content of lactose powder affected by different relative humidities and consequently the effect on the tableability.

#### **3.1.1 Effect of Relative Humidity on Moisture Content of Primary Lactose Powder**

Lactose powder was conditioned at different relative humidities between 10% and 90% RH in a step of 10% using humidity chamber at a temperature of 25°C for three days. The corresponding powder moisture content was measured using the moisture analyser. This was done by placing the Powders,

conditioned to different RH, on an aluminium pan and heating them at a temperature of 100°C using fully automatic mode. Figure 51 shows the measured moisture content of lactose powder at different relative humidities. The result showed that there is a slight increase in the moisture content of lactose powder as relative humidity increases. It can be seen from Figure 51 that the increase at the first stage was not significant, such that the increase in moisture content between relative humidity of 10 and 20 was about 0.03, about 0.01 between the 20 and 30%, 0.02 between 30 and 40%, 0.03 between 50 and 60%. However, 60% RH, the increase in moisture content between the relative humidities was higher, such that the increase in moisture content between the 60% and 70% was about 0.06, between 70 and 80% was about 0.08 and between 80 and 90% was 0.1.

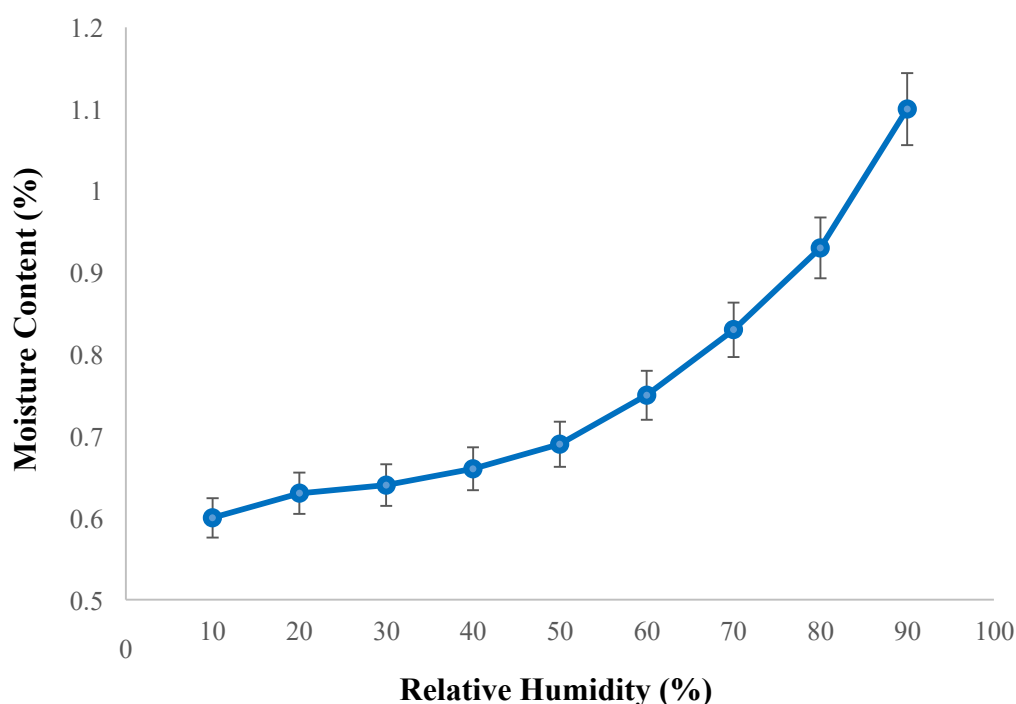


**Figure 51: Moisture content of lactose powder (150M) conditioned at different relative humidities (10% to 90% RH at a step of 10%) using humidity chamber at a temperature of 25°C for three days.**

### **3.1.2 Effect of Relative Humidity on the Tableability of the Powder**

Figure 52 shows how the relative humidity affects the tablet strength produced using different compression forces of 10, 15, 20 kN. Figure 52 generally shows that with increase in relative



humidity, there is an increase in tablet strength. However, there is a threshold above 60% RH where the tablet strength decreases significantly with increase in relative humidity. The increase in the tablet strength in the first stage could be attributed to that water acted as a plasticizer which caused “an increase in the plastic deformation of the powder” which consequently resulted in producing tablet of higher tensile strength compared to that produced by powder at lower relative humidity (Osborne et al., 2013). Further increase in relative humidity resulted in a decrease of the tensile strength of the tablets. This could be because of the powder caking which happened at higher relative humidity as it can be seen in Figure 53. This Figure shows a microscopic image of lactose powder conditioned to the two extremes of relative humidity of 10% (a) and high of 90 % (b). It can be seen from the image that the powder stored at 90 %RH is caked and transformed into big lumps (granules) compared to the single particle at 10 %RH. This increase in the size caused a decrease in the surface area and consequently caused a decrease in the contact area between the particles during the compaction. This contact area is important to produce good tablet strength.

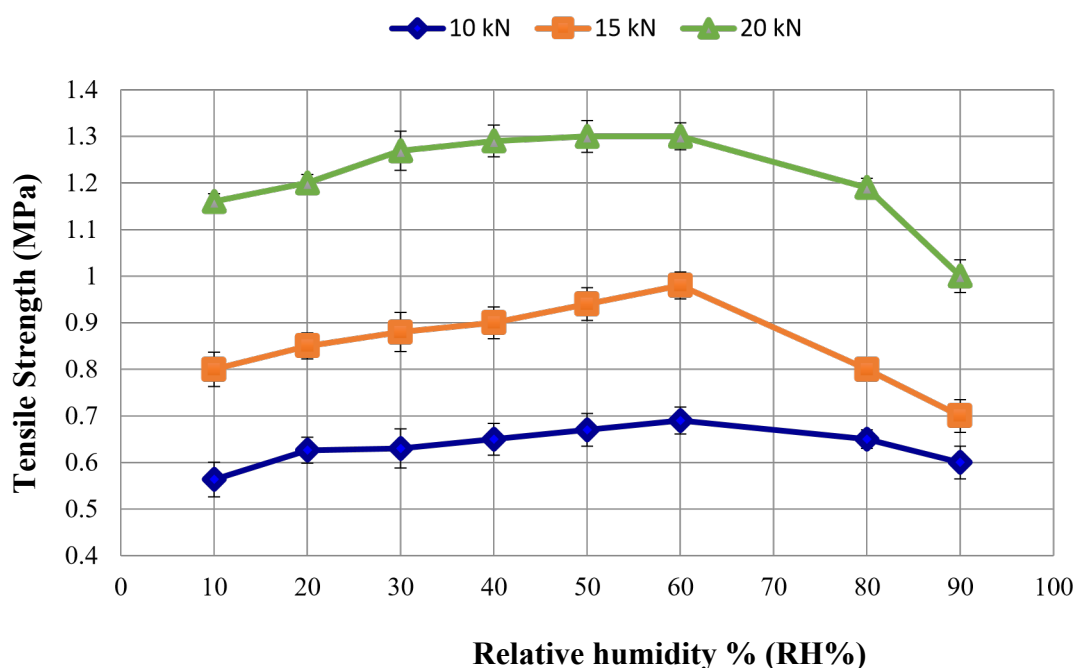


**Figure 52: The influence of relative humidity at which the feed powder is stored on the tablet strength for a range of compression forces (10,15,20kN).**

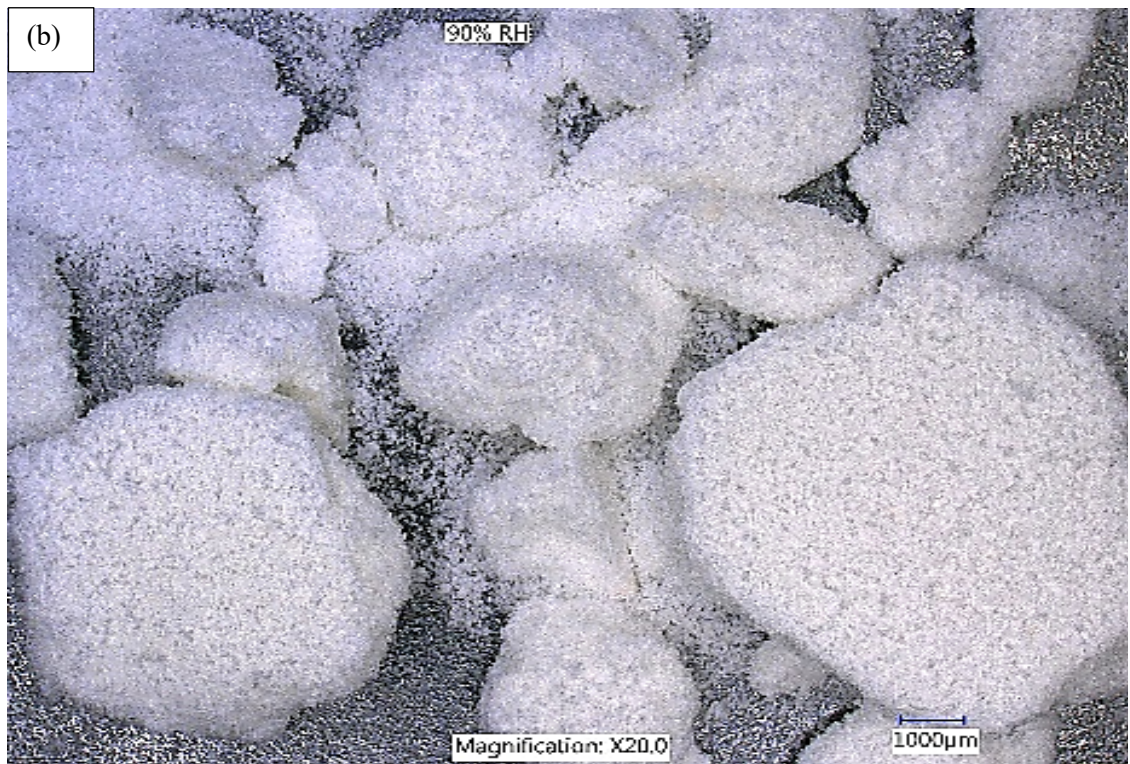
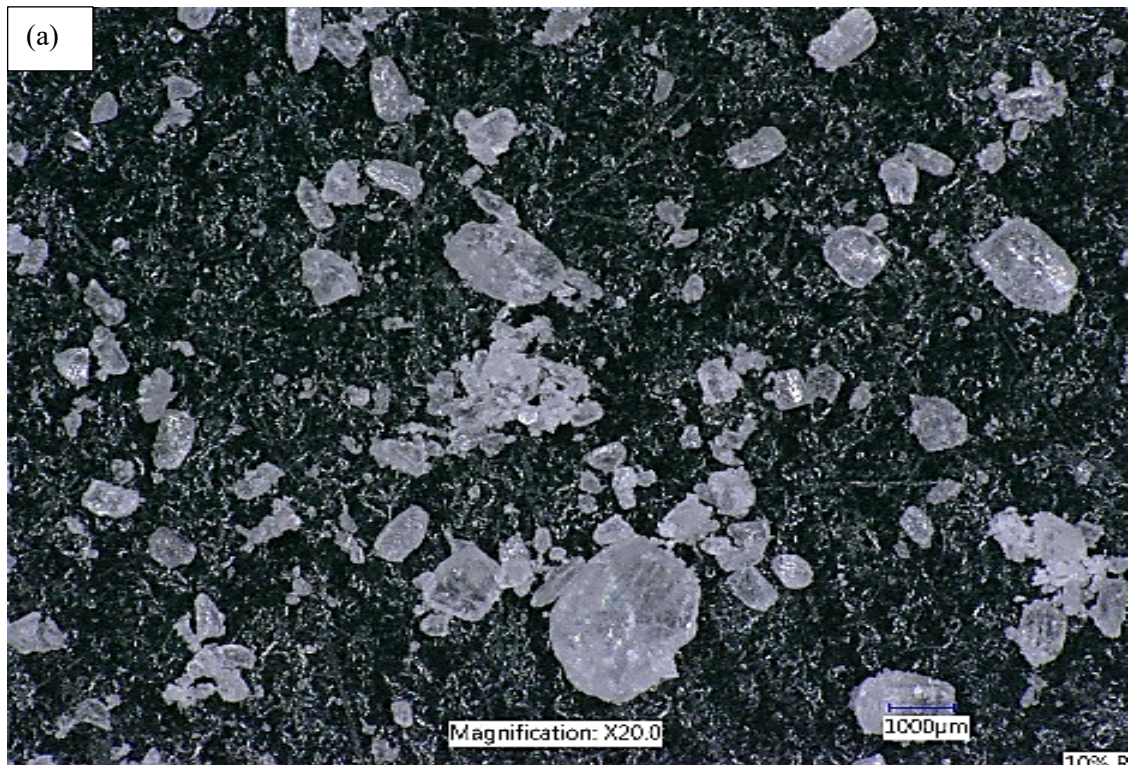


**Figure 53: Images of lactose powder stored at relative humidity for three days of (a) 10% and (b) 90% taken by Keyence microscope at the same scale/magnification (X20).**

### 3.2.0 Twin Screw Granulation

#### 3.2.1 Initial Size Distribution of Granules

Twin screw granulation (TSG) was conducted to produce granules to study the effect of fluidized bed (FB) drying on the properties of the resultant granule and tablet. The granules were produced and collected from twin screw granulator (as described in Section 2.2.3) and kept drying in the room temperature overnight for 24 hours. Figure 54 shows the size distribution of the granules dried in the room temperature. Figure 54 shows a mono-model distribution with an average  $d_{50}$  value of 1090.14  $\mu\text{m}$ . later in the result section, this TSG initial size distribution will be compared to the size distribution of the granules dried in FB. Obtaining a narrow size distribution would enhance uniformity of drying of the granule, as opposed to having over dried or under dried granules. Consequently, control of granule size at the stage of twin-screw granulation is very necessary in order to reduce as such problem during downstream processing.

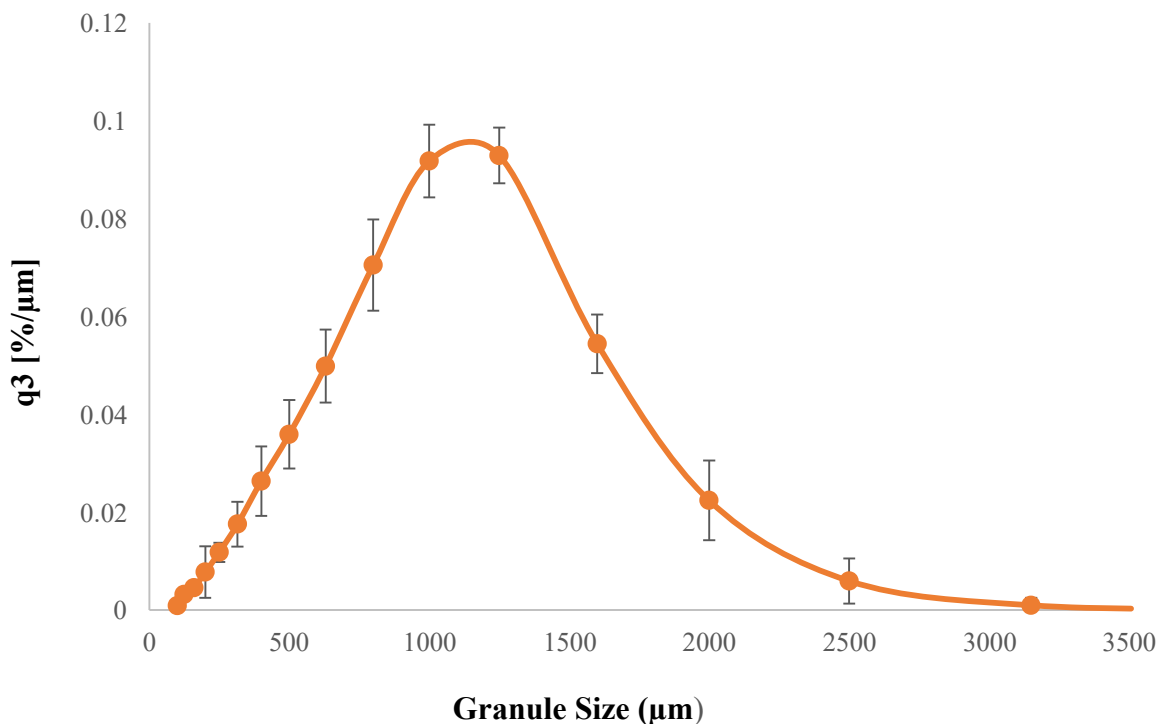


**Figure 54: Size distribution of initial granules prepared by TSG with lactose powder of 150M and water as a liquid binder, L/S of 0.10, screw speed of 250rpm, powder feed rate of 2kg/hr and 16-KE in each screw (before drying in fluidized bed).**



### 3.2.2 Moisture Content of Wet Granules

The expected moisture content of the wet granules is approximately 10 % since this is equal to liquid to solid ratio used in granulation experiment. The moisture content of wet granules taken directly from the twin screw was measured using moisture analyser. A sample of 2 g of lactose-wet granules was used in this measurement. The measurement was repeated 20 times and average moisture content was calculated to be approximately 9.5%. Figure 55 shows the moisture content of 20 measurements. It can be clearly seen that there was a slight fluctuation in the measurements; this could be attributed to the possibility of water evaporation during preparation the sample for the test.

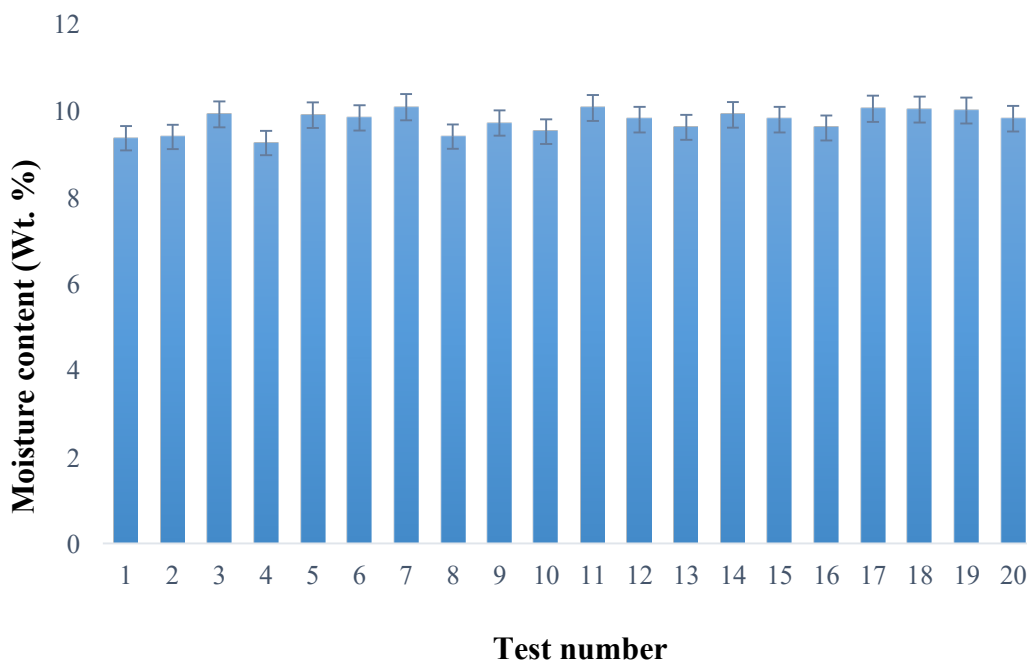


**Figure 55: Moisture content of wet granules as produced directly from TSG measured with loss on drying by moisture analysers at temperature of 105°C with fully automatic mode and a sample of 2 grams of wet granules used in each measurement.**

### 3.2.3 Drying of Granules in the Humidity Chamber

The overall drying mechanism is summarized into two main stages, the first stage is the evaporation of the liquid from the solid surface and the second stage is the evaporation from the interior of the solid. In order to investigate the drying process of wet granules, two drying techniques were used (drying at room temperature and drying in fluidized bed). Granules from twin-screw granulator were left to dry

in the humidity chamber at temperature and relative humidity of 25°C and 40% respectively. The moisture content of those granules was then measured every 20 minutes using the moisture analyser. The reason behind choosing the 20 minutes is because it is the time required to collect about 500 g granules from TSG to be dried in FB and also it is the time taken to make one batch of tablet from the granules brought from the fluidized bed. Figure 56 shows the moisture content of the granules as a function of drying time. It can be seen from this figure that the total drying time was approximately 3.40 hours. However, the weight loss in the water stopped after approximately 80 minutes. The aim from this experiment was to see how much moisture or liquid can be lost when the granules are taken from twin screw granulation unit to fluidized bed drying and from fluidized bed to tableting unit. From Figure 56, it is found that about 2% of moisture content was lost from time zero to 20 minutes and about 2.84% was lost from time 20 to 40 minutes, 1.29% from time 40 to 60 and 2.84% was lost from time 60 minutes to 80 minutes and after that the moisture loss was very little, so drying was happening faster at the first hour and 20 minutes.

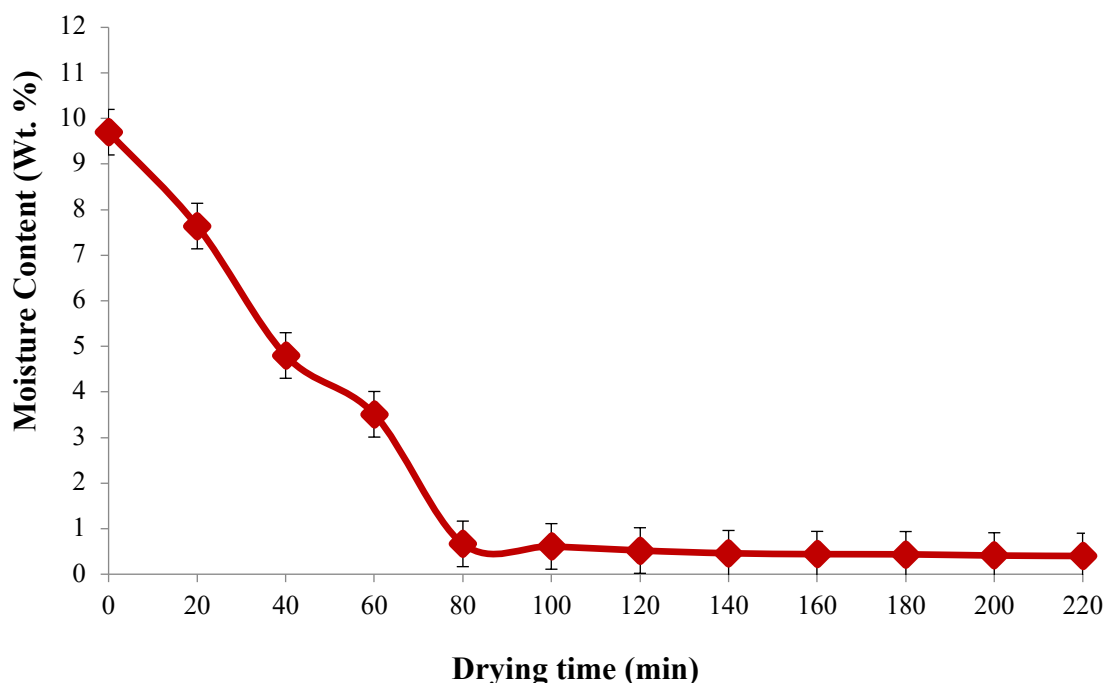


**Figure 56: Moisture content of granules produced by TSG using 150M lactose powder and water as liquid binder at a L/S of 0.1, 250rpm and 16KE in each screw and dried at standard room conditions in humidity chamber at a temperature and relative humidity of 25°C and 40% respectively with moisture content measurement performed every 20 minutes using loss on drying by moisture analyser at a temperature of 105°C and fully automatic mode.**

### 3.3 Fluidized Bed Drying of Granules

#### 3.3.1 Effect of Drying Air Velocity and Temperature on Granule Size Distribution

To investigate the effect of fluidized bed drying on the properties of the twin-screw granules, the air velocity and temperature were varied. Figure 57 shows the size distribution of granule after performing the fluidizing bed drying at different air velocities (2, 2.6 and 3.4 m/s) in blue line. The velocity numbers (2, 2.6 and 3.4 m/s) were chosen based on low, medium, high values in the velocity gauge meter. It can be seen from the figure that the size distribution of the granules dried in the fluidized bed is smaller compared to the size of the granules dried in room temperature. It can be also notice that increasing the air velocity caused a reduction in the granule size. The  $d_{50}$  for the three air velocities are 734, 710 and 686  $\mu\text{m}$  respectively, which clearly indicates the decrease in granule size as air velocity increases. This could be attributed to the breakage that resulted from the collision of the granules with other granules and granules with the wall of the fluidized bed. These results are in agreement with findings in the literatures (MacKaplow et al., 2000) and (Nieuwmeyer et al., 2007). This scenario is unwanted since the primary aim of granules drying is to only dry them to remove the moisture or liquid present within the granules and not to affect the size to either smaller (breakage) or bigger (growth). Thus, it very important to maintain the granules properties throughout the drying process especially the size. Figure 58 shows the size distribution of the granules dried at room temperature (orange line) and size of granules after performing the fluidizing bed drying (blue line) at different drying air temperatures of 25, 50 and 75°C. Similar results to the air velocity were obtained for varying air temperatures. It can be seen from the figure that the size of the granules dried in the fluidized bed at different temperature is smaller compared to the size of the granules dried at room temperature in the humidity generator. The granule size reduced after fluidized bed drying indicates that breakage of the granules was also occurring. The  $d_{50}$  for the three air temperatures are 980, 827 and 744  $\mu\text{m}$  respectively, this also indicate reduction in granule size during fluidized bed which suggests breakage that might be caused by the collision between granules and granule-wall.

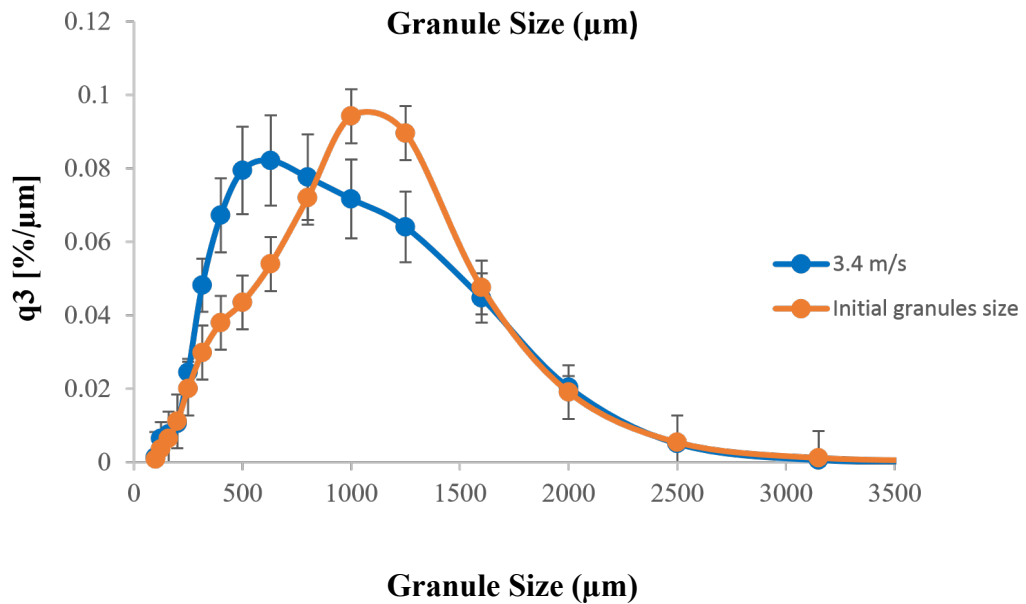
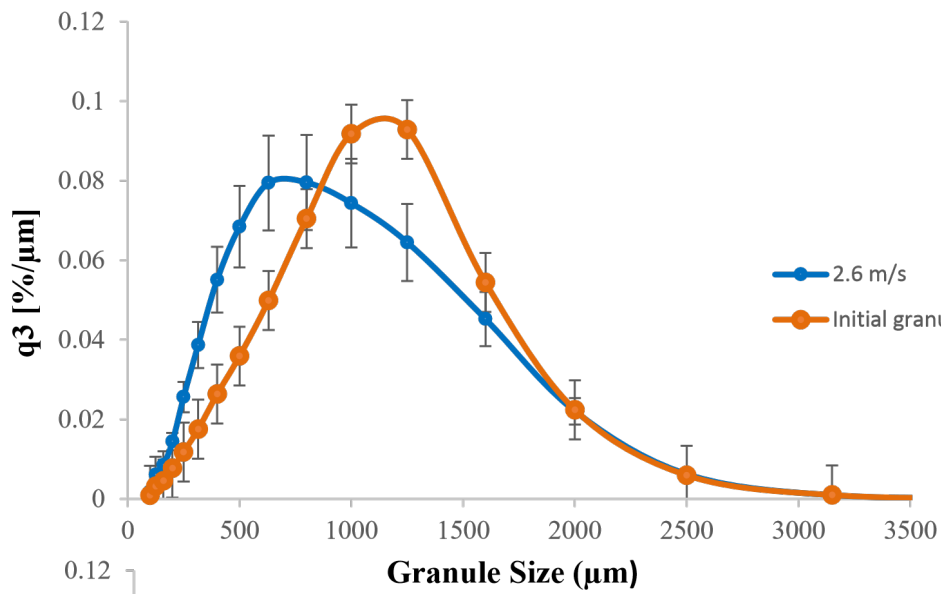
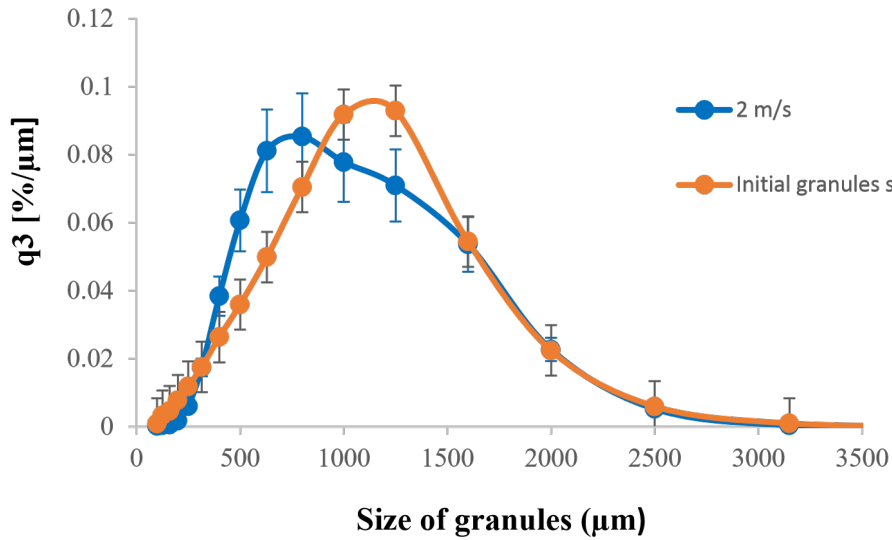
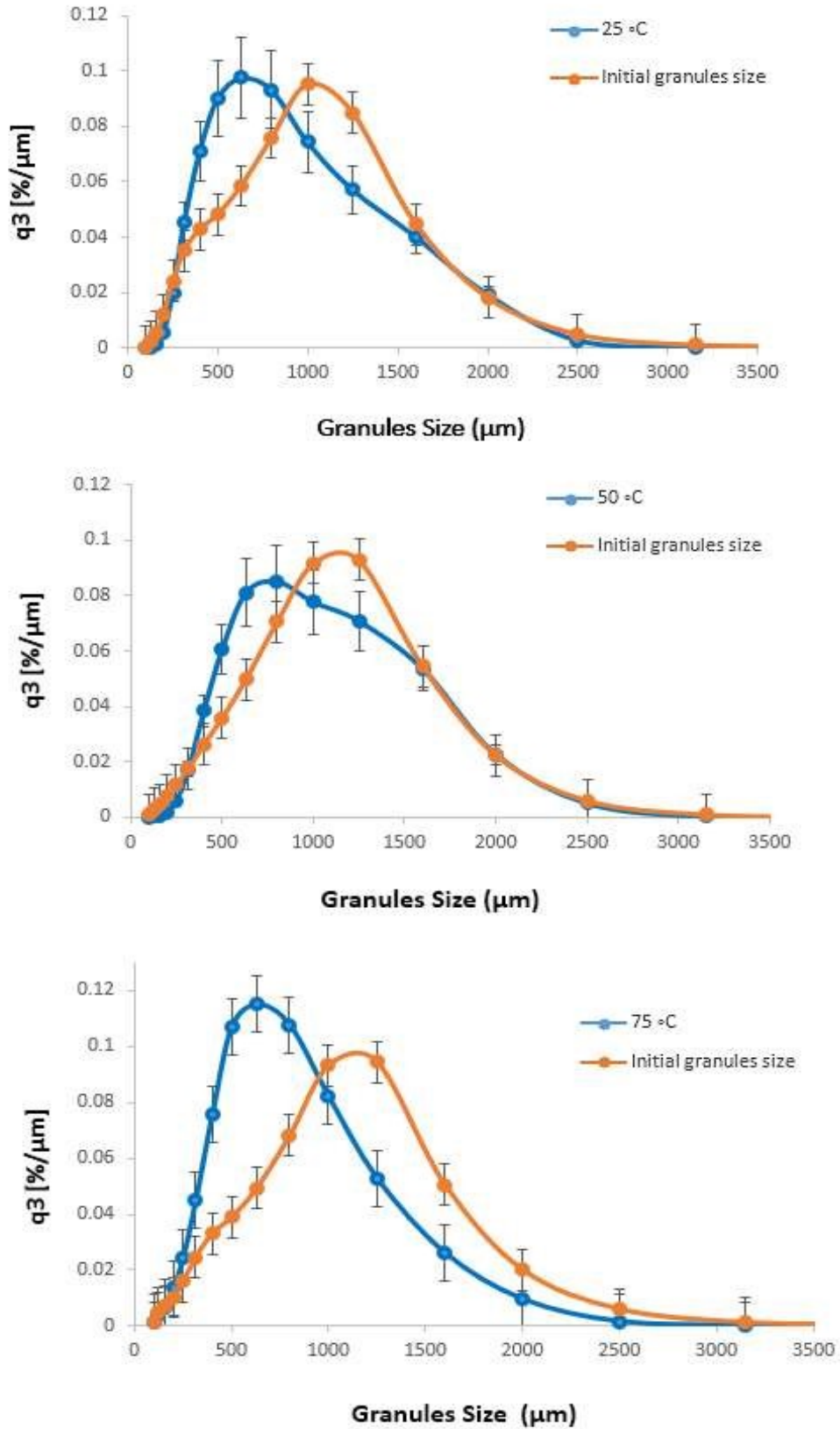


Figure 57: Effect of fluidizing air velocities on the PSD of granules produced by TSG with 150M lactose powder and water as liquid binder at a L/S od 0.1, 250rpm, 16-KE in each screw and dried with air temperature of 50°C.



**Figure 58: Effect of fluidizing air temperature on the PSD of granules produced by TSG with 150M lactose powder and water as a liquid binder at a L/S of 0.1, 250rpm, 16-KE in each screw and dried with air velocity of 2m/s.**



### 2.3.1.2 Sphericity of Granules

In twin screw granulator, there is a confined space for the materials to move. Due to the shear stress from the screws, the granule produced tend to be elongated more than spherical. Figure 59 shows a comparison between the sphericity curves for the initial granules dried in room temperature and the sphericity of the granules dried in the fluidized bed at different air velocities. The figure shows that the sphericity of the granules produced at different air velocities are higher than the sphericity of the granules dried at room temperature. This is because in fluidized bed, there is much volume and space available for the granules to be bouncing and hence sticking together to form spherical granules and the granules are colliding with each other and with the wall. Since they are wet, they are easily deformed. From this figure, the sphericity of the granules produced by TSG were ranging from 0.57 to 0.92. It can be seen that the sphericity of the granules dropped down after 1500  $\mu\text{m}$ .

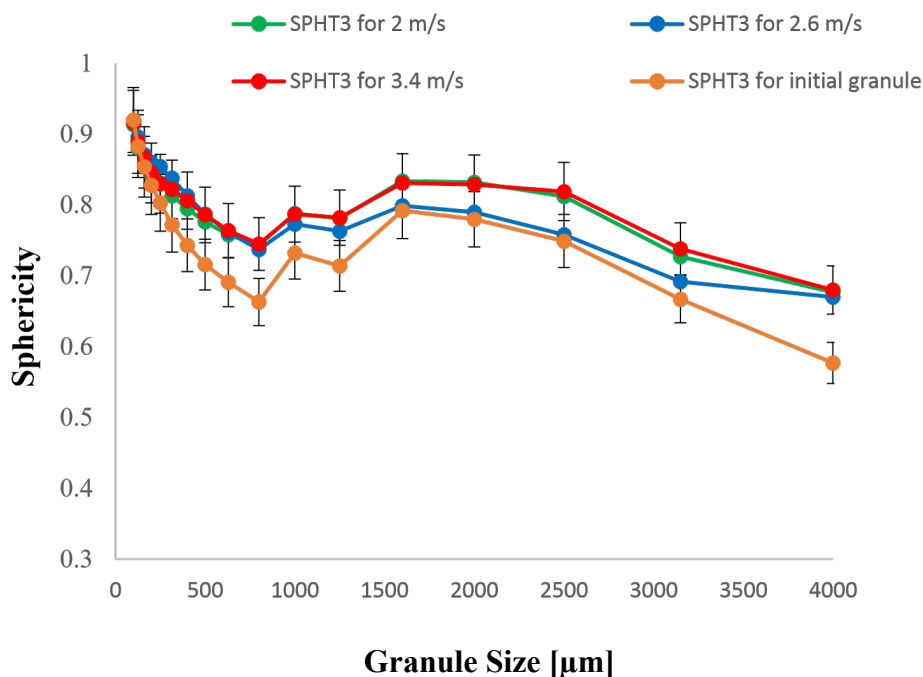


**Figure 59: Sphericity curves for granules produced by TSG with 150M lactose powder and water as a liquid binder at a L/S of 0.1 ,250 rpm and 16-KE in each screw and dried in fluidized bed at different air velocities (2m/s, 2.6m/s, 3.4m/s) and air temperature of 50°C.**

Figure 60 shows the sphericity curves for granules dried in room temperature and fluidized bed at different air temperatures. Roughly a similar result to the air velocities was obtained for different air temperatures. The sphericity of the granules dried in the fluidized bed is higher compared to the

granules dried at the room temperature. Overall, air velocity showed to less spherical granules than the granules dried at different temperature. This is due the attrition which increases as a result of air velocity. Furthermore, from observing the two figures (Figure 59 and Figure 60), it can be seen that the sphericity of the particles ranging from 1 to 100  $\mu\text{m}$  approximately were approaching a sphericity of about 0.9, which is slightly unexpected, however, this could be explained due to the fact that fine particles tend to stick to each other during the measurement when falling down towards the cameras zone making particles looks spherical to the camera, the stickiness of the fine powder though is difficult to control as their flowability is lower than big particles/ granules, hence this could be one of equipment errors/ limitations.

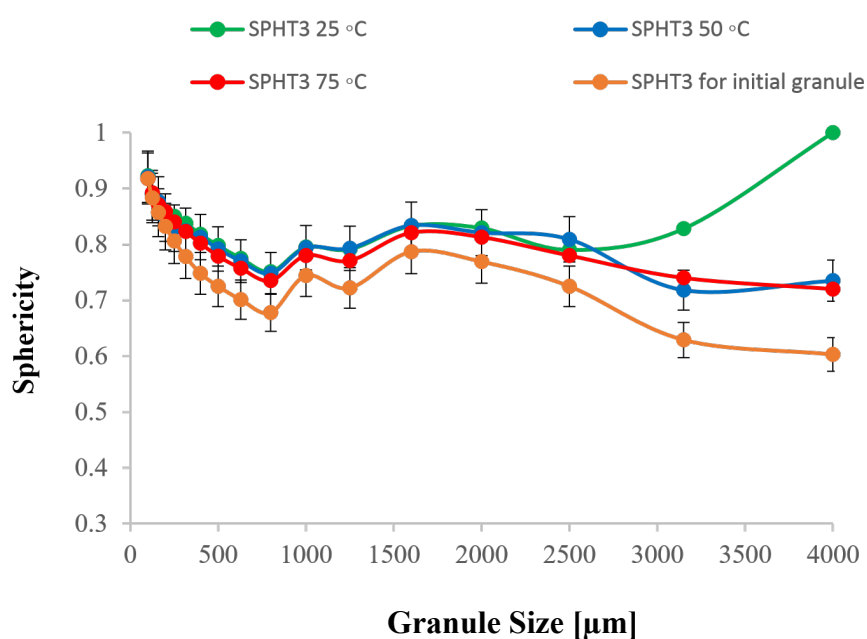


**Figure 60: Sphericity curves for granules produced by TSG with 150M lactose powder and water as a liquid binder at a L/S of 0.1, 250 rpm, 16-KE in each screw and dried in fluidized bed at different air temperature (25,50 and 75 °C) and an air velocity of 2m/s.**

### 3.3.2 Effect of Fluidizing Air Velocity on Granule Moisture Content

An experiment was conducted to determine the effects of varying drying air velocities on moisture content of granules. The moisture content of the granules was measured every minute and as described in Section 2.4.1. The drying curves of lactose granules undergoing fluidized bed drying at different fluidizing air velocities of 2, 2.6 and 3.4 m/s are shown in Figure 61. The air velocities were

chosen in the ranges where fluidization of granules was insured. The drying air temperature was maintained at 50°C for all the experiment. It has been found from these experimental results that the increase in the velocity caused a decrease in the drying time and in the moisture content of the granules. The level of moisture content was the lowest at the higher fluidizing air velocity (3.4 m/s) with the least drying time (1min) and obtained at the lower fluidizing air velocity (2 m/s) with longer drying time. This is mainly because increasing air velocity increases convective heat transfer of water from solids to air resulting in an increase in drying rate. Also, at higher air velocity, granules can fluidize faster, in such a case, granules can move more resulting in collision between the granules with each other and with the wall of the dryer. The collision led the granules to be compacted. This compaction also contributed to removing the water from the granules in addition to the heat. This argument is supported by characterizing the structure of the granules using the X-ray technique and as described in Section 2.4.3.

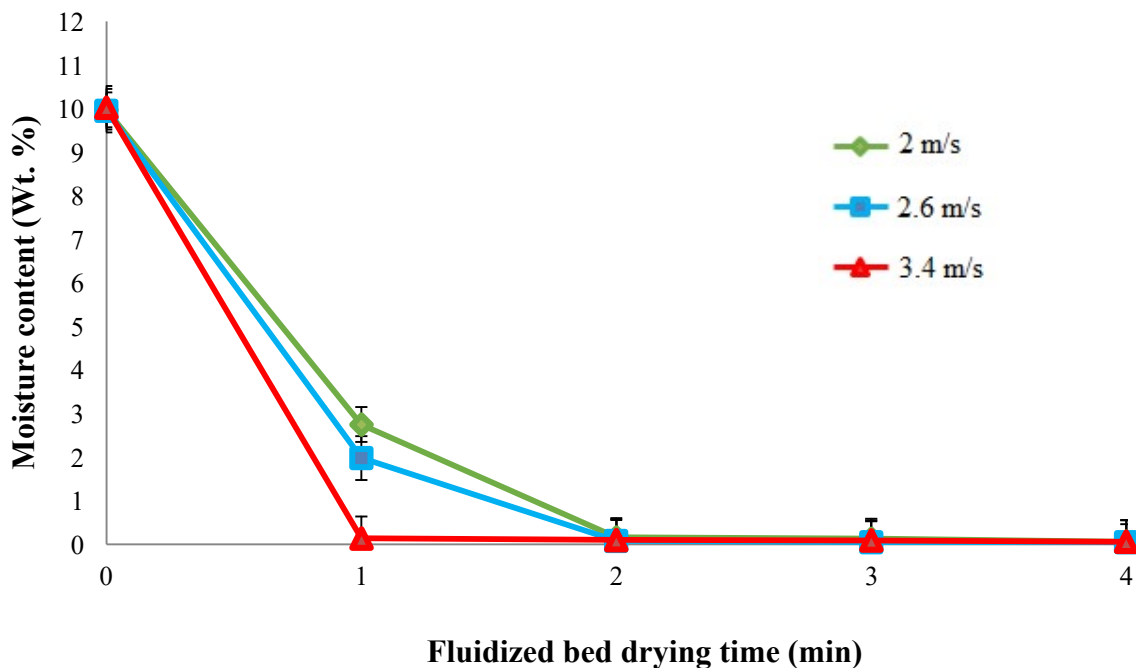


**Figure 61: Drying curves of granules produced by TSG with 150M lactose powder and water as a liquid binder at a L/S of 0.1, 250 rpm and 16-KE in each screw and dried in FB at different air velocities 2, 2.6 and 3.4 m/s using an air temperature of 50°C.**

### 3.3.3 Effect of Drying Air Temperature on Granule Moisture Content

An experiment was conducted to determine the effects of varying drying air temperature on the level of moisture content. The fluidizing air velocity was kept fixed at 2 m/s. The drying curves of lactose granules undergoing fluidized bed drying at various temperatures are shown in Figure 62. The result shows that increasing the air temperature caused a decrease in the moisture content and drying time of the granules. The removal of moisture was enhanced at higher temperatures (75°C), therefore the drying time at this temperature was almost the lowest (2 minutes) however the granules dried at (25°C) had the longest drying time (3 minutes). This result can be explained by the fact that an increase in air temperature results in higher thermal heat input into the fluidized bed system, which increases the surface temperature of the granules being dried. This therefore leads to lower the moisture content at the surface and increase the rate of evaporation.

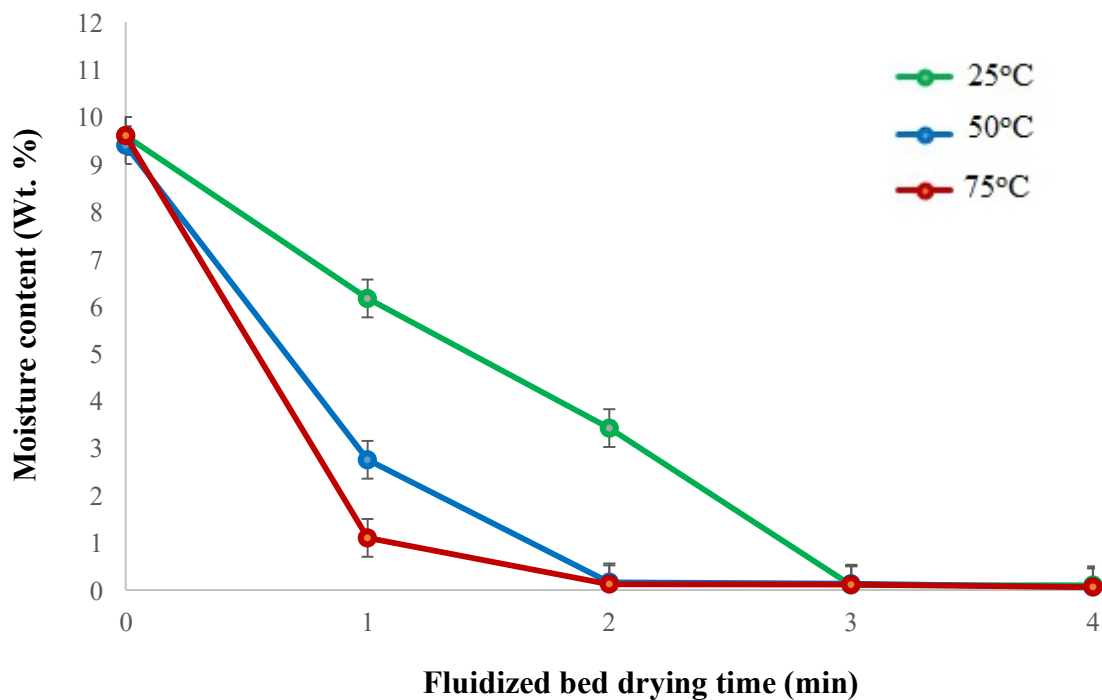


**Figure 62: Drying curves of granules produced by TSG with 150M lactose powder and water as a liquid binder at L/S of 0.1, 250 rpm and 16-KE in each screw and dried in FB at different air temperatures of 25, 50 and 75°C using an air velocity of 2 m/s.**

### 3.3.4 Granules Structure by X-Ray

CT scan x-ray tomography was used to determine the porosity and the structure of the granules dried in standard room conditions and in fluidized bed. Figure 63 shows an x-ray images of the lactose granules dried in standard room conditions (a) and in the fluidized bed (b) at a temperature of 50°C, an air velocity of 2 m/s and a drying time of 3 minute. The porosity calculation was performed using ImageJ software and as described in more details in Section 2.4.3. It was found that the porosity of the granules dried in room temperature was calculated to be approx. 40%. While the porosity for the granules dried in fluidized bed calculated to be 24%. Clearly, this indicates that the granules dried in room temperature is more porous than those dried in fluidized bed. This might be attributed to the reason that when the wet granules that produced from twin screw being subjected to agitation by the drying air in fluidized bed, the granules bounce and collide with each other and with the dryer vessel. This resulting in granules being compacted and consolidated therefore porosity decreases. It can be seen from Figure 63 (b) that one of the granules is almost has a circular shape with smooth curved edges. This is believed to be because of the collision that happening during the drying process which caused the shape to be changed to a more circular-like shape which could be the reason behind the sphericity of the fluidized bed granules is higher compared to that of the room temperature drying. This multi-collision between the granules with each other and the granules with the wall might cause chipping and abrasion to take place at the edges of some granule surface in Figure 63 (b). This could be the reason why there was an increase in the small granules (reduction in size). As seen in the granule size distribution in Figure 59 and Figure 56. The porosity study will help to understand and control the properties of the tablet properties, mainly the strength.

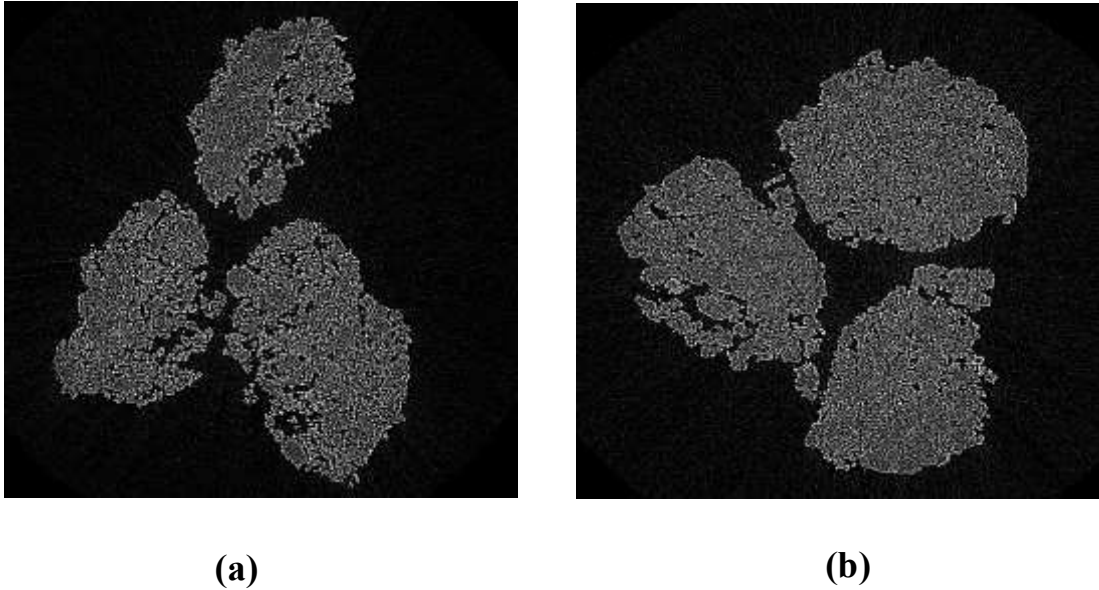


**Figure 63: X-ray images of granules produced by TSG with 150M lactose powder and water as a liquid binder at L/S of 0.1, 250rpm and 16-KE in each screw (a) Room Temperature dried granules, (b) Fluidized bed- dried lactose granules, at a temperature of 50°C, air velocity of 2 m/s and drying time of 3 minutes.**

### **3.4 Effect of Moisture on Tablet Tensile Strength**

In order to examine what effect the moisture content of granules has on tablet tensile strength, granules at different fluidized bed drying time (different moisture content) were compressed into tablets and as described in Section 2.3.3. This fluidized bed drying experiment was performed at a temperature of 25°C and air velocity of 2 m/s. The obtained tablets were then left in the humidity chamber to dry at a controlled environment of humidity and temperature (40% RH, 25°C) to be tested for their tensile strength. Figure 64 shows the relationship between the fluidized bed drying time, moisture content of the granules used to make the tablets and tablet tensile strength. The horizontal axis of Figure 64 represents the fluidized bed drying time of the granules, however, the zero time in this axis represents a wet granule taken directly from the twin-screw granulator prior to the fluidized bed drying. The vertical axis in the right-hand side represents the measured moisture content of the granules used to make the tablets; the vertical axis on the left-hand side represents the tensile strength of the tablet.

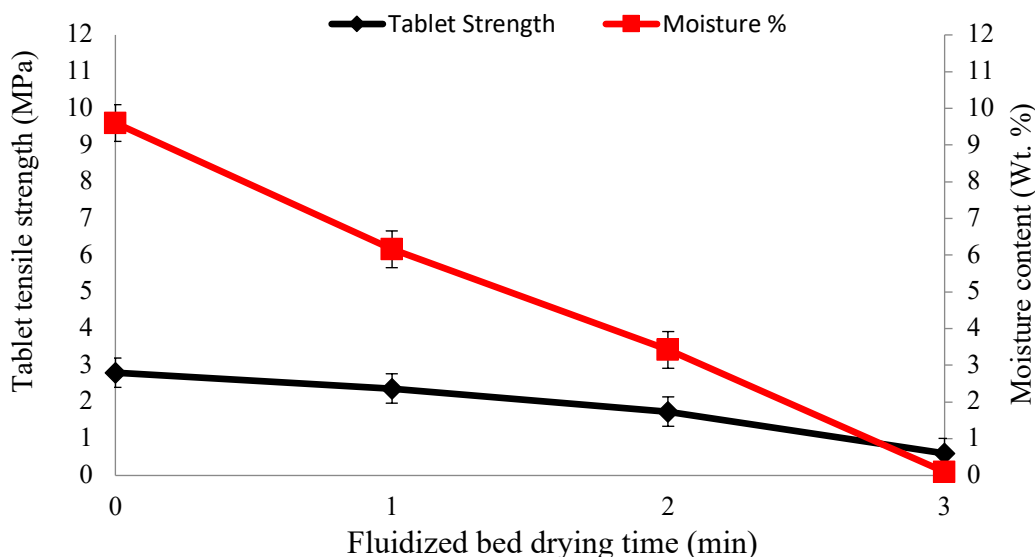


**Figure 64: Relationship between the fluidized bed drying time, moisture content of granules and tensile strength of tablet made from those granules. The granules were produced by TSG with 150M lactose powder and water as a liquid binder, L/S of 0.1, 250 rpm and 16- KE in each screw, the granules were then dried in FB at temperature of 25°C and air velocity of 2 m/s.**

It can be clearly observed from Figure 62 that as the fluidized bed drying time proceeds, the moisture content of the granule decreases. Accordingly, the tablet tensile strength decreases. In other words, higher moisture content results in a tablet with a higher tensile strength. Such findings are consistent with the result reported by (Gabbott et al., 2016), which found that higher moisture content of the granules resulted in harder tablet and concluded that the moisture content in the granules was the main and only factor that influences the tablet tensile strength when performed together with process parameters such as granulation time and granule bulk density. However, the decrease in tablet strength could be attributed to the effect of porosity and size of the granules which are both changing during the drying process in the fluidized bed which are not considered in the study of Gabbott et al. 2016. However, this needs to be investigated further to verify whether the size distribution or moisture of the granules is the dominant cause for this result.

### 3.5 Conclusion

The aim of this study is to investigate the effect of fluidized bed (FB) drying process parameters on the final properties of granules produced by twin screw granulator (TSG) and on the properties of the subsequent produced tablet from those granules. This was achieved by using the TSG to granulate lactopure lactose powder and distilled water at fixed conditions (250 rpm, L/S of 0.1) throughout this study. The produced granules were then subjected to FB drying at different air velocities (2, 2.6 and 3.4 m/s) and at different air temperatures (25, 50 and 75 °C). Granules were tested for their size distribution, sphericity, porosity and moisture content before and after drying in FB at different process parameters. It was found that the influences of the fluidized bed drying air velocity and air temperature have not only changed the moisture content of the granules, but it also had an impact on the granule size, sphericity and porosity which consequently might affect the tableability of the granules. Results have shown that the moisture content of the granules dried using high air velocity is low compared to the moisture of the granules dried at low air velocity. This is valid only in the region before the end point of the drying. Similarly, increase in drying air temperature has been found to reduce the moisture content. It was found that the decrease in the moisture content of the granules was not only as a result of the heat but also because of the compaction of the granules which is caused by the collisions of the particle with each other and with the wall of the dryer. This resulted in higher migration of liquid to the surface of the granules which make it easy for the water to evaporate. The size distribution of granules dried in FB at different air temperatures and velocities is lower than the size of the original initial granules. In addition, the porosity of the granules after FB drying is less compared to that of the initial granules from twin screw. Opposite results were observed for the sphericity of the granules where the granules after drying in fluidized bed is higher than that of the initial granules dried at room temperature. Compression of the granules before and after drying was done and the tablet strength was measured. It was found that the strength of the tablet produced by granules of different moisture content is different. The higher the drying time (less moisture content), the lower the tablet strength. The reduction in the tablet strength could be also influenced by granule size and porosity.



## **4.0 Drying in Batch Laboratory Scale Fluidized Bed: Effect of Twin-Screw Formulation Parameters**

---

### **4.1 Introduction**

The aim of this chapter is to link the properties of granules [physical (i.e., size, shape moisture content) and mechanical (structure, porosity and strength)] produced using TSG to the effect of fluidized bed drying conditions. In other words, to develop a mechanistic understanding of the granule's formation in TSG and their subsequent transformation during fluidised bed drying process. To investigate the impact of changing the L/S on the resultants granules properties and hence on the drying process, two L/S ratios were used in this study (0.08 and 0.10) and all other TSG and FB conditions were kept constant (an air temperature of 50°C, air velocity of 2 m/s). The reason behind choosing these particular liquids to solid ratios (0.089 and 0.104) is because trying to use a L/S below 0.08 tended to produce ungranulated powder and trying to use a L/S higher than 0.10 tended to produce slurry/paste.

### **4.2 Result and Discussion**

This work is conducted to link the impact on granule properties (e.g., granule size and granule structure) to variation of the L/S ratio in TSG and the inclusion of fluidized bed drying step. In this work, all other process and formulation parameters in twin screw granulation and fluidized bed drying were kept fixed. Lactose monohydrate was the granulated powder with distilled water as the liquid binder. Figure 65 below shows a flow diagram summarizing the work methodology process and parameters used for this chapter.

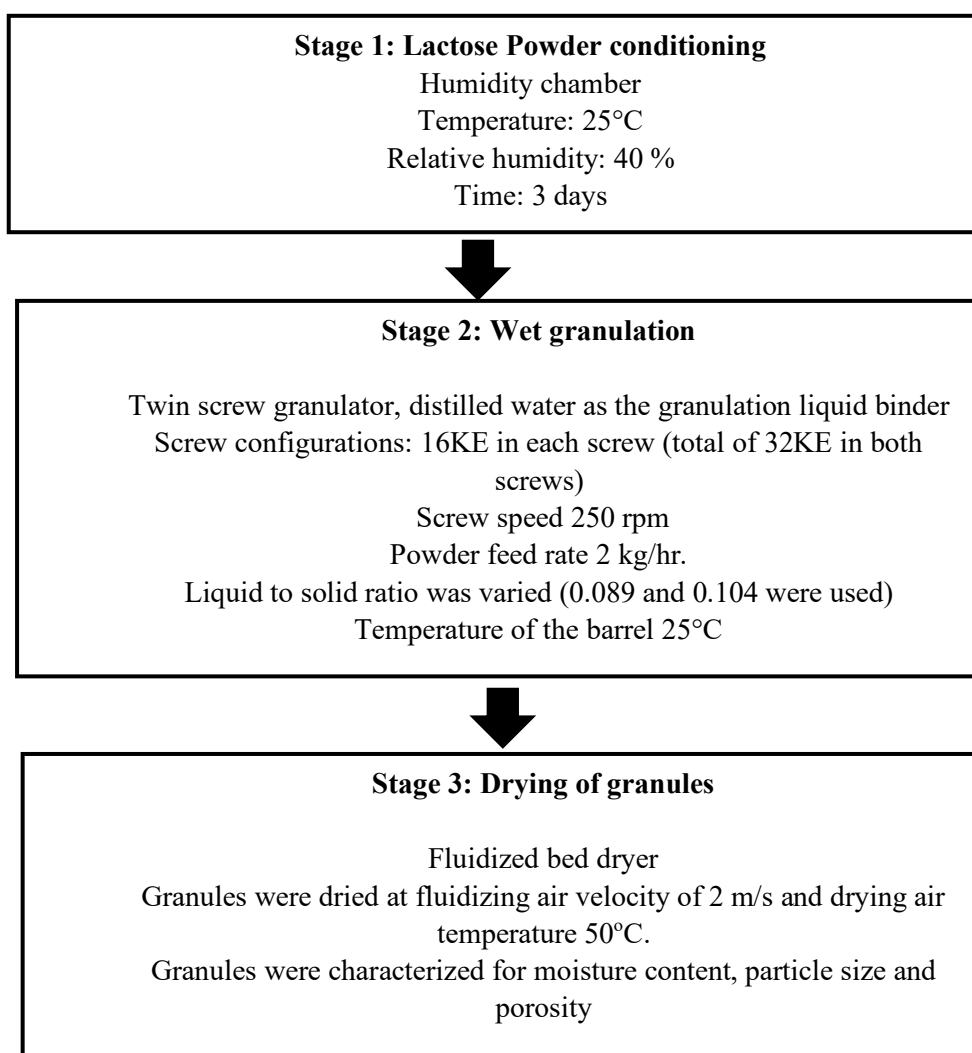


**Figure 65 :Flow diagram showing the experimental conditions and variables used in the TSG and FB in this study.**

Figure 66 shows the size distribution of granules produced by the twin-screw granulator with two different liquids to solid ratio: L/S (0.104) and L/S (0.089). It can be clearly observed from Figure 66 that both L/S ratios shows a monomodal distribution, however, there a shift to the right of the x-axis as the L/S is increased. This indicating a growth of the granules and a narrow distribution. The highest liquid to solid ratio (0.104) resulted in a uniform distribution of granules size with a peak around 1000 $\mu$ m marking approximately the  $d_{50}$  value which is presented later in this section. However, the lowest liquid to solid ratio (L/S 0.089) shifted more towards a lower granules size fraction. The  $d_{50}$  of the lowest liquid to solid ratio was 830.6 $\mu$ m. Dhenge et al. 2010, altered the same parameter (i.e.,

L/S) and they observed a granule growth as well as longer residence time which they believed it allowed more time for the fine to adhere/coalesce.

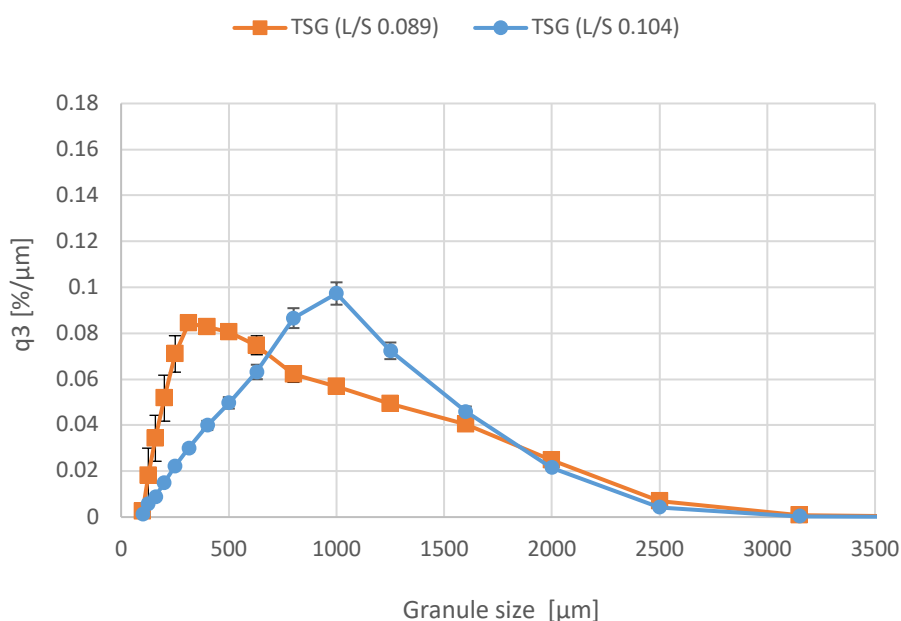


**Figure 66: Size distribution of granules produced by the Twin screw granulator using 150M lactose powder and water as a liquid binder with screw speed of 250rpm, 16-KE in each screw at two different liquids to solid ratios (L/S of 0.089 and 0.104) before FB drying.**

The porosity of granules before drying was measured with x-ray tomography and so the images for both set of experiment are shown in Figure 67.

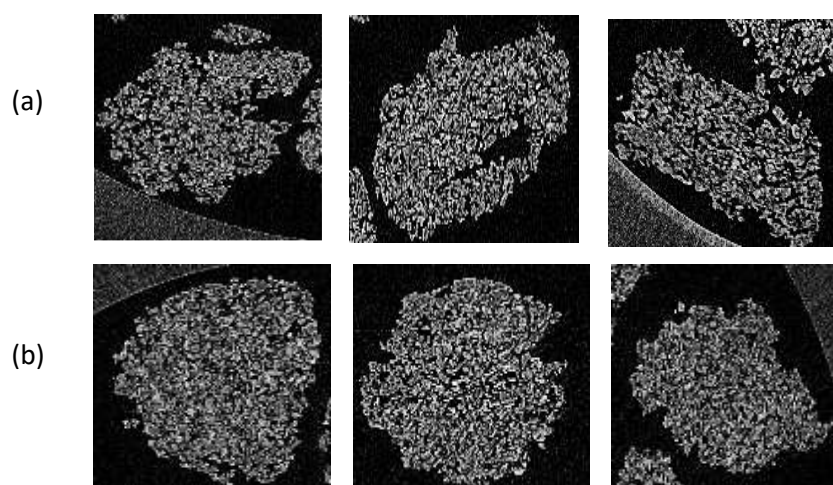
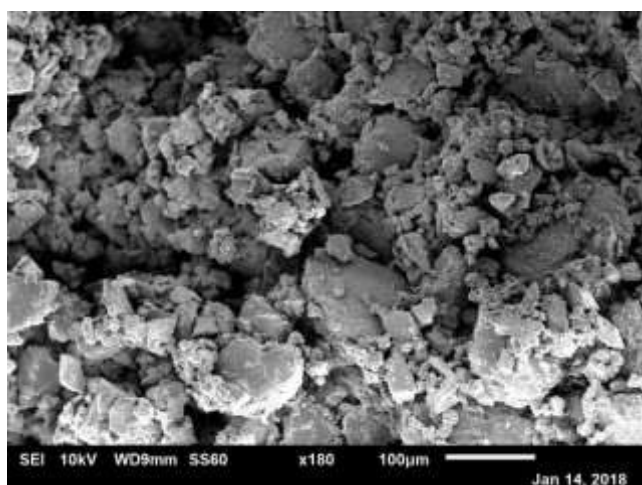


**Figure 67: X-ray tomographic images of undried granules produced by TSG with 150M lactose powder with water as liquid binder, screw speed of 250 rpm and 16-KE in each screw at two different L/S ratios (a) L/S 0.089 with a porosity of 48% (b) L/S 0.104 with a porosity of 40%.**

It can be seen from Figure 67 that granules with lower liquid to solid ratio tend to be elongated in shape with higher porosity compared the ones produced with higher liquid content they tend to be more spherical and less porous. Figure 68 shows the scanning electron microscopy of the two liquid to solid ratio used in this study. Figure 68 supports the observes in the size distribution of granules presented in Figure 66 above and in the X-ray images in Figure 67. It can be clearly seen from the SEM images that the granules produce with higher liquid content had a smoother surface and larger particle than the granules produced with the lowest liquid to solid ratio which was smaller with rougher surface. The granules with the two different liquid to solid ratios were then subjected to fluidized bed drying separately. The moisture content of each batch during drying was measured by moisture analyser and recorded as a function of drying time, obtaining a drying curve for each liquid to solid ratio experiment. Figure 69 shows the effect of increasing water content on the fluidised bed drying process of granules. It can be clearly seen that the drying was faster in the granules produced with lower liquid to solid ratio (0.089) compared to the ones produced with higher liquid to solid ratio (0.104). There are different main factors that can have an influence on the rate of evaporation during drying of material, such as the concentration of the evaporating substance in the air, drying air flow rate, material temperature and surface area of the material. However, the latter factor is the most possible reason behind the obtained trend since all other factors were kept fixed for the two drying experiments. In other words, the granules produced with higher liquid to solid ratio had larger granules as seen in the size distribution shown in Figure 66 above, and so they have lower surface to volume ratio, thus dried slower than the granules produced with lower liquid to solid ratio which had a mixture of some large, small and large granules with higher amounts of fines, this was also clearly seen in the size distribution in Figure 66 above. Fines and smaller granules have higher surface to mass ratio and so they tend to dry much faster than the larger granules, thus, the water at the core of smaller granules, tend to reach the granules surface much faster than in larger granules. This is believed to be reason behind getting this result trend. This is also in agreement with the study conducted by (Fonteyne et al., 2014) which dried granules of different size fractions by means of Karl Fischer titration.

L/S 0.089



L/S 0.104

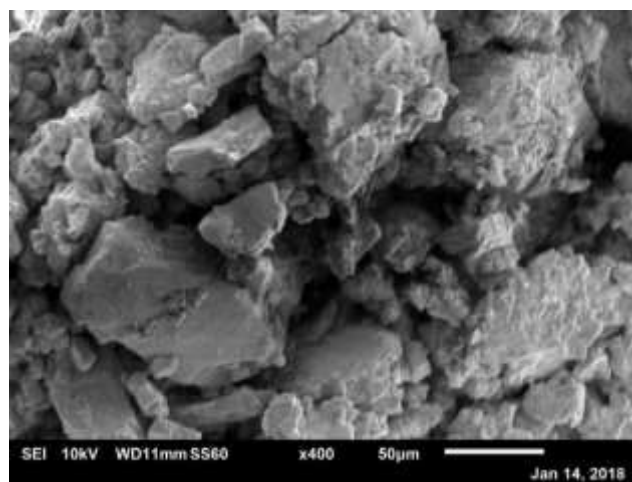
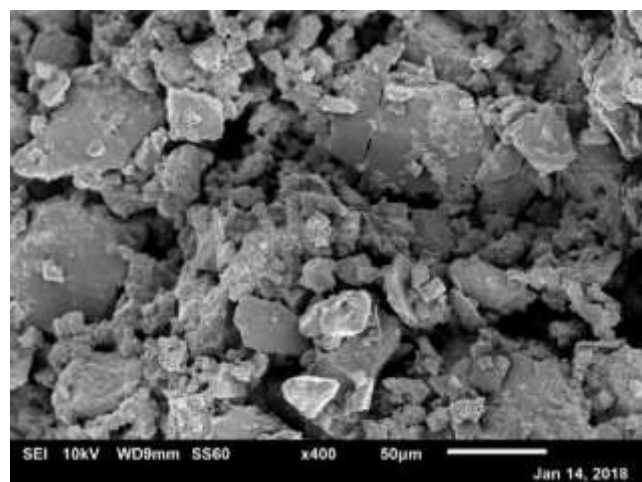
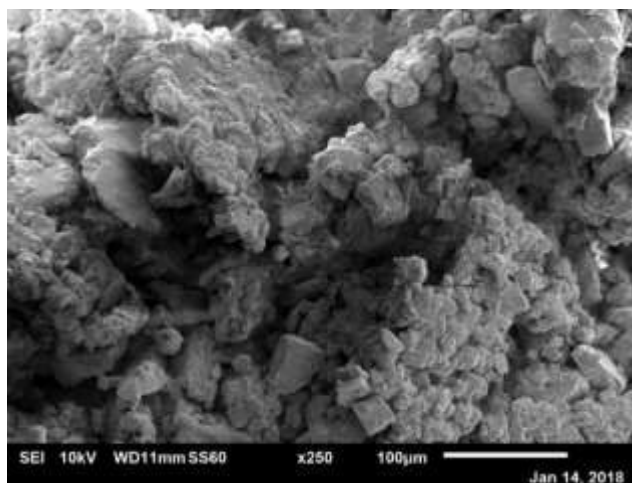
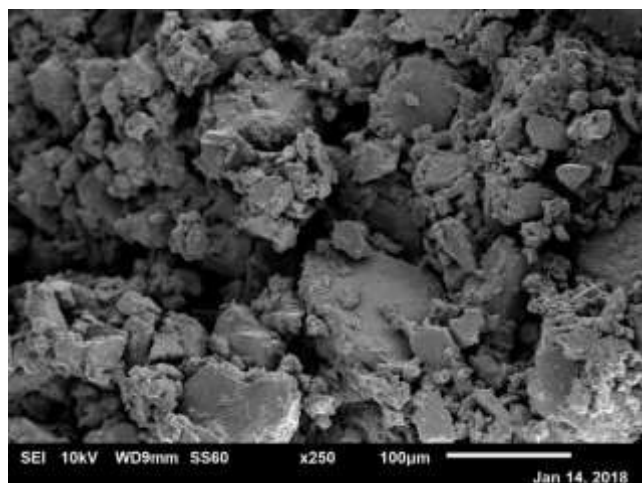
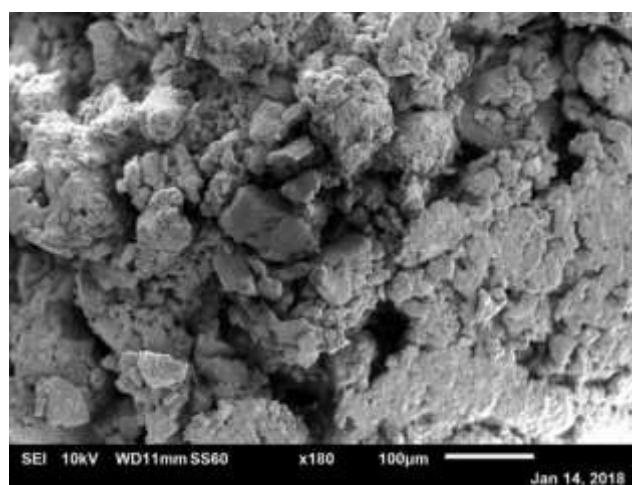
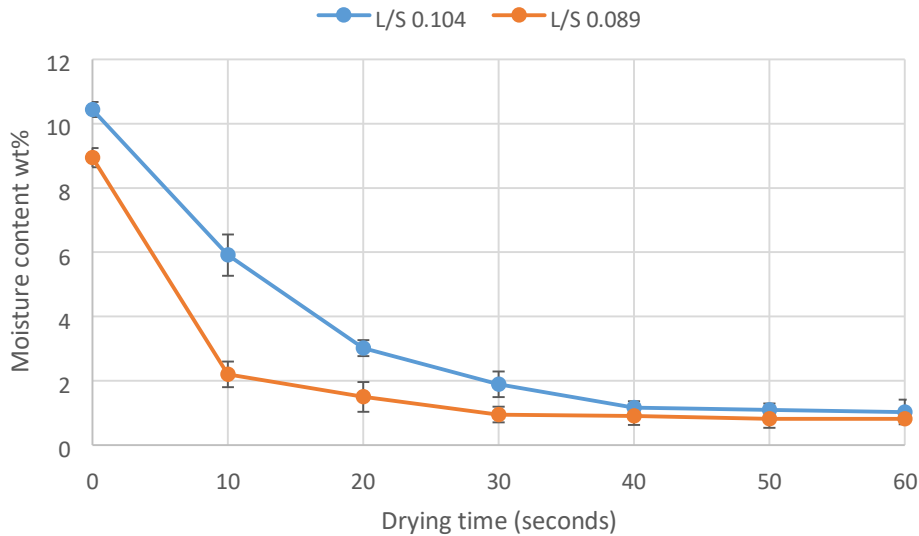


Figure 68: SEM images of granules produced by TSG with 150M lactose powder and water as a liquid binder with screw speed of 250rpm, 16-KE in each screw and at two different L/S ratio (L/S of 0.089 and L/S of 0.104) as indicated above.



**Figure 69: Effect of varying liquid to solid ratios on the FB drying of granules produced by TSG with 150M lactose powder and water as a liquid binder, screw speed of 250 rpm, 16-KE in each screw and dried in FB at temperature of 50°C and an air velocity of 2m/s.**

The reason why Figure 62 and Figure 69 are different with respect to comparing the blue drying curves which were done at similar conditions (i.e., L/S 0.10 and air velocity in FB 50°C) is that in Figure 62, samples for offline moisture measurements were taken out of fluidized bed dryer every 1 minute in which this was done by opening the FB, however, in Figure 69 samples were taken every 10 seconds, which is obviously shorter time interval than the 1 minute, this shorter time interval (10 seconds) disturbed the heat stability of the FB dryer and contributed to higher reduction in moisture content compared with the Figure 69. Figure 70 shows the size distribution of the granules produced at different liquid to solid ratio before and after fluidized bed drying. In both Figures (a and b), the blue curve represents the size distribution of granules produced with twin screw prior to fluidized bed drying. And the orange curve represents the size distribution of granules after fluidized bed drying process. It can be clearly seen from Figure 70 that the granules produced at the lower liquid to solid ratio shows more reduction in size than the one produced with higher liquid content. This is attributed to the reason that higher liquid content resulted in granules with more liquid bridges and therefore stronger granules that when subjected fluidized bed drying will have more resistance to breakage than the case in the granules produced with lower water content. The granules produced with lower water content tend to be more fragile and weaker due to the absence of more liquid bridges and therefore will have more reduction in granule size. Figure 71 shows the  $d_{10}$ ,  $d_{50}$  and  $d_{90}$  before and after drying

for the two different liquid to solid ratio used (0.089 and 0.104) respectively. The overall trend in Figure 71 is that as the liquid content increase, the granule size increases, however, after the granules were subjected to fluidized bed drying, a clear reduction in size occurs and that's can be attributed to the attrition and breakage that took place during fluidized bed drying. The reason why more breakage occurred in granules batch produced with the lowest moisture content was explained above as its to do with the formation of liquid bridges between particles and the strength of the granules.

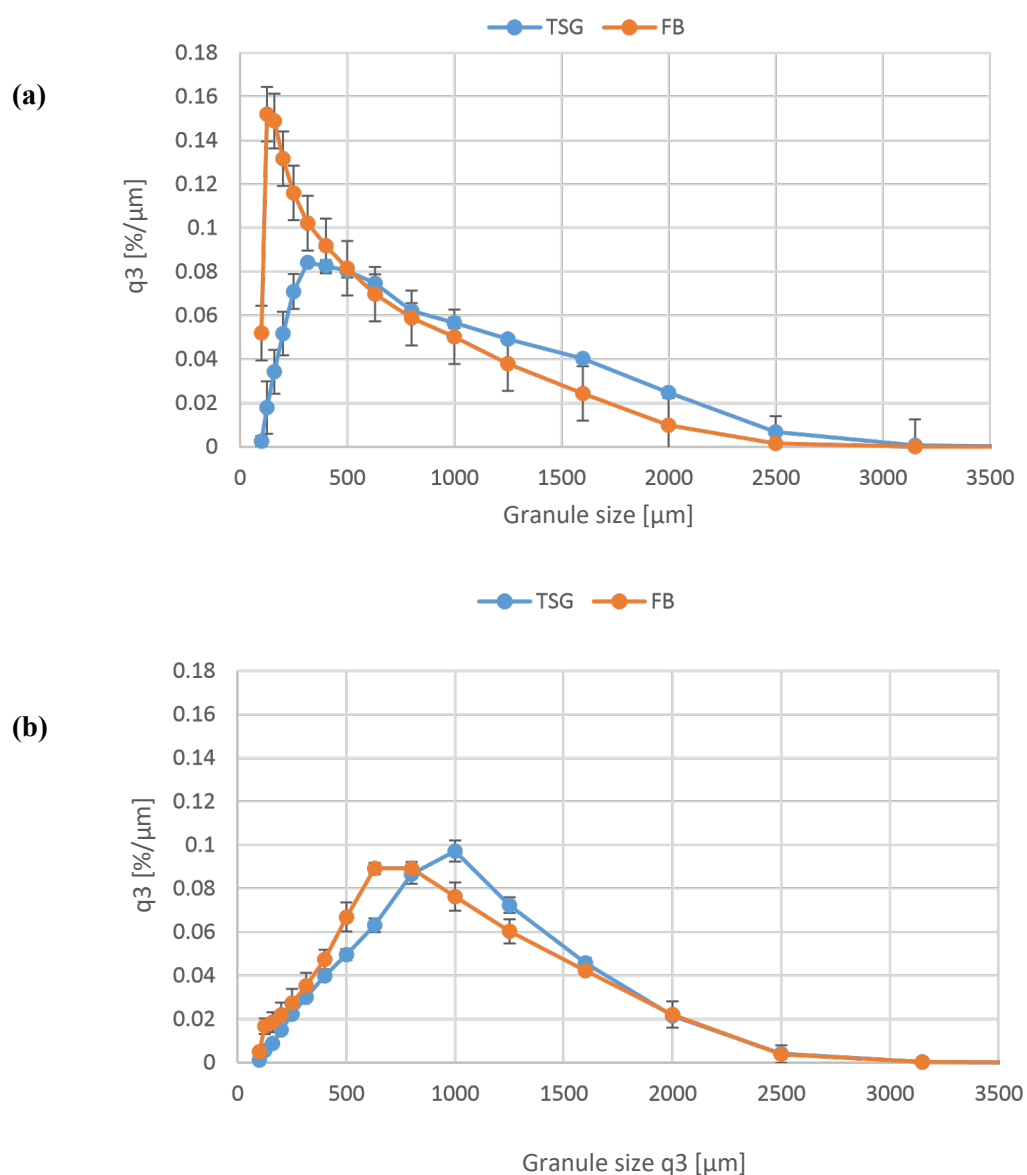


**Figure 70: Size distribution of granules produced by TSG with 150M lactose powder and water as a liquid binder at a screw speed of 250 rpm, 16-KE in each screw at two different liquids to solid ratios before and after fluidized bed drying (temperature of 50°C and an air velocity of 2m/s. (a) L/S 0.089 (b) L/S 0.104.**

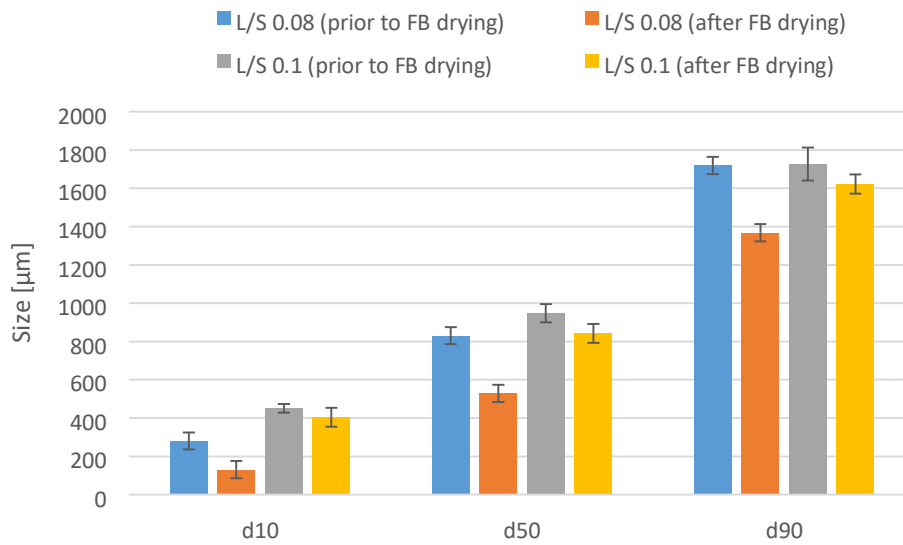


**Figure 71: Particle size (d10, d50, d90) of the batch of the granules that produced by TSG with 150M and water as liquid binder, 250 rpm, 16-KE in each screw at two different liquids to solid (L/S 0.089 and 0.104) and dried in FB at a temperature of 50°C and an air velocity of 2m/s.**



## **4.3 Effect of Viscosity of Granulation Liquid Binder**

### **4.3.0 Introduction**

Binder viscosity and concentration has a significant impact on the size distribution and the flowability of material through the twin-screw granulator. Increasing the liquid binder viscosity increases the torque in the screw, this leads to a reduction to the flow as the viscous binder produced big and strong granules that resist conveyance within the barrel. To date, there are no studies found in literature to link the properties of granules produced with twin screw granulator at different binder viscosity to the drying process in the fluidized bed, namely the subsequent effect on dried granules physical and mechanical properties. Therefore, the aim of this work is to provide a linkage between the properties of granules resulted from using different binder viscosities at the twin-screw granulation and the fluidized bed drying process for those granules. To fulfil this objective, the other formulation and process parameters during both granulation and fluidized bed drying was maintained fixed (250 rpm for the screw speed, 2kg/hr for the powder feed rate, 50°C for the drying air temperature and 2 m/s for the drying air velocity).

### **4.3.1 Results and Discussions**

Lactose monohydrate was used as the primary powder and HPC at different concentrations was used as the liquid binder in this work. An experiment with water as liquid binder was also conducted in this section to compare it with the result of the other HPC solutions of different viscosity. HPC solution of 2,5,10 and 15% concentration were prepared and the viscosity of these solution and water were measured with the Rheometer. Figure 72 below shows a flow diagram summarizing the work methodology process and parameters used for this chapter.

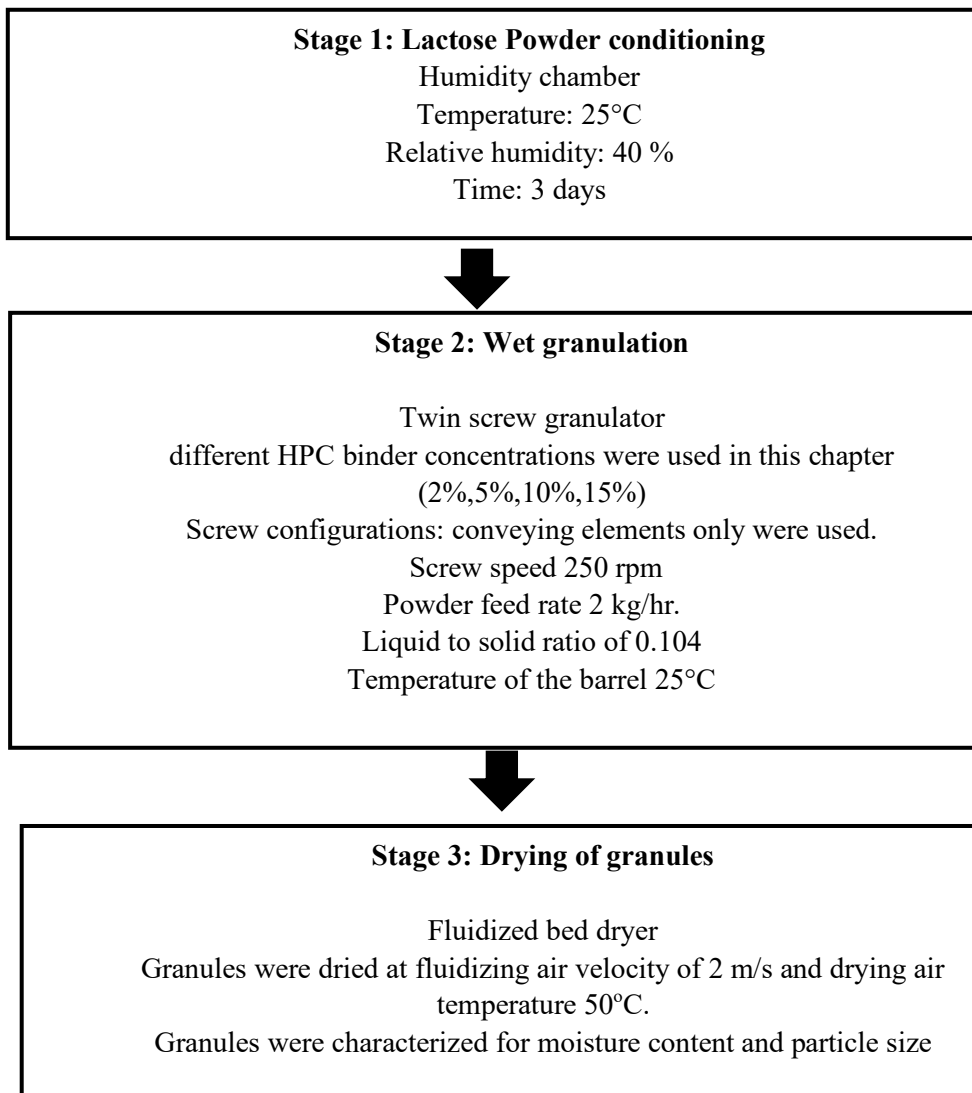


**Figure 72: Flow diagram showing the experimental conditions and variables used in the TSG and FB in this study.**

Figure 73 shows shear viscosity versus shear rate for water and different HPC solution concentrations. Figure 74 shows the average shear viscosity for different concentrations of HPC solution. The mean viscosity as shown in Figure 74 was calculated by averaging all the shear viscosities values (Pa s) across all the shear rate values (0-1000  $s^{-1}$ ) for every single concentration. In the x-axis, 0% represent the liquid binder with no HPC (distilled water only) which had the lowest viscosity of 0.001 Pa-s.

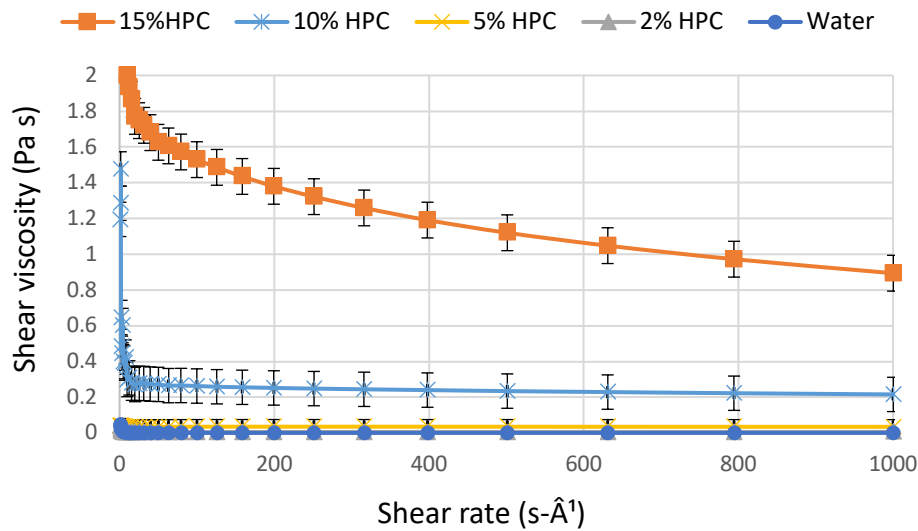


Figure 73: Shear viscosity versus shear rate for water and different HPC solution concentrations

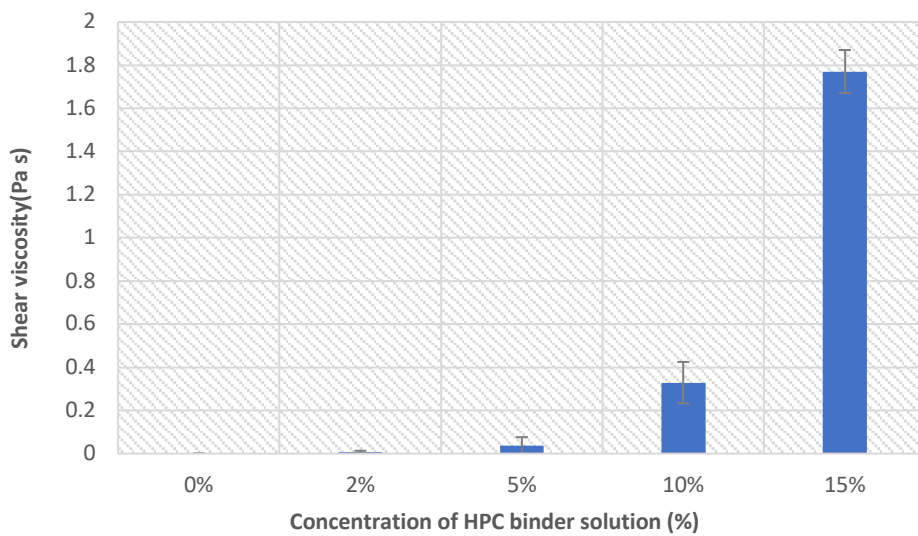
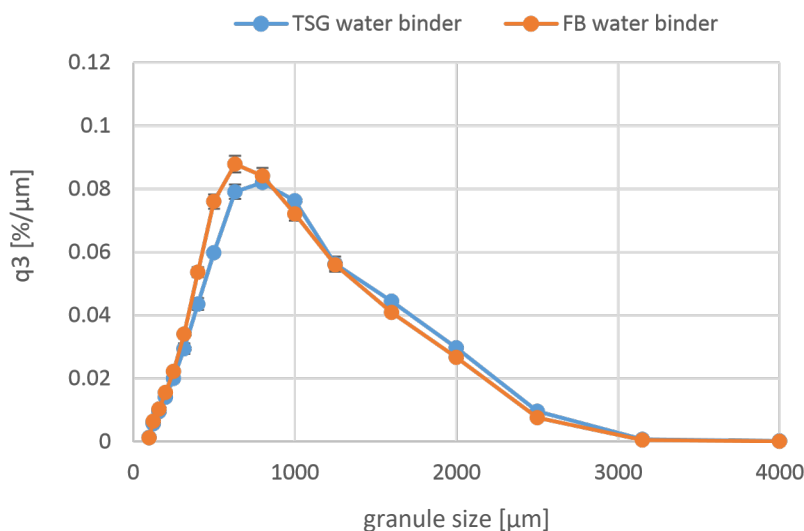


Figure 74: The average shear viscosity for different concentrations of HPC solution including distilled water.

Granulation with different HPC liquid binder concentration was conducted followed by fluidized bed drying for each experiment separately. Figure 75 shows the size distribution of granules before and after fluidized bed drying when water was used as the liquid binder during granulation. Figure 76-79 show the size distribution of granules when HPC solution was used as the liquid binder at different

concentrations 2,5,10 and 15% respectively. From Figure 75, it can be clearly seen that there was a minimal difference between the size distribution of granules before and after fluidized bed drying and that was when water was the liquid binder. However, a difference in the granule size distribution started to increase as the concentration of HPC increases and therefore as the viscosity of these solution increases. The granules produced with the lowest viscosity binder had lower reduction in granule size during fluidized bed drying compared with the granules produced with the highest viscosity binder which had higher reduction in granules size during the fluidized bed drying process. This suggests the occurrence of breakage and attrition of granules during the fluidized bed process. The breakage and attrition of granules was found to increase as the viscosity of the liquid binder used during twin screw granulation increases. The granule size increased more noticeably as the binder viscosity increased. However, the binder distribution within these granules may have not been sufficient to provide constant strength throughout the granule and hence results in granules with weaker edges that susceptible to attrition and breakage during drying in fluidized bed. This can be supported by considering all the Figures (76-79); where it can be looked at the distribution of large end (i.e., the right of the x-axis) and it can be seen the lower the binder viscosity, the smaller change, whereas the higher the viscosity of the binder, the high the drop in that region.



**Figure 75: Size distribution of granules produced by TSG with 150M lactose powder and water as liquid binder (0% HPC) at 250 rpm, L/S of 0.10 and conveying elements only. This plot shows the PSD of granules before and after fluidized bed drying which was performed at a temperature of 50°C and an air velocity of 2m/s.**

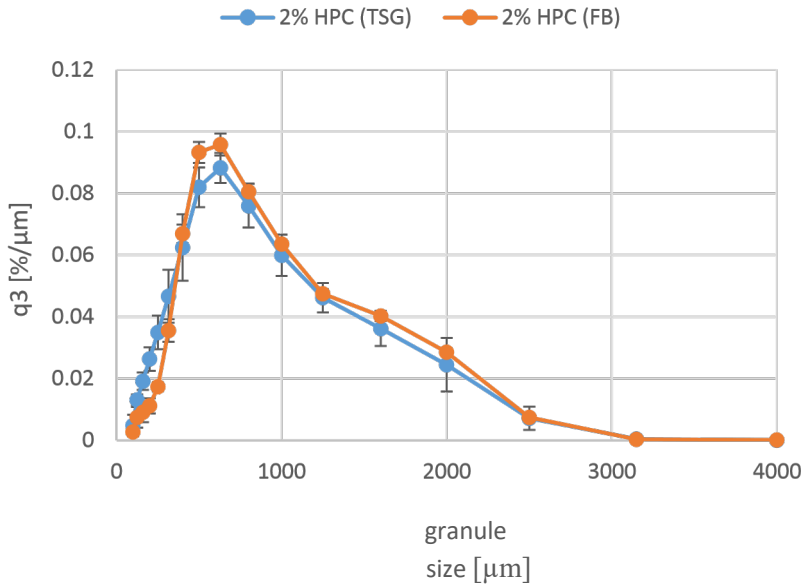


**Figure 76:** Size distribution of granules produced by TSG with 150M lactose powder and HPC as liquid binder (2% HPC) at 250 rpm, L/S of 0.10 and conveying elements only. This plot shows the PSD of granules before and after fluidized bed drying which was performed at a temperature of 50°C and an air velocity of 2m/s.

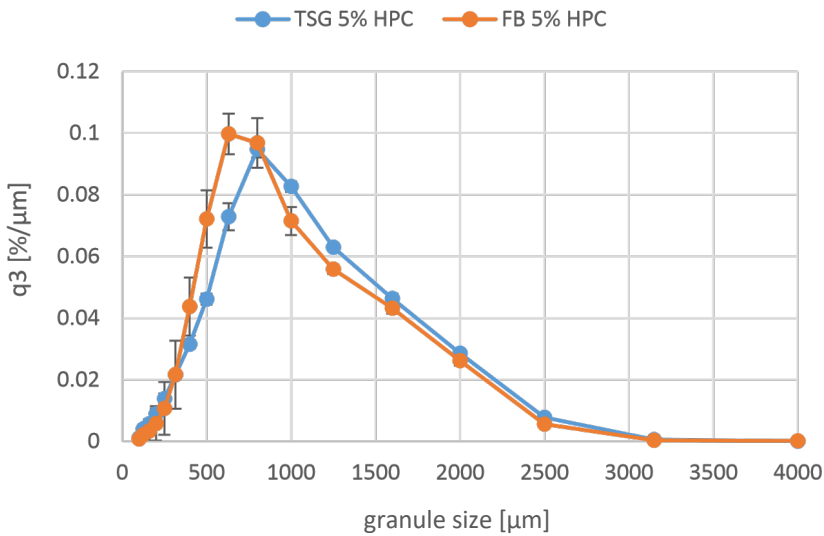


**Figure 77:** Size distribution of granules produced by TSG with 150M lactose powder and HPC as liquid binder (5% HPC) at 250 rpm, L/S of 0.10 and conveying elements only. This plot shows the PSD of granules before and after fluidized bed drying which was performed at a temperature of 50°C and an air velocity of 2m/s.

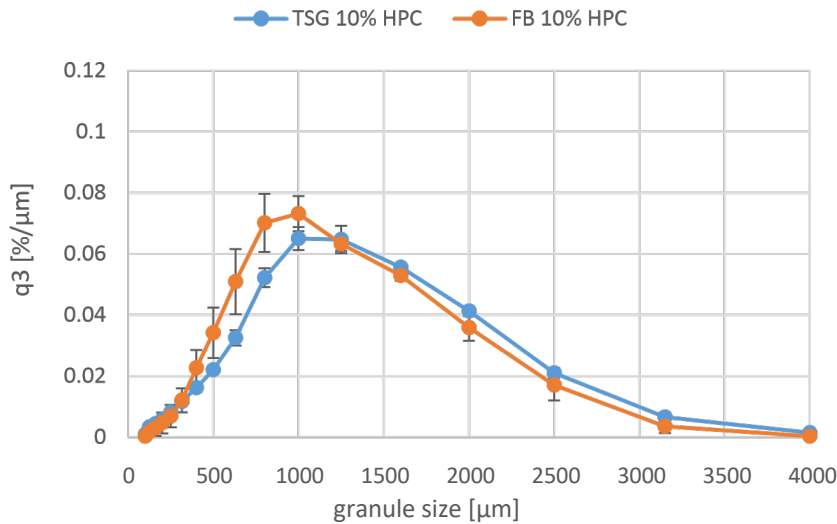


**Figure 78:** Size distribution of granules produced by TSG with 150M lactose powder and HPC as liquid binder (10% HPC) at 250 rpm, L/S of 0.10 and conveying elements only. This plot shows the PSD of granules before and after fluidized bed drying which was performed at a temperature of 50°C and an air velocity of 2m/s.

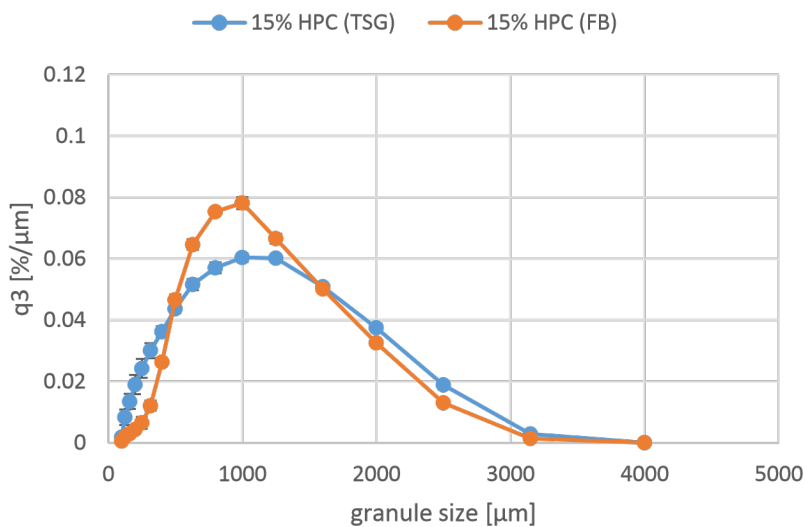


**Figure 79:** Size distribution of granules produced by TSG with 150M lactose powder and HPC as liquid binder (15% HPC) at 250 rpm, L/S of 0.10 and conveying elements only. This plot shows the PSD of granules before and after fluidized bed drying which was performed at a temperature of 50°C and an air velocity of 2m/s.

Figure 80 shows the  $d_{10}$ ,  $d_{50}$  and  $d_{90}$  before and after drying as the binder viscosity increases. It can be clearly seen that the median granules size is increasing as the HPC liquid binder viscosity increases.

However, it reduced when the highest viscosity liquid binder was used. As previously seen in Figure 79 above, the liquid binder which was made with 15% concentration of HPC, had the highest viscosity and there was significant difference between the 10% and 15% liquid binder viscosity, and that explained why the median size of granules reduced only at the highest liquid binder viscosity as the

penetration of this liquid into the lactose powder was much slower than the others liquid binders, resulting in forming loose small granules. The median granule size when the water only was used as the liquid binder was bigger than median size of granules when the HPC solution was used. The finding above is supported by (Dhenge et al., 2013).

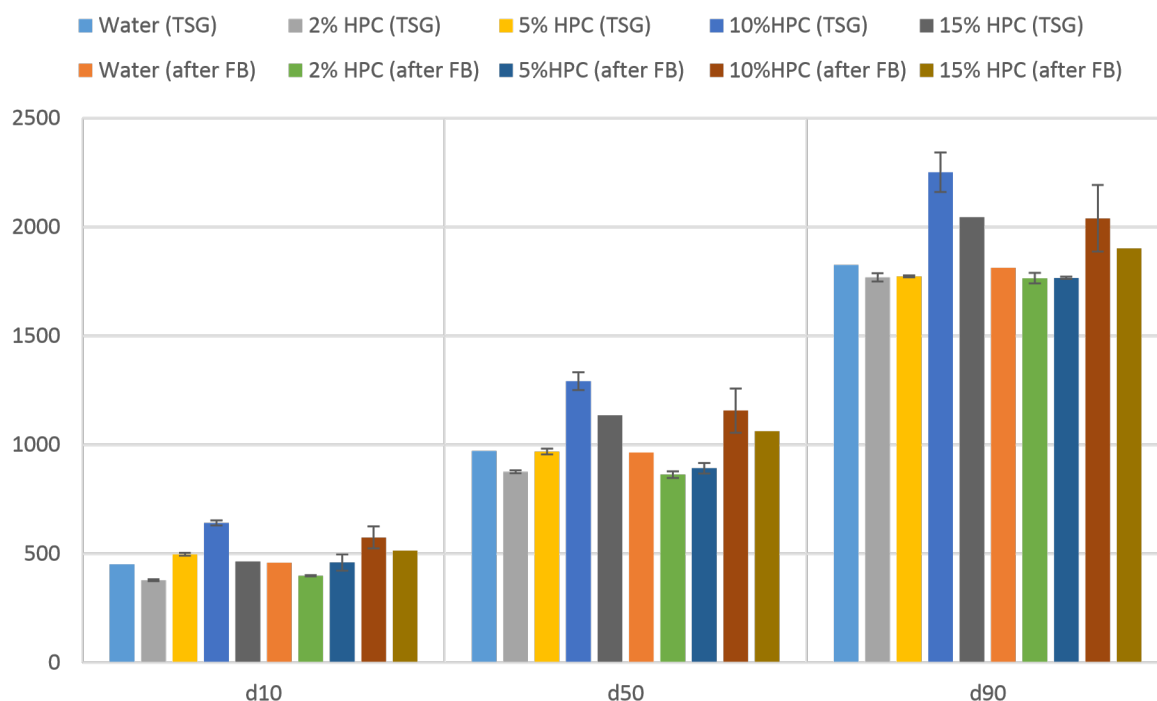


**Figure 80: PSD (d10, d50, d90) of granules produced by TSG using 150M lactose powder with water and HPC of different concentrations were used as a liquid binder, the screw speed was 250rpm and screw configuration of conveying element only. This Figure shows PSD before and after FBD which was performed at a temperature of 50 and an air velocity of 2m/s as binder concentration varies.**

#### 4.4 Conclusion

A mechanistic understanding of the granule’s formation in TSG as the liquid to solid ratio and binder viscosity varied and the subsequent transformation of those granules during fluidised bed drying process was attained. The extent of granules breakage taking place during the fluidized bed drying process was found to be significantly dependent on the liquid to solid ratio and binder viscosity used during the twin-screw granulation stage. Using higher liquid to solid ratio (0.104) appeared to produce stronger granules with less fines and porosity due to the fact that higher liquid to solid ratio stimulate higher granules growth and more liquid bridges. This caused ultimately the granules to have had

higher resistance to breakage in fluidized bed during drying compared with the lowest liquid to solid ratio which result in worse breakage. After conducting this work, it can be also, concluded that the drying regime can be optimised by controlling the initial granules properties such as size distribution. For both studies linking the twin-screw granulation formulation parameters to the fluidized bed drying process of granules, was generally found to affect the drying curves of granules. The granules batches produced with higher amounts of fines, bigger proportion of small granules and higher porosity (i.e., in the cases of using lower L/S ratio) tended to dry much faster than the granules batch produced with less amounts of fines, bigger proportion of large granules and lower porosity (i.e., higher L/S ratios). This was mainly attributed to the reason that the fines or small particles dries much faster than large particles due to its higher surface to volume ratio and that the water in the inside of the small granules will reach out to the surface faster than in the large granules. Therefore, the surface area availability is the limiting factor in getting such trend.



## 5.0 Drying in Batch Laboratory Scale Fluidized Bed: Effect of Twin-Screw Process Parameters

### 5.1 Introduction

This chapter of work attempts to link the impact of changing the screw configuration on the properties of granules during twin screw granulation to their consecutive impact on the fluidized bed drying process and so on the granule's properties. Four screw configurations are used in this study. Figure 81 shows the experimental conditions and variables used in the TSG in this study. The process variables at the fluidized bed dryer (an air temperature of 50°C and an air velocity of 2 m/s) were all kept constant in order to determine the effect of changing the screw configurations at the twin-screw granulator.

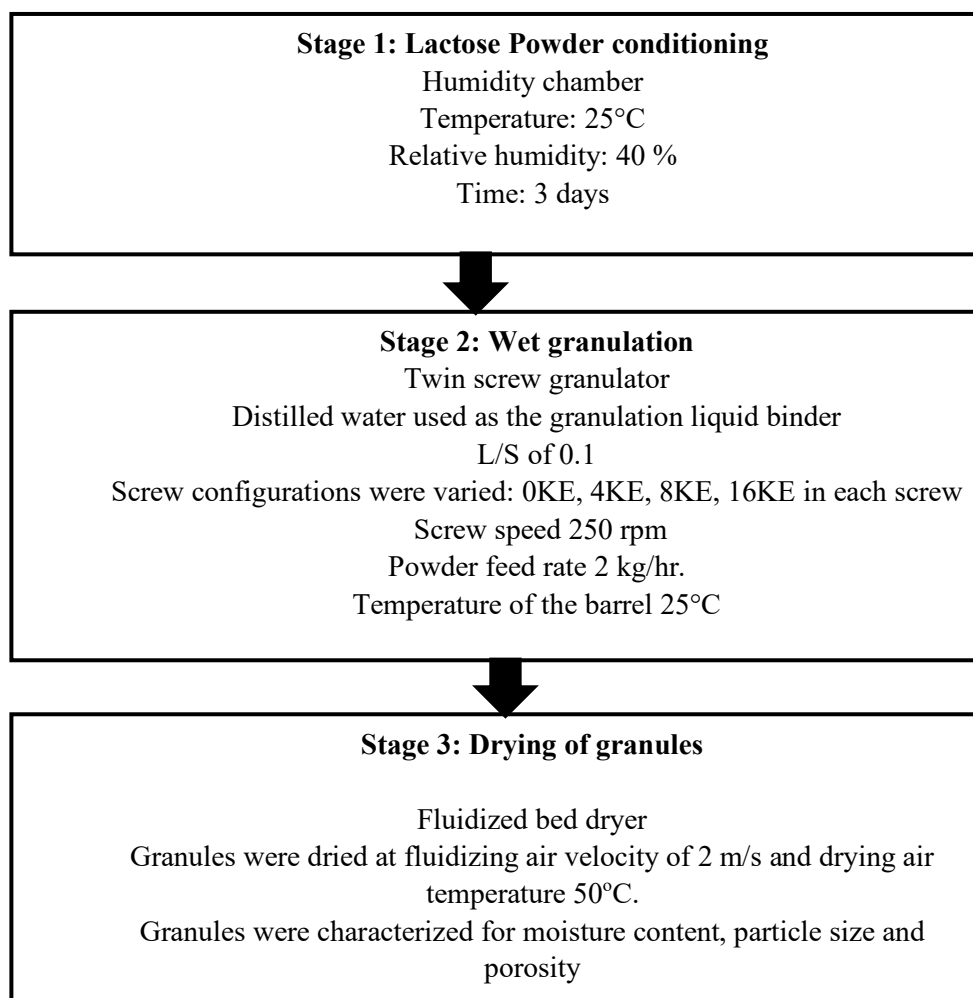


**Figure 81: Flow diagram showing the experimental conditions and variables used in the TSG and FB in this study.**

## 5.2 Screw Configuration

Figure 82 shows the four different screw configurations used in this study. These were, 4 kneading elements in each screw as shown in Figure 82 (a), 8 kneading elements in each screw as shown in Figure 82 (b) and 16 kneading elements in each screw as shown in Figure 82 (c) and conveying elements only (0 kneading elements) in each screw as shown in Figure 82 (d). The kneading discs were placed at 60° pitch. The length of the screw elements was kept fixed (16 mm).

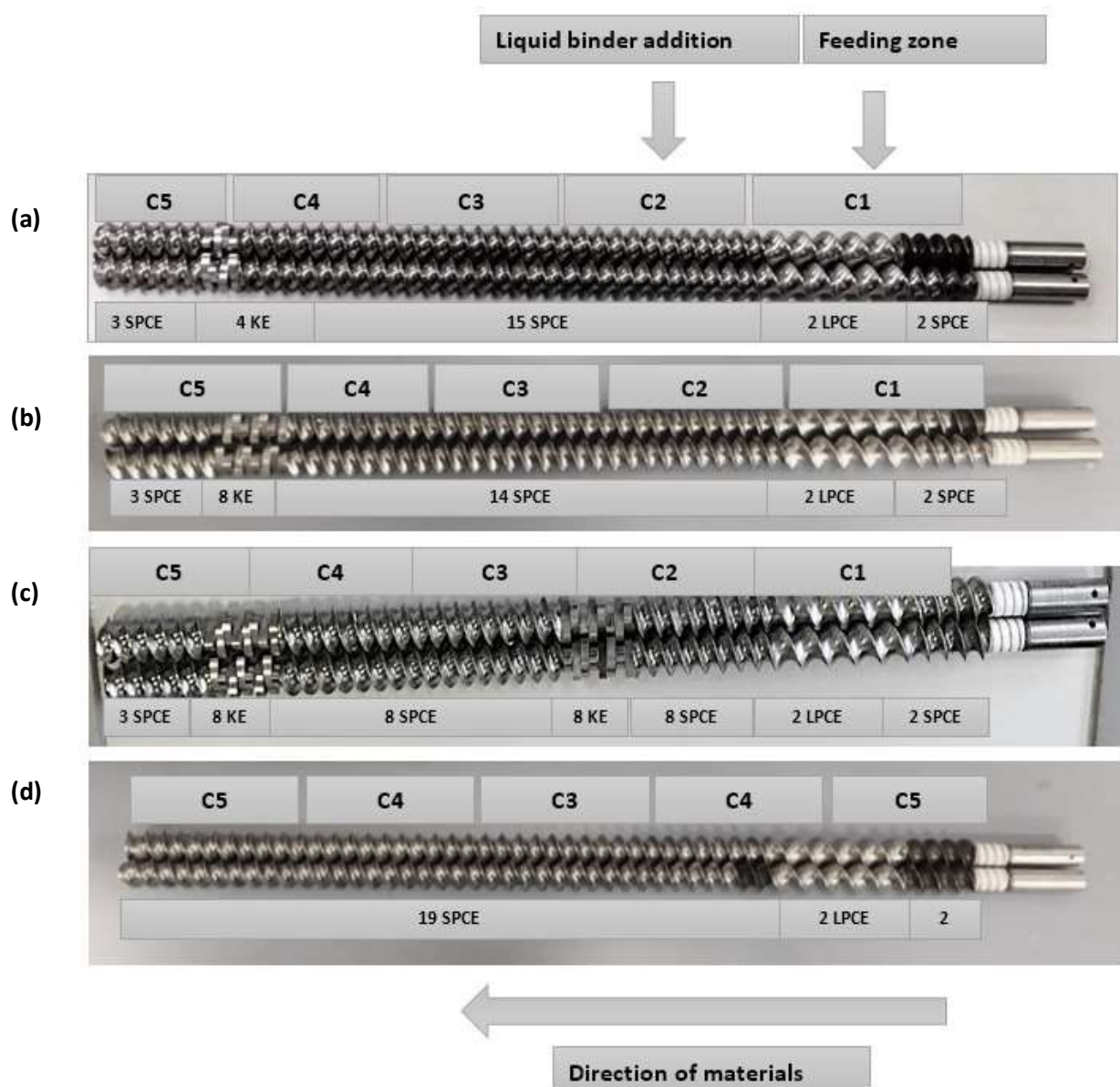


**Figure 82: Screw configurations used in this study with (a) 4KE in each screw (b)8 KE in each screw (c) 16 KE in each screw (d) conveying elements only (0KE). The angle at which the Kneading element are placed is 60°.**

### 5.3 Results and Discussions

Figure 83 shows the size distribution of granules produced at different screw configuration before fluidized bed drying. It can be clearly seen that as the number of kneading elements increases in the screw configuration, the size distribution of granule shifted towards big sized granules. So, for the granules produced with conveying elements only, where no kneading elements were presented in the screw configuration, the size distribution of granules had the highest proportion of small granules.

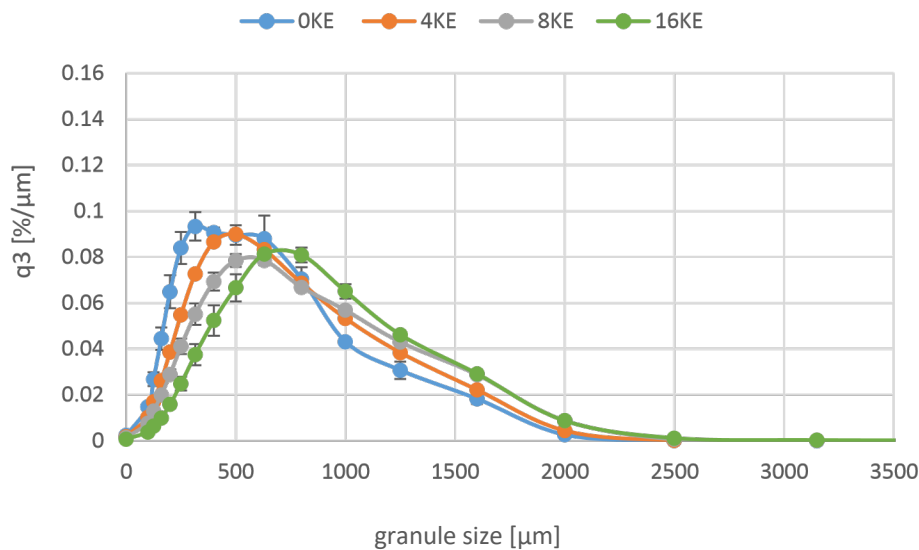


**Figure 83: Size distribution of granules produced by TSG using 150M lactose monohydrate powder with water used as the liquid binder, L/S of 0.1, screw speed of 250 rpm at four different screw configurations (conveying elements only; 0KE, 4KE, 8KE, 16KE in each screw). This Figure shows the PSD of granules before fluidized bed drying.**

This can be attributed to the reason that presence of kneading elements in the screw configuration would enhance the mixing between the liquid binder (water) and powder (lactose). Hence, resulting in higher contact between the primary particles and liquid binder (water) and so this assist with dissolving lactose partially and creating liquid bridges, resulting the granules to grow in size. So, the higher the number of kneading elements used in the screw configuration, the higher the energy imparted into the materials, and therefore the higher the mixing of liquid binder with powder consequently results granules to grow in size.

The opposite scenario occurs when using less kneading or only conveying elements. So, in the case of using only conveying elements, a much lower energy can be imparted into the material to improve the mixing between the liquid binder which is water in this study and the lactose powder. Thus, using only conveying or less kneading elements tend to result in poor spreading of the liquid binder (water) and therefore resulting in poor compaction which lead to formation of smaller weak granules. This is in agreement with the finding of Saleh et al. (2015). Moreover, if Figure 83 above were to be compared with Figure 57 (a) in chapter 3 (section 3.31), Figure 83 above show bigger granules (before drying) than the granules in Figure 57 (a) before drying although both performed at similar process conditions. The only reason for this could be due to the difference in time interval when opening of FB for taking samples for measurement of moisture. In Figure 83, the FB was opening every 10 seconds rather every 1 minute (as in Figure 57 a). Figure 84 shows the effect of changing the screw configurations on the particle size ( $d_{10}$ ,  $d_{50}$  and  $d_{90}$ ). It can be clearly seen that increasing the kneading elements in the configurations, was found to increase the granules size and that trend was observed in all the three particle sizes ( $d_{10}$ ,  $d_{50}$ , and  $d_{90}$ ).

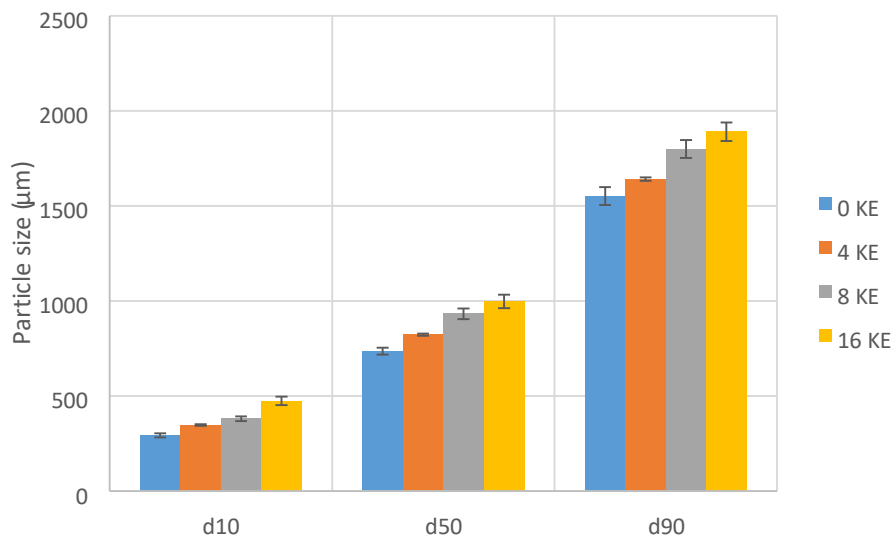
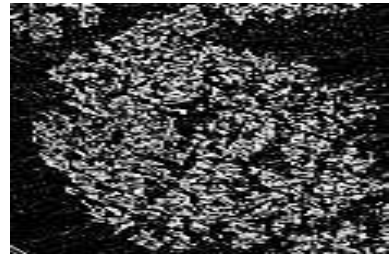
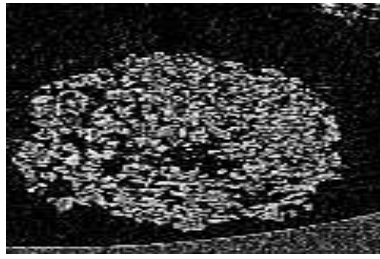
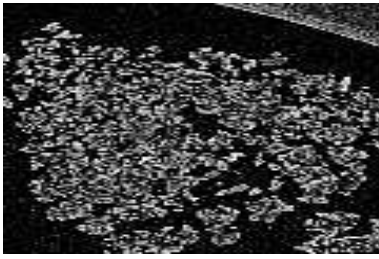
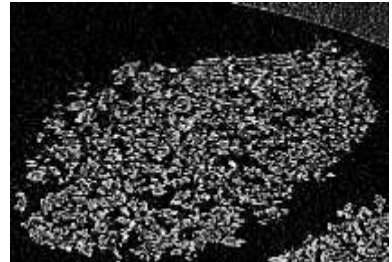
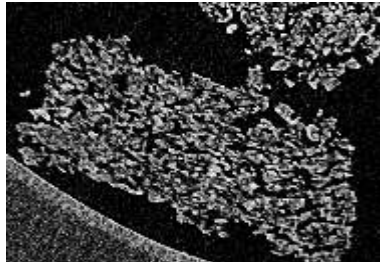
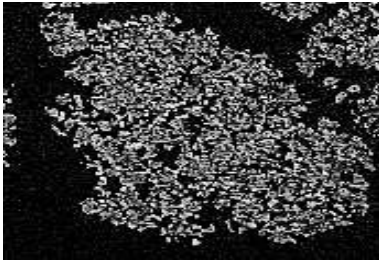


**Figure 84: Particle size ( $d_{10}$ ,  $d_{50}$  and  $d_{90}$ ) of granules produced by TSG using 150M lactose monohydrate powder with water used as the liquid binder, L/S of 0.1, screw speed of 250 rpm at four different screw configurations (conveying elements only; 0KE, 4KE, 8KE, 16KE in each screw). This Figure shows the PSD of granules before fluidized bed drying.**

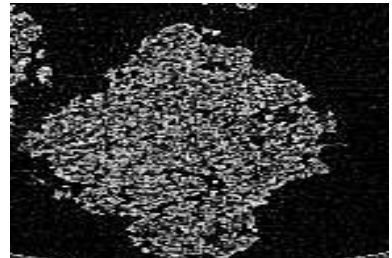
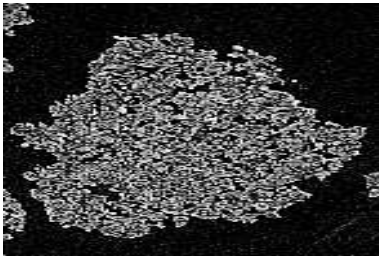
Granule's porosity measurement was then conducted to support the findings above. X-ray tomography was used to scan the granules in the  $d_{50}$  size class. X-ray tomographic images of granules produced using lactose granules at different screw configurations are shown in Figure 85. The images were then processed with ImageJ software to calculate the porosity of the granules. The result of the calculated porosity is shown in Figure 86, it can be seen from this Figure that the granules porosity was significantly affected by altering the screw configurations and that is well support the finding above. This finding also in agreement with the study conducted by Djuric and Kleinebudde, 2008. The highest number of kneading elements used in this study produced the least porous granules. And screw configuration used without any kneading elements (conveying only) produced the most porous granules in this study. This can be attributed to reason explained earlier in this chapter that is more kneading elements tend to put higher energy into the material and thus more compaction and improved mixing of the lactose powder with the liquid binder is achieved where the voids and gaps between particles are closed producing less porous granules. Screw configuration with less kneading element or conveying elements only tend to impart a minimum energy into the material resulting in poor spreading and mixing of the liquid binder into the powder forming weak porous granules.



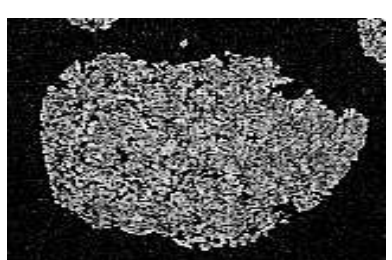
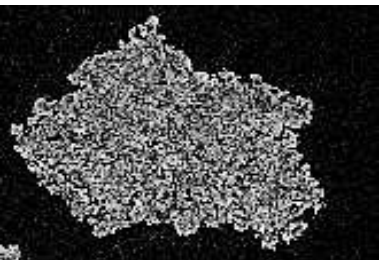
(a) 0 KE (Conveying elements only)



(b) 4 KE (total of 8 kneading elements)



(c) 8 KE (total of 16 kneading elements)



(d) 16 KE (total of 32 kneading elements)

**Figure 85: X-Ray images of granules produced by TSG using 150M lactose monohydrate powder with water used as the liquid binder, L/S of 0.1, screw speed of 250 rpm at four different screw configurations (a)conveying elements only;0KE (b) 4KE (c) 8KE (d) 16KE in each screw. These are X-Ray images of granules before fluidized bed drying.**

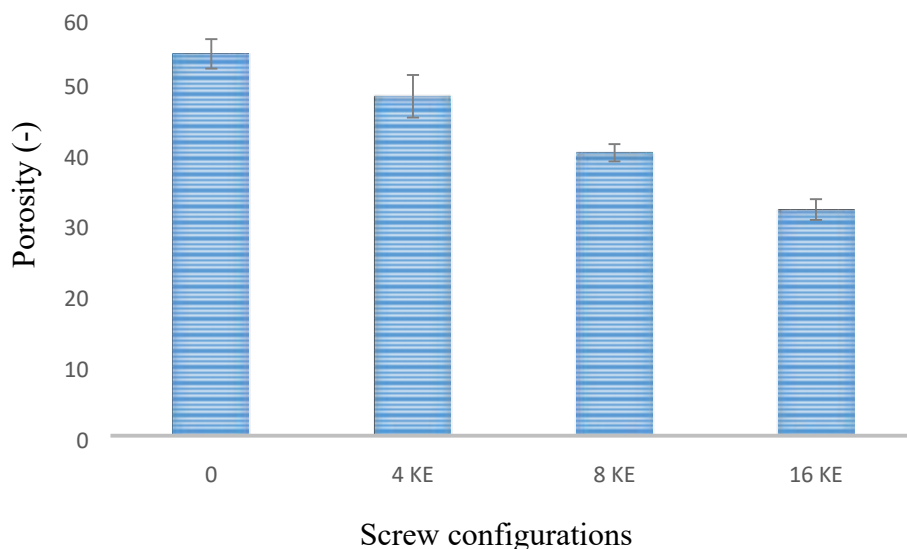


**Figure 86: Average porosity of granules produced by TSG using 150M lactose monohydrate powder with water used as the liquid binder, L/S of 0.1, screw speed of 250 rpm at four different screw configurations (conveying elements only; 0KE, 4KE, 8KE, 16KE in each screw). The porosity was measured by using X-Ray topography for granules before fluidized bed drying.**

As well as to the porosity characterization, granules were then taken to the scanning electron microscopy (SEM) to look at their structure and surface topography as seen in Figure 87. It can be clearly seen from the SEM images that the granules produced with only conveying elements where no kneading elements existed were the roughest with bigger voids and gaps and as the number of kneading elements existed in the screw configuration increases, the granules become softer and more deformed with smaller voids and gaps existed. This supports the size distribution and the porosity measurement presented above. Post the twin-screw granulation, each experiment batch was immediately subjected to fluidized bed drying where all the drying process parameters kept fixed throughout all the four experiments. Samples after every 10 seconds were taken for offline moisture content measurement by moisture analyser to obtain the drying curves at each experimental batch where the screw configuration was changing. Figure 88 shows these drying curves which shows the moisture content of granules as a function of fluidized bed drying time for all the four screw configuration experiments. However, the zero minute in the x-axis represents granules collected immediately from the TSG before going into the fluidized bed for drying. this was added to the graph just to show the initial moisture content of the granules.



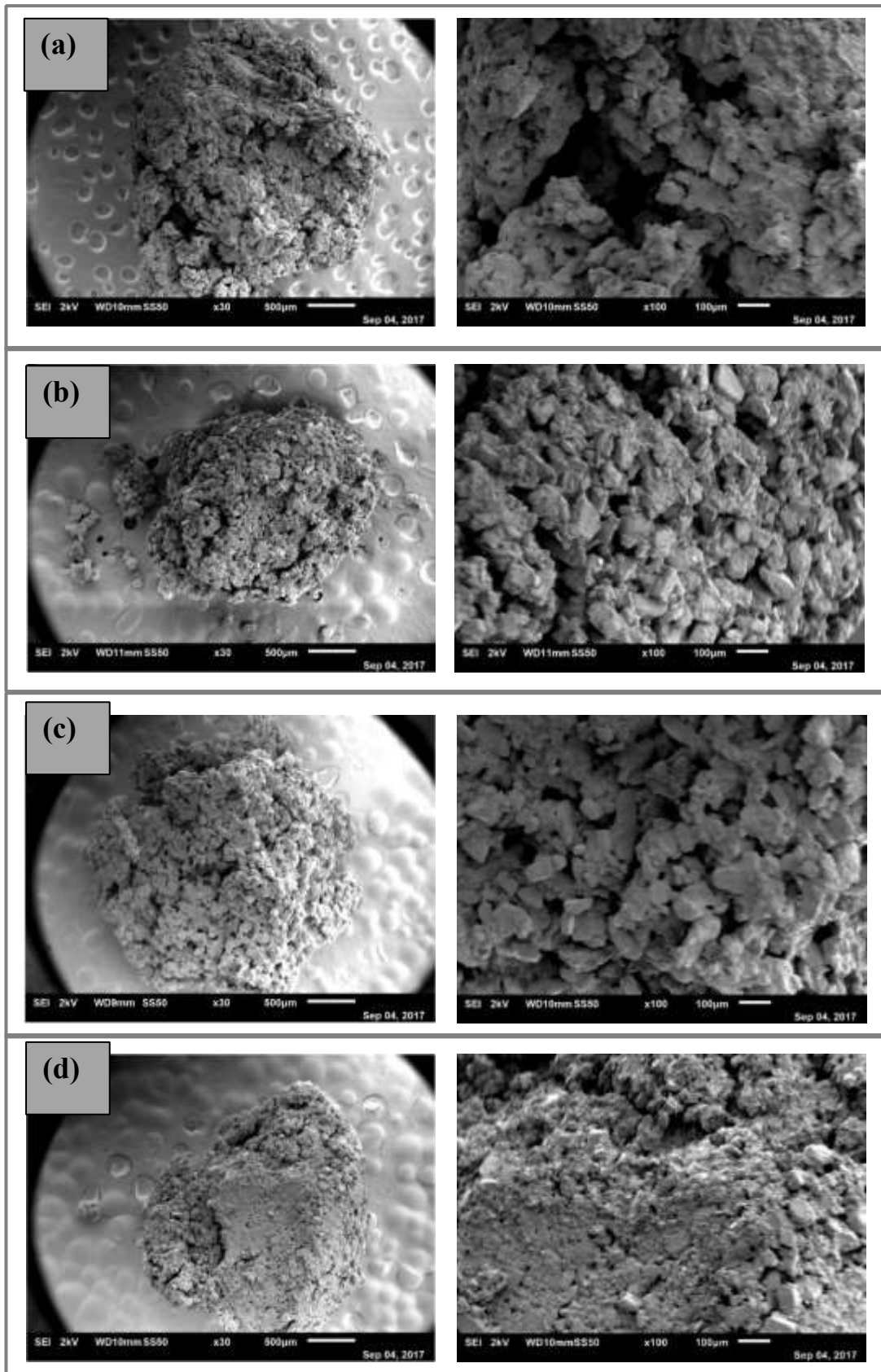


**Figure 87: Scanning electron microscopy of granules produced by TSG with 150M lactose powder and water used as a liquid binder, 250rpm and at different screw configurations (a) 0 KE (b) 4 KE (c) 8 KE (d) 16 KE before FB drying.**



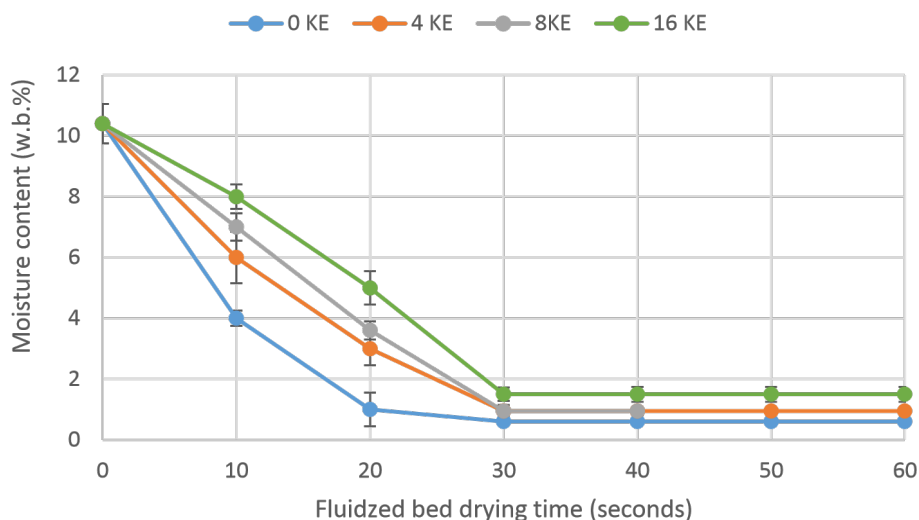


**Figure 88: Effect of varying screw configurations (0KE, 4KE, 8KE, 16KE) on the FB drying of granules produced by TSG with 150M lactose powder and water as a liquid binder, screw speed of 250 rpm, L/S of 0.1 and dried in FB at temperature of 50°C and an air velocity of 2m/s.**

### 5.3.1 Drying curves for granules made with different screw configurations

It can be clearly seen from Figure 88 above that the granules batch made with no kneading elements (conveying only) in the twin-screw granulation was found to be the fastest drying among all other granules batches which were produced with kneading elements. Moreover, granules batch produced with the highest number of kneading elements during the twin-screw granulation was found to be the slowest in drying. This clearly suggest that the initial properties of granules prior to drying and hence the screw configurations that helped with the production of the granules with such properties has significantly affected the drying process of these granules. In other words, since the granules produced with kneading elements tend to be bigger in size, this would mean that bigger granules produce less surface for the air to evaporates (have smaller surface to mass ratio) so they dried slower. While for the granules batch produced with less kneading elements tended to have the faster the drying process and that is because using fewer kneading elements or only conveying elements tend to form smaller granules. These granules would have smaller surface to mass ratio. Figure 89-92 shows the size distribution of granules produced with different screw configurations, 0,4,8,16 kneading elements in each screw respectively. These Figures (89-92) shows a comparison between the size distribution of

granules before and after fluidized bed drying. It can be noticeably seen that granules were significantly reduced in size after drying in the case where 0 kneading elements (conveying elements only) were used (Figure 89). And a little difference in the size before and after fluidized bed was noticed with the case when the highest kneading elements were used. Thus, it can be said that the highest the number of kneading elements were used in the screw configuration, the least the size reduction was. This size reduction can be attributed to the breakage /attrition occurred during drying. However, how big is the granule size reduction is determined by the initial granule's properties at the twin-screw granulation stage (i.e., how porous and compacted the granules). As mentioned earlier, granules produced with higher number of kneading elements tend to be large, compacted and less porous. Therefore, when such granules are subjected to fluidized bed drying, they tend to withstand the fluidization during drying more than the granules produced with a smaller number of kneading elements in screw configuration at the granulation stage. This is due to their initial properties before drying (less porous and compacted granules), hence, more resistance to breakage and attrition during fluidized bed drying. However, the attrition and breakage were found to increase during the drying of the granules produced with lower number of kneading elements. This suggests that is the initial granules properties made at different screw configuration is very well correlated with the extent of breakage and attrition that take place during the drying of the granules.

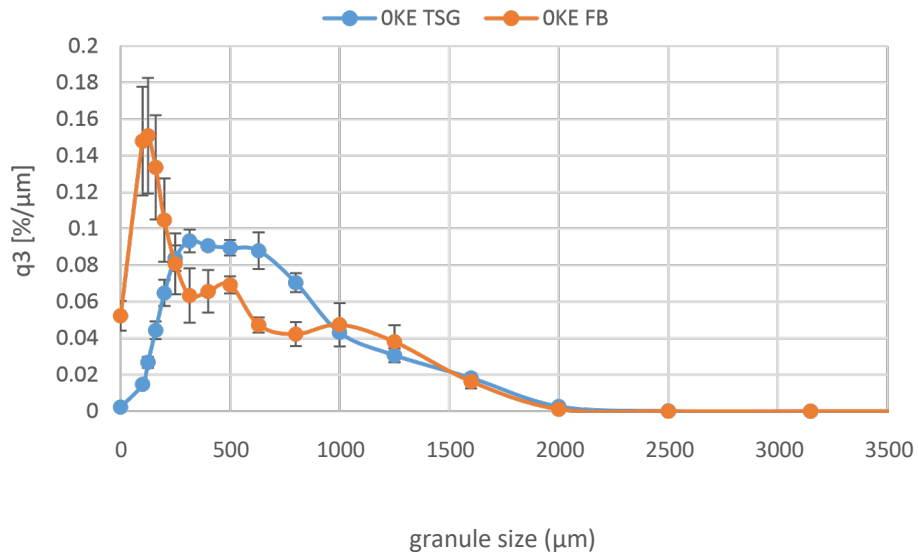


**Figure 89:** Size distribution of granules produced by TSG with 150M lactose powder and water used as a liquid binder at a screw speed of 250 rpm, L/S of 0.1 and a screw configuration of 0KE conveying elements only in each screw. This figure shows the PSD of granules before and after Fluidized bed drying which was performed at a temperature of 50°C and an air velocity of 2m/s.

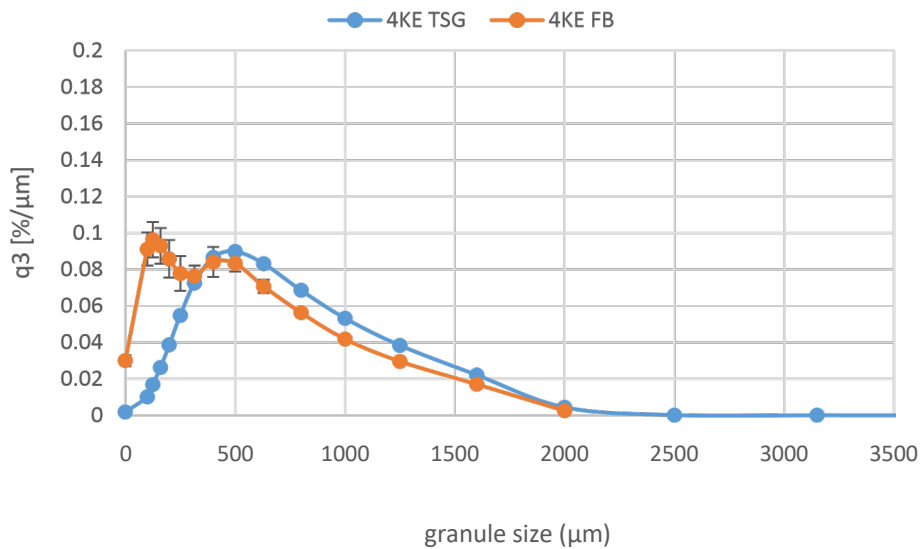


**Figure 90:** Size distribution of granules produced by TSG with 150M lactose powder and water used as a liquid binder at a screw speed of 250 rpm, L/S of 0.1 and a screw configuration of 4 kneading elements in each screw. This figure shows the PSD of granules before and after Fluidized bed drying which was performed at a temperature of 50°C and an air velocity of 2m/s.

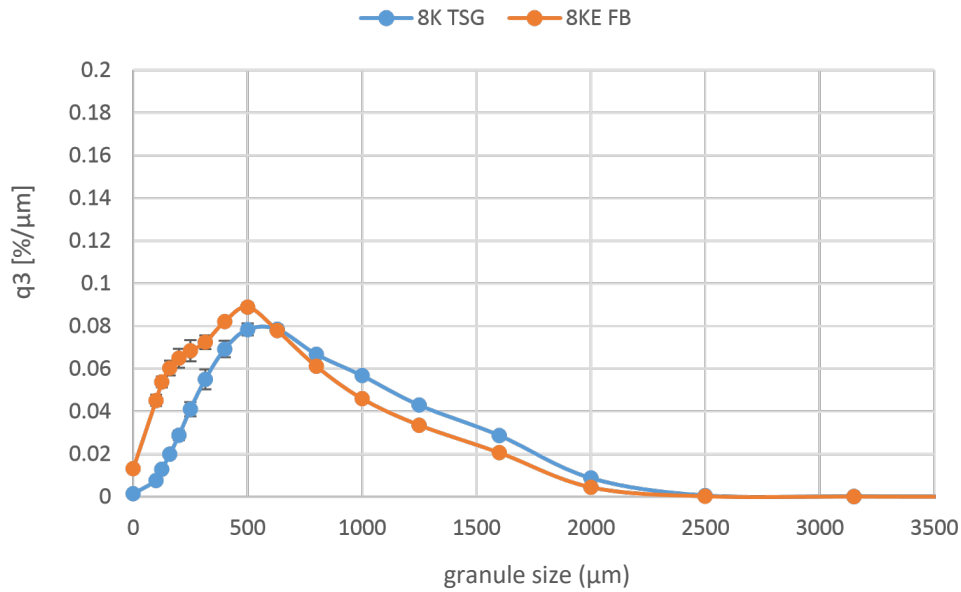


**Figure 91:** Size distribution of granules produced by TSG with 150M lactose powder and water used as a liquid binder at a screw speed of 250 rpm, L/S of 0.10 and a screw configuration of 8 kneading elements in each screw. This figure shows the PSD of granules before and after Fluidized bed drying which was performed at a temperature of 50°C and an air velocity of 2m/s.

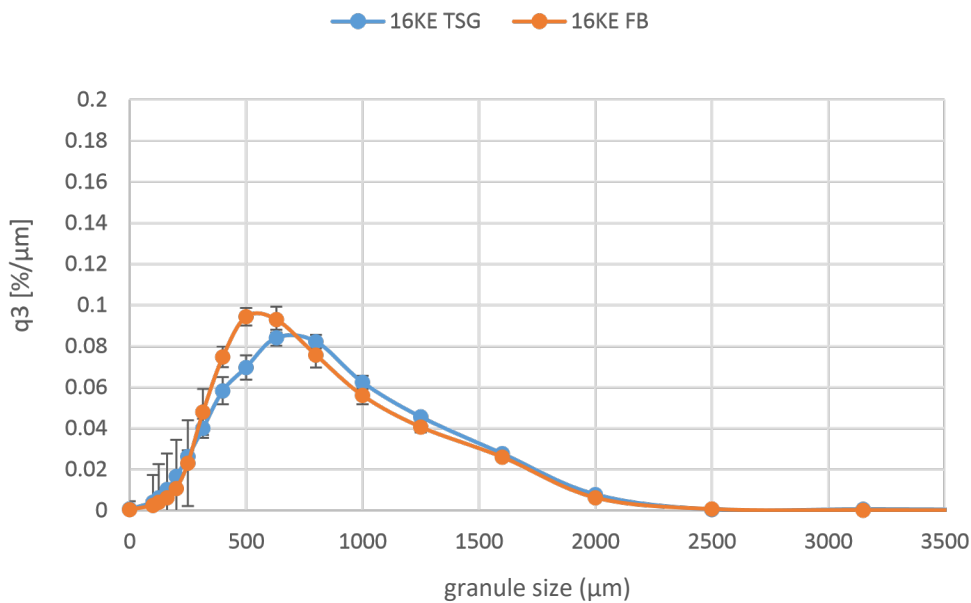


**Figure 92:** Size distribution of granules produced by TSG with 150M lactose powder and water as a liquid binder at a screw speed of 250 rpm, L/S 0.1 and a screw configuration of 16kneading elements in each screw. This figure shows the PSD of granules before and after Fluidized bed drying which was performed at a temperature of 50°C and an air velocity of 2m/s.

## 5.4 Conclusion

The conclusion that can be drawn out of this study that changing the screw configuration during twin screw granulation stage can alter the produced granules properties and therefore this would significantly be altering the drying process accordingly. As the number of kneading elements increases in the screw configuration, the extent of granules breakage/ attrition in the fluidized bed drying decreases. This is believed to be attributed to the chief reason that increase of kneading elements results in the production of large, compacted granules with lower porosity, that have higher resistance to breakage/ attrition when subjected to drying in fluidized bed. Moreover, the granules drying regime at the drying stage is significantly dependent on the granules initial properties prior to drying. Particularly, increasing the kneading elements led to production of large granule (granule growth), these large granules have smaller surface to mass ratio making them follow slower drying regime and vice versa. Hence, one can optimize the desired drying regime and size distribution based on optimizing the granules properties at the twin-screw granulation stage.

## **6.0 Drying in a Continuous Wet Granulation ConsiGma 25 line: Investigation of the Effect of the Screw Configuration**

---

### **6.1 Introduction**

Over the upcoming years, the significance of the continuous manufacturing concept is expected to face an increase in the pharmaceutical industry. This is mainly due to several reasons such as its lower costs, lower production of waste, better efficiency and flexibility, rapid throughput and the growing demand for solid dosage forms (Vercruyssen et al., 2012). The most common method to improve the materials characteristic such as flowability, homogeneity and compressibility prior to the process of tableting is known to be the wet granulation. Continuous wet granulation process is of a supreme significance for the manufacturing of solid dosage forms, as by doing this, wet granules can be produced in a continuous manner. This process utilises liquid binder and is commonly used in the pharmaceutical industry, especially for products with particularly high or low percentages of active pharmaceutical ingredients, or particularly poor flowing materials.

Nearly all-pharmaceutical continuous wet granulation processes are equipped with a twin-screw granulator to produce granules, the wet granules need to be dried to remove the moisture and form granules which are acceptable for further processing. The continuous powder to tablet line which was used in this study has a twin-screw granulator and required the addition of a dryer. The dryer which was fitted in the line for this study is a segmented fluidised bed dryer and is divided in 6 cells, (each segment is referred to as a cell). The wet granules from the granulator are directed to a cell via a valve positioned at the top of the fluidised bed, the cell is then filled for a finite amount of time, which is defined as the filling time. When the filling time for one cell has been reached the valve turns and the next cell is loaded. After the granules have been in a cell for a specified drying time (which includes the filling time) or when they reach a target temperature the cell is unloaded via a rotary valve at the bottom of the fluidised bed dryer and a pneumatic conveying system. The process can continue indefinitely as the cells are loaded and unloaded sequentially. Each cell of the fluidised bed dryer is

equipped with a temperature probe situated just above the air distributing plate. Given its location, the probe will measure a combination of the air and product temperature depending on its coverage.

The dryer has the biggest impact on the residence time of the material along the line taking up to an order of magnitude more time than any other operations in the line. It is also one of the highest energy drawing devices as it requires multiple fans and heating elements to work. For these reasons, it is important to understand the drying behaviour in this particular fluidised bed to be able to optimise the time required for drying, not only to have a smaller residence time but also to optimise the power efficiency of the fluidised bed. The understanding of the behaviour of this fluidised bed could also lead to a simple model that could be used in a control system to obtain dry granules up to specification even when fluctuations are detected. Although a few studies on the segmented fluidised bed present in the ConsiGma-25 line have been published, most of them focused on varying the process parameters in the dryer while not focusing on the effect of the conditions of the twin-screw granulator feeding the dryer. The effect of the parameters selected during the granulation process on the behaviour of the dryer is the focus of this study. The understanding of how each unit in a continuous process affects the downstream units is key to provide scientists and companies with the knowledge to optimise and further develop these complex processes. The aim of this work was to study the granules formation, drying and subsequent production of tablets at different screw configurations in a unique and first of its kind industrial scale ConsiGma system (GEA Pharma Systems), paying particularly more attention to the drying process of the granules, which is monitored with an inline NIR system and temperatures sensor. Moreover, to validate some of the outcomes obtained using the laboratory scale co-rotating twin screw granulator. Three screw configurations were implemented in this study to examine their effect on the drying process of granules on the six-segmented fluidized bed dryer. All other parameters were fixed throughout the experiment.

## **6.2 Design of Experiment**

Figure 93 shows the process parameters used in all of the three experiments which were carried out to investigate the effects of changing the screw configurations on the drying process of granules and consequently on the tableting process. Tap water was the liquid binder used in all of the experiments.

The L/S ratio used in this chapter was 0.1. In response to the experimental results, granules size distribution after twin-screw granulation was measured for each experiment. Moreover, inline NIR-probe (FP710e, NDC Technology, Dayton, Ohio, USA) and temperature sensors measured the moisture content and temperature profiles of the granules during fluidized bed drying respectively. For the final product (tablet), the breakage force of the entire produced tablet was measured.

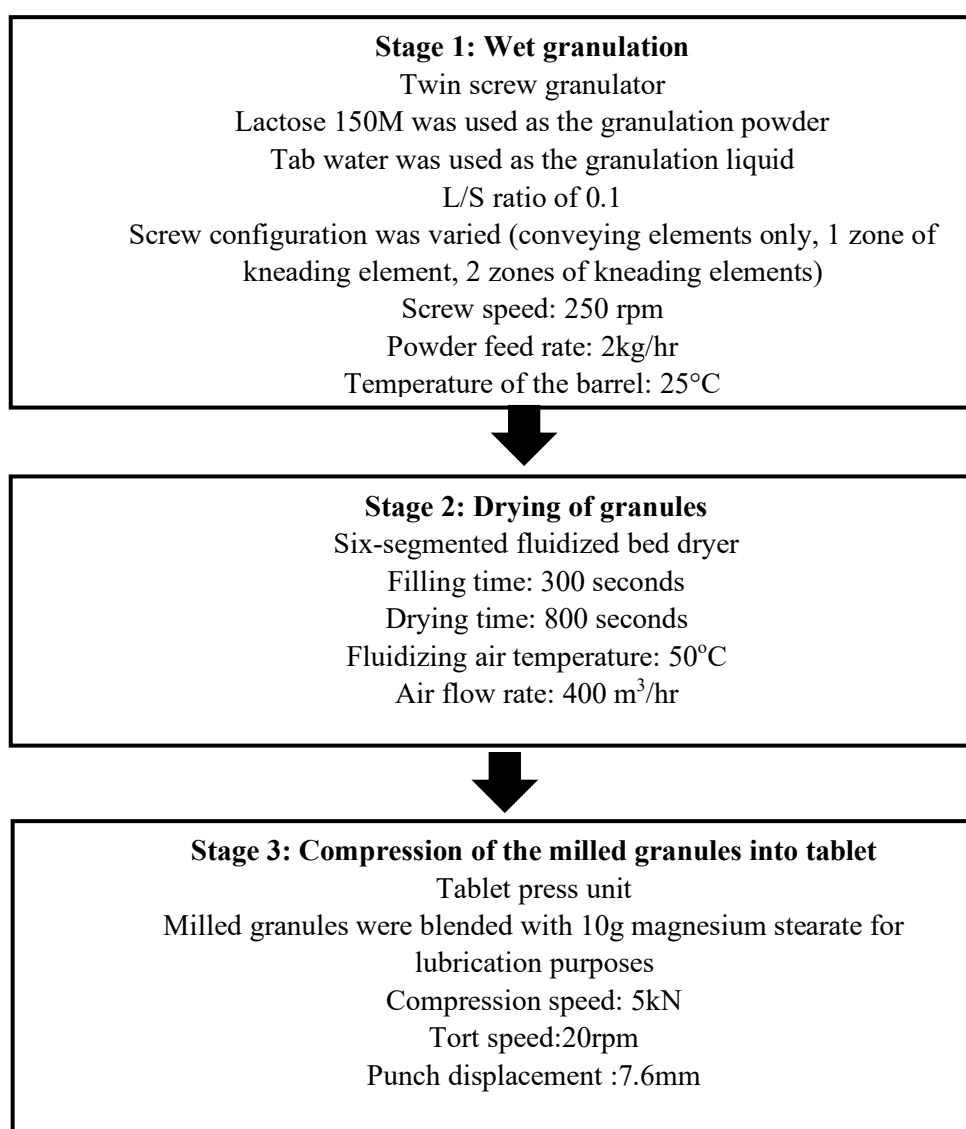
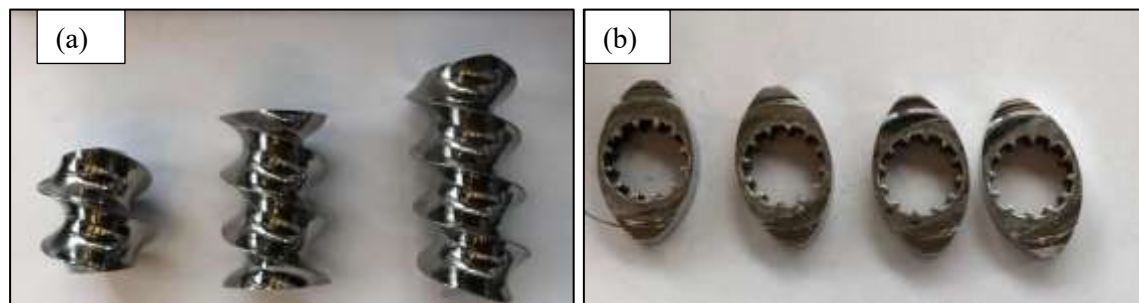


**Figure 93: Flow diagram showing process parameters used in TSG, fluidized bed dryer and tablet press unit of the ConsiGma -25 line as screw configurations vary.**



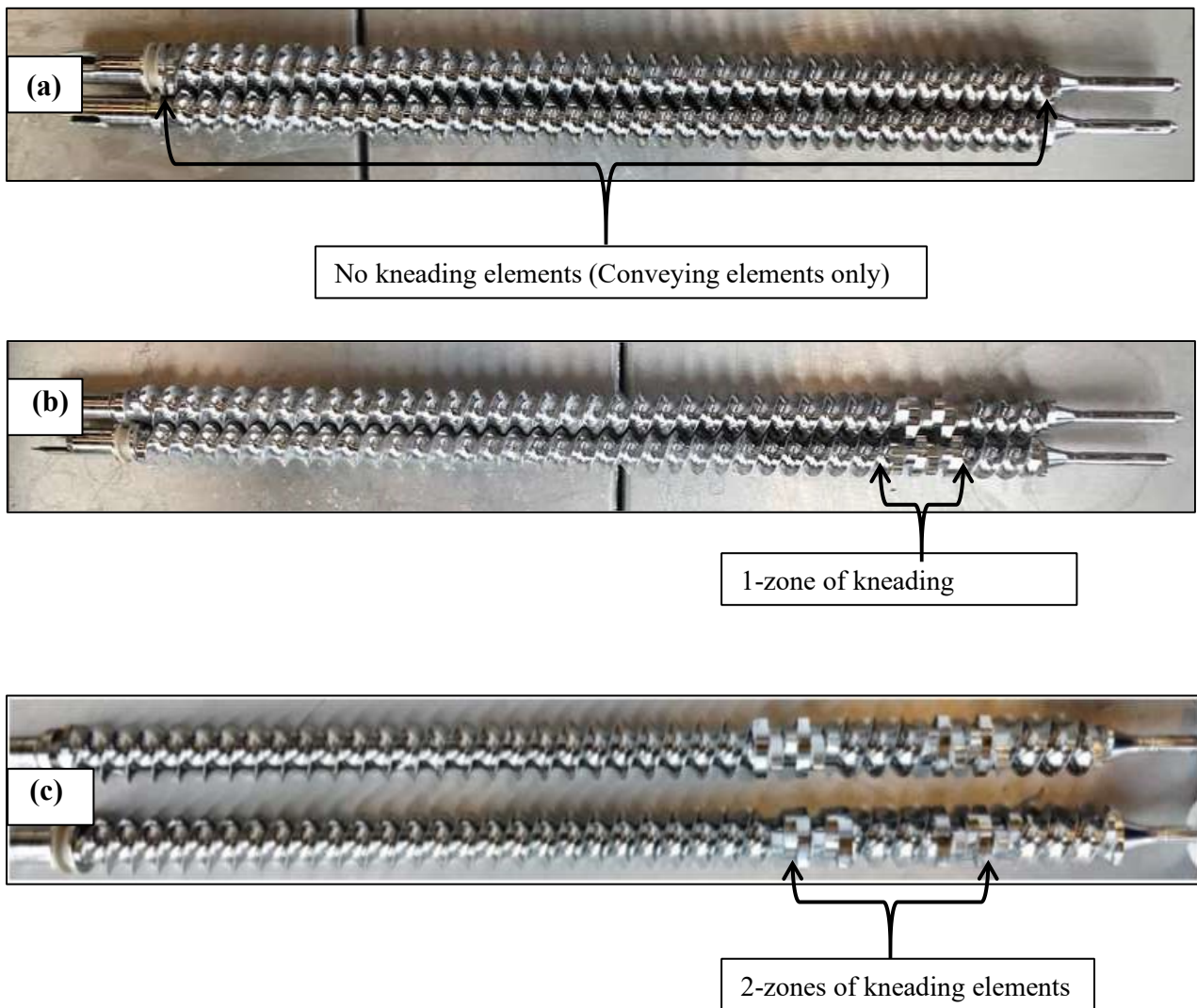
### 6.3 Screw Configuration

There are different screw element types used in the ConsiGma-25 twin screw granulator, these are the long pitch conveying element (LPCE), short pitch conveying elements (SPCE) and kneading elements. These are all illustrated in Figure 94.



**Figure 94: Pictures of (a) Short and long pitch conveying elements (LPCE) (b) Kneading elements used in the screw configuration of this study.**

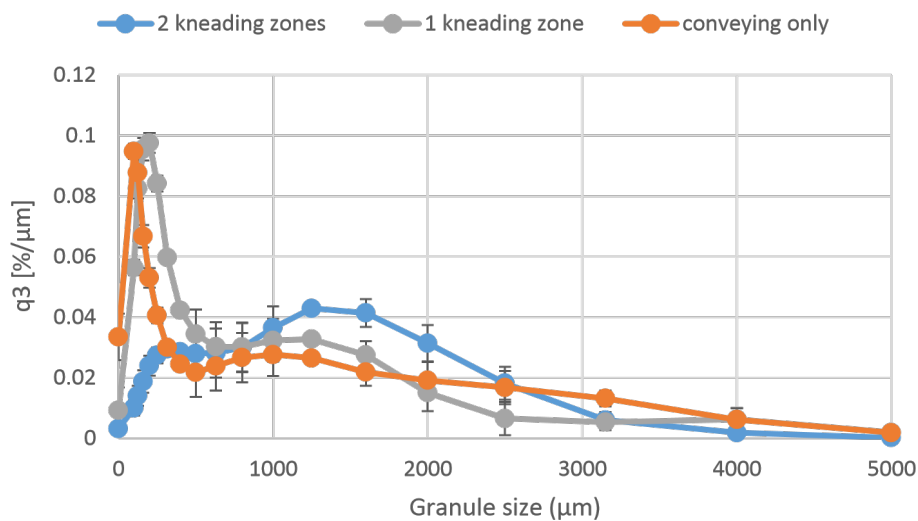
Figure 95 illustrate the three different screw configurations used in this study. Figure 95 (a) shows screw configuration of conveying elements only. Each screw consists of only long and short pitch conveying elements. These elements tend to rotate in a self-wiping motion, in which the powder is pushed forward as the screws are rotating. Figure 95 (b) shows screw configuration of conveying elements with one zone of kneading discs. Each screw consists of 6 kneading discs placed at  $60^\circ$  and separated by conveying elements. Figure 95 (c) shows screw configuration of conveying elements with two zones of kneading disc. Each screw consists of 12 kneading elements. The function of kneading element helps with better liquid distribution and granule growth (Dhenge et al., 2013) and breaking the larger formed granules into smaller ones and therefore produce a more uniform particle size distribution (Kumar et al., 2016).



**Figure 95: Screw configurations used in this study (a) Conveying elements only (b) conveying and 1-kneading elements zones (c) conveying and 2-kneading elements zones. The angle at which the kneading elements are placed is 60 degree.**

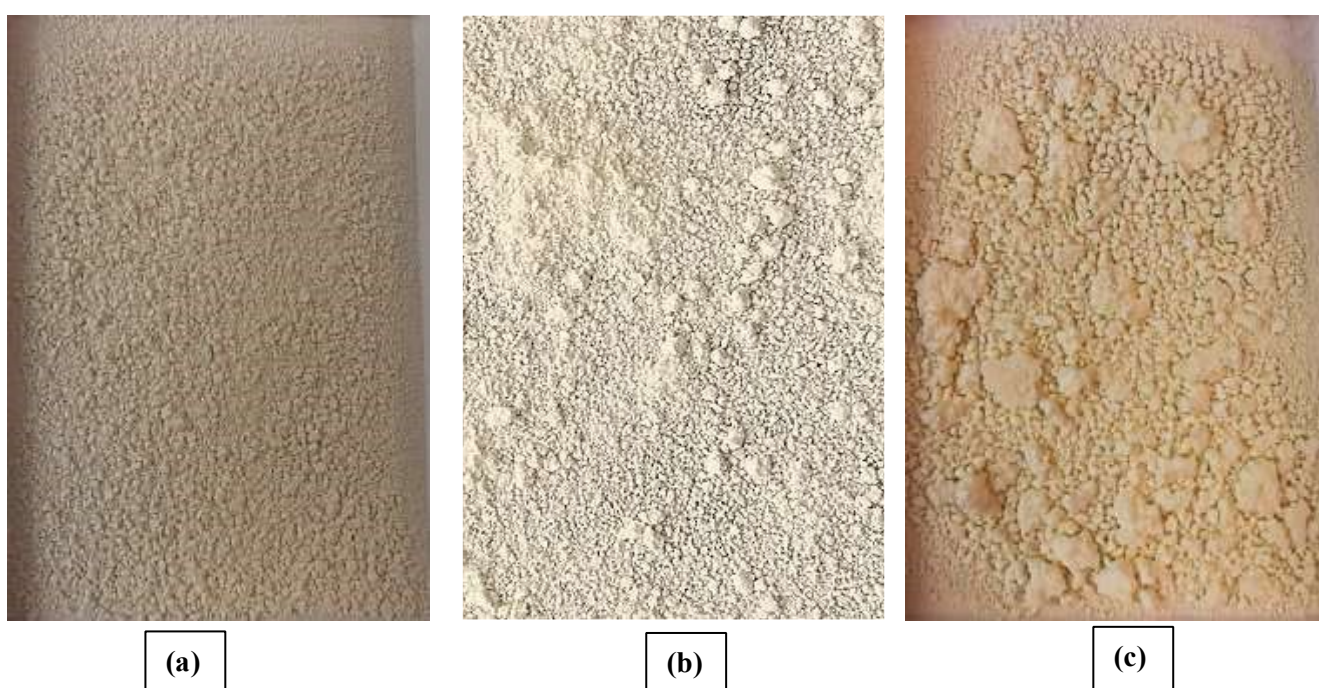
## 6.4 Results and Discussion

Figure 96 shows the size distribution of granules prior to the fluidized bed drying for the three screw configurations used. It can be clearly seen from the size distribution that granules produced with conveying elements and one kneading zone have higher proportions of fines and smaller granules than when the one produced with two kneading elements zones. Generally, when conveying elements are used in the screw design, they tend to impart a minimal mechanical energy when moving material, however, using kneading elements in the screw design would intensively mix the components of solid and liquid. In other words, using a higher number of kneading elements in the screw design would result in intensive mixing of the powder with the granulation liquid binder, therefore, yielding less amounts of fines. Additionally, using the more kneading element would enhance the distribution of liquid binder through the powder bed and hence the material becomes more densified resulting in granules with higher strength and that are less liable to mechanical stress. This result is in agreement with the finding of (Vercruysse et al., 2012) and (Saleh et al., 2015).



**Figure 96: Size distribution of granules produced by the TSG of the Conigma line using 150M lactose powder and water used as al liquid binder with L/S of 0.1 and screw speed of 250 rpm at three different screw configurations (conveying elements only, 2 kneading zone, and one kneading zone before drying.**

Figure 97 shows images of batches of granules produced with (a) two kneading elements zones (b) one kneading zone and (c) with conveying elements only before drying in the fluidized bed dryer. These three images correspond to the granules size distribution presented above. As shown in Figure 97(c), it can be noticed that the granules produced with conveying elements only had higher number of fines with large ungraduated lumps. These lumps have formed due to the poor mixing of the granulation liquid binder with the powder, dissimilar to the granules which were produced when using the highest number of kneading elements, which is seen to be fairly uniform distribution indicating the good mixing of the liquid binder with the powder. This is again in agreement with the findings of (Verduyck et al., 2014) and (Saleh et al., 2015)



**Figure 97: Images of granules batches produced by TSG using 150M lactose powder and water as a liquid binder, L/S of 0.1, and screw speed of 250 rpm at (a) 2-kneading zones (b) 1kneading zone (c) conveying elements before drying in the segmented fluidized bed dryer.**

To compare this result (Figure 96 above) with the PSD of granules obtained at different screw configurations using the small laboratory scale TSG prior to drying in FB (chapter 5, Figure 83), it can be noticed that the trend is generally the same for both scales as number of kneading elements increases, in other words, as kneading elements increases, bigger granules are obtained with less amounts of fines, however, it can be seen that the result is not precisely the same, this is because the number and arrangement of a stack of kneading elements can result in different outcomes.

And currently, the number of kneading elements and the position where they are placed within the screw varies among the two scales, thus, this resulted in getting slightly different result. For instance, looking at the screw configurations Figures for both scales, small laboratory scale (Figure 82) and industrial scale TSG (Figure 94), it can be clearly seen the number and the arrangement of the kneading elements are different in both scale and this implies the result would be accordingly altered. Figure 98 shows the particle  $d_{10}$ ,  $d_{50}$  and the  $d_{90}$  of the granules corresponding to the batches produced at the three different screw configurations above.

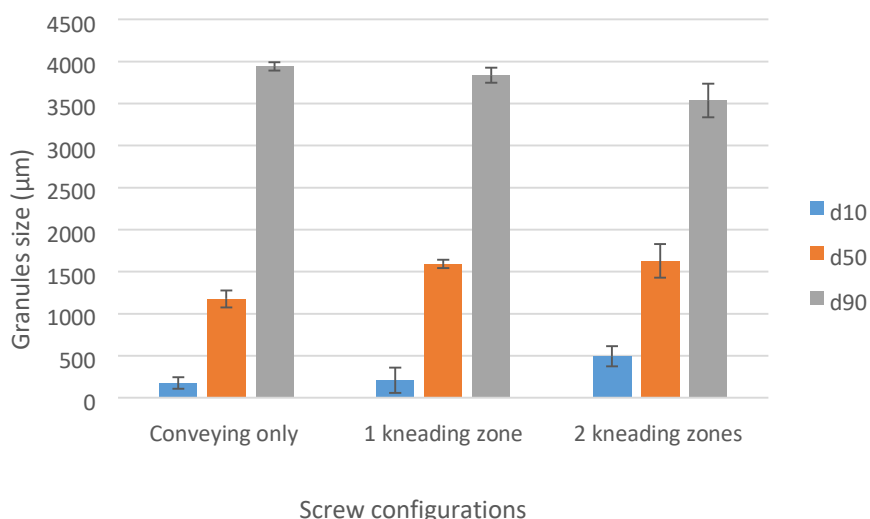


**Figure 98: PSD ( $d_{10}$ ,  $d_{50}$  and  $d_{90}$ ) of granules produced by the TSG of the ConsiGma line using 150M lactose powder and water used as a liquid binder with L/S of 0.1 and screw speed of 250 rpm at three different screw configurations (conveying elements only, 2 kneading zone, and one kneading zone) before drying.**

#### 6.4.1 Temperature Profiles of Granules During Drying in the Fluidized bed

The main aim of this study is to link the effect of the screw configurations to the behaviour of the drying process at the dryer cell, as there were no studies in the literature to report such link, therefore this missing gap is explored further in this section. Following the production of granules in the twin-screw granulator, the three batches of granule produced using different screw configurations were subjected to drying in the six-segmented fluidized bed dryer separately, while monitoring both the

moisture content and the temperature of granules by using NIR and a temperature probe respectively, as a function of drying time. The filling time per cell was 300 seconds which results in a cell load of 0.83 kg granules at a powder feed rate of 10 kg/hr. The inlet drying air temperature, humidity and flow rate of the were set at 50 °C, 10% and 400 m<sup>3</sup>/h, respectively. The time of drying was fixed at 800 seconds. These conditions were all kept constants for all the experiment while the screw configurations at the twin-screw granulation stage were varied. Figure 99 shows the temperature profiles at the dryer cell 5, produced at different screw configurations (screw configuration with 2 kneading zones, screw configuration with 1 kneading zone and with conveying elements only). It is generally clear to see how these temperature profiles behave similarly for each of the three different screw configurations used.

In all of the three cases, it can be noticed that the temperature abruptly decreases when the granules started filling the cell. It is also possible to observe that the decrease in temperature profile for the cell filled with granules made with conveying elements only is being slightly less steep compared to the other screw configuration conditions. Once the cell loaded with granules, the temperature was constant for a period of time, except for the batch made with conveying elements only. This could be properly due to filter clogging with fines and activation of the filter have caused this disruption to the stability of the temperature at this stage. This period represents the constant rate-drying period. What this means is that the heat transferred from the air evaporates the liquid at the surface of the granules. The temperature was relatively maintained constant near the equilibrium wet bulb temperature until all of the moisture at the surface of granules is evaporated. There does not seem to be any difference between the temperature profiles of the granules made with one kneading zone and two kneading zone. This process was a bit shorter for the granules prepared with conveying elements only. After most of the water at the surface had evaporated, the temperature begins to increase and kept rising until all of the internal moisture content is evaporated. This represents the falling rate period. Once the liquid had fully evaporated from the granule, the high temperature from the inlet air (due to elevated temperature of 50°C) will start to heat the granules and as the drying ends. The dry granules are then heated to reach a balance with the drying medium. The temperature then stabilizes and reaches a steady state



similar to the drying air temperature, as all of the moisture is evaporated, and granules become dried. This stage represents the equilibrium period. Overall, the temperature profile of the granules produced with conveying elements only showed a visible difference in the drying behaviour among the two screw configuration conditions, this could be associated with the relatively small granules size and the amounts of fines exist within this batch compared to other two batches which produced with kneading elements. Overall, difference in product temperature was bigger at the beginning of the process and then it gets smaller as the drying process come to an end. This is defined as the end point of drying. The end point of drying can be also determined by using the temperature of product data (Fonteyne et al., 2014), whenever the product temperature reaches steady state (reached stabilization), it can be said that the drying come to an end. The temperature of the product is a more reliable way of determining the end point of drying in the six-segmented fluidized bed dryer since each cell of the fluidized bed has its own installed temperature sensor and that the temperature sensor is embedded actually in the product. Unlike the NIR probe for reading the moisture content which is installed at higher position from the bottom of the cell, which could be slightly less accurate compared to the temperature probe. For example, the state of the bed fluidization can affect the reading of the NIR probe, this will be explained in more details later at the moisture profiles section. Now, to assess the drying process of these three screw configuration conditions, moisture content profiles are obtained and discussed further.

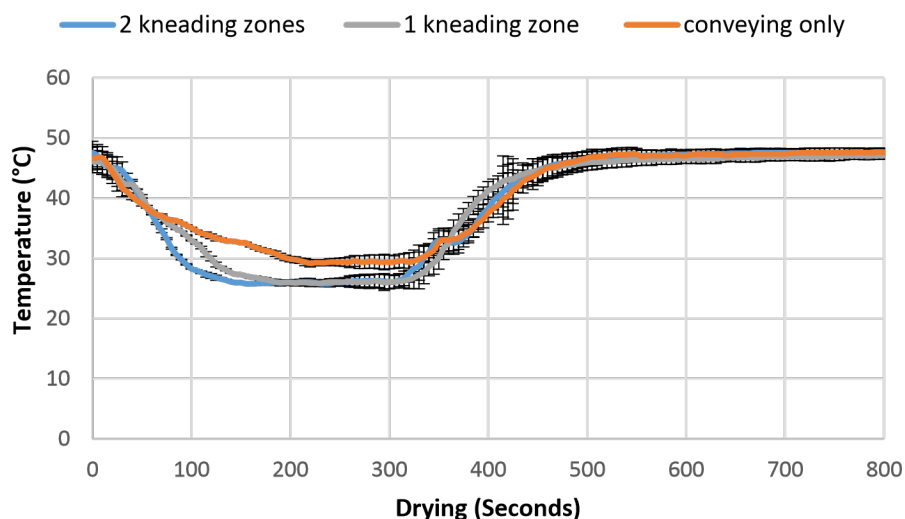


**Figure 99: Temperature profiles at different screw configuration (conveying element only, 1 kneading zone and 2 kneading zones) inside the dryer cell 5 of the segmented fluidized bed dryer at an air temperature of 50 (°C), an air flow rate of 400 m<sup>3</sup>/hr, cell filling time of 300 seconds and a total drying time of 800 seconds.**

#### **6.4.2 NIR online measurements of Moisture content in Fluidized Bed**

To further assess the behaviour of granules drying process in the segmented fluidized bed dryer, an online NIR probe was used to obtain the granule moisture content every 5 seconds. As mentioned earlier, the NIR probe was fixed in the probe port of cell 5 of the fluidized bed. Besides the solid moisture content measurement, the NIR probe can also detect and quantify the product around the probe, this is called product presence. Figure 100 shows the profiles of moisture content of granules produced using the three different screw configurations. During the cell filling time, the moisture content reading generally increases, the increase in moisture content is steady as the system is drying the granules as it comes into the cell. During the filling period, as the granules are loaded into the cell continuously, they are also drying at the same time. At the start of the filling period, the moisture content increases to then decreases and begin to increase again. This is because as the first wet granules are coming into the cell, they contact the probe closely as they come in and then are fluidizing away, resulting in the probe to be unable to provide sensible readings again. This hypothesis is supported by the product presence obtained by the same NIR probe as seen in Figure 101 which indicates the amounts of granules near the NIR probe capable of reflecting the light of the NIR. As it can be observed from both Figures (Figure 100 and Figure 101) that the readings of moisture content and product presence slightly dropped at the same time which emphasise the hypothesis. The product presence tends to stay constant almost during the whole process of drying. However, overall, the presence of product during the drying process for the three conditions tend to be different. For instance, the more uniform the granule size distribution the more organised the fluidization state and the more product is detected by the NIR probe. For the batch prepared with conveying only, there was a large amount of fines and small granules, which made random fluidization which tends to result in less product being sensed by the NIR probe. Also, the batch of granules prepared with conveying elements only had unstable fluidization state due to its batch having more fines compared to the one with prepared with more kneading elements, which caused the holes in the bed distributor to become easily clogged by the fine particles. In other words, product presence can be useful to have an insight



about the state of the bed fluidization as well. After the completion of the granules filling, which is marked with a vertical black dotted line at 300 seconds, the moisture content decreases for the two screw configurations cases (with 2 kneading zones and 1 kneading zone) at a fairly constant rate as expected until reaching the critical moisture content point which was different for each of the two cases. For the drying curve of granules prepared with conveying elements only, an almost steady state was reached at the beginning of the drying process (300 seconds) and stabilized to the end of the drying process. This could be related to the granules size distribution of this batch which had the highest amounts of fines and un-granulated loose powder, which are when susceptible to fluidization during drying, which causes further break resulting in even more fine formations. In turn, small granules and fines tend to dry much faster, due to its higher surface to volume ratio (Fonteyne et al., 2014), than the bigger granules, which have smaller surface area available for and require more time to dry. Moreover, water in the inside of the small granules will reach the surface faster than in large granules. The moisture content of the granules which were prepared by conveying elements only never went under 2%, which is lower than the initial moisture content of the granules recorded by the probe when were wet, indicating that the product is dried. The granules produced with kneading elements tend to dry much slower than the granules produced with conveying elements. This because large granules have smaller surface area available for drying and require more time to dry. To look closely at the impact of screw configuration on the drying curves of granules produced with different screw configurations, the line slope for all curves between time 300 seconds (starts of the drying) and 400 seconds (starts of equilibrium point) were plotted as shown in Figure 102. As the number of kneading elements increases, the steepness of the lines decreases, which align well with the obtained regimes of the drying. The lowest steepness was obtained for the granules prepared with conveying elements only (0 kneading elements), which was the fastest batch in drying and vice versa. The residual moisture content of the granules at the end of the drying process for all the three screw configurations conditions was plotted as shown in Figure 103. As the kneading elements number increases, the residual moisture content decreases, the difference between the residual moisture content of the granules prepared with 2 kneading zone and 1 kneading zone is not significant. Overall, it can be seen from both the temperature and the moisture profiles of granules that the temperature of the granules

made with conveying elements is higher than the temperature of the granules made with kneading elements. This trend supports the results obtained in the moisture content profiles. Since the granules produced with conveying elements dries faster, i.e., loses water faster, its temperature will also increase faster until it reaches a steady state. Whereas granules produced with kneading elements tend to have lower temperature and that is also associated with the moisture content profiles, since the granules here dried slower, then its temperature will increase slower.

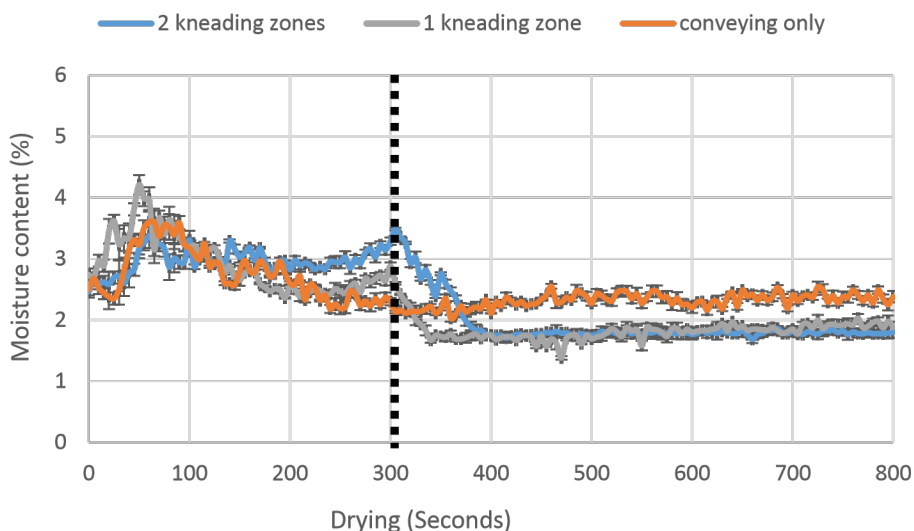


**Figure 100: Moisture content profiles at different screw configuration (conveying element only, 1 kneading zone and 2 kneading zones) inside the dryer cell 5 of the segmented fluidized bed dryer at an air temperature of 50 (°C), an air flow rate of 400 m<sup>3</sup>/hr, cell filling time of 300 seconds and a total drying time of 800 seconds.**

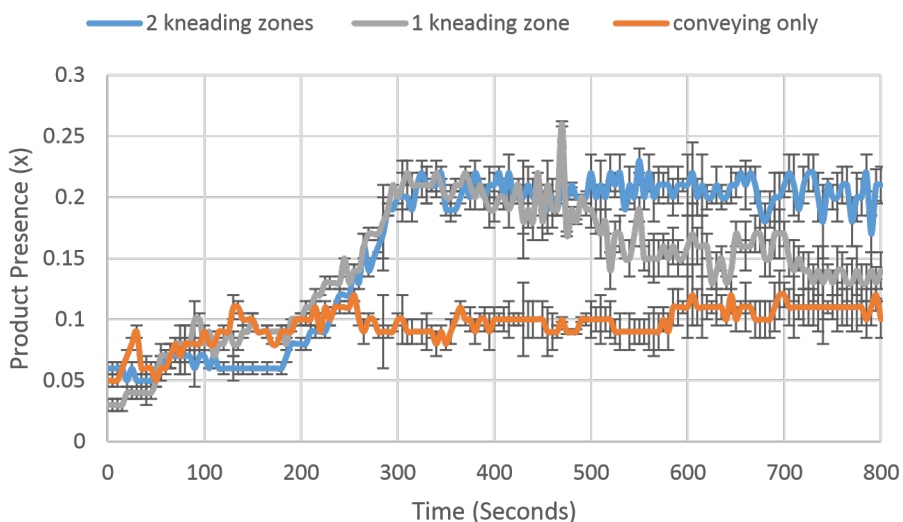


**Figure 101: Product presence profile of granules inside the dryer cell 5 measured by the NIR probe at different screw configurations (conveying element only, 1 kneading zone and 2 kneading zones).**

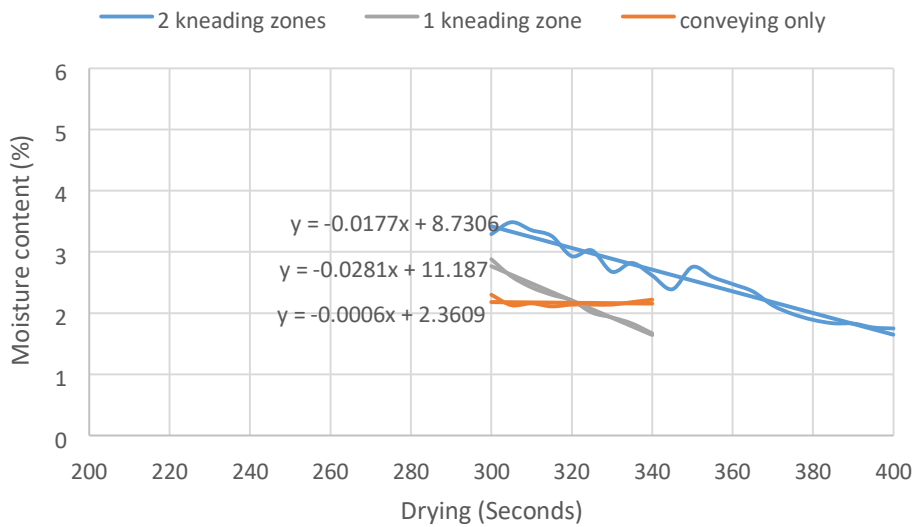


**Figure 102: Slopes of the drying curve between time 300 seconds and 400 seconds at the dryer cell at different screw configurations (conveying element only, 1 kneading zone and 2 kneading zones).**

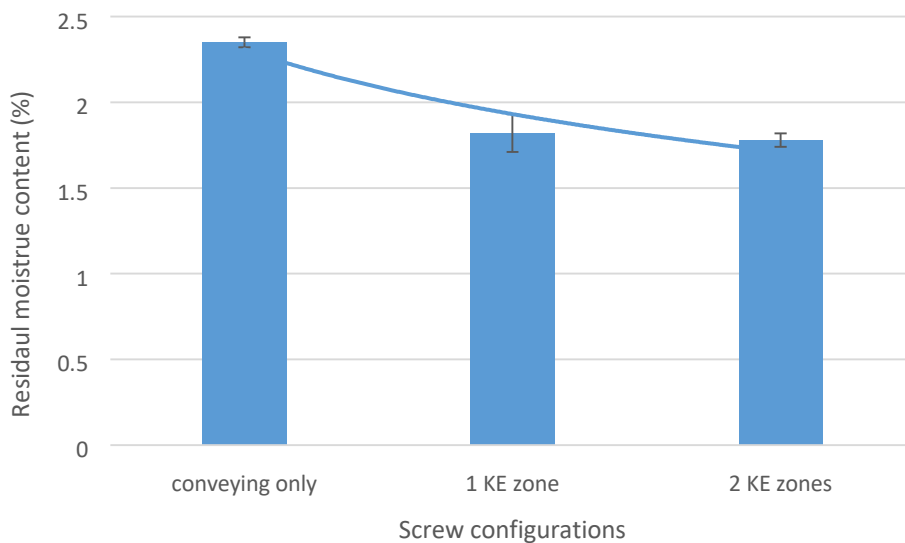


**Figure 103: The residual moisture content of granules at the dryer cell at different screw configurations (conveying element only, 1 kneading zone and 2 kneading zones).**

Post drying, it was not possible to take samples of granules out of fluidized bed dryer for determination of size distribution; this was even not possible after drying is completed, as doing so will disturb the whole system of the powder to tablet line. Therefore, no size distribution of granules during or after drying is presented in this work. The granules were then flowed to the milling unit (Quadro comil U10,

Quadro Engineering, Ontario, Canada) for size reduction and then for blending with magnesium stearate ready for compression into tablet form which is the final product in the line.

### 6.4.3 Tablet Evaluation

As mentioned above the tablets were produced using the milled granulation product lubricated with magnesium stearate at the blending unit. The conditions at the tableting press were kept constant throughout all the experiments. This is to allow the determination of the impact of screw configuration on the tablet properties. The shape of the tablets as produced from the tablet press is complex concave. To evaluate the characteristics of the tablet produced, mass, thickness, diameter and breaking force for a sample of 100 tablets of each condition were evaluated by hardness tester (Pharmatron, AG-Multitest 50 G2, Switzerland) as presented in Table 3.

**Table 3:** Variation in the tablet thickness, diameter and weight at three different screw configurations

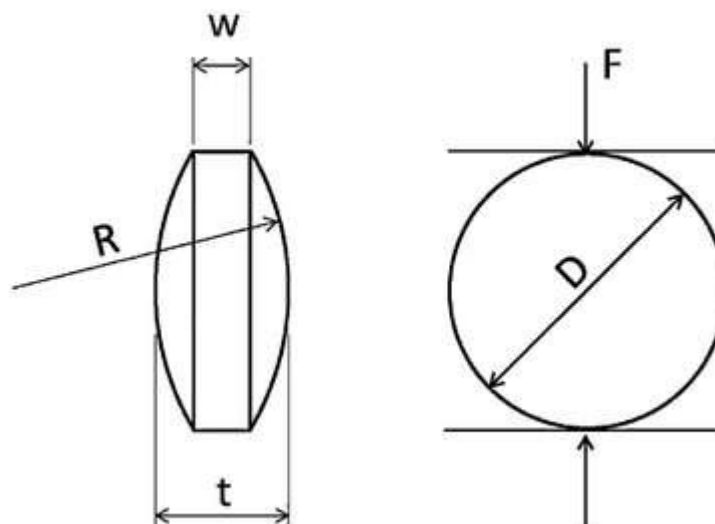
Screw configurations	Tablet Mass (g)	Tablet Thickness (mm)	Tablet Diameter (mm)
2 kneading zones	0.75±0.011	6.5±0.079	12.10±0.008
1 kneading zones	0.74±0.004	6.4±0.035	12.11±0.007
Conveying only	0.96±0.003	6±0.043	12.07±0.01

#### 6.4.3.1 Tablet Tensile Strength

Equation 4 which was developed by Pitt and Newton (1988) was used to calculate the curved faced tablet tensile strength from the breaking forces loaded across the tablet diameter (Shang et al., 2013).

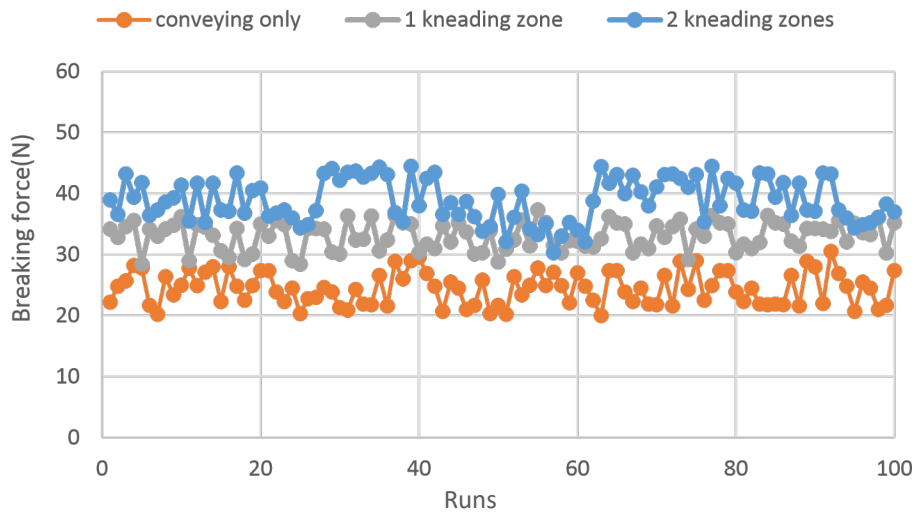
$$\sigma_t = \frac{10P}{\pi D^2} \left( 2.84 \frac{t}{D} - 0.126 \frac{t}{W} + 3.15 \frac{W}{D} + 0.01 \right)^{-1} \quad \text{Eq. 4}$$

Figure 104 shows a schematic diagram of curved faced tablets geometry where the parameters in the equation above is illustrated.  $P$  represents the fracture load (N),  $D$  is diameter of the tablet (mm),  $t$  is the overall thickness (mm) of the tablet and  $W$  is the central cylinder thickness (mm).



**Figure 104: Curved faced tablets geometry with the illustration of strength equation parameters.**

Figure 105 shows the variation in the breaking force of 100 tablets made with three different screw configurations: one zone of kneading elements, two zones of kneading elements and zero kneading elements (conveying elements only). Figure 106 shows the average breaking force of the 100 tablets for the three screw configurations used. It can be clearly seen from these Figures that as the kneading elements increases, the tablet breaking force increases. In other words, tablet produced with conveying element only had the lowest breaking force. To explain this further the tensile strength of all the tablets of each condition was plotted as seen in Figure 107 for 100 tablets and as in Figure 108 for the average tensile strength of the 100 tablets. It can be clearly observed from these figures that higher number of kneading elements resulted in production of stronger tablets and the absence of kneading elements resulted in a weaker tablet. The reason behind this result can be related mostly to the amount of stress exerted on the material by the kneading elements during the granulation stage and therefore affecting its deformability. Lactose is a brittle material and increasing the number of kneading elements increase the compaction of the materials and thus this increases the chance of breaking/ fracturing of the particles during granulation. Therefore, the contact surface area and the bonding strength between the particles increases, and thus resulting in stronger tablets as evidenced in Figure 107 and Figure 108.



**Figure 105: Variation in the tablet hardness at three different screw configurations (conveying element only, 1 kneading zone, 2 kneading zones). The compression force used for tableting was 5kN for all the three experiments and measurement was repeated for 100 tablets of each condition.**

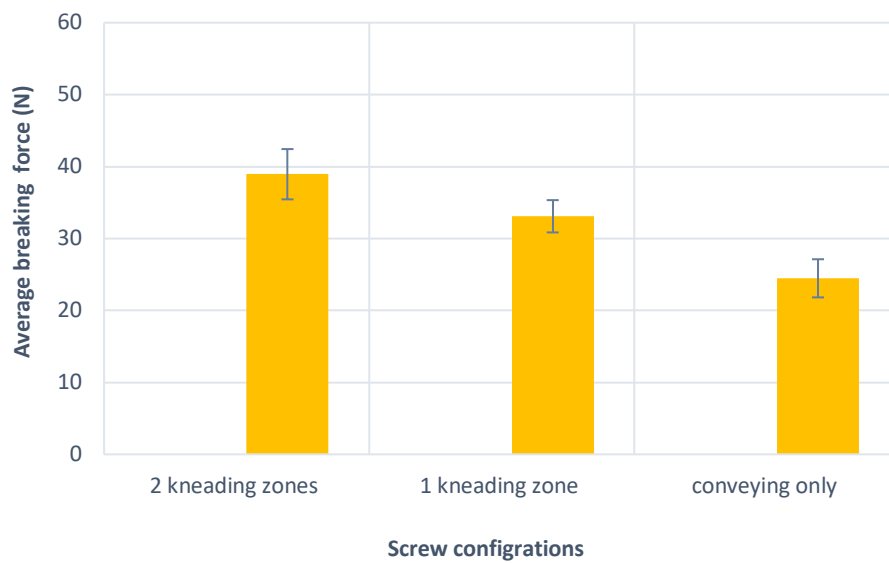


**Figure 106: Average breaking force of 100 tablets produced with three different screw configurations (conveying element only, 1 kneading zone, 2 kneading zones). The compression force used for tableting was 5kN for all the three experiments.**

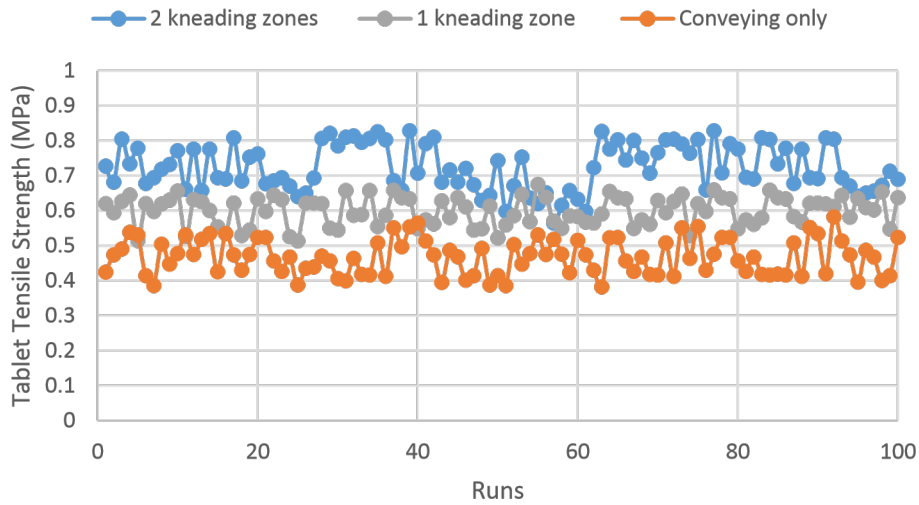


Figure 107: Tensile strength of 100 tablets as calculated by the equation developed by Pitt and Newton (1988) at the three different screw configurations (conveying element only, 1 kneading zone, 2 kneading zones). The compression force used for tableting was 5kN for all the three experiments.

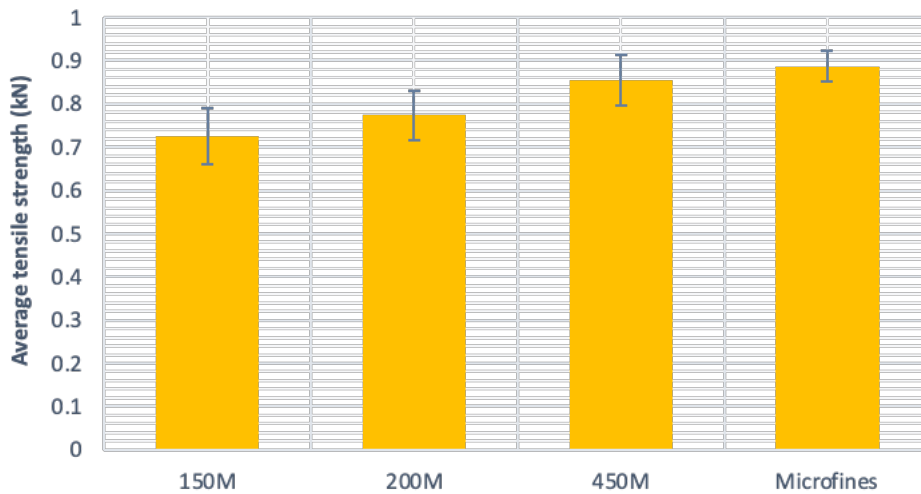


Figure 108: Average tensile strength of 100 tablet produced with three different screw configurations (2 kneading zone, 1 kneading zones, conveying element only,). The compression force used during tableting was 5kN for all the three screw configuration experiments.

### 6.4.3.2 Tablet Dissolution

As mentioned previously in this thesis, oral solid dosage forms are considered to be the most effective and flexible available treatments to patients. Therefore, testing the dissolution of all the oral solid dosage forms is a requirement, it is used throughout the life cycle development for testing the product release and stability. It is a fundamental analytical test used to detect any physical changes in the API and formulated product in the pharmaceutical and biopharmaceutical industry. In the early stages of the development process of the drug, the dissolution testing (in-vitro) strengthens the optimisation process of the release of the drug from a specified formulation. The oral dosage form effectiveness relies on the drug fundamental ability to dissolve in the gastrointestinal tract fluids before being absorbed into the systemic circulation. Thus, tablet dissolution rate is of a paramount importance to this process. In pharmaceutical development, one of the main encountered problems is the need for the optimisation of the drug level that should be available to the body to achieve the full desired therapeutic effect of the drug. Inadequate bioavailability and consequently absence of efficiency could potentially result in case of incorrect optimisation of the drug level outside the therapeutic frame. On the other hand, too high bioavailability can lead to the production of undesirable adverse toxic effects to the patient. Therefore, it is imperative that the test of dissolution is robust and reproducible with the capability of detecting any important changes in the performance of the product for instance distinguishing between different batches and formulations. The exact employed technique of dissolution is determined by the characteristics of the dosage form and the planned administration route. There are several industry standard methodologies for testing dissolution of solid dosage forms within the United States Pharmacopoeia (USP), however, for the purpose of this project USP Apparatus I (basket) is implemented as it is the most common technique used for tablets.

The dissolution profile for the lactose tablets made from different screw configuration is shown in Figure 109. It can be seen from the Figure that the response of the lactose to the conductivity is very low. This is because lactose naturally is non-conductive material, however, since there are some impurities in lactose, it is still giving a signature of conductivity. Moreover, during the granulation stage, tap water was used as liquid binder which also have impurities that remain in the tablet. From Figure 109, the tablets produced with 2 kneading elements shows a slightly fast dissolution rate at the



first 50 seconds compared to tablet produced with 1 kneading element and 0 kneading elements. Overall, the dissolution profiles for the three conditions are overlapping suggesting there is no obvious difference in the dissolution for the three experiment. This could be attributed to the fact that the granules prior to compression were subjected to milling of the same class size as well as they were compressed to the same compression force, so this contributed to have a trivial difference between their dissolution profiles.

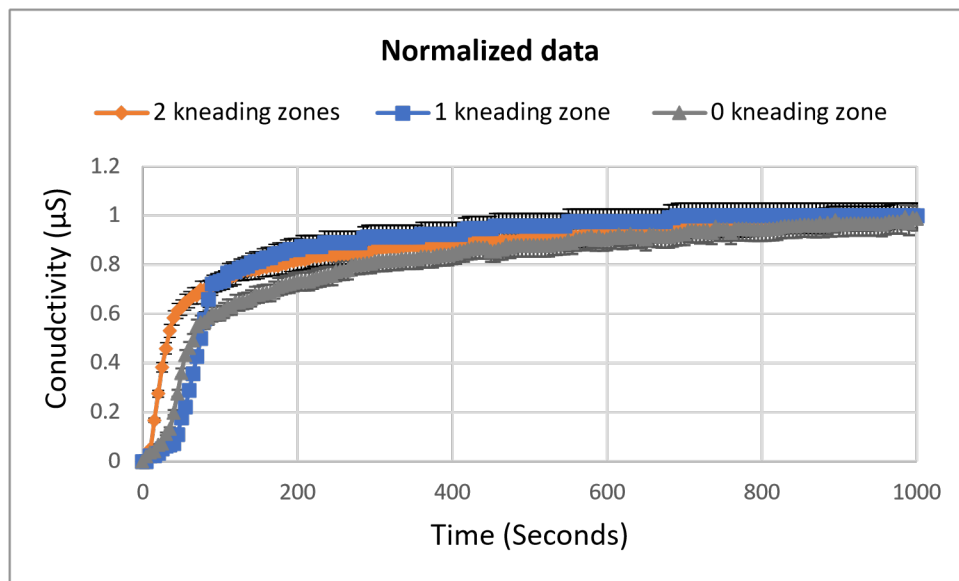


**Figure 109: Dissolution profiles for the tablets produced with three different screw configurations (2 kneading zones, 1 kneading zone, conveying element only). Measurements were repeated 10 times for all the three conditions, distilled water was being used as the dissolution medium with solution temperature of 37 °C and motor speed of 700 rpm.**

## 6.5 Conclusion

This part of work investigated the effect of varying the screw configuration on drying of granules and tabletability using a pilot plant scale (ConsiGma-25, Powder to tablet line). Varying the screw configuration has significantly affected the formation of the granules at the twin-screw granulation stage and ultimately this affected the drying process of the granules in fluidized bed and tabletability. The kneading elements provide more compaction and densification to granules due to its high shearing and mixing energy and this in turn led to the formation of well compacted granules with less amounts of fines. As the number of kneading elements decreases, fines formation increases, this was particularly observed with the absence of kneading elements (conveying only) in which high amounts

of fines and ungranulated powder was formed. This therefore has affected the drying process, the granules which were formed with using conveying elements only was the fastest in drying compared to the drying of granules which were produced with kneading elements. This may be attributed to the fact that small granules and fines, such as in the case of conveying elements, tend to dry faster due its higher surface area, dissimilar to the bigger and well compacted granules which tend to dry a bit slower because of its lower surface area available for drying. Also, the internal water reaches out to the surface at a slower rate in large granules compared to smaller ones. Moreover, screw configurations appeared to have an impact on the tableability of the milled granules. It was found that increasing the number of kneading elements led to the production of stronger tablet compared with the tablets produced with conveying element only. This could be attributed to that kneading elements exerting higher shearing and stress on the particles during the granulation stage and therefore affecting the deformability of particles. Lactose is a brittle material and increasing the number of kneading elements increases the compaction of the materials and thus this increases the chance of breaking/ fracturing of the particles during granulation. Therefore, the contact surface area and the bonding strength between the particles increases, and thus resulting in stronger tablets. The opposite scenario occurs when no kneading elements is used (conveying elements only). Tablet dissolution was also studied in this work; it was found that tablet produced with more kneading element dissolves slightly faster than the tablet produced with a smaller number of kneading elements or conveying elements. Furthermore, this work has given an insight about the impact of varying the screw configuration on the granules drying and tableting at larger scale pilot plant compared to the laboratory scale twin-screw granulator and fluidized bed dryer equipment. Regardless of the scale of the equipment, it was found in this study that the small-scale lab equipment and large-scale pilot plant gave the same conclusion in term of drying curves behaviour at different screw configuration, however investigation of the tablet tensile strength at different screw configuration was additionally investigated in the pilot plant study. Based on the above work, one can optimise the quality of granules and tablet by altering specific process and formulation parameters during the granulation stage using a continuous twin-screw granulator in both small and large scale.

## 7.0 Drying in a Continuous Wet Granulation ConsiGma 25 Line: Investigation of the Effect of Using Different Primary Particle size of Lactose Powder

---

### 7.1 Introduction

This chapter introduces the effect of varying the lactose primary particle size on drying of granules in the six-segmented fluidized bed dryer and tableability using a pilot plant scale (ConsiGma-25, Powder to tablet line). The temperature and moisture content profiles of the granules produced from different primary particle size of lactose monohydrates are analysed. Primary particle size of the starting material is one of the important parameters affecting the quality of the granules produced in a twin-screw granulator (Lute, et al 2018) and it is expected to be the parameter which affects the drying behaviour significantly. Both the moisture content and temperature of the granules can be used as an available control method to define the end point of the drying process in the line ratio (Fonteyne et al., 2014). However, this is not the focus of this study. An online NIR probe was also employed to measure the moisture content of the granules throughout the drying cycle. In the industry of pharmaceuticals, the granulation of powders to produce structured granules is one of the most significant processes in the manufacturing of oral dosage forms. This is done to enhance flowability, homogeneity, and compaction of powders. Lactose is considered one of the most common powders in the pharmaceutical industry among numerous excipients (filler/diluent) that are used in dry/wet granulation and tableting processes. It is available commercially in different grades (sieved, milled, spray-dried, granulated, etc.) giving different characteristics of particle (i.e., size, distribution of size, level of fines, shape, surface, flowability, and compressibility) (Lute, et al 2018). Lactose exists in two forms:  $\alpha$  and  $\beta$ , resulting in different solubility, melting points and hardness. It is well known that different lactose grades have different compression and granulation characteristics (Keleb, et al 2004). It has been reported by Lute, et al 2018, for instance, in direct compression, sieved  $\alpha$ -lactose monohydrate is used, while milled  $\alpha$ -lactose is wet granulated before tableting because of its poor compressibility under direct compaction. Lactose particles characteristics can play significant roles in granulation and consequently on drying and tableting processes.

In other words, the particle size of the primary powder plays a very significant role in determining the nuclei size at the stage of nucleation in wet granulation (Lute, et al 2018), which consequently affects the final attributes of granules. Therefore, the impact of the primary particle size and its properties need to be taken into account during the development of products using the platform of wet granulation. This work aims to study the effect of using different size grade of lactose monohydrates; 150M, 200M, 450M and microfine by comparing the effect of their physical properties on the granulation behaviour and consequently on the granules drying behaviour and tableability. All the powders were supplied from the DFE pharma except for the 150M lactose powder which was provided from a different supplier.

## 7.2 Lactose Powders Used

In this study, four different primary particle size of  $\alpha$ -lactose monohydrate (Pharmatose) were used; 150M, 200M, 450M and micro fines.  $\alpha$ -Lactose Monohydrate (Pharmatose) is white or almost white, odourless, crystalline powder freely soluble in water (Rowe et al., 2006). It is extensively used in industry of pharmaceuticals especially in wet and dry granulation, this being due to its low hygroscopicity, good compaction and compressibility properties. 200M, 450M and microfine were provided from the same supplier (DFE pharma) and 150M was provided from a different supplier (FrieslandCampina Domo, Netherland). Tap water was used as the liquid binder in the granulation process. Lactose powder morphology (i.e., size and shape) were analysed and therefore discussed in this section. Camsizer XT (Retsch Technology GmbH, Germany) was used to measure the size distribution of the four different size grade lactose monohydrates. Table 4 shows the  $d_{10}$ ,  $d_{50}$  and  $d_{90}$  of the four lactose monohydrate powders and Figure 109 shows the particle size distribution of each powder. It can be seen that the lactose 150M and 200M had the largest particle size ( $d_{50}$ ) amongst other lactose powder (i.e., 450M and the microfine) respectively.

**Table 4:** Particle size  $d_{10}$ ,  $d_{50}$  and  $d_{90}$  of the four lactose monohydrate powders used in this study

Lactose Powder Grade	Particle Size ( $\mu\text{m}$ )		
	$d_{10}$	$d_{50}$	$d_{90}$
Micro fines	3.8	6	9.1
450M	7.9	25.3	46.3
200M	11.6	41.9	77
150M	12.8	50	111.9

### 7.2.1 Morphology of the Powder

The scanning electron microscopy (SEM) images were generated to analyse the particle shape and morphology of  $\alpha$ -lactose monohydrate of different size grade (Figure 110.) The SEM images clearly show the difference in the size and shape. Lactose monohydrate powder is crystalline milled lactose with tomahawk like shape. Lactose powder particles tend to be elongated with some particle sticking on the larger ones. Overall, all powder used in this study tend to have similar morphology as presented in the SEM images in Figure 111.

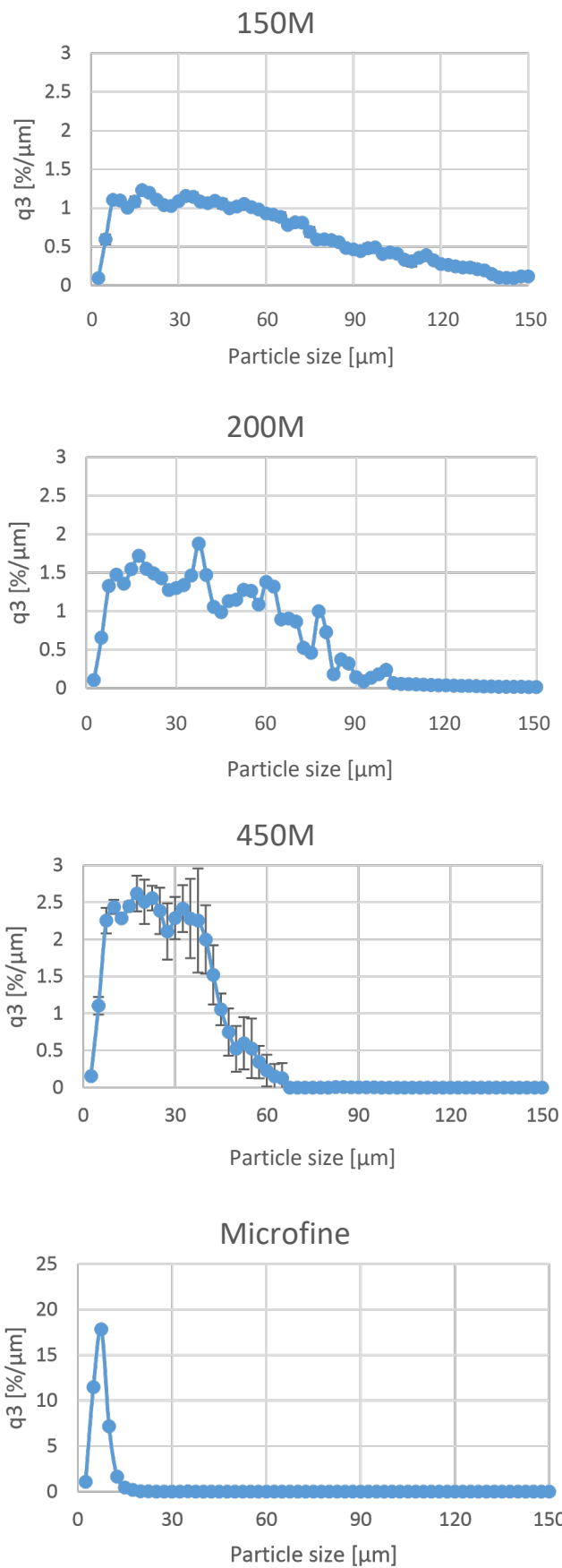
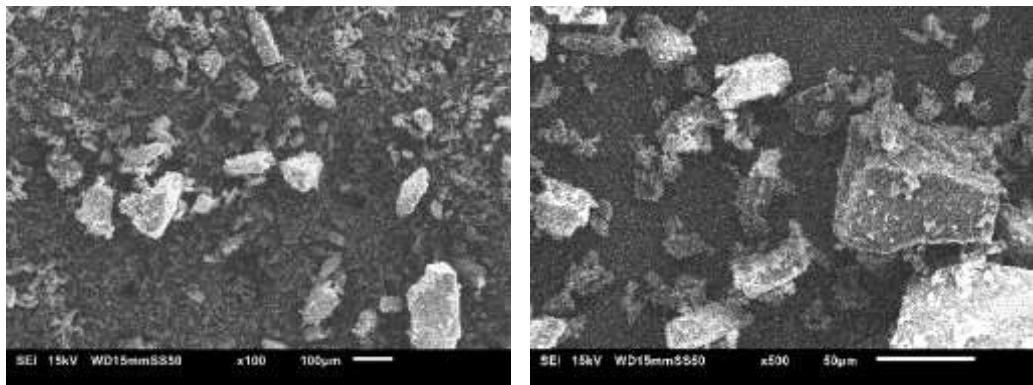
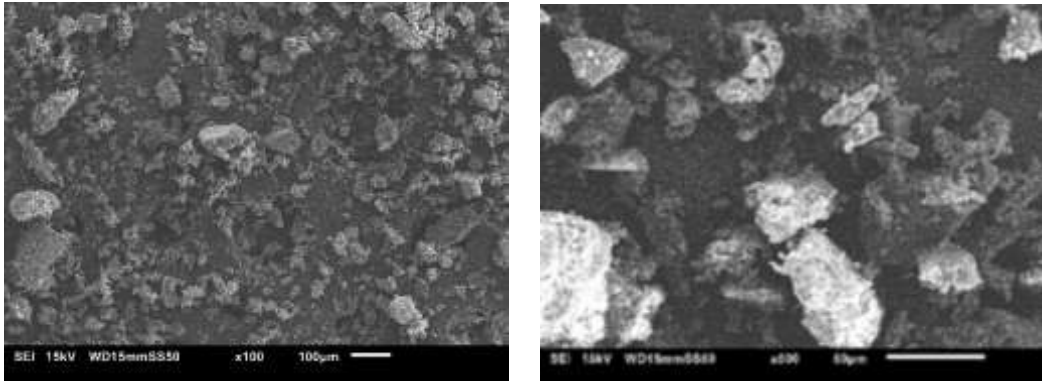


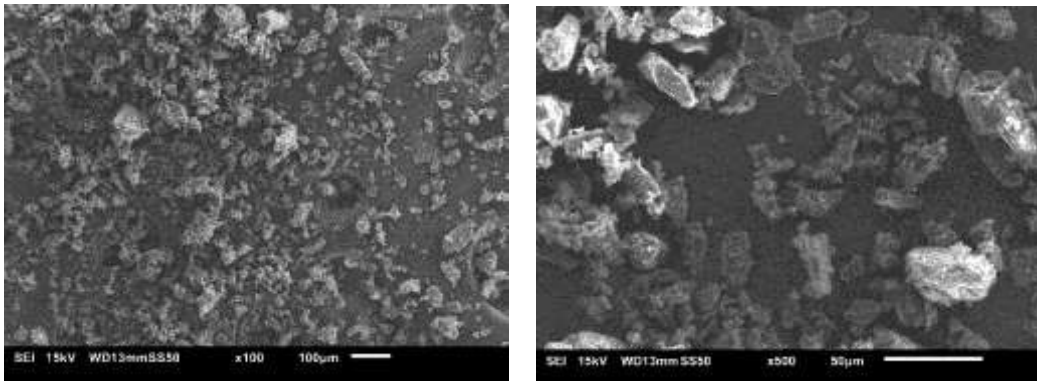
**Figure 110: Primary Particle size distribution of lactose monohydrate with different size grades (150M,200M,450M and microfine) measured by Camsizer XT.**



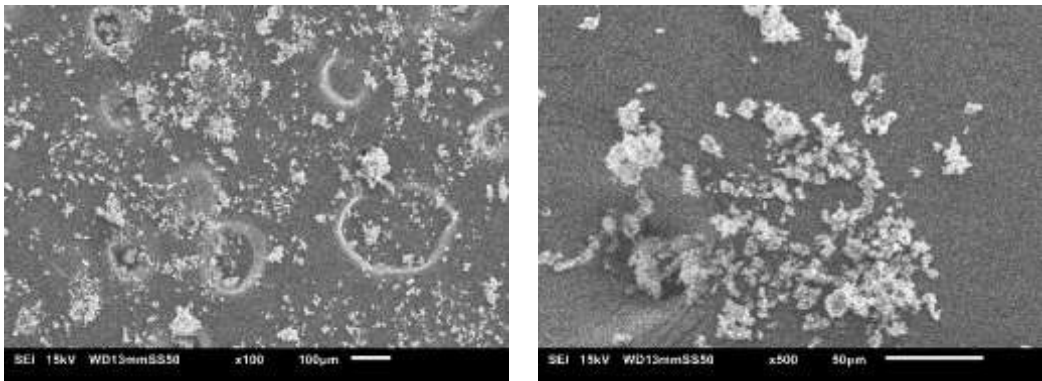
**150M lactose Monohydrate ( $d_{50}$  50µm)**



**200M lactose Monohydrate ( $d_{50}$  41.9µm)**



**450M lactose Monohydrate ( $d_{50}$  25.3µm)**



**Micro fines lactose Monohydrate ( $d_{50}$  6µm)**

**Figure 111: SEM of lactose monohydrate of different primary particle size.**

### 7.3 Lactose Powders Density

The bulk density and the tapped density of the four size grades of lactose monohydrate powder (150M, 200M, 450M and microfine) are measured. The bulk densities of the powder were obtained by pouring powders into 100 cm<sup>3</sup> cylinder through a funnel, based on the American standard for testing of material (ASTM D1895-96 2010, ASTM International 2015). The mass of the dispensed powder into the cylinder and the corresponding volume were measured. The bulk density of the powder was obtained by dividing the mass of powder by the volume of the cylinder to give the following values of lactose monohydrates powders respectively 0.62 ±0.02, 0.59 ±0.01, 0.51 ±0.02, 0.28 ±0.03 (Table 5). The tapped density of the four lactose size grades is obtained by mechanically tapping on the cylinder containing the powder sample, using Copley tapped density tester (Copley Scientific JV2000, UK) in accordance with the ASTM B527 standards. The powder is tapped inside the cylinder until no further change in product volume is observed. The tapped density is then determined by dividing the mass of the powder by the final tapped volume to give the following tapped density values of the four-lactose monohydrate powders; 150M, 200M, 450M and microfine respectively, 0.78 ±0.02, 0.73 ±0.02, 0.67 ±0.03, 0.37 ±0.03 (Table 5). The measurements were repeated three times and the standard deviation was below 5% for all the measurements. The closeness values of densities are important as different tap densities suggest different packing efficiencies of particles, which can independently have an impact on the properties of granule (Lute et al., 2018).



**Table 5:**The measured bulk and tapped density of the four-lactose powder monohydrate

<b>Lactose Powder Size Grade</b>	<b>Bulk Density g/cm<sup>3</sup></b>	<b>Tapped density g/cm<sup>3</sup></b>
<b>150M</b>	0.62 ±0.02	0.78 ±0.02
<b>200M</b>	0.59 ±0.01	0.73 ±0.02
<b>450M</b>	0.51 ±0.02	0.67 ±0.03
<b>microfine</b>	0.28 ±0.03	0.37 ±0.03

#### **7.4 Design of Experiment**

Figure 112 shows the conditions used (process parameters) in all of the four experiments which were carried out to investigate the effects of changing the primary particle size of the starting material (lactose monohydrate) on the drying process of granules and consequently on the tableting process. Tap water was the liquid binder used in all of the experiments. Temperature of the barrel (25 °C), twin screw configuration, screw speed (250 rpm), powder feed rate (10 kg/hr), liquid feed rate (1 kg/hr), filling time (300 seconds), drying time (800 seconds), drying air temperature (50 °C), air flow rate (400 m<sup>3</sup>/hr) and tableting compression force (5kN) were all kept fixed throughout the entire experiments. In response to the experimental results, granules size distribution after twin-screw granulation was measured for each experiment. Moreover, inline NIR-probe (FP710e, NDC Technology, Dayton, Ohio, USA) and temperature sensors measured the moisture content and temperature profiles of the granules during fluidized bed drying respectively. For the final product (tablet), the breakage force of the entire produced tablet was measured.

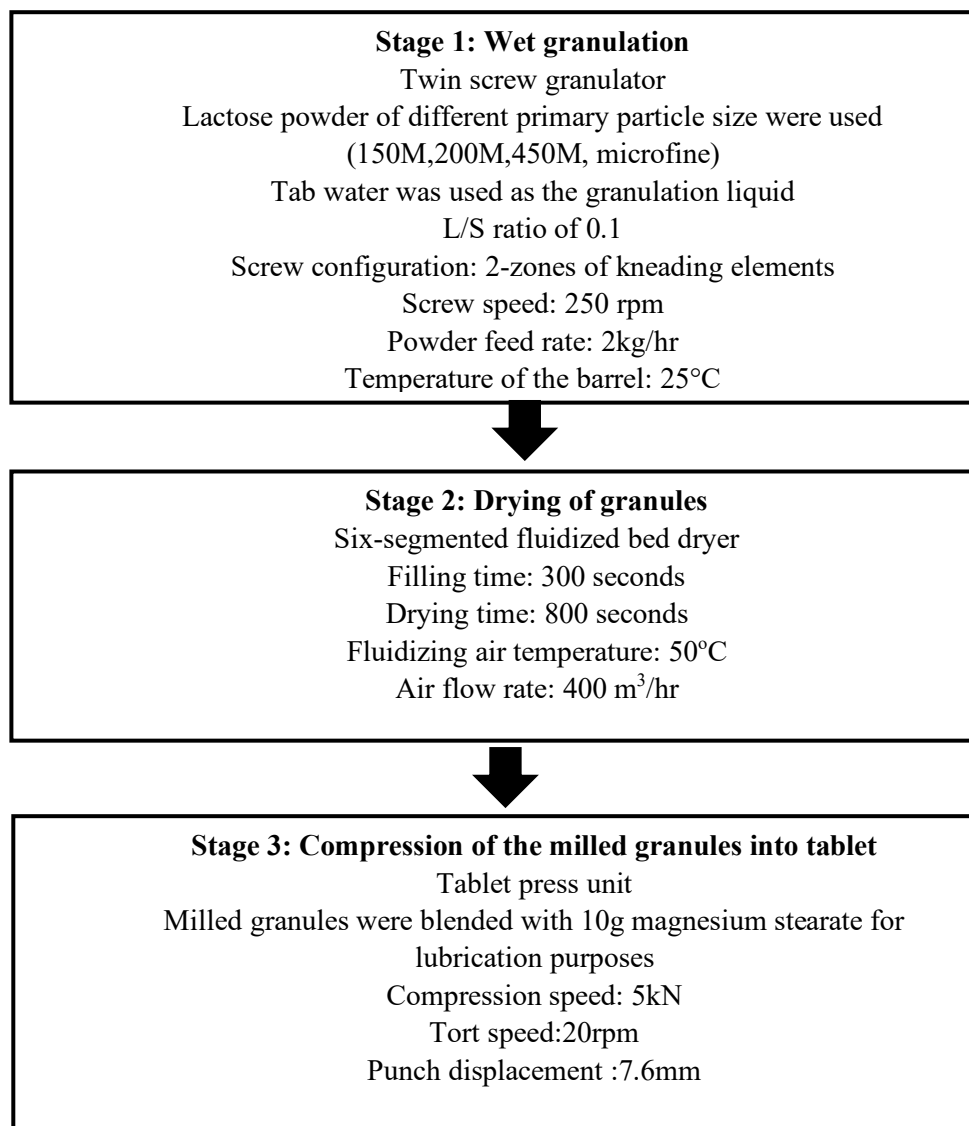


**Figure 112: Flow diagram showing the process parameters used in TSG, FBD and tableting respectively for this chapter.**

Figure 113 shows the screw configuration used throughout all the experimentation of this chapter; this configuration consisted of conveying elements with two zones of kneading discs in each screw. Each screw consists of 12 kneading discs placed at 60° and separated by conveying elements. The function of kneading element assists with breaking the larger formed granules into smaller ones and therefore produce a more uniform particle size distribution. All twin-screw conditions were kept fixed in order to determine the impact of different primary particle size on drying of granules.



**Figure 113: Screw configuration used in this stud which consisted of long pitch conveying elements and two kneading zones each contain 6 kneading discs placed at an angle of 60 degree so a total of 12 kneading discs in each screw.**

To study the rate of growth and kinetics of the granules made at the twin-screw granulation process; the connector between the TSG and the fluidized bed dryer was dismantled to collect granules from the TSG. Samples of granules were then collected in metal trays from the twin-screw granulator after the twin-screw granulator reached a steady state. The collected granules were left in room temperature to dry for 24 hours prior to the size distribution measurement in the Camsizer equipment. The granules size distribution was determined as a function of changing the primary particle size of the starting material (lactose monohydrate). To proceed with the experiment so that the powder is processed through the entire line, the connection between the twin-screw granulator and the fluidized bed dryer was resorted back. After the granules have been produced in the twin-screw granulator, then they are transferred through pneumatic conveying system to the fluidized bed dryer for drying. The fluidized bed dryer consists of six-segmented cell, which are filled with granules in an anticlockwise direction from cell 1 to cell 6. However, only one cell (cell 5) has been used in all of the experiment, as it is the only cell where the NIR probe can be fitted for measurement of moisture content throughout the drying process. Each cell is fitted with a temperature probe located at the centre just above the distributive plate of air. Both the temperature and the moisture content readings are recorded automatically every 5 seconds. The NIR probe is an inline tool to measure the moisture content profiles of the granules inside the cell. Replicate experiment was done for this cell to confirm the reproducibility of the result. The fluidized bed dryer was set to an airflow rate of 400 m<sup>3</sup>/hr, an inlet drying air temperature of 50 °C, filling time of 300 seconds, and drying time of 800 seconds. These conditions were maintained the same for all the experiments. After the drying of granules is completed, dry granules were then transferred to the milling unit in which it runs for 100 seconds. The milled granules are then transferred to a lubricant the milled granules were blended with 10g of

magnesium stearate for lubrication purpose prior to tableting. The tablet machine was set to a compression force of 5kN and a punch displacement of 7-7.

6mm. The rate at which the tableting machine was producing the tablets is 12000 tablets/hr. A set of 100 tablets from each experiment were collected and tablets were then subjected to weight, thickness, diameter and hardness measurement.

## **7.5 Result and Discussion**

### **7.5.1 TSG Granules Size Distribution**

The samples of the granules (Figure 114) which were taken from the twin-screw granulator at each experiment were analysed in the Camasizer for the size measurement. Figure 115 shows the size distribution of the granules produced using lactose powder of different primary particle size (150M, 200M, 450M and microfine). As mentioned earlier in this chapter (Section 7.2) that the  $d_{50}$  of each of powder is different they are 51  $\mu\text{m}$ , 41  $\mu\text{m}$ , 24 $\mu\text{m}$  and 6  $\mu\text{m}$ , respectively. It can be clearly seen from Figure 115 that the size of the granules increased as the primary particle size of lactose powder increases. The microfine lactose powder produced the highest amounts of fines compared to the others powders as seen in the size distribution and the images in Figure 115. Moreover, the size distribution of granules produced from 150M, 200M and 450M lactose powder has the lowest proportions of fines and overall, the distribution of the granules using these powder size grades was broad compared to the microfine granule size distribution. In other words, the distribution was seen to be broad at increased  $d_{50}$  of the starting material (450M, 200M and 150M). The reason for such trend can be ascribed to that liquid binder covers a larger particle size of lactose monohydrate more efficiently than that of the smaller particle size due to larger particles have smaller surface area and vice versa.

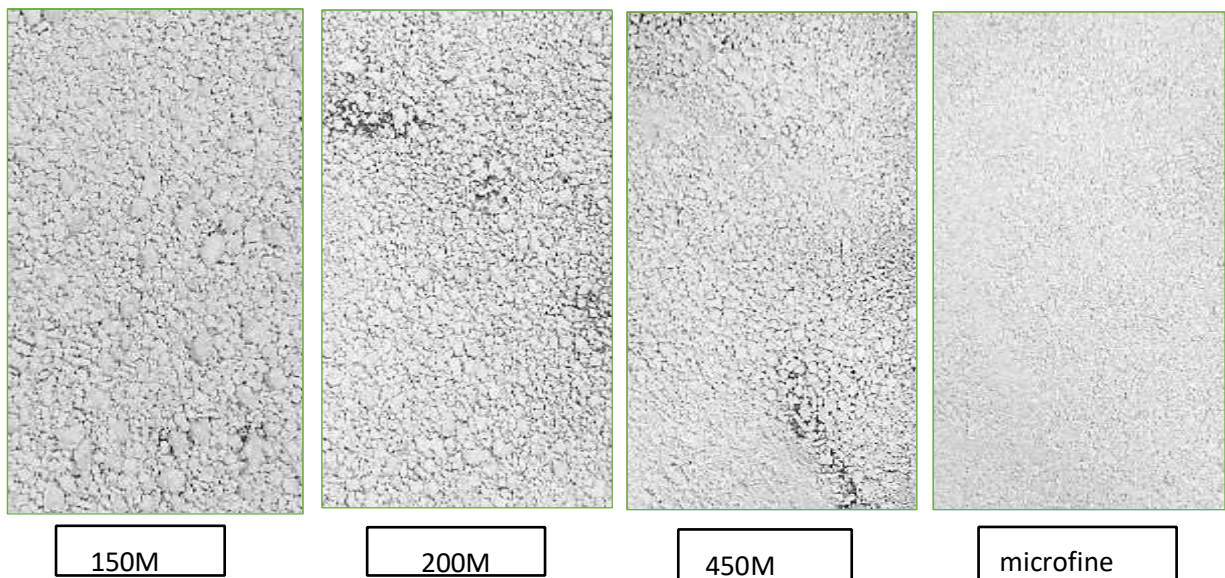


**Figure 114: Images of granules samples produced b TSG at different lactose primary particle size (150M,200M,450M and microfine) with water used as the granulation liquid binder, screw speed of 250rpm, L/S of 0.1 and 2 kneading zones prior to drying process.**

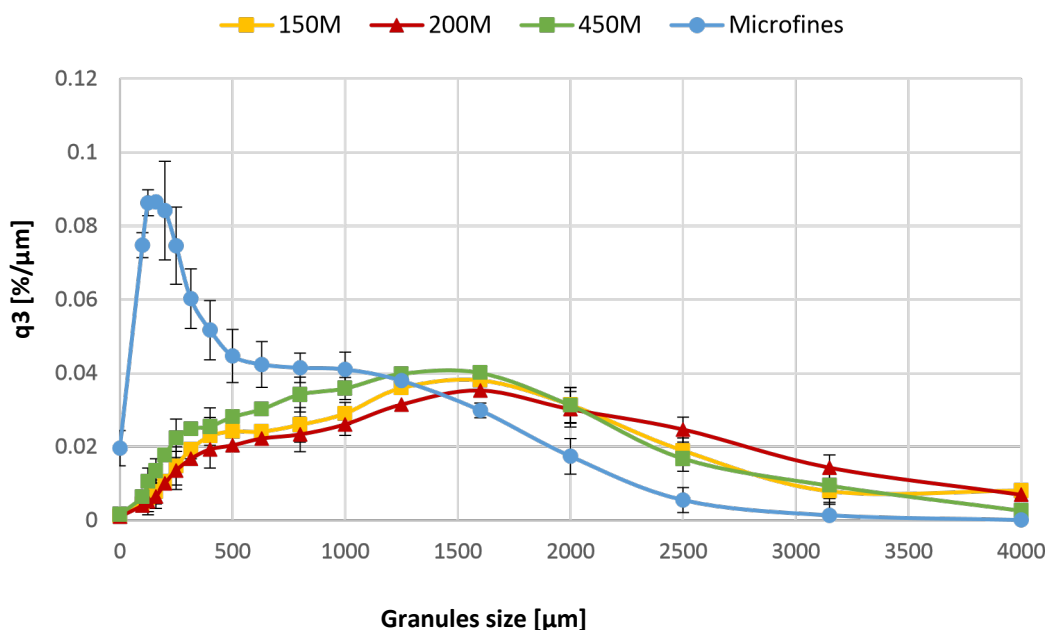


**Figure 115: Size distribution of granules produced at different primary particle size of lactose (150M, 200M, 450M and microfine). All other parameters during granulation and drying kept fixed throughout i.e., water as a liquid binder, L/S of 0.1, 2 kneading zones, screw speed of 250rpm and drying air temperature, flow rates and drying time of 50°C,400 m<sup>3</sup>/hr and 800 seconds respectively.**

Figure 116 shows the  $d_{10}$ ,  $d_{50}$  and  $d_{90}$  for the granules produced by twin screw granulator at the 4 different lactose size grade experiments. The Figure suggests the same conclusion drawn out for the granules size distribution in Figure 115. However, it can be observed from the figure that the

difference in size of the granules produced from 150M, 200M and 450M is not very significant this is due to the small difference in the  $d_{50}$  between the initial lactose powder of 150M, 200M and 450M.

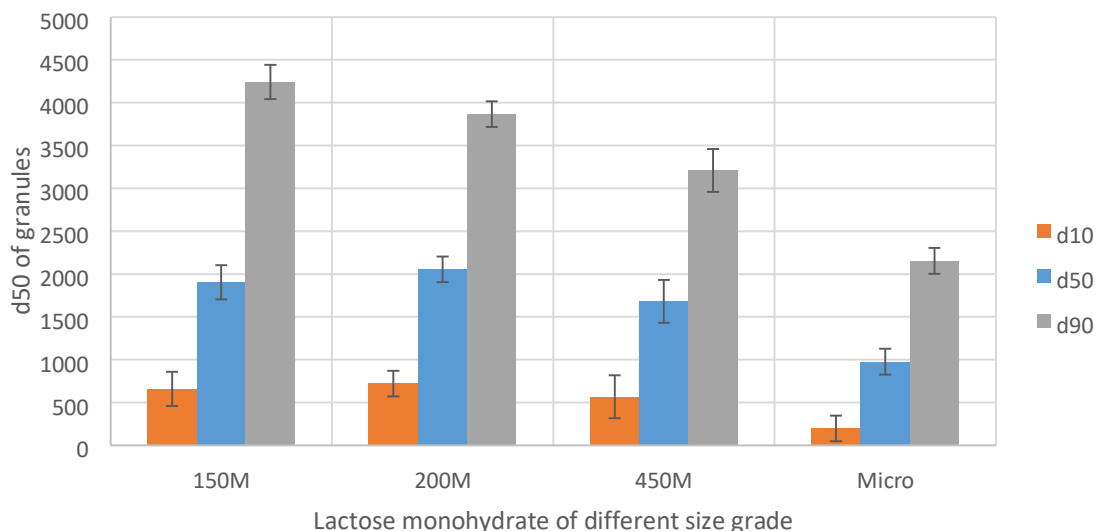


**Figure 116:  $d_{10}$ ,  $d_{50}$  and  $d_{90}$  of the granules produced by TSG prior to fluidized bed drying at different lactose monohydrate primary particle size (150M, 200M, 450M and microfine). All other parameters during granulation and drying kept fixed throughout i.e., water as a liquid binder, L/S of 0.1, 2 kneading zones, screw speed of 250rpm and drying air temperature, flow rates and drying time of 50°C, 400 m<sup>3</sup>/hr and 800 seconds respectively.**

### 7.5.2 Behaviour of Granules Drying Process in the Segmented Fluidized Bed Dryer

The filling time per cell was 300 seconds making a cell load of 0.83 kg granules at a powder feed rate of 10 kg/hr. The inlet drying air temperature, humidity and flow rate of the drying air were set at 50 °C, 10% and 400 m<sup>3</sup>/h, respectively. The drying time was fixed at 800 seconds. These conditions were all kept constants for all the experiment while the primary particle size of the starting materials was varied. The product temperature inside the dryer cells were monitored by a temperature probe. When the temperature profiles are plotted for all the four conditions (Figure 117), it is possible to see how these temperature profiles behave similarly throughout the four conditions. In all of the four cases, it can be noticed that the temperature abruptly decreases when the granules started filling the cell. It is also possible to observe that the temperature profiles for the cell filled with granules made from microfine lactose powder was slightly less steep compared to the other material size conditions. Having the cell loaded with granules, the temperature maintained constant for a period of time, this represents the constant rate-drying period. The temperature relatively maintained constant near the equilibrium wet bulb temperature until all the moisture at the surface of granules is evaporated. This

processes a bit shorter for the microfine condition. After most of the water at the surface is evaporated, the temperature begins to increase. And continues to rise until all the internal moisture content is evaporated. This represents the falling rate period. After all the internal water is evaporated, the temperature then begins to stabilise (reaches a steady state similar to the drying air temperature) this is when all of the moisture content is evaporated, and granules become dry. This stage represents the equilibrium period. Overall, the temperature profile of the granules produced from microfine showed a slightly visible difference in the drying behaviour among the three other powders, this could be due to its relatively smaller particle size compared to other three powder sizes. To assess the drying process of these four conditions, moisture content profiles are obtained and discussed further.

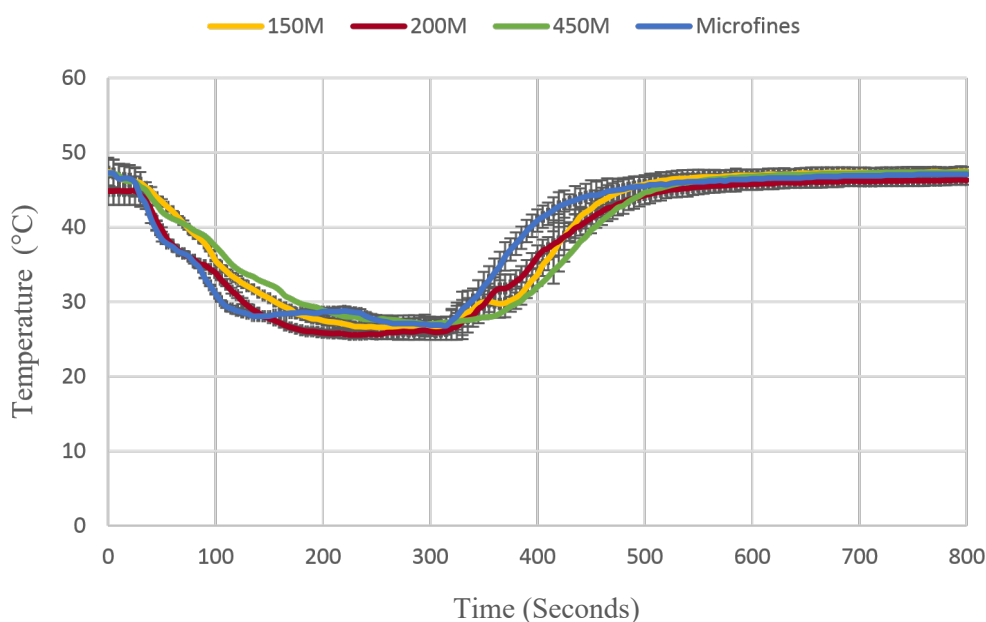


**Figure 117: Granule's temperature profiles plot at different lactose monohydrate primary particle size (150M, 200M, 450M and microfine). All other parameters during granulation and drying kept fixed throughout i.e., water as a liquid binder, L/S of 0.1, 2 kneading zones, screw speed of 250rpm and drying air temperature, flow rates and drying time of 50°C, 400 m<sup>3</sup>/hr and 800 seconds respectively.**

### 7.5.3 NIR Online Measurements of Moisture Content in the Fluidized Bed Dryer

To further assess the behaviour of granules drying process in the segmented fluidized bed dryer, an online NIR probe was used to obtain the granule moisture content every 5 seconds. As mentioned earlier, the NIR probe was fixed in the probe port of cell 5 of the fluidized bed. Besides the solid moisture content measurement, the NIR probe can also detect and quantify the product around the probe, this is called product presence which is discussed later in this section for all the drying experiments. Figure 118 shows the profiles of moisture content of granules produced using four different size grades of lactose monohydrate: 150M, 200M, 450M and microfine respectively. During the cell filling time, the moisture content reading generally increases, the increase in moisture content is steady as the system is drying the granules as it comes in the cell. During the filling period, as the granules are loaded into the cell continuously, they are also drying at the same time. At the start of the filling, the moisture content increases to then decreases and then begin to increase again. This is because as the first wet granules are coming into the cell, they contact the probe closely as they come in and then are fluidizing away resulting in the probe to be unable to provide sensible readings again. This hypothesis is supported by the product presence obtained by the same NIR probe as seen in in Figure 119 which indicates the amounts of granules near the NIR probe that is capable of reflecting the light of the NIR. As it can be observed from both Figures (Figure 118 and Figure 119) that the readings of moisture content and product presence dropped at the same time which emphasise the hypothesis. This behaviour is existing for all four different conditions presented. The product presence tends to stay constant during the whole process of drying. However, overall, the presence of product during the drying process for the four conditions tend to be different. For instance, as the particle size of the starting materials increases, the product presence around the probe decreases. It was observed from the window of the dryer cell that faster fluidization occurred during the drying of the granules produced from microfine powder, this could be the reason behind getting higher product presence values for the granules made from microfine. The opposite scenario occurs when the batch has larger granules, the product presence, then decreases because the granules are fluidizing away from the probe resulting in sensing less amount of product. In other words, this is can be useful piece of information by the NIR probe; to have an insight about the state of the bed fluidization.



After the completion of the granules filling, which is marked with a vertical black dotted line at 300 seconds, the moisture content decreases for all the four cases at a fairly constant rate as expected until reaching the critical moisture content point which was different for each of the four materials. In this case the moisture content never goes under 1.7%, which is lower than the moisture content of the starting blend recorded by the probe indicating that the product is dried. The observed difference in moisture content is most likely due to the difference in granules size as large primary particle size of lactose monohydrate produces bigger granules which have small surface area than the small granules and fines which were produced from smaller particles of lactose monohydrate. It seemed that closeness of the starting material  $d_{50}$  has led a small difference in the drying curves especially for the 150M and 200M. However, a great difference can be observed in the drying process when using the microfine powder as it has a very low  $d_{50}$  values among the other three lactose powders.

To look closely at the effect of using different primary particle sizes on the drying curves of granules, the line slope for all curves between time 300 seconds (starts of the drying) and 380 seconds (starts of equilibrium point) were plotted as shown in Figure 120. It can be seen that as the lactose primary particle size increases, the steepness of the lines increases, this implies granules produced from microfine powder had faster drying rate. This was very noticeable among the other three sizes. Only trivial difference is seen between the other three sizes 150M, 200M and 450M, this is due to the small difference between their  $d_{50}$  of the initial powder. Microfine had much lower  $d_{50}$  compared to all of the three powders, therefore a very visible difference can be observed. Moreover, the residual moisture content of the granules at the end of the drying process for all the four conditions was plotted as shown in Figure 121. As the particle size increases, the residual moisture content decreases. The difference between the residual moisture content of the granules prepared from 150M, 200M and 450M is not very significant. Again, this is believed to be related to the small difference in the initial  $d_{50}$  of the powder used to make these granules.

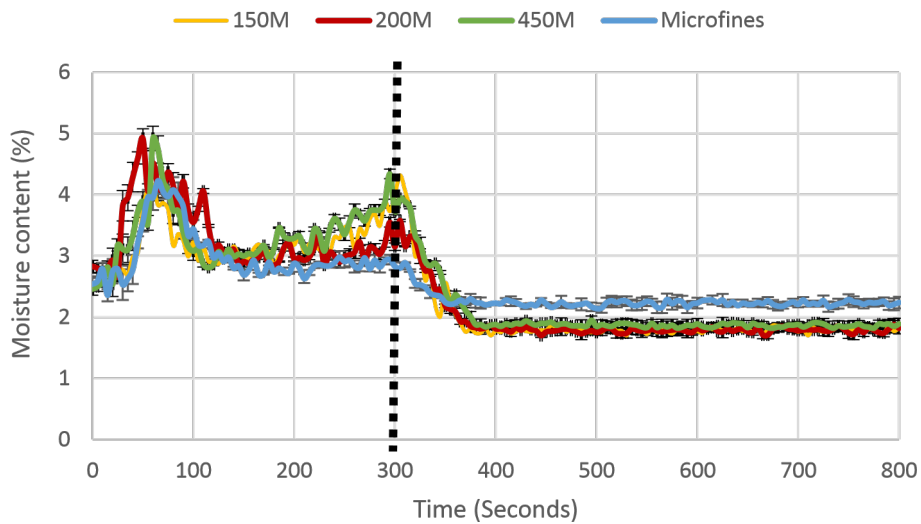


**Figure 118: Granule's moisture content profiles obtained from the NIR probe at the four different lactose monohydrate particle size (150M, 200M, 450M and microfines). The black dotted line shows the end of the filling time and the start of the drying time. All other parameters during granulation and drying kept fixed throughout i.e., water as a liquid binder, L/S of 0.1, 2 kneading zones, screw speed of 250rpm and drying air temperature, flow rates and drying time of 50°C,400 m<sup>3</sup>/hr and 800 seconds respectively.**

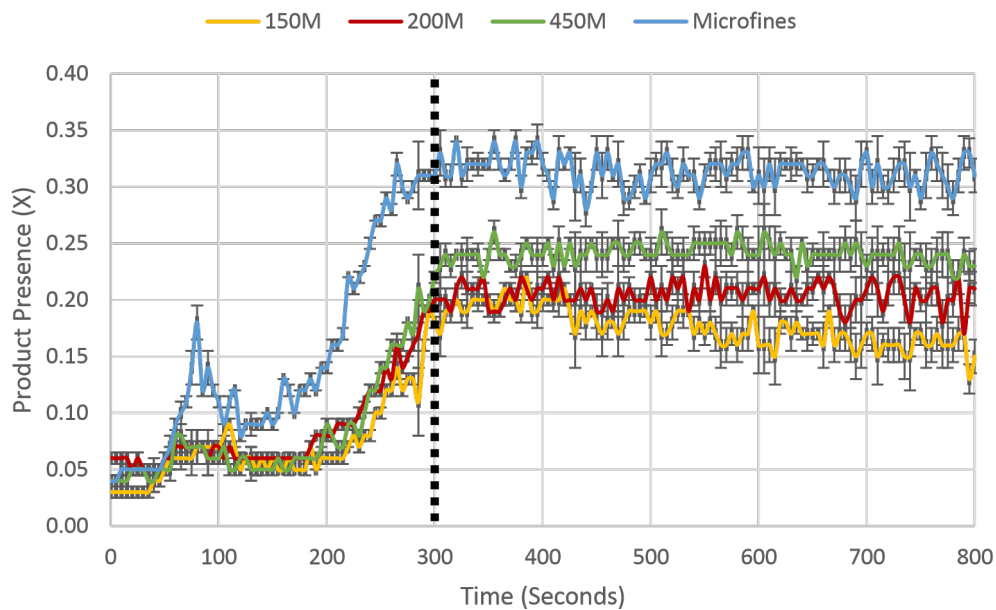


**Figure 119: Presence of product obtained from the NIR probe at the four different lactose monohydrate particle size (150M, 200M, 450M and microfines). The black dotted line shows the end of the filling time and the start of the drying time. All other parameters during granulation and drying kept fixed throughout i.e., water as a liquid binder, L/S of 0.1, 2 kneading zones, screw speed of 250rpm and drying air temperature, flow rates and drying time of 50°C,400 m<sup>3</sup>/hr and 800 seconds respectively.**

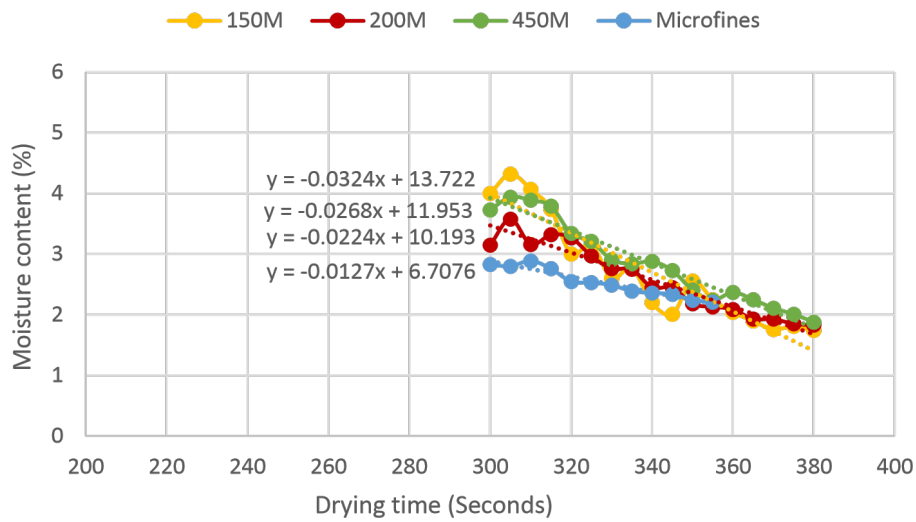


**Figure 120: Slopes of the drying curve between time 300 seconds and 380 seconds at the dryer cell at different primary particle size of lactose.**

Again, as mentioned in the previous chapter, it was not possible to take samples of granules out of the fluidized bed dryer for determination of size distribution; this was even not possible after drying is completed, as doing so will disturb the continuous process of the powder to tablet line system. Therefore, no size distribution of granules during or after drying is presented in this work. The granules were then flowed to the milling unit for size reduction, the screen size is 1596  $\mu\text{m}$  (~1.5mm) the milling is to ensure uniform size of granules. Milled granules then get blended with magnesium stearate ready for compression into tablet form which is the final product in the line.

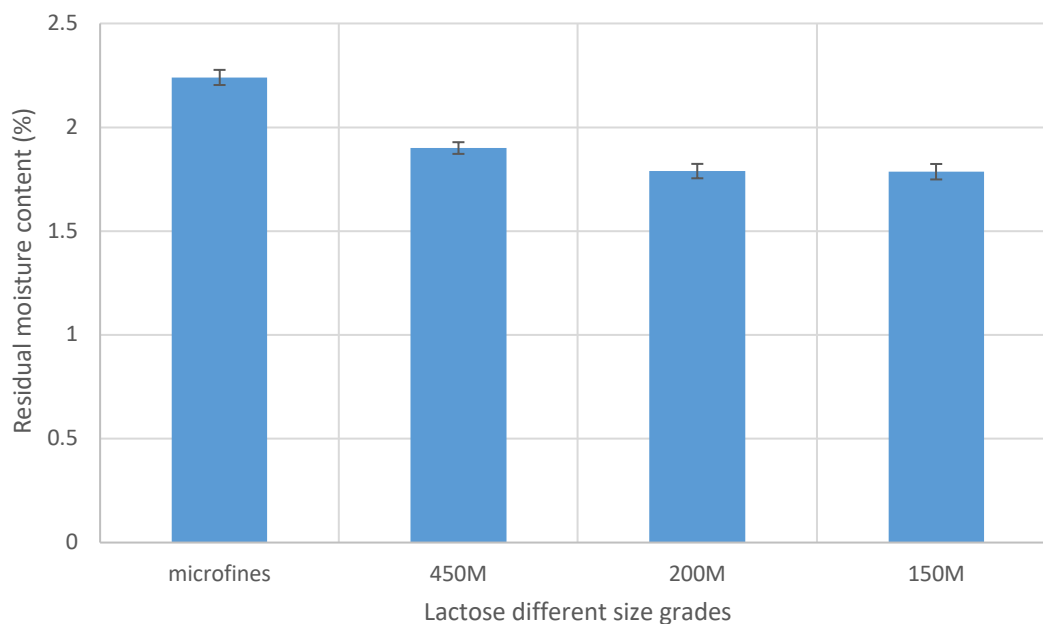


**Figure 121: Residual moisture content at the dryer cell 5 as a function of primary particle size (150M, 200M, 450M and microfine) extracted from the moisture content profiles. All other parameters during granulation and drying kept fixed throughout i.e., water as a liquid binder, L/S of 0.1, 2 kneading zones, screw speed of 250rpm and drying air temperature, flow rates and drying time of 50°C, 400 m<sup>3</sup>/hr and 800 seconds respectively.**

#### 7.5.4 Tablet Attributes

As mentioned above, the tablets were produced using the milled granulation product lubricated with magnesium stearate at the blending unit. The conditions at the tableting press were maintained constant throughout all the four experiments. This is to allow the determination of the impact of varying the starting material powder particle size on the tablet attributes. In this work, tablets were evaluated for their physical characteristics like weight, breaking force, thickness, tensile strength and dissolution. These characteristics were evaluated for 100 tablets of each condition were evaluated by Pharmatron AG -Multitest 50 G2 machine as presented in Table 6.

**Table 6:** Variation in the tablet mass, thickness and diameter as the primary particle size of the starting materials (lactose monohydrate) changes.

Starting Material	Tablet Mass (g)	Tablet Thickness (mm)	Tablet Diameter (mm)
150M Lactose	0.74±0.011	6.75±0.079	12.10±0.008
200M Lactose	0.74±0.004	6.82±0.035	12.11±0.006
240M Lactose	0.74±0.003	6.86±0.036	12.11±0.006
Microfine	0.72±0.0047	6.65±0.045	12.10±0.0075

Figure 122 shows the variation in the breaking force of 100 tablets made of different particle sizes of lactose. Figure 123 shows the average breaking force of the 100 tablets made from the different size grades of lactose. It can be clearly seen from these Figures that as the particle size of the starting material (lactose) increases, the breaking force of the tablet decreases. In other words, tablet produced from microfine showed the highest breaking force and tablet produced from the highest particle size showed the lowest breaking force



**Figure 122:** Breaking force variation for 100 tablets of each condition made of different lactose primary particle size (150M, 200M, 450M and microfine). All other parameters during granulation and drying kept fixed throughout i.e., water as a liquid binder, L/S of 0.1, 2 kneading zones, screw speed of 250rpm and drying air temperature, flow rates and drying time of 50°C, 400 m<sup>3</sup>/hr and 800 seconds respectively. The compression force used for tableting was 5kN for all experiment.

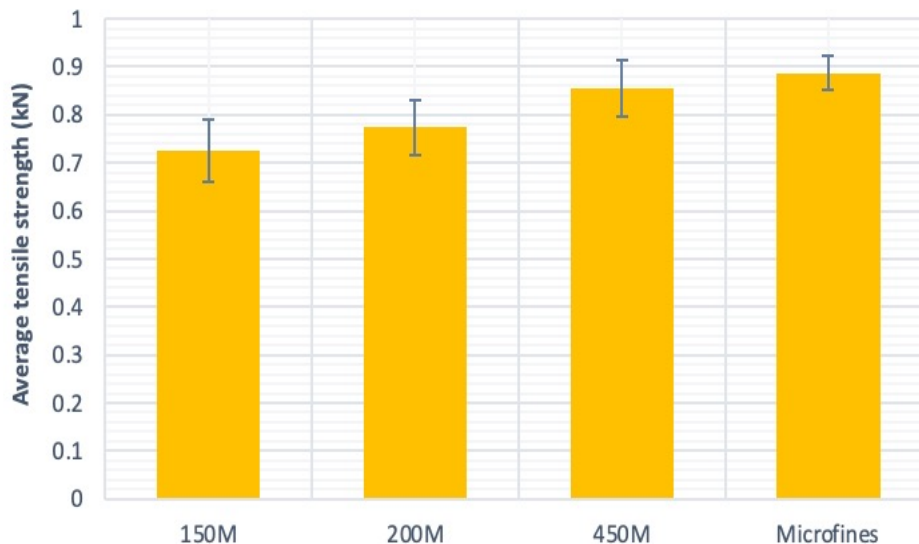


**Figure 123: Average breaking force for 100 tablets produced at different primary particle sizes of lactose monohydrate; 150M,200M,450M and microfines) with other parameters kept fixed i.e., water as a liquid binder, L/S of 0.1,2 kneading zones and screw speed of 250rpm. The compression force used during tableting was 5kN for all the four experiments.**

#### 7.5.4.1 Tablet Tensile Strength

To explain this further the tensile strength of all the tablets of each condition was determined. As mentioned in the previous chapter, the shape of the tablets as produced from the tablet press is curved faced as illustrated in Figure 100 in previous chapter. Therefore Equation 1 in the previous chapter which is developed by Pitt and Newton (1988) was used to calculate the curved faced tablet tensile strength from the breaking forces loaded across the tablet diameter (Shang et al., 2013). Figure 124 shows the variation of tensile strength for 100 tablets at different particle size of lactose. And Figure 125 shows the average tensile strength for the 100 tablets presented in the previous figure. It can be clearly observed from these figures that as the primary particle size increases, the tensile strength decreases. The effect of the lactose particle size on the breaking force and therefore on the tensile strength can be explained by the fact that smaller particles have a higher surface area available for bonding within the tablets and hence lead to a stronger tablet. It appeared that tablets compressed from small particles (microfine and 450M) were generally stronger than the tablets prepared from larger coarse particles (150M and 200M).

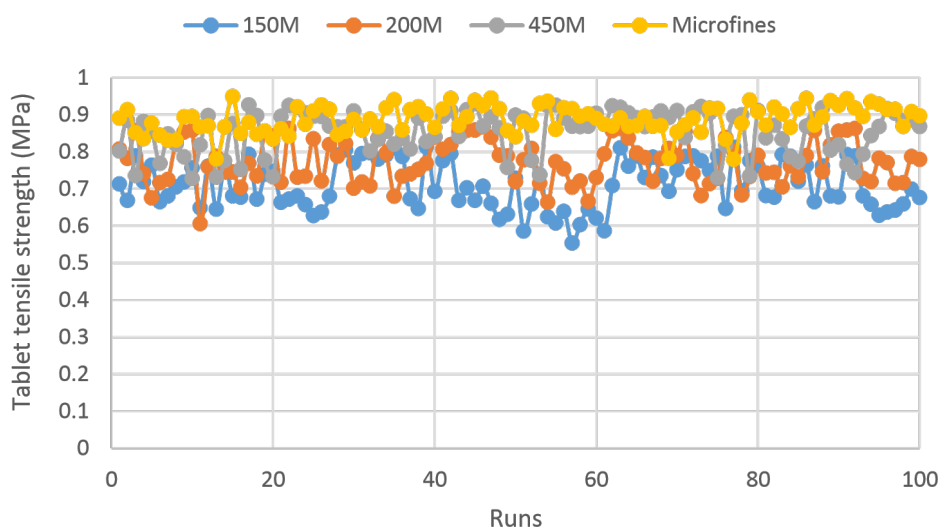


**Figure 124:** Tensile strength of 100 tablets of each condition (four different lactose primary particle size (150M,200M,450M and microfine) as calculated by the equation developed by Pitt and Newton (1988). All other parameters during granulation and drying kept fixed throughout i.e., water as a liquid binder, L/S of 0.1, 2 kneading zones, screw speed of 250rpm and drying air temperature, flow rates and drying time of 50°C,400 m<sup>3</sup>/hr and 800 seconds respectively. The compression force used for tableting was 5kN for all experiment.

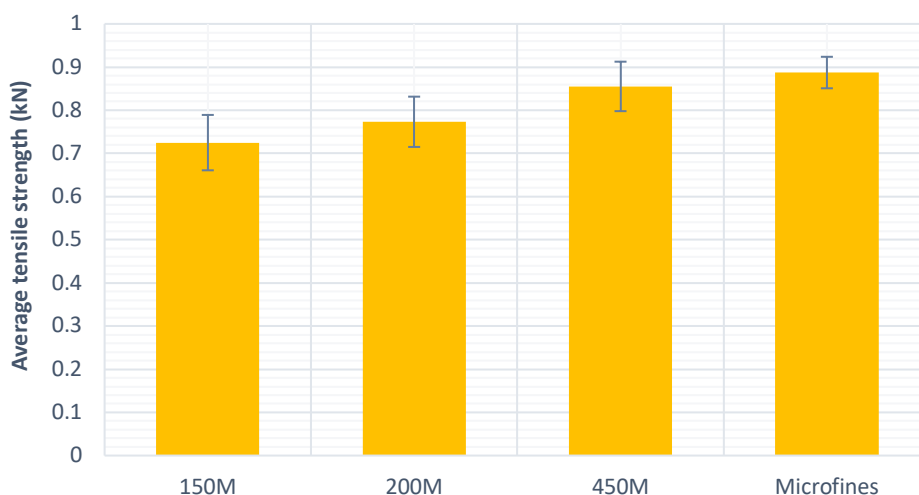


**Figure 125:** Average tensile strength for the 100 tablets made of different particle sizes of lactose (150M,200M,450M and microfine) with other parameters kept fixed i.e., water as a liquid binder, L/S of 0.1,2 kneading zones and screw speed of 250rpm. The compression force used during tableting was 5kN for all the four experiments.

#### 7.5.4.2 Tablet dissolution

As explained in the previous chapter under the topic of dissolution that studying the dissolution of the tablet is a very important aspect in the development process of the drug. Dissolution test was carried

out in this study for all the tablets using the same setup and conditions used in the previous chapter. Prior to testing the dissolution profiles of the tablets made from using different primary particle size of lactose, initial conductivity of powder used to make these tablet was measured. 150M lactose powder had initial conductivity of  $0.5\mu\text{S}$  while 200M,450M and microfine powder had a conductivity of  $2.5\mu\text{S}$  before normalization. it can be said overall that the response of the lactose to the conductivity measurement is very low. This is because lactose naturally is non-conductive material, however, since there are some impurities in lactose, it is still giving a signature of conductivity. There are also impurities as a result of the addition of tap water (binder) during the granulation stage. Impurities in tap water such as salt, calcium, and magnesium ions are charged, when they move through water, electricity can flow through the liquid and hence more conductivity is obtained. Moreover, the reason for the difference in the initial conductivity between 150M and the other three lactose size grades powder (200M, 450M and microfine) due to that 150M powder is being provided from a different supplier to the other three powders (200M,450M and microfine). This implies that the 150M (lactopure lactose) as its name suggest it purer (with less impurities) than the other three powders and that is why it is conductivity is much lower than the other three lactose powders. Furthermore, tablet produced from 150M was excluded from the measurement. Figure 126 shows the dissolution profiles of tablet produced from lactose powder of different size grades. For all the dissolution tests, distilled water was used which has a conductivity of approximately 0 to  $0.05\mu\text{S}/\text{cm}$ . In term of the dissolution rate for the three conditions tablet, it can be seen that there is no clear difference between the three experiments. This could be attributed to the fact that the granules prior to the compression into tablets were subjected to milling of the same class size as well as they were compressed into tablet with the same compression force (5kN). Plus, there is a very small difference between their tablet tensile strength, hence this maybe led to having no evident difference in the dissolution result.



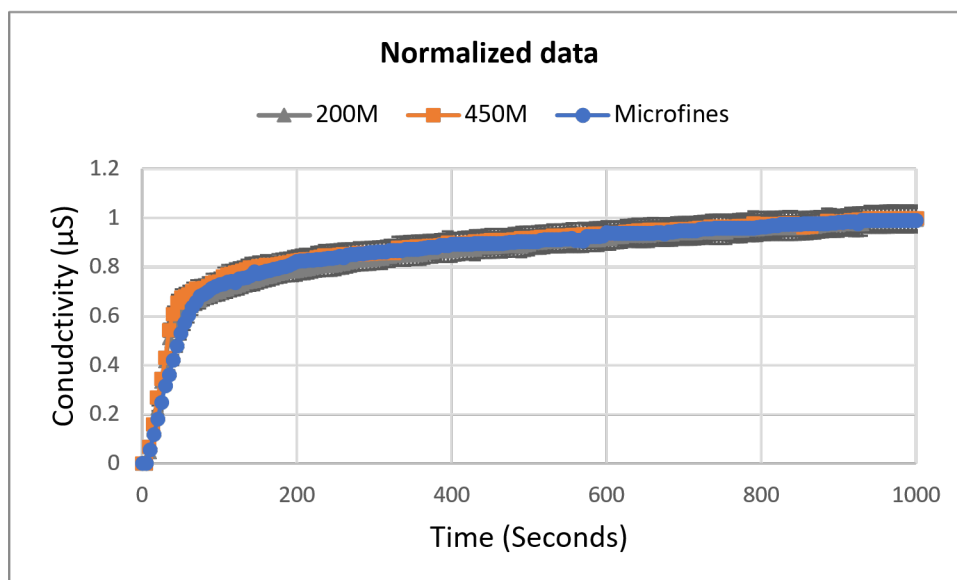


**Figure 126: Dissolution profiles of tablet produced with different lactose primary particle size (200M,450M and microfine) with other parameters kept fixed during granulation i.e., screw configuration of 2 kneading zones, L/S of 0.1 and screw speed of 250rpm. Dissolution measurements were repeated 10 times for each of the condition with distilled water was being used as the dissolution medium with temperature of 37 °C and motor speed of 700 rpm.**

## 7.6 Conclusion

The impact of using different primary particle size powder on the granule's formation at the twin-screw granulation stage, the subsequent drying stage of those granules at the fluidized bed dryer and on the attributes of the tablet made from those granules was studied. The work was carried out in a unique and first of its kind industrial scale ConsiGma system (GEA Pharma Systems), paying particularly more attention to the drying process of the granules which was monitored with an inline NIR system and temperatures sensor. It was found that the primary particle size of the starting material has significantly affected the granules size distribution at the granulation stage, however, this was mainly observed when a very small primary particle size was used. Smaller primary particle size resulted in the formation of smaller granules with higher amounts of fines and larger primary particle size led to the formation of larger granules with less amounts of fines. This is believed to be attributed to the fact that liquid binder covers a larger particle size of lactose monohydrate more efficiently than that of the smaller particle size due to larger particles have smaller surface area and vice versa. Moreover, due to the small difference in  $d_{50}$  of the primary particles for 150M,200M and 450M, a very

small difference was observed in their drying behaviour (temperature and moisture content profiles measured by the temperature and NIR probe respectively). Whereas a clear difference in drying was seen for the granules prepared from microfine among the other three powder sizes. This is because microfine powder as a starting material has a very low  $d_{50}$  (primary particle size) compared with the other three powders. In other words, microfine granules dried much faster in the segmented fluidized bed dryer than the granules prepared from 150M, 200M, and 450M and this is mainly attributed to the smaller granules and amounts of fines that formed in the batch of microfine. Smaller granules and fines have much higher surface area than the larger granules and thus more area available for drying (mass and heat transfer) to occur.

Furthermore, using smaller primary particle size powder material produced stronger tablets than the one made from larger primary particle size. This is ascribed to that smaller particles having a higher surface area available for bonding within the tablets and hence lead to a stronger tablet. It appeared that tablets compressed from small particles (microfine and 450M) were generally stronger than the tablets prepared from larger coarse particles (150M and 200M). Tablet tensile strength has directly affected the dissolution of the tablets accordingly. Also, it was found that there are no obvious differences between the dissolution profiles for the tablet made from different primary particle size.

## 8.0 Investigating the Drying Mechanism Using Near Infrared Chemical Imaging (NIR-CI)

---

### 8.1 1 Introduction

Fluidized bed drying of wet granules is a common process in many industrial sectors and monitoring the granules moisture content in drying is of paramount importance to ensure the quality of the final product. The drying of moist particles is a complex process involving simultaneous heat and mass transfer. Therefore, a greater understanding of the drying mechanisms taking place for granules will enable a better control of the drying process. In this chapter, a non-destructive method using NIR chemical imaging technique has been developed to visualize the spatial distribution of moisture content, as well as provide a quantitative information of the moisture in single FB-dried granules as a function of drying time. This is particularly imperative in controlling the properties of the dried materials for the downstream processes such as tableting. In this chapter, a calibration model which consisted of five constituents of different moisture content granules is developed. The produced images are known as chemical images, these images present the distribution of water content throughout the granule and allow the mechanism of drying taking place within single granules to be monitored. This technique enables fast assessment of quality parameters of pharmaceutical products that could comprehensively be defined not only by its external features (i.e., colour, shape and size) but also by its chemical composition and water content spatial distribution (Elmasry and Jens Petter Wold, 2008).

## 8.2 Experimental Methodology on NIR-CI

### 8.2.1 Chemical Imaging Equipment and Software

Granules at different moisture content are scanned by an offline near infrared diode array spectrometer (EVKHelios G2-320 class, EVK DI Kerschhaggl). This instrument has Indium Gallium Arsenide (InGaAs) detector with spatial and spectral resolution of 312x256 pixels respectively. In this work, the highest magnification lens was used, this lens was provided by the manufacturer, which has a field of view of (1cm-width) and a pixel size of approximately 32 $\mu$ m. This NIR-CI instrument works based on diffuse reflectance mode, which records spectral images in the range of 900 to 2300 nm at a frame rate of 120 Hz. The instrument has a broadband quartz tungsten halogen light, the intensity of this light source should be controlled to be the same throughout the entire experiment by using the same voltage (this study used 100V). This is to avoid variation in the result. Moreover, the NIR-CI is fitted with a conveyer belt which moves at a constant velocity. The sample is placed on this conveyer belt and moves at a constant velocity under the detector. The belt velocity is coordinated with the frame rate of the camera; this is to avoid any stretching or shrinking to the image. The camera records one line per frame, each line has 312 pixels and so as the conveyer belt is moving, more lines are recorded. Figure 127 illustrates a schematic diagram of the NIR-CI instrument used in this study. The software, which was used in this work, is SQALAR. This software was used to process the spectral images taken by Helios camera and convert it into a quantitative meaningful chemical image (QCI) in which quantification of the moisture content of the granules can be obtained.

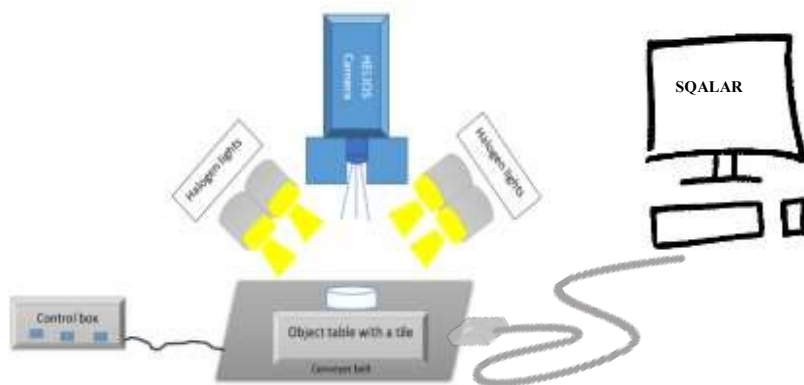


**Figure 127: Schematic of the near infrared chemical imaging equipment used in this study**

### 8.2.2 Data processing

The software which was used to process the data in this work is SQALAR (EVK SQALAR software package, Austria). This software was used to process the spectral images taken by Helios camera and convert it into a quantitative meaningful chemical image. There are two primary multivariate data analyses (MVDA) that this software uses to analyse the spectral data (i.e., qualitative and quantitative modes):

- 1- EC3: this is a qualitative analysis mode; it functions by performing principal component analysis (PCA) on the spectral data. Principal component analysis in brief is a mathematical procedure which is used to lessen large sets of data into smaller one with observing most of the information in the large set. So, for instance, according to its spatial resolution, 312 spectra (data for 1 line) are being collected by the detector at the same time and scanning more lines to cover the entire sample results in generating huge amount of data, the role of PCA then comes to reduce this large amount of data based on the largest variance within the spectra. In the spectral data, the highest variation wavelength is known as the first principal component and the following component correspond for the second highest variation etc. (M. Blanco et al., 1998) and (Manley, 2014b).
- 2- Quantitative chemical imaging (QCI): this is a quantitative analysis mode which apply partial least analysis to construct quantitative predicting model. Partial least square provides a quantitative dimension to the principal component analysis by allocating each PC to a reference value.

### **8.2.3 Quantitative Calibration Model for NIR-CI Experiment on Granules:**

In order to start using the chemical imaging as a technique to quantify the moisture content in the granules as a function of drying time, a calibration curve was needed. Twin screw granulator was used to produce granules at different water content starting from dry powder 0% and ending with wetted granules with 20% liquid content. The water concentrations which used to make the calibration curve were 0.3, 5, 10, 15 and 20%. The obtained samples were then directly scanned in the chemical imaging. Spectral information was then obtained for each scanned image. The spectral data was first analysed by partial least –squares (PLS), and then the pixel spectra were converted into a meaningful distribution map of moisture contents under the quantitative chemical imaging (QCI). The calibration model can be generated and updated once the number of used latent variables LV has been chosen. In this project, the number 3 has been used for the latent variables. Then, it is all ready to be used for analysing the drying behaviour.

### **8.2.4 Chemical Imaging Measurement and Processing**

Granules were spread on the conveyor belt of the NIR-CI equipment. The granules were scanned line by line; this is to ensure gathering the entire spectral image. The collection of data is therefore occurring as  $I(x, \lambda)$  and then scanned alongside the belt movement direction (i.e., in the y direction). MATLAB R2017b (Image Processing Toolbox) was used for processing the resultant chemical images to get the average distribution profile of moisture content across the radial distance of the granules. For less complexity, the analysis was performed on grey images rather than RGB. The grey scale images were obtained directly from the chemical imaging software (Helios optimizer, SQALAR) by changing the scale colour bar from RGB to grey scale one. The computation was performed at a pixel wise step. A total of 10 granules were analysed for this measurement and the average distribution of the ten granules was plotted. When doing the image analysis, the black background was excluded from the computation and only the non-zero values was included. So, pure

black colour has value of zero when the lowest moisture content of the granules was calibrated to be 0.8.

## **8.3 Results and Discussions**

### **8.3.1 Penetration Depth of the NIR-CI**

As discussed in the literature review of near infrared chemical imaging that there is not an agreed value for the penetration depth of the near infrared radiation light into a sample. Its therefore crucial to know the penetration depth of the light prior to performing the main experiment (NIR-CI as a tool in granules drying). Hence, this section aims to investigate the penetration depth of NIR-CI radiation into a sample for the equipment used in this project. This is to get an insight whether the light is penetrating only to the immediate particle surface layer or its penetrating to several layers underneath the surface. To begin with this experiment, lactose tablet of 3.8mm thickness and layers of plastic weighing boat bases each with a thickness of 300 $\mu$ m were prepared to carry out this experiment. Figure 128 shows a schematic diagram of the experimentation set up used in this study in which layers of plastic material were stacked on top of the lactose tablet. The experiment started by scanning lactose tablet only with no plastic layer on top, this was then followed by the scan of one plastic layer only, at that point the spectral information was recorded for these two competent. Then lactose tablet with 1 plastic layer on the top of it was scanned and spectral information was obtained and recorded. Then another plastic layer was then added and so on until 5 layers were all placed on the top of the lactose tablet as illustrated in Figure 128. The raw reflectance/intensity profiles of spectra were all converted into 2<sup>nd</sup> derivatives for improving the identification of the unique peaks of NIR. This pre-processing step was necessary to improve the definition of the spectra as well as to remove any further baseline variations in the spectra (Clarke et al., 2002). Figure 129 shows a 2<sup>nd</sup> derivative spectral profile changes of lactose tablet when the interacting radiation had to penetrate increasing layers of plastic to reach the lactose tablet. for all the scanned components. The red colour

represents lactose tablet only, green colour represents plastic layer only, blue colour represents lactose tablet with one layer placed in top of it, purple colour represents lactose tablet with two layers of plastic placed on top of it, pink colour represents lactose tablet with three layers of plastic placed in top of it, olive green colour represents lactose tablet with four layers of plastic placed on top of it and lastly orange colour represents lactose tablet with five layers of plastic placed on top of it. The yellow shaded box represents the 2<sup>nd</sup> derivative spectral information for the wavelength region between 1905-1969nm. This region represents the water peaks as well as is the region where the fingerprint of lactose presented. At this wavelength, the extent of the NIR-CI penetration depth used in this project can be determined. However, for more clarity, this region of wavelength was zoomed in as seen in Figure 130. It can be clearly seen that the lactose tablet has some distinctive spectra that's distinguish it from other material such the plastic spectra in this occasion. Therefore, one of its distinctive spectra was highlighted here to carry the explanation of penetration on it (1905-1969nm).

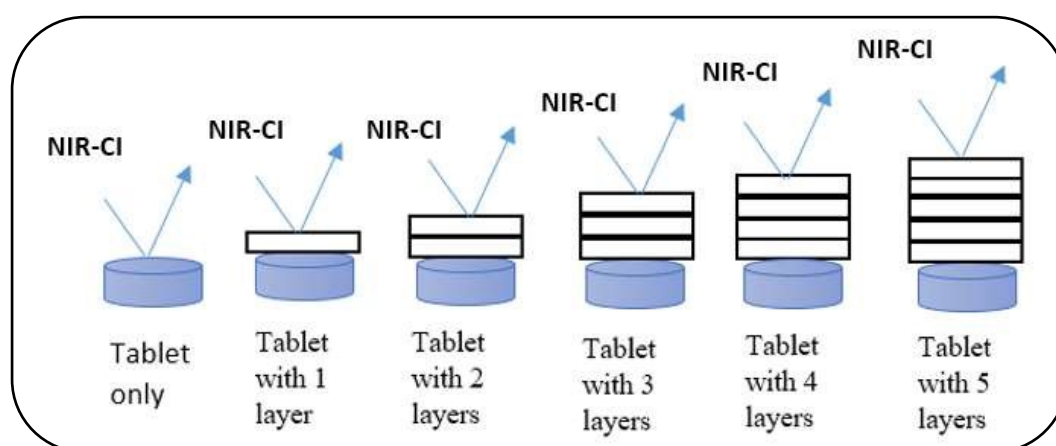


**Figure 128: Experimentation set up for the study of near infrared chemical imaging penetration depth. The thickness of each plastic layer is measure with the Keyence microscope to be 300 $\mu$ m and the thickness of the tablet was measured to be 3.8mm.**



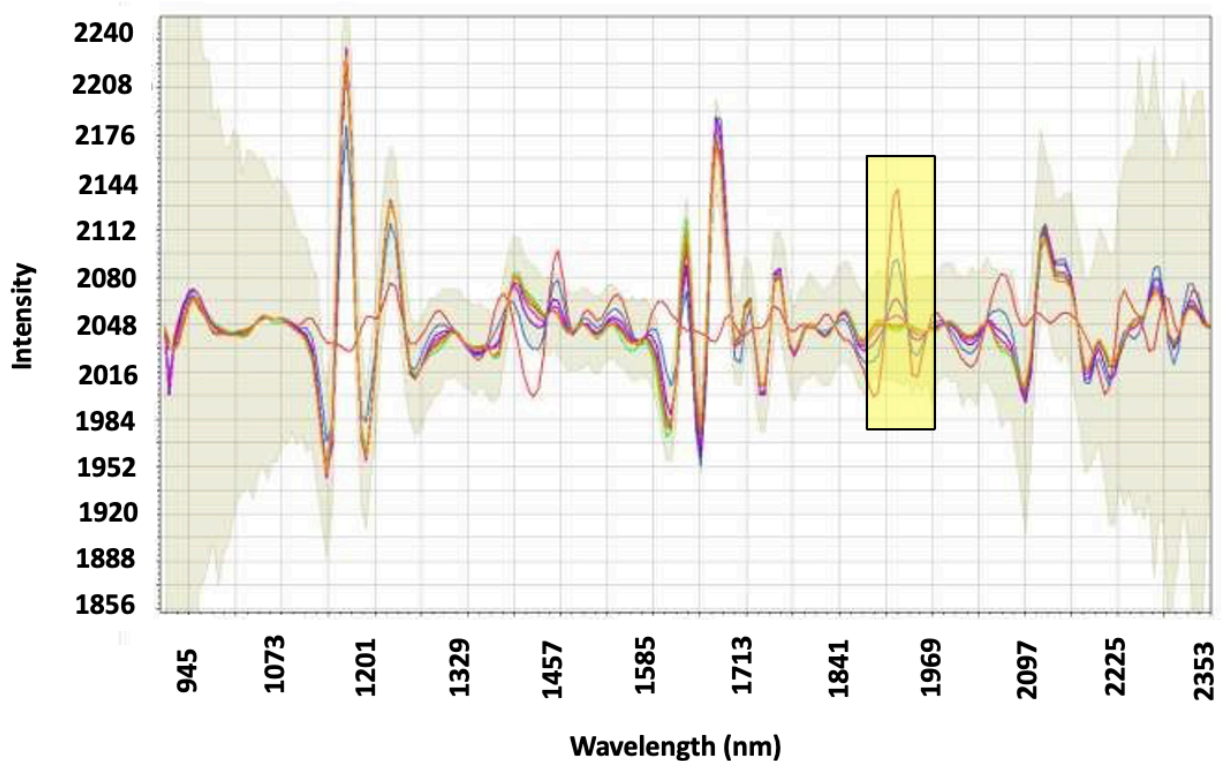


**Figure 129: The 2<sup>nd</sup> derivative spectral data for the lactose tablet with 0-5 layers of plastic layers placed on it at the wavelength region between 1905-1969nm. This highlighted region (yellow shade) represent the water peak.**

In Figure 130, it can be observed that the spectra (blue curve) which includes tablet with one plastic layer on its top was significantly close to the pure lactose tablet spectra (red curve). This means that the NIR radiation penetrated to reach the lactose tablet with this plastic layer on top of the tablet. Moreover, placing a 2<sup>nd</sup> layer of plastic on top of the lactose tablet has shifted the intensity down as seen in the purple curve with still observing the distinctive peaks of lactose through the plastic layers. and so on, this suggests that there is clear relationship between the thickness and the extent of the penetration depth of the NIR radiation into the sample material. In other word, the lower the thickness of the layer placed on the top of the tablet, the higher the penetration depth of the light into the sample material and vice versa. Ultimately, the lactose distinctive peak at 1918nm was still noticeable when the 4<sup>th</sup> plastic layer was placed on the top of the tablet. However, placing the 5<sup>th</sup> layer of plastic on the

top of the lactose tablet still showed a signature of the lactose spectra but that was a trivial one compared to when less layers was used. Putting more layers on top of the tablet after the 5<sup>th</sup> plastic layer would not permit the NIR light to penetrate to the sample material any further as the spectra of pure plastic was nearly visible at the 5<sup>th</sup> plastic layer. Hence, based on this obtained result, the penetration of NIR light to reach for lactose tablet was clearly evidenced at a total of 4 plastic layers each with a thickness of 300 $\mu$ m which can added up to approximately 1200 $\mu$ m.

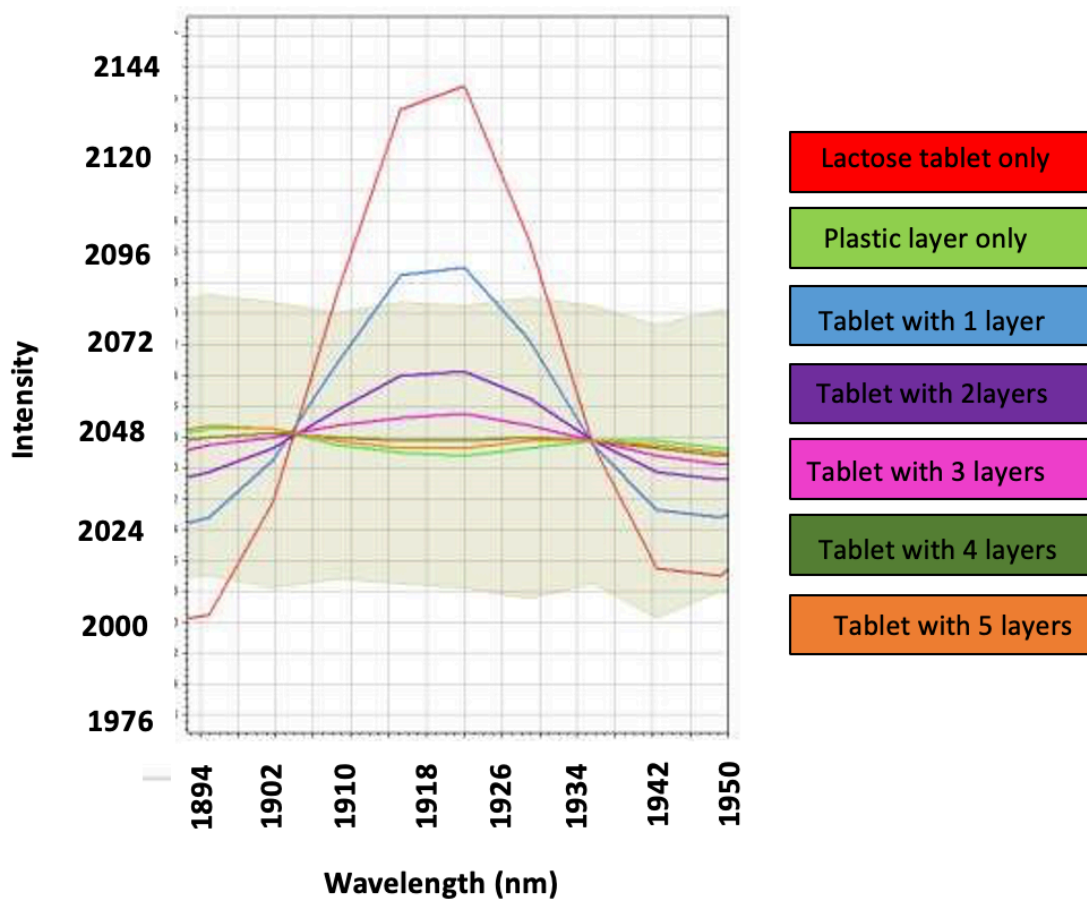


**Figure 130: The 2<sup>nd</sup> derivative spectral data for the lactose tablet with 0- 5 layers of plastic placed on it. This peak for the wavelength region between 1905-1969nm in which this region represents the water peaks as well as is the region where the fingerprint of lactose is presented.**

### 8.3.2 Surface Roughness Effect on the NIR-CI Predictability.

The main aim of using the near infrared chemical imaging in this project is to visualize the spatial distribution of moisture content, as well as to provide a quantitative information of the moisture in single FB-dried granules as a function of drying time. Based on similar research conducted on this

field, the spatial distribution obtained could be affected by the optical/technical limitation of the instrument used (NIR-CI). This limitation in turn could make it difficult to distinguish between the real information of moisture content and the information as a result of other effect such surface morphology (roughness) of the material being examined or the depth of field of the NIR-CI instrument used. The limitation of surface roughness is going to be investigated further in this work.

There are also some other technical limitations that should be considered before performing any experimentation in the NIR-CI. These include sample preparation and illumination. The former, involves correct sample positioning in the field of view of the lens and the latter involves providing correct illumination that can be sufficient to reflect a detectable signal to the detector. Though, intensity of the light should not be too high that can result in damage to the sample. In addition, illumination across the sampling area should be uniform, otherwise, the reflected light intensity can show a considerable discrepancy. This discrepancy can be a very challenging problem as the majority do not take the uniformity of the illumination into consideration, instead intrinsically assume that there is an equivalence among the collected spectra.

#### **8.3.2.1 Surface Roughness**

The roughness and the curvature of the surface could alter the length of the relative path between the surface of the sample and the detector, which in turn could have an impact on the quality of the reflected signal. Studies reported in the literature that when using NIR-CI to scan a curved surface, the light will not be uniformly reflected back, consequently, making meaningless conclusion. For this purpose, processing technique was developed to isolate the impact of surface roughness on the reflected spectra quality. Surface roughness can be awkward if the examined surface roughness is higher than the lens depth of field (DOF). The depth of field can be defined as the distance between the nearest and the farthest objects that are in acceptably sharp focus in an image. In general, when using near infrared chemical imaging, it is always essential to make sure that there is not an impact by any source of variation on the reflected signal. Overall, there is lack of information exists in literature about the depth of field and surface roughness of the scanned surfaces. Therefore, in order to investigate this further, determination of the depth of field of the NIR-CI lens should be taken further.

Moreover, detailed work has been done in this research project addressing the challenge of surface roughness that could be faced when using the chemical imaging technique in determination of moisture content. This work was detailed in a conference published paper which is attached in the appendix of this thesis. The work investigated the effect of surface roughness by using tablet of different surface roughness which were produced by means of different compression forces and different moisture content. From this study, it was found that the surface roughness highly influences the result of chemical imaging when determining the moisture content of the materials and therefore could mislead NIR-CI result.

### **8.3.2.2 Determination of Depth of Field of the NIR-CI Instrument**

This preliminary experiment conducted to determine the DoF of the lens of the near infrared chemical imaging instrument used in this project. Therefore, a plastic micro scaled ruler is used to investigate this further. The experiment started with focusing the chemical imaging lens on the plastic micro scaled ruler. The ruler was then gradually moved up  $50\mu\text{m}$  in each step toward the detector by placing number of round plates of  $50\mu\text{m}$  thickness (as measured by the Keyence microscope) underneath the plastic micro scaled ruler in a stepwise manner. Figure 131 shows the images obtained at each  $50\mu\text{m}$  step moving toward the detector. So, by looking at this Figure, it can be seen that the image become blurry as the distance to the detector (distance of focus) was changes by  $\sim 400\text{-}500\ \mu\text{m}$ . This was taken as the depth of field of the lens. This experiment assisted with knowing that there is a certain field of depth to this equipment and from there we know that it is something to be considered when using the chemical imaging

### **8.3.2.3 Granule Surface Roughness**

To investigate the role of surface roughness of the granules in the NIR-CI study, microscope measurement for granules surface profiles was conducted. Roughness of surface can be expressed by different parameters which are carefully chosen based on the desired application. To link the surface roughness with the DoF of the lens, Ra value was chosen to express the surface roughness of the

granules used in this study due to its suitability for quantitatively determining the surface roughness of the of the studied granule in this work.

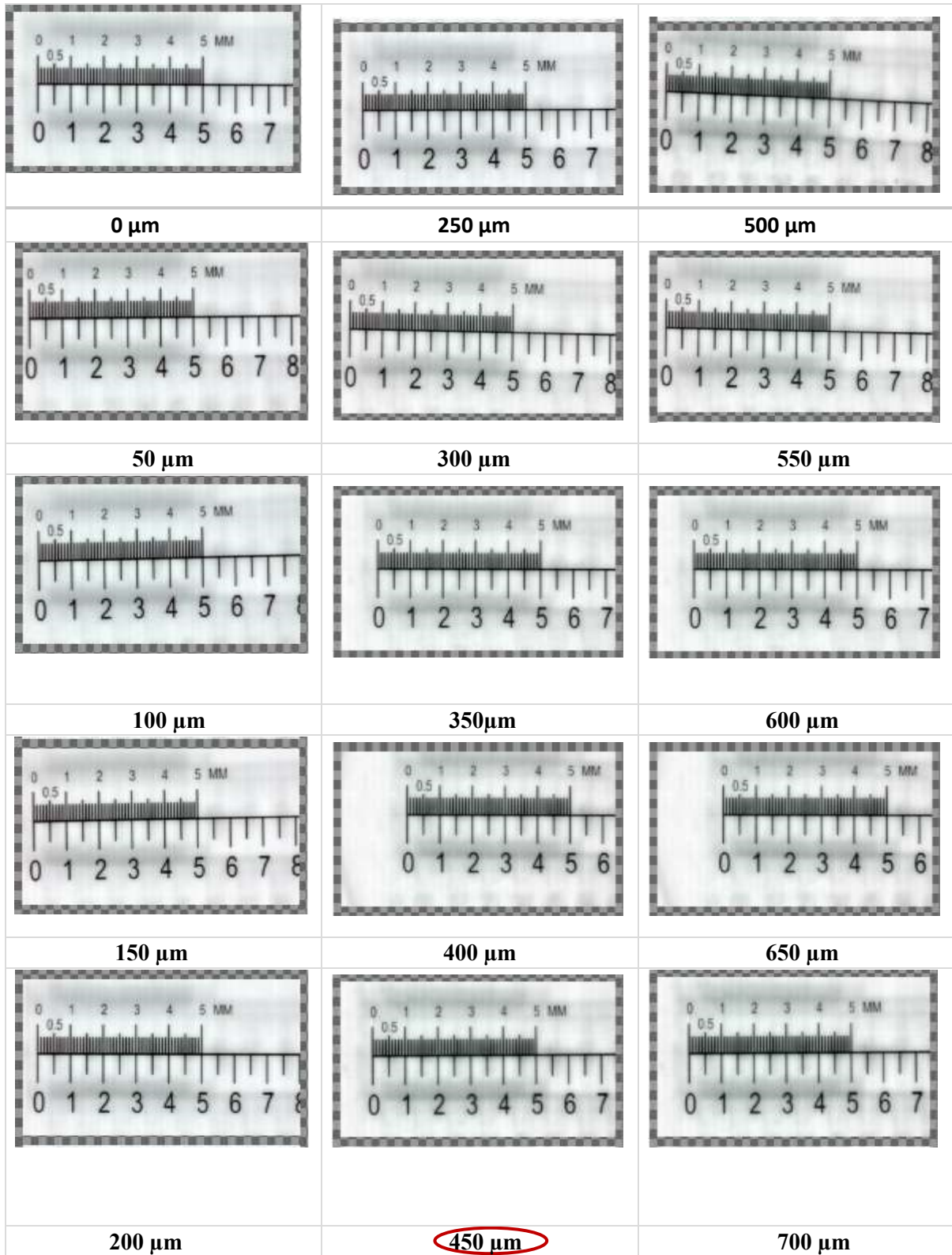
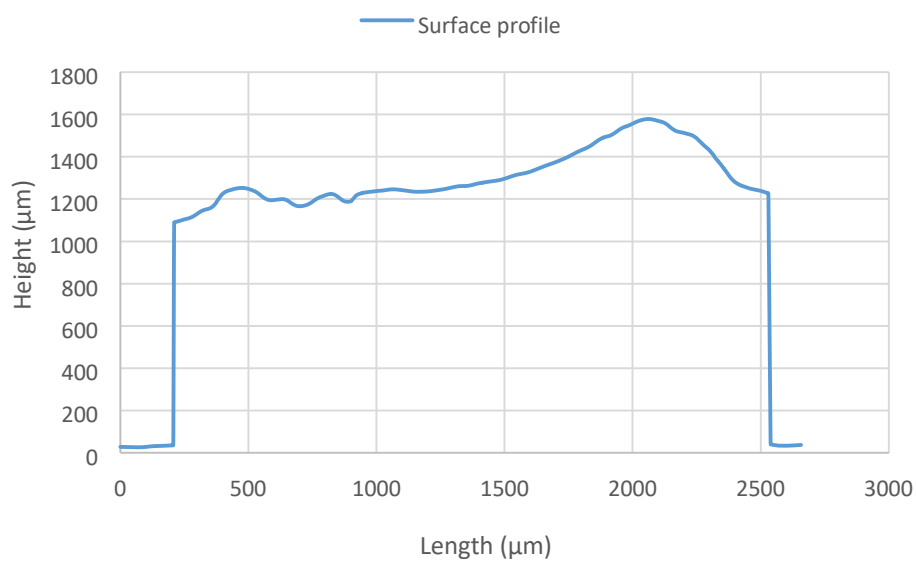


Figure 131: Raw images of plastic micro ruler obtained with Near infrared chemical imaging instrument at different distance to the spectrometer detector to determine the DoF of the lens.

### 8.3.2.3.1 Granules Surface Profile Measurement

A good number of granules with a diameters range between 1.5-2.5mm were subjected to surface profile measurement using a digital microscope (Keyence VHX-5000). For the surface profile measurement of granule, a horizontal line was selected across the granule. A file from this measurement was then generated and exported as a comma-separated values (CSV) spreadsheet and so profiles were plotted as shown in Figure 132. The profile will be used for further surface roughness analysis.



**Figure 132: Example of surface roughness profile of the granule obtained from the digital Keyence microscope (granules with diameter between 1.5-2.5mm).**

The surface roughness ( $R_a$ ) which is the average of a surfaces measured microscopic peaks and valleys was calculated from the obtained surface profiles using Eq. 5.

$$R_a = \frac{1}{n} \sum_i^n |y_i - \bar{y}| \quad \text{Eq. (5)}$$

Where  $R_a$  is the universally recognised parameter of surface roughness for arithmetic mean deviation,  $n$  represents the number of points in the profile,  $i$  is the  $i$ th data point,  $y_i$  is the  $i$ th height,  $\bar{y}$  is the height of the centreline.

The first step was to draw a centreline for all surface profiles as illustrated in Figure 133. The centreline was obtained as the arithmetic mean of all the height points of the profile. Figure 133 shows an example of granule surface profiles with the centre line.

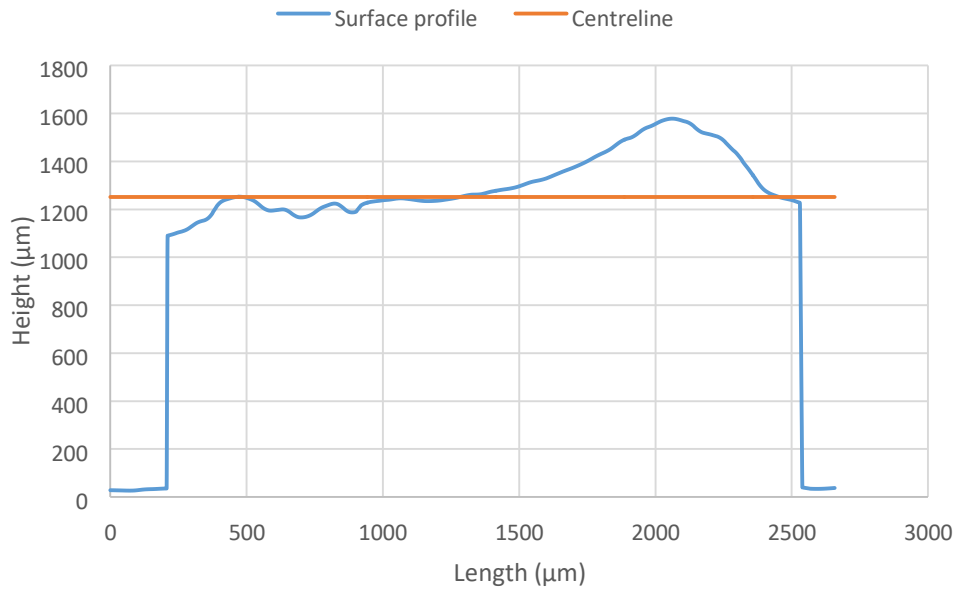


**Figure 133: Surface profile of granule (diameter between 1.5-2.5mm) with determination of the centreline which was obtained as the arithmetic mean of all the height points of the profile. Surface profile measurement was performed with the use of Keyence microscope.**

The average computed Ra values for all granules (10 granules of each condition) used in this study are shown in Figure 134. It can be seen from the figure that the Ra values of the granules are much lower than the depth of field of the lens. Therefore, all the granules used in this work are always in focus.

This consequently allows the next step of this work to be achieved.

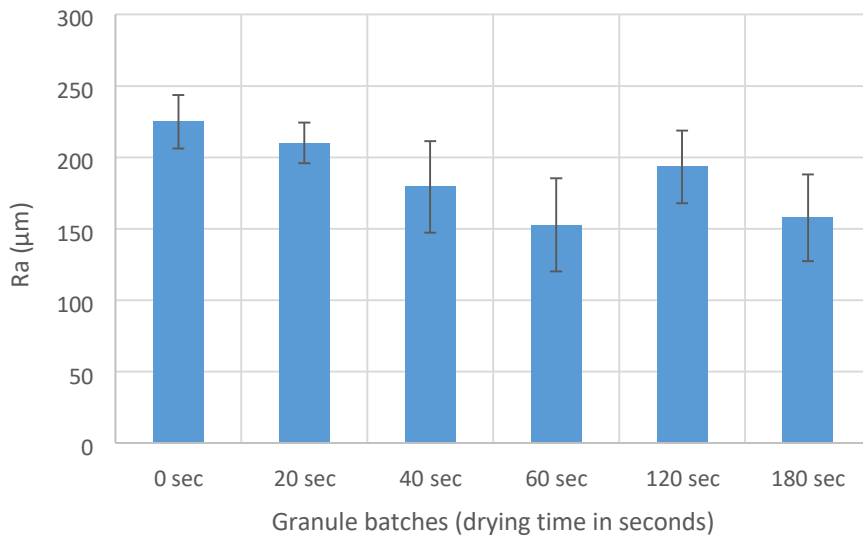


**Figure 134 : Roughness (Ra values) for all the granules produced at different fluidized bed drying times calculated using equation 5 above. The measurement was repeated ten times for each drying time.**



## 8.4 Moisture Content Calibration Curve

In order to start using the chemical imaging as a technique to quantify the moisture distribution in granules as a function of drying time, a calibration model was needed to be constructed from the average spectra extracted from known moisture content of granules. The calibration is based on the relationship between the reflected light intensity and granule moisture content. Twin screw granulator was used to produce granules at different water content starting from dry powder 0% and ending with wetted granules of 20% liquid content in a step of 5%. Therefore, the water concentrations which were used to make the calibration curve were 0, 5, 10, 15 and 20%. The obtained samples were then directly scanned using the NIR chemical imaging. Spectral information was then obtained for each scanned image as seen in Figure 135. Spectral colour representation of each component is presented in the same figure. The two shaded area represents the water NIR spectrum; 1450nm and 1950nm (M Blanco et al., 1998). These two water peaks were used to obtain an information about the accuracy of the calibration model ( $R^2$ ). Figure 136 shows the relationship between the moisture content and the intensity of the reflected light using the two water peaks (1450nm and 1940nm). This can give an indication on how good the model prediction ability for moisture content. By looking at  $R^2$  value for both curve in Figure 136, it can be said that the model ability in predicting the moisture content is very high. This permits to continue further with this work as NIR-CI found to be a reliable tool in such application.

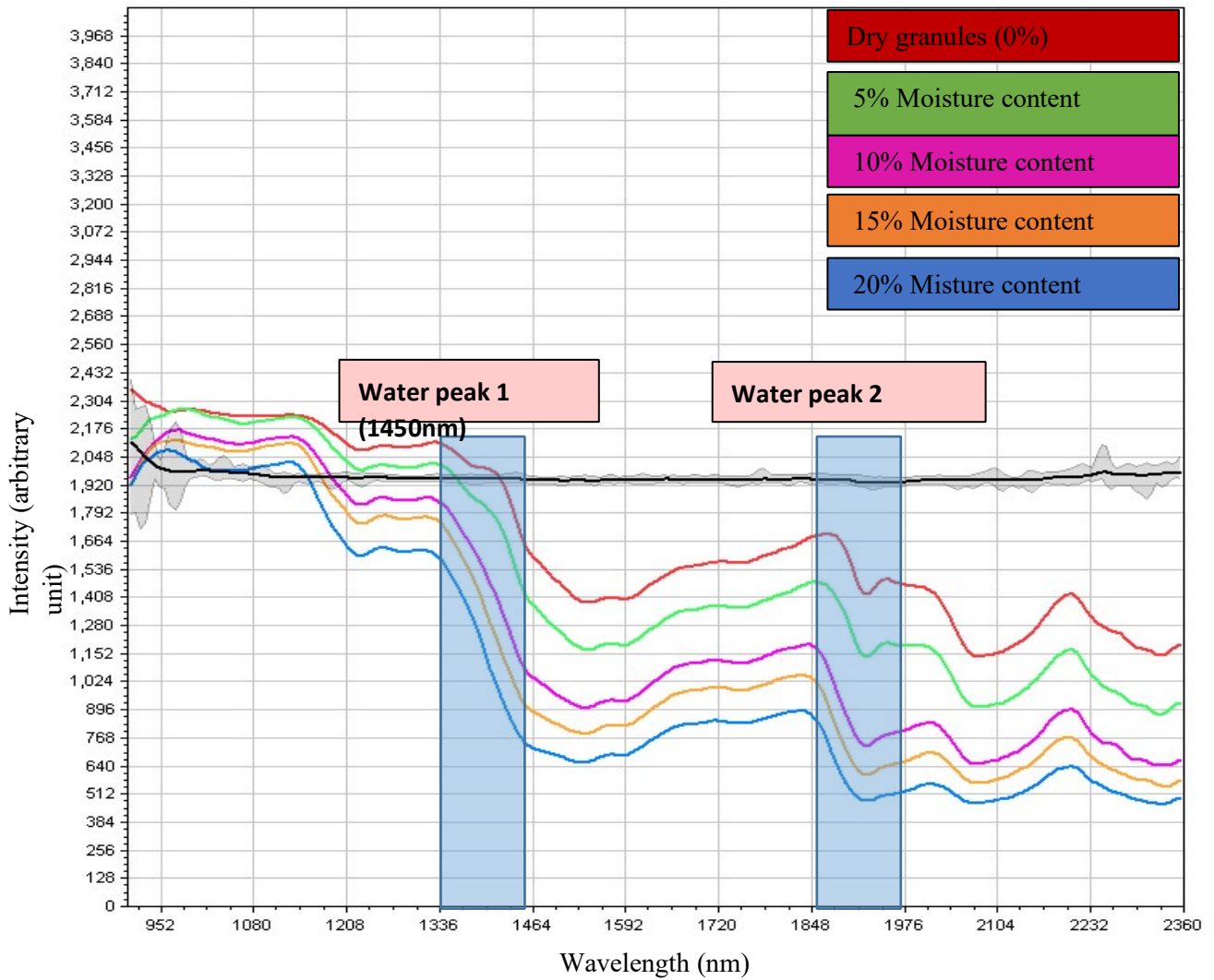


**Figure 135: Raw NIR spectrum of lactose granules at different moisture contents (0%,5%,10%,15%,20%) with the two water peaks highlighted at 1450nm and 1950nm. The spectral colour representation of each component is that red colour represents dry granules, green represents 5% moisture content, purple represents 10% moisture content, orange represents 15% moisture content, blue represents 20% moisture content and black represents ceramic background which has no spectra.**

The model was tested with a set of validation granules of known moisture content, these were not included in the calibration stage. The results for the validation of the calibration model of the granules are shown in Figure 137.

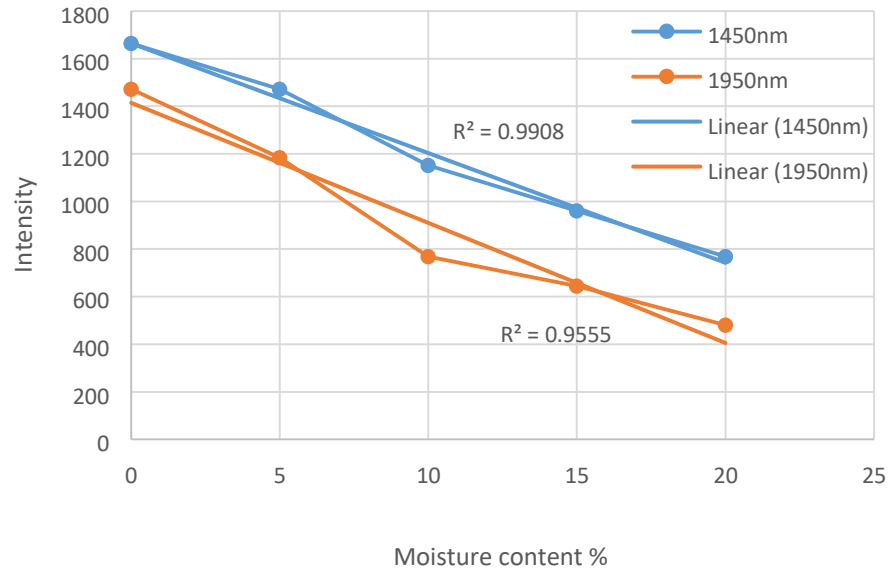


**Figure 136: Calibration curves show a correlation between the moisture content and the intensity of reflected light at the two water peaks (1450nm, and 1940nm). This Figure plotted to give an indication on how good the model prediction in determining moisture content.**

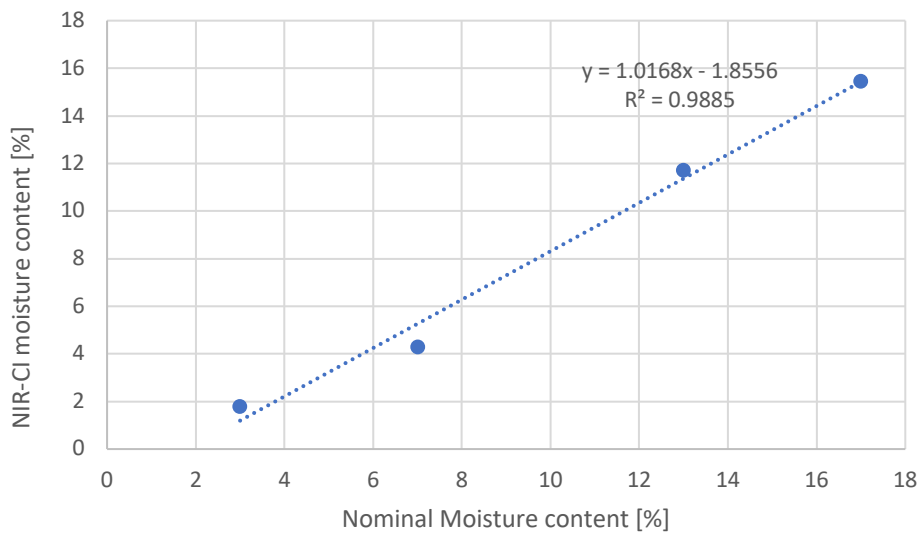


**Figure 137: Predicted NIR-CI moisture content vs. nominal moisture content of granules for calibration curve validation. This was performed using four set of validations with granules of known moisture content.**

## 8.5 Calibration Model and Granule Moisture Content Distribution

### 8.5.1 Quantitative Calibration Model (QCI)

Now to obtain the QCI model, the spectral data was first analysed by partial least –squares (PLS), and then the pixel spectra were converted into a meaningful distribution map of moisture contents under the quantitative chemical imaging (QCI). The calibration model can be generated and updated once the number of used latent variables LV has been chosen. Then, it is all ready to be used for further work i.e., drying purpose. Figure 138 shows the QCI images of the calibration curve. The QCI measurement values in the output images are encoded using a colour scale bar. By clicking on this colour map in the chemical imaging software, different colouring can be obtained. Figure 138 (a) shows the RGB scale and Figure 138 (b) shows in grey scale. Each of the five moisture content constituents in the grey scale was processed in ImageJ software (National Institutes of Health (NIH), USA) to obtain an information about the average intensity for each moisture content constituents since this was not possible to be done in the SQLAR chemical imaging software. Therefore, Figure 139 which shows a correlation between the grey value and the moisture content. This figure is particularly used to analyse moisture content distribution within every single granule.

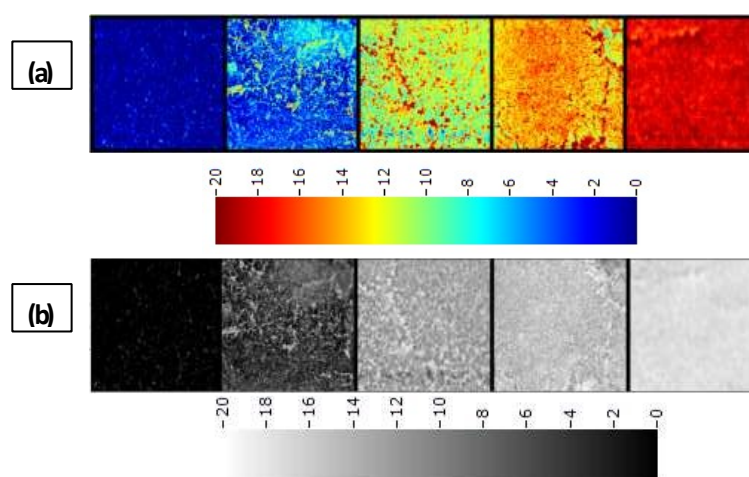


**Figure 138: QCI images of the calibration curve including the different five moisture content components 0%, 5%, 10%, 15%, 20% in which (a) RGB (b) Grey obtained by the Partial least square quantitative model.**

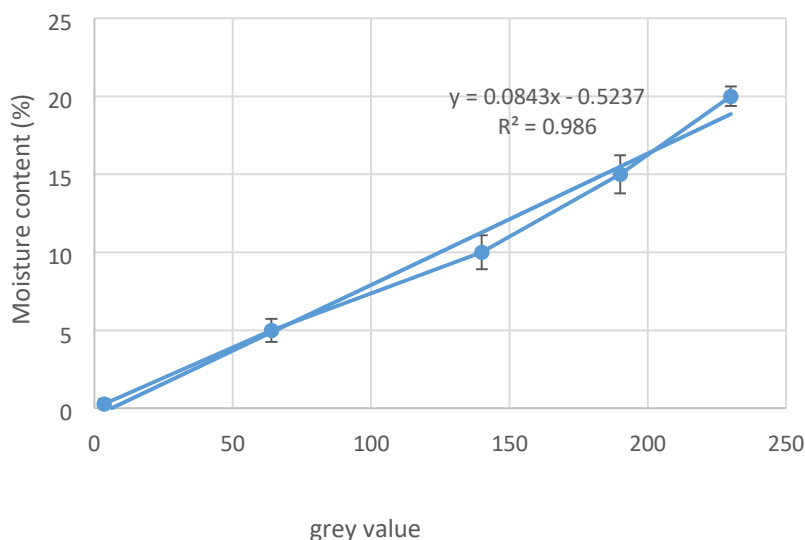


**Figure 139: Calibration curve generated using QCI shows a correlation between the grey value and the moisture content. This plot is particularly useful to analyse moisture content distribution within every single granule.**

### 8.5.2 Image Processing for Granules

The distribution information of moisture content across the radial distance of the granule was not possible to be obtained in the SQLAR software, hence MATLAB (R2017b, Image Processing Toolbox) was used for processing the resultant chemical images to get the average distribution profile of moisture content across the radial distance of the granules. For less complexity, the analysis was performed on grey images rather than RGB. The grey scale images were obtained directly from the chemical imaging software (Helios optimizer, SQALAR) by changing the scale colour bar from RGB to grey scale one. Figure 140 illustrates an example of how the average radial profile was computed in every single granule. The computation was performed at a pixel wise step, however, for simplicity of visualization, 20 circles only were drawn. A total of 10 granules were analysed for this measurement and the average distribution of the ten granules was plotted. When doing the image analysis, the black background was excluded from the computation and only the non-zero values was included. So, pure black colour has value of zero when the lowest moisture content of the granules was calibrated to be 0.

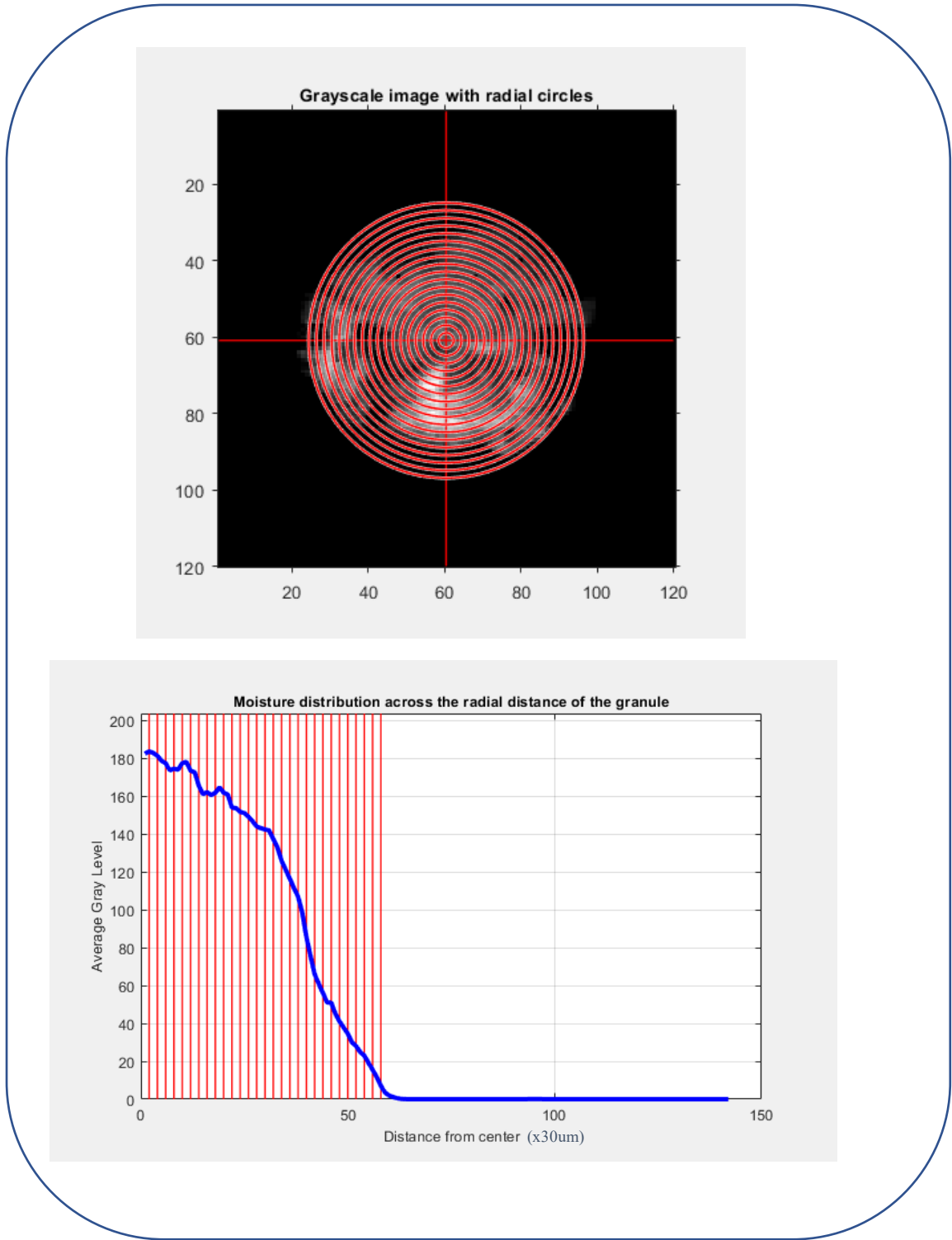


**Figure 140: Example to illustrate the computation of moisture content distribution in single granule in MATLAB. This was computed in every single granule in which computation was performed at a pixel wise step, however for less complexity, only 20 circles were drawn. A total of 10 granules of each condition were analysed and the average distribution of the 10 granules was plotted.**

### 8.5.3 Critical Investigation of Moisture Content Analysing Technique

The conventional method, loss on drying (LOD) by moisture analyser and the NIR chemical imaging are both an offline technique that can be used to measure the moisture content of the granules. However, chemical imaging technique remain to be the most robust and powerful way to predict the moisture content of the sample because it can give pixel information in terms of moisture content. It can qualitatively and quantitatively determine the average moisture content and moisture distribution in single pharmaceutical granules. While LOD can only give the average moisture content of the sample with no information of how the water is distributed. It also can be considered as a fast method to determine the stages of drying process at any point of time during the drying process once the calibration model is established. Figure 141 illustrates the drying curves of lactose granules dried at different times in the fluidized bed using loss on drying and chemical imaging method. It can be seen that there is a good correlation between the two techniques in relation to the LOD method and chemical imaging method. Chemical imaging technique can be used as predictive tool to measure the moisture content of the granules. The chemical imaging prediction curve has not only given the average moisture content of the sample, but it also gave a visualized chemical image that were processed to give a radial distribution of the average moisture content in single granules.

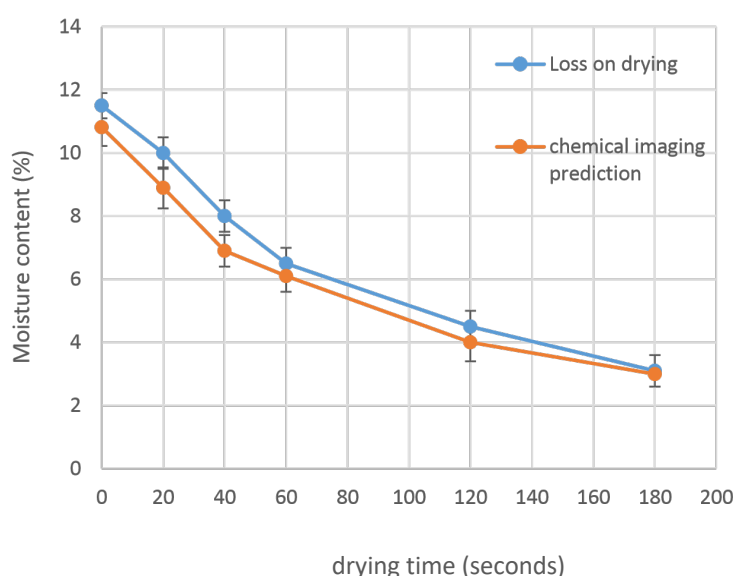


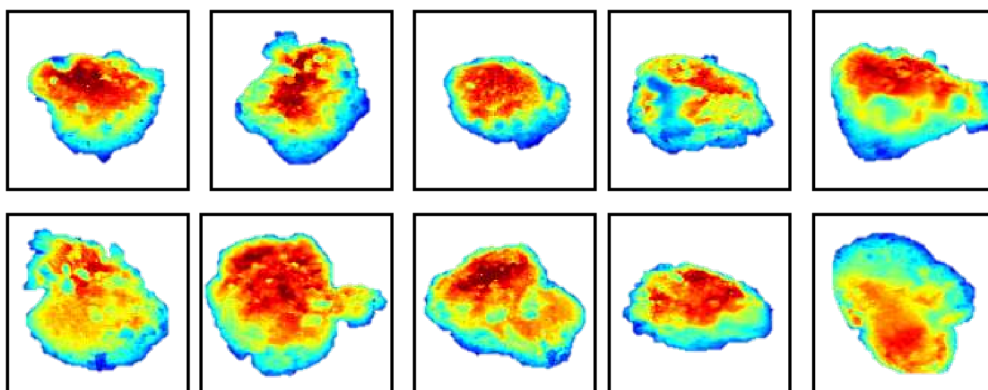
**Figure 141: Drying curve of lactose granules at different fluidized bed drying times using loss on drying (LOD) and NIR chemical imaging methods.**

### 8.5.3.1 Distribution of Moisture Content in Single FB Dried Granules

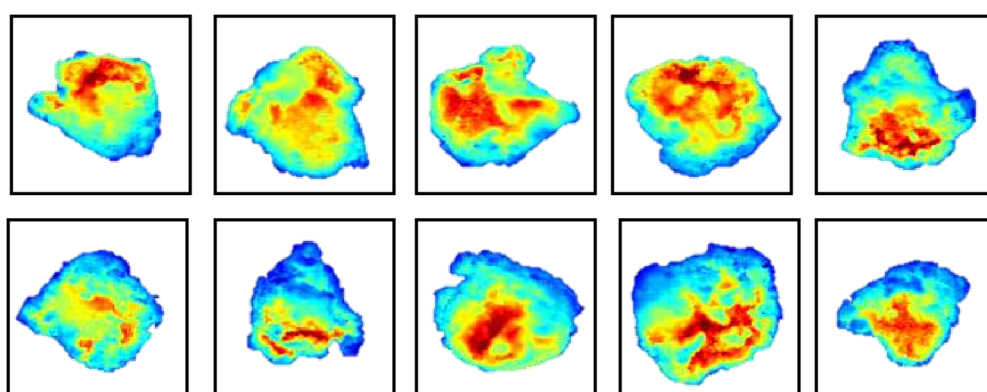
As mentioned previously, the majority of the existing literature research with the regards to the drying of wet solids/ granules have depend on the theory to explain the drying mechanism. However, this work highlights the use of chemical imaging technique to investigate the mechanism of drying of wet granules (the stages of drying) with visualized chemical images and quantitative moisture distribution. Figure 142 shows single granules chemical images that correspond to the drying curve (Figure 141) at different drying times (20, 40, 60, 120, 180 seconds). As it has been reported in the literature in many researches, the drying stages split into two main phases; the first stage is the surface evaporation and the 2<sup>nd</sup> stage is the internal evaporation (Mezhericher et al., 2010), (Mezhericher, Levy and Borde, 2009), (Poutiainen et al., 2012), (Mezhericher et al., 2008), (Walton, 2004), (Mortier et al., 2013), and (Mezhericher, Levy and Borde, 2007). As the name suggests, the first stages imply the evaporation of the free water that is available at the surface whereas the second stages imply the evaporation of the bound water that is located inside the granule. Figure 141 exhibited the two main aforementioned drying stages in which chemical images in Figure 142 is in agreement with it. From the chemical images and by looking at the colour bar scale (Red colour represent highest amount of liquid water, blue colour represents lowest amount of liquid water- dry granule), it can be clearly seen that there is clear trend in term of the colour map at different drying times. Chemical images of fresh granules were taken immediately after the granules been produced from the TSG; therefore, it tends to have almost a wet surface all around the granule (almost red colour). Images of granules at 20 seconds FB showed a slight reduction in the red colour, in other words, water shrunk towards the core of the granule and so on. Figure 143 shows the moisture distribution across the radial distance of the granules, it can be seen from this Figure that the distribution of the wet fresh granules coming directly from the twin-screw granulator had the highest moisture distributed across the radial distance of the granules at the core and the surface/edges of the granule compared to the rest of the measurements.



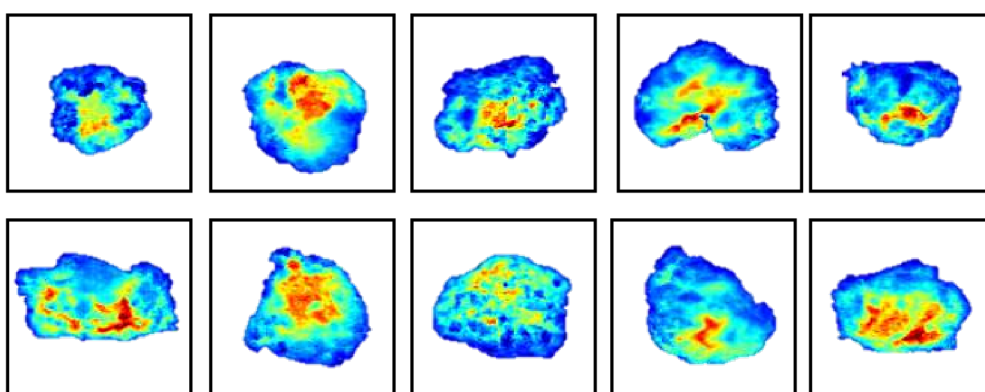
As the drying time proceeds, the granules moisture content distributed at the core and the surface/edges reduced with time, until the granules are dried (blue colour was dominant). In other words, and by looking at the chemical images, the granules at time 20 and 40 seconds, correspond to the 1<sup>st</sup> surface evaporation constant drying stage. At this stage, the chemical image indicates that the liquid is still distributed at the centre of the granule with water already evaporated at the granule surface / (edges). However, at time 60 seconds and by observing both the drying curve obtained with the LOD method (Figure 141) and the chemical images Figure 142, it can be said that this describes the critical moisture content (the end of the constant rate period and at the start of the falling rate period) at which the drying become internally inhibited. Preceding with the drying, chemical images of the granule at time 120, 180 seconds describe the drying of the internal bound water. Time 180 seconds represents the equilibrium moisture content which is the granules reaches equilibrium with the environment surrounded the granules and therefore at time 180 seconds the granules are said to be dried.



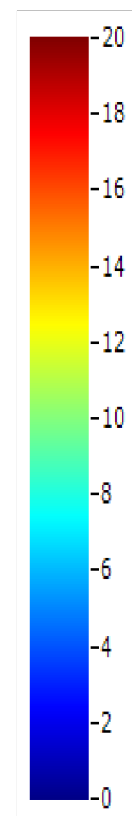
(a) Fresh granules directly from twin screw granulator

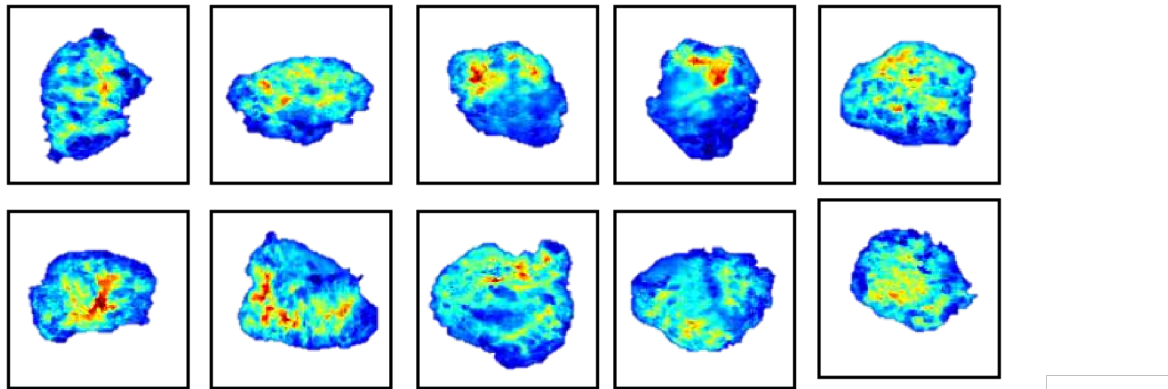


(b) 20 seconds FB-dried granules

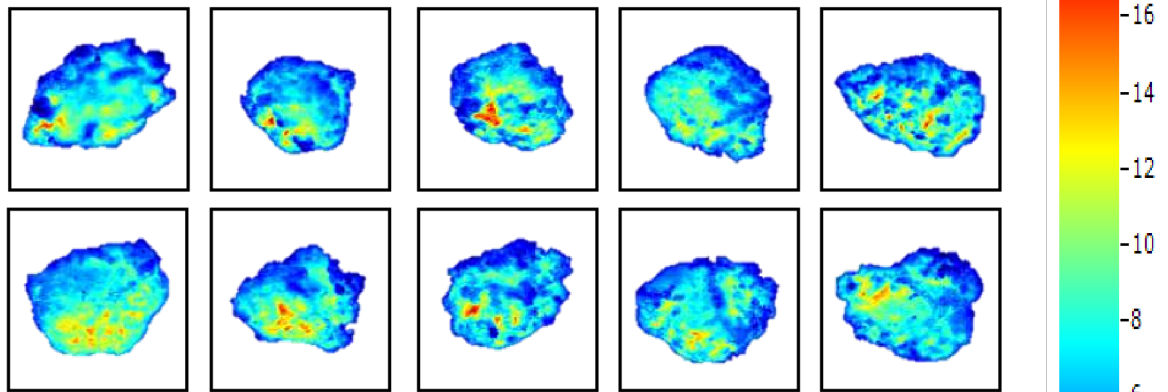


(c) 40 seconds -FB dried granules

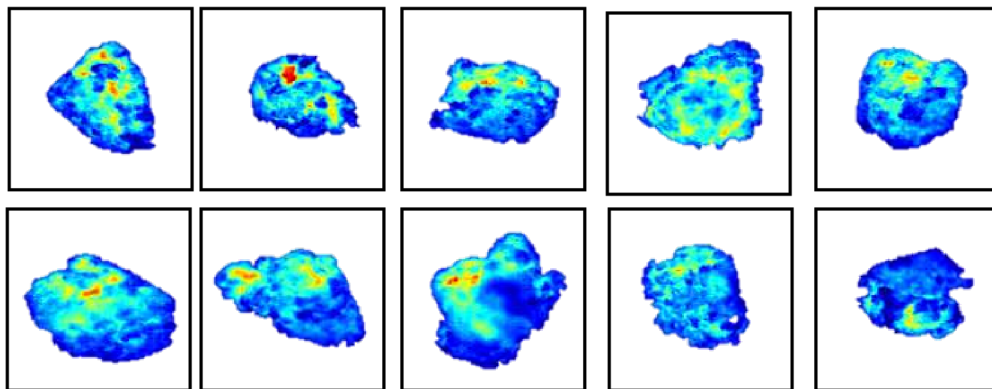




(c) 60 seconds –FB dried granules



(d) 120 seconds –FB dried granules



(e) 180 seconds –FB dried granules

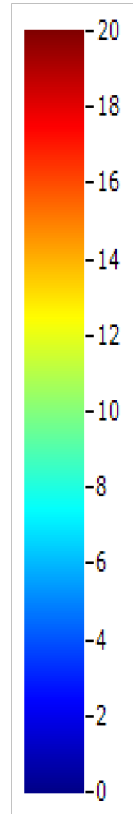


**Figure 142: Prediction map of moisture distribution content in single granules at different fluidized bed drying times including fresh granules prior to drying (a) fresh granules (b) 20 seconds FB-dried granules (c) 40 seconds FB-dried granules (d) 60 seconds FB- dried granules (e) 120 seconds FB- dried granules (f) 180 seconds FB-dried granules. The figure present 10 granules from each condition.**

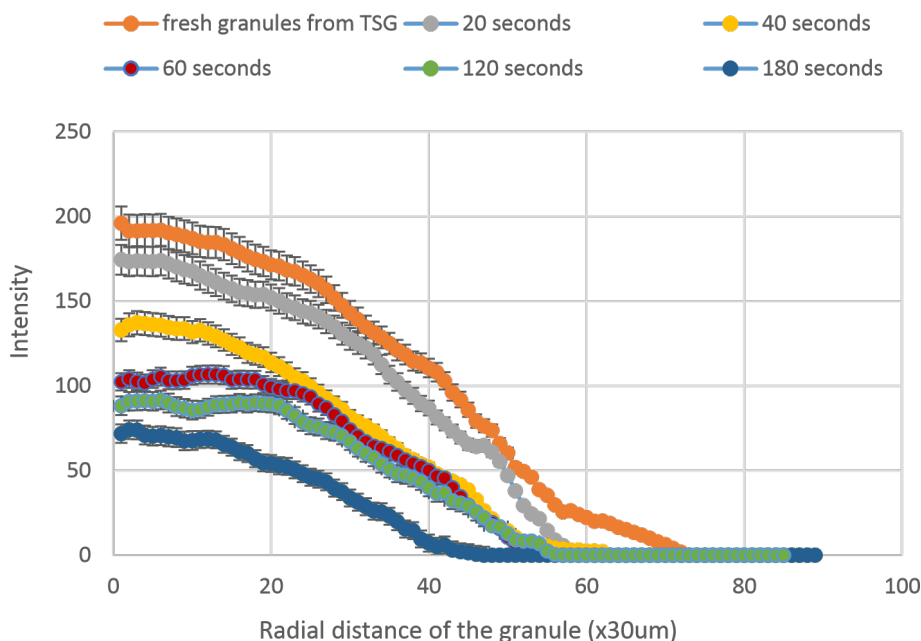


**Figure 143: Moisture content distribution across the radial distance of single fluidized bed dried granule as a function of FB drying time, this also includes fresh granules prior to drying. This plot obtained with using MATLAB/imaging processing tools.**

## 8.6 Conclusion

This is the first reported work on the utilization of NIR chemical imaging for the determination of moisture content in single FB-dried granules. This work has also enabled the quantifying or tracking the distribution and movement of liquid as a function of fluidized bed drying time across the radial distance of the granule. This was implemented with NIR spectral chemical imaging system of spectral region between 1000-2500 nm. A robust quantitative NIR-CI analytical method was developed and successfully obtained a spatial moisture content distribution across the radial distance of a single granule with MATLAB image processing software. In other words, this study determined the moisture distribution across the radial distance of single granules dried at different FB times. In addition, this technique enabled a good prediction of the average moisture content of the sample at different fluidized bed drying times. Drying is a very important unit operation that is mostly used in all industry producing solid product ranging from food to pharmaceutical industry. Obtaining the moisture distribution across the radial distance of single granules can potentially contribute to the understanding and hence optimization and better control of the resultant granule attributes and downstream process post drying.

Table 7 shows some highlight of the advantages of using the chemical imaging over LOD method.

**Table 7:** Highlight of the advantages of using the NIR chemical imaging technique over LOD.

	Loss on drying (LOD)	Chemical imaging
Moisture distribution	Not available neither at single granular nor whole sample level, it deduces only the average moisture content.	Available and at a single granular and whole sample level. It gives quantitative information in where the liquid is distributed within each single granule.
Speed	Slow in determination at which stage the drying is at until whole batch of drying is completed and then drying stages will be clear from the drying curve.	Very fast prediction of moisture content at any point of time during drying.
Visualization images	Not possible	QCI –colour-based images
Usefulness in further work	Not useful in term of getting data that could be modelled for single granules	Useful to carry out modelling work with it especially distribution data of moisture across the single granule.
Using of sample after test	Cannot be used for further test- as sample could be already degraded due to the introduction of heat during the test.	Non – destructive technique - sample can be re- used for different test.



---

## CHAPTER 9

### Main Conclusion, Future Work, References and Appendix

---



## 9.0 Main Conclusions

---

This research project is the first attempt to shed the light on to how the fluidized bed drying of granules can be influenced by altering the process and formulation parameters at the twin-screw granulation. Therefore, the uniqueness of this project is the combination of the twin-screw granulation with fluidized bed drying process to set the parameters of processing and formulation on two scale production (batch laboratory scale and continuous pilot plant scale). The effect of batch fluidized bed drying process parameters on the final properties of granules and on the subsequent properties of tablet produced from those granules are investigated. Moreover, the effect of both the formulation and process parameters at the twin-screw granulation on the granules drying process at the fluidized bed were carefully investigated.

It was generally found that the variation of the twin-screw formulation and process parameters affected the drying process of granules in the fluidized bed. Breakage of granules occurred during all the performed drying experiments in this project, however, there were an occasion where the breakage was minimal. The extent of granules breakage during conventional batch fluidized bed drying process was found to be dependent on changing these parameters (i.e., L/S ratio, binder viscosity and screw confirmation). Using higher L/S ratio appeared to produce larger granules with a smaller amount of fines and lower porosity as higher L/S ratio stimulates higher granules growth and more liquid bridges. This caused ultimately the granules to have had higher resistance to breakage in fluidized bed during drying compared with the lowest L/S ratio which result in worse breakage. Moreover, from the study of varying the viscosity of the binder solution, it was evident that using the lowest viscosity binder solution (water) has led to the least breakage of granules in the fluidized bed, this might be due to the higher probability that water as a binder mixed well with powder during granulation than HPC binder, thus, resulting in the formation of well compacted and less porous granules that can withstand the fluidization during drying. In addition, varying the screw configuration at the twin-screw granulation stage had significantly affected the formation of the granules and ultimately the drying process of the granules in batch fluidized bed dryer. Conveying elements led to more breakage during drying due to the granules being the most porous and friable which makes it more susceptible to

breakage, whereas more kneading elements led to the least breakage due granules being the densest and least friable and therefore less susceptible to breakage when subjected to fluidized bed drying. Adding more kneading elements was found to result in much less granules breakage during fluidized bed drying, this was attributed the reason that the densest and least friable granules produced with kneading elements has higher resistance to breakage due to its properties and vice versa. With respect to the granules drying curves, it was generally found that the granules produced with using higher L/S ratios, lower binder viscosities, the existence of more kneading blocks in the screw configurations tended to dry much slower than the granules prepared from lower L/S ratios, higher binder viscosities, and a smaller number of kneading elements.

Furthermore, determination of moisture content is important for many industrial sectors. It is used to ensure achieving the required quality of the final product. This research project also used an inline real-time near infrared (NIR) to measure the moisture content of granules manufactured using a pilot plant production scale-continuous twin-screw granulator fluid-bed dryer (ConsiGma-25, powder to tablet line). The behaviour of drying for granules produced at different screw configurations and lactose powder of different primary particle size was studied and observed through inbuilt temperature sensor and NIR probe. Generally, regardless of the scale of the equipment used, screw configuration has had a significant impact on the formation and consequently on the drying of granules. It was found that using different screw configuration had an impact on the formation and drying of granules and also on the consecutive tableting of those granules. Similarly, varying the primary particle size of lactose powder was found to affect the formation and the drying of granules and their tableability. However, the effect of particle size of 150M,200M and 450M lactose seems to have only had a slight effect on the drying rate, dissimilar to the microfine granules which showed a visible difference among them all.

Moreover, a greater understanding of the drying mechanisms taking place in granules will enable a better control of the drying process, thus this project is the first to report the development of a novel quantitative analytical method by utilizing NIR chemical imaging to determine the moisture content and quantify or track the distribution and movement of liquid at single granular level as a function of



fluidized bed drying time. The study determined the moisture distribution across the radial distance of single granules dried at different FB times. Obtaining the moisture distribution across the radial distance of single granules can potentially contribute to the understanding and hence optimization and better control of the resultant granule attributes and downstream process post drying such as tableting.

In conclusion, continuous twin screw wet granulation has become one of the most prominent continuous manufacturing technologies in the pharmaceutical industry and academics in the last ten years. However, currently, there is a gap in the literature studying the impact of twin-screw granulation on subsequent fluidized bed drying and downstream processes, signalling that there is a missing link between granule quality and drying behaviour and changes in twin-screw formulation and process parameters. This research project therefore is the first to establish in-depth process knowledge regarding the integration of the two-unit operations, twin-screw granulation and fluidized bed drying process. Specifically, it addressed optimum process and formulation factors in TSG that contribute to controlling granule size during drying, avoiding growth or size reduction, and monitoring moisture content; avoiding over drying or under drying conditions, achieve quality attributes for granules and downstream product (tableting). This project, consequently, will be useful for providing an enhanced understanding on how process and formulation variables in the twin screw granulation affect the fluid bed drying behaviour of granules. Furthermore, the new findings from this project, especially the granules breakage data and moisture content distribution across the radial distance of granules are very useful in the development of a generic drying model or a flowsheet model used for the simulation of granule size in future. This is important in formulation and process optimization and process control in pharmaceutical and food industry. Additionally, the findings of this research project in general will also have the potential to benefit the broader field of powder technology across several industrial sectors such as pharmaceuticals, food, detergent, agriculture, polymer etc., potentially boosting pharmaceutical research output significantly. It will also give an overview of recent developments in continuous twin screw wet granulation, emphasising the importance of formulation and raw material properties, as well as process-related considerations for drying and other downstream processes. So, one can optimise the quality of granules and tablet by

altering specific process and formulation parameters during the granulation stage using a continuous twin-screw granulator. Besides, this project will offer numerous practical information for both novice and experienced users of this technique, as well as highlighting some unmet needs that deserve future investigation.

## 9.1 Future Work

---

### Use of NIR-CI in Further Single Granule Drying Model

Having established a robust NIR-CI quantitative analytical method for determination of moisture content and the spatial distribution of the moisture content within the single granule as a function of fluidized bed drying time, a promising modelling work on the drying behaviour of single granule will be potentially implemented. Hence, carrying out such work will enable the introduction of a unique protocol to be used for granule drying process at both laboratory and pilot scale in pharmaceutical industry. The modelling work will consider the porosity as well as the moisture content distribution across the radial distance of the granule a function of FB drying time. This will be an attractive addition to the existing modelling work that was implanted by Mortier et al. (2012). Figure 144 shows a schematic diagram of the proposed modelling future work.

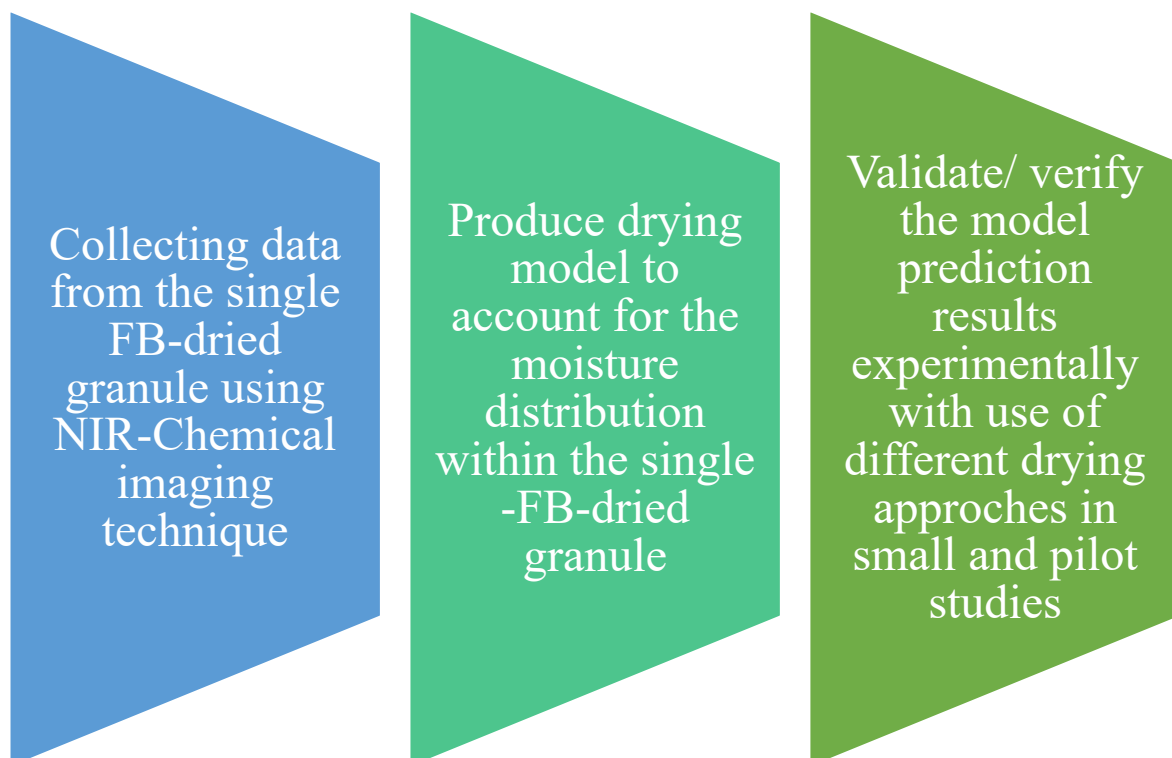


**Figure 144: Schematic diagram of the proposed future work**

## 9.2 References

---

- Amigo, J.M., 2010. Practical issues of hyperspectral imaging analysis of solid dosage forms. *Analytical and bioanalytical chemistry*, 398(1), pp.93-109.
- Amigo, J.M., Cruz, J., Bautista, M., MasPOCH, S., Coello, J. and Blanco, M., 2008. Study of pharmaceutical samples by NIR chemical-image and multivariate analysis. *TrAC Trends in Analytical Chemistry*, 27(8), pp.696-713.
- Augsburger, L.L. and Hoag, S.W. eds., 2017. *Pharmaceutical dosage forms: capsules*. CRC Press.
- Aulton, M.E., 2002. *Pharmaceutics: The science of dosage form design*. Churchill livingstone.
- Bemrose, C.R. and Bridgwater, J., 1987. A review of attrition and attrition test methods. *Powder Technology*, 49(2), pp.97-126.
- Blanco, M., Coello, J., Iturriaga, H., MasPOCH, S. and De La Pezuela, C., 1998. Near-infrared spectroscopy in the pharmaceutical industry. *Analyst-London- society of public Analyst then royal society of chemistry-*, 123, pp.135R-150R.
- Briens, L. and Bojarra, M., 2010. Monitoring fluidized bed drying of pharmaceutical granules. *Aaps Pharmscitech*, 11(4), pp.1612-1618.
- Bronlund, J. and Paterson, T., 2004. Moisture sorption isotherms for crystalline, amorphous and predominantly crystalline lactose powders. *International Dairy Journal*, 14(3), pp.247-254.
- Clarke, F.C., Hammond, S.V., Jee, R.D. and Moffat, A.C., 2002. Determination of the information depth and sample size for the analysis of pharmaceutical materials using reflectance near-infrared microscopy. *Applied spectroscopy*, 56(11), pp.1475-1483.

- De Leersnyder, F., Vanhoorne, V., Bekaert, H., Vercruyse, J., Ghijs, M., Bostijn, N., Verstraeten, M., Cappuyns, P., Van Assche, I., Vander Heyden, Y. and Ziemons, E., 2018. Breakage and drying behaviour of granules in a continuous fluid bed dryer: Influence of process parameters and wet granule transfer. *European Journal of Pharmaceutical Sciences* 115, pp.223-232.
- Dhenge, R.M., Fyles, R.S., Cartwright, J.J., Doughty, D.G., Hounslow, M.J. and Salman, A.D., 2010. Twin screw wet granulation: Granule properties. *Chemical Engineering Journal*, 164(23), pp.322-329.
- Dhenge, R.M., Washino, K., Cartwright, J.J., Hounslow, M.J. and Salman, A.D., 2013. Twin screw granulation using conveying screws: Effects of viscosity of granulation liquids and flow of powders. *Powder technology*, 238, pp.77-90.
- Djuric, D. and Kleinebudde, P., 2008. Impact of screw elements on continuous granulation with a twin-screw extruder. *Journal of pharmaceutical sciences*, 97(11), pp.4934-4942.
- Elkhider, N., Chan, K.A. and Kazarian, S.G., 2007. Effect of moisture and pressure on tablet compaction studied with FTIR spectroscopic imaging. *Journal of pharmaceutical sciences*, 96(2), pp.351-360.
- ElMasry, G. and Wold, J.P., 2008. High-speed assessment of fat and water content distribution in fish fillets using online imaging spectroscopy. *Journal of agricultural and food chemistry*, 56(17), pp.7672-7677.
- Farber, L., Tardos, G.I. and Michaels, J.N., 2003. Evolution and structure of drying material bridges of pharmaceutical excipients: studies on a microscope slide. *Chemical engineering science*, 58(19), pp.4515-4525.
- Fonteyne, M., Gildemyn, D., Peeters, E., Mortier, S.T.F., Vercruyse, J., Gernaey, K.V., Vervaet, C., Remon, J.P., Nopens, I. and De Beer, T., 2014. Moisture and drug solid-state monitoring during a continuous drying process using empirical and mass balance models. *European Journal of Pharmaceutics and Biopharmaceutics*, 87(3), pp.616-628.

- Gabbott, I.P., Al Husban, F. and Reynolds, G.K., 2016. The combined effect of wet granulation process parameters and dried granule moisture content on tablet quality attributes. *European Journal of Pharmaceutics and Biopharmaceutics*, 106, pp.70-78.
- Gombas, A., Szabó-Révész, P., Kata, M., Regdon, G. and Erős, I., 2002. Quantitative determination of crystallinity of  $\alpha$ -lactose monohydrate by DSC. *Journal of Thermal Analysis and Calorimetry*, 68(2), pp.503-510.
- Hegedűs, Á. and Pintye-Hódi, K., 2007. Comparison of the effects of different drying techniques on properties of granules and tablets made on a production scale. *International journal of pharmaceutics*, 330(1-2), pp.99-104.
- Hernandez, E., Pawar, P., Keyvan, G., Wang, Y., Velez, N., Callegari, G., Cuitino, A., Michniak-Kohn, B., Muzzio, F.J. and Románach, R.J., 2016. Prediction of dissolution profiles by non-destructive near infrared spectroscopy in tablets subjected to different levels of strain. *Journal of pharmaceutical and biomedical analysis*, 117, pp.568-576.
- Huang, M., Kim, M.S., Chao, K., Qin, J., Mo, C., Esquerre, C., Delwiche, S. and Zhu, Q., 2016. Penetration depth measurement of near-infrared hyperspectral imaging light for milk powder. *Sensors*, 16(4), p.441.
- Huang, W., Shi, Y., Wang, C., Yu, K., Sun, F. and Li, Y., 2013. Using spray-dried lactose monohydrate in wet granulation method for a low-dose oral formulation of a paliperidone derivative. *Powder technology*, 246, pp.379-394.
- Hwang, K.M., Cho, C.H., Yoo, S.D., Cha, K.I. and Park, E.S., 2019. Continuous twin screw granulation: Impact of the starting material properties and various process parameters. *Powder Technology*, 356, pp.847-857.
- Iveson, S.M., Litster, J.D., Hapgood, K. and Ennis, B.J., 2001. Nucleation, growth and breakage phenomena in agitated wet granulation processes: a review. *Powder technology*, 117(1-2), pp.3-39.

- Jørgensen, K., Bach, P. and Jensen, A.D., 2005. Impact and attrition shear breakage of enzyme granules and placebo particles-application to particle design and formulation. *Powder technology*, 149(2-3), pp.157-167.
- Keleb, E.I., Vermeire, A., Vervaet, C. and Remon, J.P., 2004. Single-step granulation/tableting of different grades of lactose: a comparison with high shear granulation and compression. *European journal of pharmaceutics and biopharmaceutics*, 58(1), pp.77-82.
- Kelkar, V.V. and Ng, K.M., 2002. Development of fluidized catalytic reactors: Screening and scale-up. *AIChE journal*, 48(7), pp.1498-1518.
- Koide, T., Yamamoto, Y., Fukami, T., Katori, N., Okuda, H. and Hiyama, Y., 2015. Analysis of distribution of ingredients in commercially available clarithromycin tablets using nearinfrared chemical imaging with principal component analysis and partial least squares. *Chemical and Pharmaceutical Bulletin*, 63(9), pp.663-668.
- Kumar, A., Vercruyse, J., Toiviainen, M., Panouillot, P.E., Juuti, M., Vanhoorne, V., Vervaet, C., Remon, J.P., Gernaey, K.V., De Beer, T. and Nopens, I., 2014. Mixing and transport during pharmaceutical twin-screw wet granulation: experimental analysis via chemical imaging. *European Journal of Pharmaceutics and Biopharmaceutics*, 87(2), pp.279-289.
- Lee, S.L., O'Connor, T.F., Yang, X., Cruz, C.N., Chatterjee, S., Madurawe, R.D., Moore, C.M., Lawrence, X.Y. and Woodcock, J., 2015. Modernizing pharmaceutical manufacturing: from batch to continuous production. *Journal of Pharmaceutical Innovation*, 10(3), pp.191-199.
- Lute, S.V., Dhenge, R.M. and Salman, A.D., 2018. Twin Screw Granulation: Effects of Properties of Primary Powders. *Pharmaceutics*, 10(2), p.68.
- Mackaplow, M.B., Rosen, L.A. and Michaels, J.N., 2000. Effect of primary particle size on granule growth and endpoint determination in high-shear wet granulation. *Powder Technology*, 108(1), pp.32-45.

- Malamataris, S., Goidas, P. and Dimitriou, A., 1991. Moisture sorption and tensile strength of some tableted direct compression excipients. *International journal of pharmaceutics*, 68(1-3), pp.51-60.
- Mangal, S., Larson, I., Meiser, F. and Morton, D.A., 2015. Particle Engineering of Polymers into Multifunctional Interactive Excipients. In *Handbook of Polymers for Pharmaceutical Technologies* (pp. 1-31). John Wiley & Sons Inc.
- Manley, M., 2014. Near-infrared spectroscopy and hyperspectral imaging: non-destructive analysis of biological materials. *Chemical Society Reviews*, 43(24), pp.8200-8214.
- Mezhericher, M., 2014. Development of drying-induced stresses in pharmaceutical granules prepared in continuous production line. *European Journal of Pharmaceutics and Biopharmaceutics*, 88(3), pp.866-878.
- Mezhericher, M., Levy, A. and Borde, I., 2007. Theoretical drying model of single droplets containing insoluble or dissolved solids. *Drying technology*, 25(6), pp.1025-1032.
- Mezhericher, M., Levy, A. and Borde, I., 2008. Modelling of particle breakage during drying. *Chemical Engineering and Processing: Process Intensification*, 47(8), pp.1404-1411.
- Mezhericher, M., Levy, A. and Borde, I., 2009. Heat and mass transfer and breakage of particles in drying processes. *Drying Technology*, 27(7-8), pp.870-877.
- Mezhericher, M., Levy, A. and Borde, I., 2010. Spray drying modelling based on advanced droplet drying kinetics. *Chemical Engineering and Processing: Process Intensification*, 49(11), pp.1205-1213.
- Mortier, S.T.F., De Beer, T., Gernaey, K.V., Remon, J.P., Vervaet, C. and Nopens, I., 2011. Mechanistic modelling of fluidized bed drying processes of wet porous granules: a review. *European journal of pharmaceutics and biopharmaceutics*, 79(2), pp.205-225.
- Mortier, S.T.F., De Beer, T., Gernaey, K.V., Vercruyssen, J., Fonteyne, M., Remon, J.P., Vervaet, C. and Nopens, I., 2012. Mechanistic modelling of the drying behaviour of single



pharmaceutical granules. *European journal of pharmaceutics and biopharmaceutics*, 80(3), pp.682-689.

- Mortier, S.T.F., Gernaey, K.V., De Beer, T. and Nopens, I., 2013. Development of a population balance model of a pharmaceutical drying process and testing of solution methods. *Computers & chemical engineering*, 50, pp.39-53.
- Nieuwmeyer, F., van der Voort Maarschalk, K. and Vromans, H., 2008. The consequences of granulate heterogeneity towards breakage and attrition upon fluid-bed drying. *European journal of pharmaceutics and biopharmaceutics*, 70(1), pp.402-408.
- Nieuwmeyer, F.J., Damen, M., Gerich, A., Rusmini, F., van der Voort Maarschalk, K. and Vromans, H., 2007. Granule characterization during fluid bed drying by development of a near infrared method to determine water content and median granule size. *Pharmaceutical Research*, 24(10), pp.1854-1861.
- Niskanen, T. and Yliruusi, J., 1994. Attrition of theophylline granules during drying in a fluidized bed granulator. *Pharmazeutische Industrie*, 56(3), pp.282-285.
- Nokhodchi, A., 2005. Effect of moisture on compaction and compression. *Pharm. Tech*, 6, pp.46-66.
- NOKHODCHI, A., FORD, J.L., ROWE, P.H. and RUBINSTEIN, M.H., 1996. The influence of moisture content on the consolidation properties of hydroxypropylmethylcellulose K4M (HPMC 2208). *Journal of pharmacy and pharmacology*, 48(11), pp.1116-1121.
- Nokhodchi, A., Rubinstein, M.H., Larhrib, H. and Guyot, J.C., 1995. The effect of moisture content on the energies involved in the compaction of ibuprofen. *International journal of pharmaceutics*, 120(1), pp.13-20.
- Osborne, J.D., Althaus, T., Forny, L., Niederreiter, G., Palzer, S., Hounslow, M.J. and Salman, A.D., 2013. Investigating the influence of moisture content and pressure on the bonding mechanisms during roller compaction of an amorphous material. *Chemical engineering science*, 86, pp.61-69.

- Owen, S.C., 2006. Sorbitol. Handbook of pharmaceutical Excipients, Rowe, RC, Sheskey, PJ, Owen, SC, eds., 5th ed., Pharmaceutical Press, USA, pp.718-721.
- Poutiainen, S., Honkanen, M., Becker, J., Nachtweide, D., Järvinen, K. and Ketolainen, J., 2012. X-ray microtomography analysis of intragranular drug migration during fluidized bed and oven tray drying. Journal of pharmaceutical sciences, 101(4), pp.1587-1598.
- Ravn, C., Skibsted, E. and Bro, R., 2008. Near-infrared chemical imaging (NIR-CI) on pharmaceutical solid dosage forms—comparing common calibration approaches. Journal of Pharmaceutical and Biomedical Analysis, 48(3), pp.554-561.
- Saleh, M.F., Dhenge, R.M., Cartwright, J.J., Hounslow, M.J. and Salman, A.D., 2015. Twin screw wet granulation: Effect of process and formulation variables on powder caking during production. International journal of pharmaceutics, 496(2), pp.571-582.
- Shamlou, A.A., Liu, Z. and Yates, J.G., 1990. Hydrodynamic influences on particle breakage in fluidized beds. Chemical Engineering Science, 45(4), pp.809-817.
- Shang, C., Sinka, I.C., Jayaraman, B. and Pan, J., 2013. Break force and tensile strength relationships for curved faced tablets subject to diametrical compression. International journal of pharmaceutics, 442(1-2), pp.57-64.
- Srinivas, G. and Setty, Y.P., 2013. Drying behavior of uniform and binary mixture of solids in a batch fluidized bed dryer. Powder technology, 241, pp.181-187.
- Syahrul, S., Hamdullahpur, F. and Dincer, I., 2002. Thermal analysis in fluidized bed drying of moist particles. Applied Thermal Engineering, 22(15), pp.1763-1775.
- Taghavivand, M., Choi, K. and Zhang, L., 2017. Investigation on drying kinetics and tribocharging behaviour of pharmaceutical granules in a fluidized bed dryer. Powder Technology, 316, pp.171-180.
- Takasaki, H., Yonemochi, E., Ito, M., Wada, K. and Terada, K., 2016. The effect of water activity on granule characteristics and tablet properties produced by moisture activated dry granulation (MADG). Powder Technology, 294, pp.113-118.

- Van den Dries, K., de Vegt, O.M., Girard, V. and Vromans, H., 2003. Granule breakage phenomena in a high shear mixer; influence of process and formulation variables and consequences on granule homogeneity. *Powder technology*, 133(1-3), pp.228-236.
- Vandevivere, L., Portier, C., Vanhoorne, V., Häusler, O., Simon, D., De Beer, T. and Vervaet, C., 2019. Native starch as in situ binder for continuous twin screw wet granulation. *International Journal of Pharmaceutics*, 571, p.118760.
- Vanhoorne, V., Vanbillemont, B., Vercruyssen, J., De Leersnyder, F., Gomes, P., De Beer, T., Remon, J.P. and Vervaet, C., 2016. Development of a controlled release formulation by continuous twin screw granulation: influence of process and formulation parameters. *International Journal of Pharmaceutics*, 505(1-2), pp.61-68.
- Varmuza, K. and Filzmoser, P., 2016. Introduction to multivariate statistical analysis in chemometrics. CRC press.
- Vercruyssen, J. et al., 2012. Continuous twin screw granulation: Influence of process variables on granule and tablet quality. *European Journal of Pharmaceutics and Biopharmaceutics*, 82(1), pp.205–211.
- Vercruyssen, J., Delaet, U., Van Assche, I., Cappuyns, P., Arata, F., Caporicci, G., De Beer, T., Remon, J.P. and Vervaet, C., 2013. Stability and repeatability of a continuous twin screw granulation and drying system. *European journal of pharmaceutics and biopharmaceutics*, 85(3), pp.1031-1038.
- Vercruyssen, J., Peeters, E., Fonteyne, M., Cappuyns, P., Delaet, U., Van Assche, I., De Beer, T., Remon, J.P. and Vervaet, C., 2015. Use of a continuous twin screw granulation and drying system during formulation development and process optimization. *European Journal of Pharmaceutics and Biopharmaceutics*, 89, pp.239-247.
- Vercruyssen, J., Toiviainen, M., Fonteyne, M., Helkimo, N., Ketolainen, J., Juuti, M., Delaet, U., Van Assche, I., Remon, J.P., Vervaet, C. and De Beer, T., 2014. Visualization and understanding of the granulation liquid mixing and distribution during continuous twin screw

granulation using NIR chemical imaging. *European Journal of Pharmaceutics and Biopharmaceutics*, 86(3), pp.383-392.

- Verkoeijen, D., Meesters, G.M., Vercoulen, P.H. and Scarlett, B., 2002. Determining granule strength as a function of moisture content. *Powder technology*, 124(3), pp.195-200.
- Verstraeten, M., Van Hauwermeiren, D., Lee, K., Turnbull, N., Wilsdon, D., am Ende, M., Doshi, P., Vervaet, C., Brouckaert, D., Mortier, S.T. and Nopens, I., 2017. In-depth experimental analysis of pharmaceutical twin-screw wet granulation in view of detailed process understanding. *International journal of pharmaceutics*, 529(1-2), pp.678-693.
- Wade, J.B., Martin, G.P. & Long, D.F., 2013. A methodological approach for determining the effect of moisture content on the compaction properties of powders: Granular hydroxyapatite. *Powder Technology*, 246, pp.511–519.
- Walton, D.E., 2004. The evaporation of water droplets. A single droplet drying experiment. *Drying technology*, 22(3), pp.431-456.
- Watano, S., Yeh, N. and Miyanami, K., 1998. Drying of granules in agitation fluidized bed. *Journal of chemical engineering of Japan*, 31(6), pp.908-913.
- Wold, S., Sjöström, M. and Eriksson, L., 2001. PLS-regression: a basic tool of chemometrics. *Chemometrics and intelligent laboratory systems*, 58(2), pp.109-130.
- Zhuikova, N.N., Sablina, O.S. and Gavrilov, A.S., 2009. Effects of moisture on the pressing of pharmaceutical powders. *Pharmaceutical chemistry journal*, 43(1).
- Chablani, L., Taylor, M. K., Mehrotra, A., Rameas, P., & Stagner, W. C. (2011). Inline real-time near-infrared granule moisture measurements of a continuous granulation-drying-milling process. *AAPS PharmSciTech*, 12(4), 1050–1055.
- De Leersnyder, F., Vanhoorne, V., Bekaert, H., Vercruyse, J., Ghijs, M., Bostijn, N., Verstraeten, M., Cappuyns, P., Van Assche, I., Vander Heyden, Y., Ziemons, E., Remon, J. P., Nopens, I., Vervaet, C., & De Beer, T. (2018). Breakage and drying behaviour of granules in a continuous fluid bed dryer: Influence of process parameters and wet granule transfer. *European Journal of Pharmaceutical Sciences*, 115(September 2017), 223–232.

- Dhenge, R. M., Cartwright, J. J., Doughty, D. G., Hounslow, M. J., & Salman, A. D. (2011). Twin screw wet granulation: Effect of powder feed rate. *Advanced Powder Technology*, 22(2), 162–166.
- Dhenge, R. M., Cartwright, J. J., Hounslow, M. J., & Salman, A. D. (2012). Twin screw granulation: Steps in granule growth. *International Journal of Pharmaceutics*, 438(1–2), 20–32.
- Fonteyne, M., Correia, A., De Plecker, S., Vercruyssen, J., Ilić, I., Zhou, Q., Vervaet, C., Remon, J. P., Onofre, F., Bulone, V., & De Beer, T. (2015). Impact of microcrystalline cellulose material attributes: A case study on continuous twin screw granulation. *International Journal of Pharmaceutics*, 478(2), 705–717.
- Fonteyne, M., Gildemyn, D., Peeters, E., Mortier, S. T. F. C., Vercruyssen, J., Gernaey, K. V., Vervaet, C., Remon, J. P., Nopens, I., & De Beer, T. (2014). Moisture and drug solid-state monitoring during a continuous drying process using empirical and mass balance models. *European Journal of Pharmaceutics and Biopharmaceutics*, 87(3), 616–628.
- Fonteyne, M., Wickström, H., Peeters, E., Vercruyssen, J., Ehlers, H., Peters, B. H., Remon, J. P., Vervaet, C., Ketolainen, J., Sandler, N., Rantanen, J., Naelapää, K., & Beer, T. De. (2014). Influence of raw material properties upon critical quality attributes of continuously produced granules and tablets. *European Journal of Pharmaceutics and Biopharmaceutics*, 87(2), 252–263.
- Lute, S. V., Dhenge, R. M., Hounslow, M. J., & Salman, A. D. (2016). Twin screw granulation: Understanding the mechanism of granule formation along the barrel length. *Chemical Engineering Research and Design*, 110, 43–53.
- Lute, S. V., Dhenge, R. M., & Salman, A. D. (2018). Twin screw granulation: Effects of properties of primary powders. *Pharmaceutics*, 10(2).
- Portier, C., Pandelaere, K., Delaet, U., Vigh, T., Di Pretoro, G., De Beer, T., Vervaet, C., & Vanhoorne, V. (2020). Continuous twin screw granulation: A complex interplay between formulation properties, process settings and screw design. *International Journal of*

Pharmaceutics, 576(October 2019), 119004.

- Portier, C., Pandelaere, K., Delaet, U., Vigh, T., Kumar, A., Di Pretoro, G., De Beer, T., Vervaet, C., & Vanhoorne, V. (2020). Continuous twin screw granulation: Influence of process and formulation variables on granule quality attributes of model formulations. *International Journal of Pharmaceutics*, 576(January), 118981.
- Qiao, Z., Wang, Z., Zhang, C., Yuan, S., Zhu, Y., & Wang, J. (2012). PVAm-PIP/PS composite membrane with high performance for CO<sub>2</sub>/N<sub>2</sub> separation. *AIChE Journal*, 59(4), 215–228.
- Ryckaert, A., Ghijs, M., Portier, C., Djuric, D., Funke, A., Vervaet, C., & Beer, T. De. (2021). The Influence of Equipment Design and Process Parameters on Granule Breakage in a Semi-Continuous Fluid Bed Dryer after Continuous Twin-Screw Wet Granulation.
- Stauffer, F., Vanhoorne, V., Pilcer, G., Chavez, P. F., Vervaet, C., & De Beer, T. (2019). Managing API raw material variability in a continuous manufacturing line – Prediction of process robustness. *International Journal of Pharmaceutics*, 569(July).
- Stauffer, Fanny, Ryckaert, A., Van Hauwermeiren, D., Funke, A., Djuric, D., Nopens, I., & De Beer, T. (2019). Heat Transfer Evaluation During Twin-Screw Wet Granulation in View of Detailed Process Understanding. *AAPS PharmSciTech*, 20(7), 1–13.
- Van Hauwermeiren, D., Verstraeten, M., Doshi, P., am Ende, M. T., Turnbull, N., Lee, K., De Beer, T., & Nopens, I. (2019). On the modelling of granule size distributions in twin-screw wet granulation: Calibration of a novel compartmental population balance model. *Powder Technology*, 341, 116–125.
- Vandevivere, L., Denduyver, P., Portier, C., Häusler, O., De Beer, T., Vervaet, C., & Vanhoorne, V. (2020). Influence of binder attributes on binder effectiveness in a continuous twin screw wet granulation process via wet and dry binder addition. *International Journal of Pharmaceutics*, 585(May), 119466.
- Vanhoorne, V., Janssens, L., Vercruyssen, J., De Beer, T., Remon, J. P., & Vervaet, C. (2016). Continuous twin screw granulation of controlled release formulations with various HPMC

grades. *International Journal of Pharmaceutics*, 511(2), 1048–1057.

- Vercruyssen, J., Córdoba Díaz, D., Peeters, E., Fonteyne, M., Delaet, U., Van Assche, I., De Beer, T., Remon, J. P., & Vervaet, C. (2012). Continuous twin screw granulation: Influence of process variables on granule and tablet quality. *European Journal of Pharmaceutics and Biopharmaceutics*, 82(1), 205–211.
- Vercruyssen, J., Delaet, U., Van Assche, I., Cappuyns, P., Arata, F., Caporicci, G., De Beer, T., Remon, J. P., & Vervaet, C. (2013). Stability and repeatability of a continuous twin screw granulation and drying system. *European Journal of Pharmaceutics and Biopharmaceutics*, 85(3 PART B), 1031–1038.
- Vercruyssen, J., Peeters, E., Fonteyne, M., Cappuyns, P., Delaet, U., Van Assche, I., De Beer, T., Remon, J. P., & Vervaet, C. (2015). Use of a continuous twin screw granulation and drying system during formulation development and process optimization. *European Journal of Pharmaceutics and Biopharmaceutics*, 89, 239–247.
- Verstraeten, M., Van Hauwermeiren, D., Lee, K., Turnbull, N., Wilsdon, D., am Ende, M., Doshi, P., Vervaet, C., Brouckaert, D., Mortier, S. T. F. C., Nopens, I., & Beer, T. De. (2017). In-depth experimental analysis of pharmaceutical twin-screw wet granulation in view of detailed process understanding. *International Journal of Pharmaceutics*, 529(1–2), 678–693.
- Willecke, N., Szepes, A., Wunderlich, M., Remon, J. P., Vervaet, C., & Beer, T. De. (2017). Identifying overarching excipient properties towards an in-depth understanding of process and product performance for continuous twin-screw wet granulation. *International Journal of Pharmaceutics*, 522(1–2), 234–247.
- Willecke, N., Szepes, A., Wunderlich, M., Remon, J. P., Vervaet, C., & De Beer, T. (2018). A novel approach to support formulation design on twin screw wet granulation technology: Understanding the impact of overarching excipient properties on drug product quality attributes. *International Journal of Pharmaceutics*, 545(1–2), 128–143.
- Yu, S., Reynolds, G. K., Huang, Z., De Matas, M., & Salman, A. D. (2014). Granulation of increasingly hydrophobic formulations using a twin screw granulator. *International Journal of*

Pharmaceutics, 475(1–2), 82–96.



### 9.3 Appendix

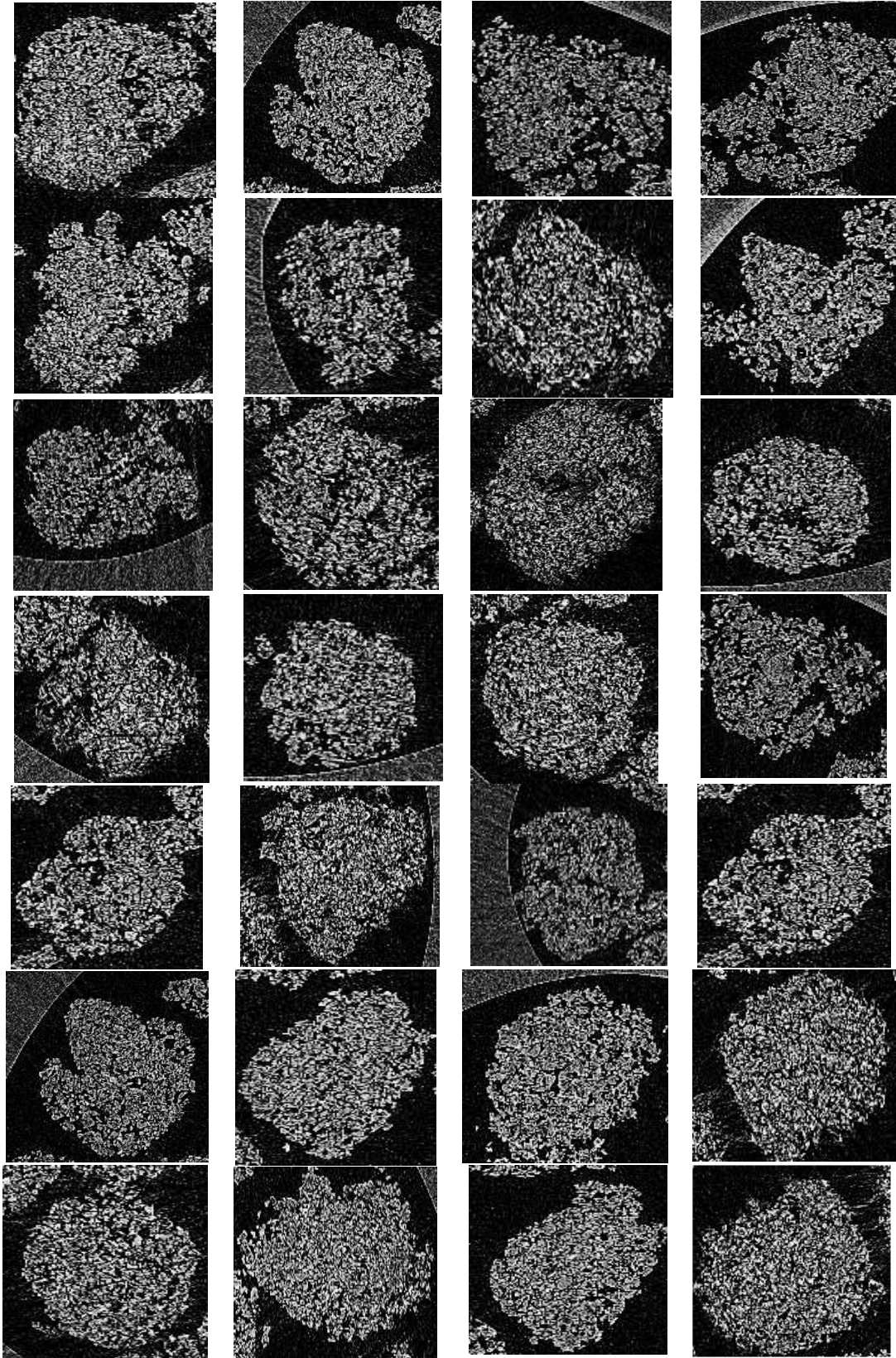


**Fig.142:X-ray images of granules prepared with conveying elements at the twin screw granulation**

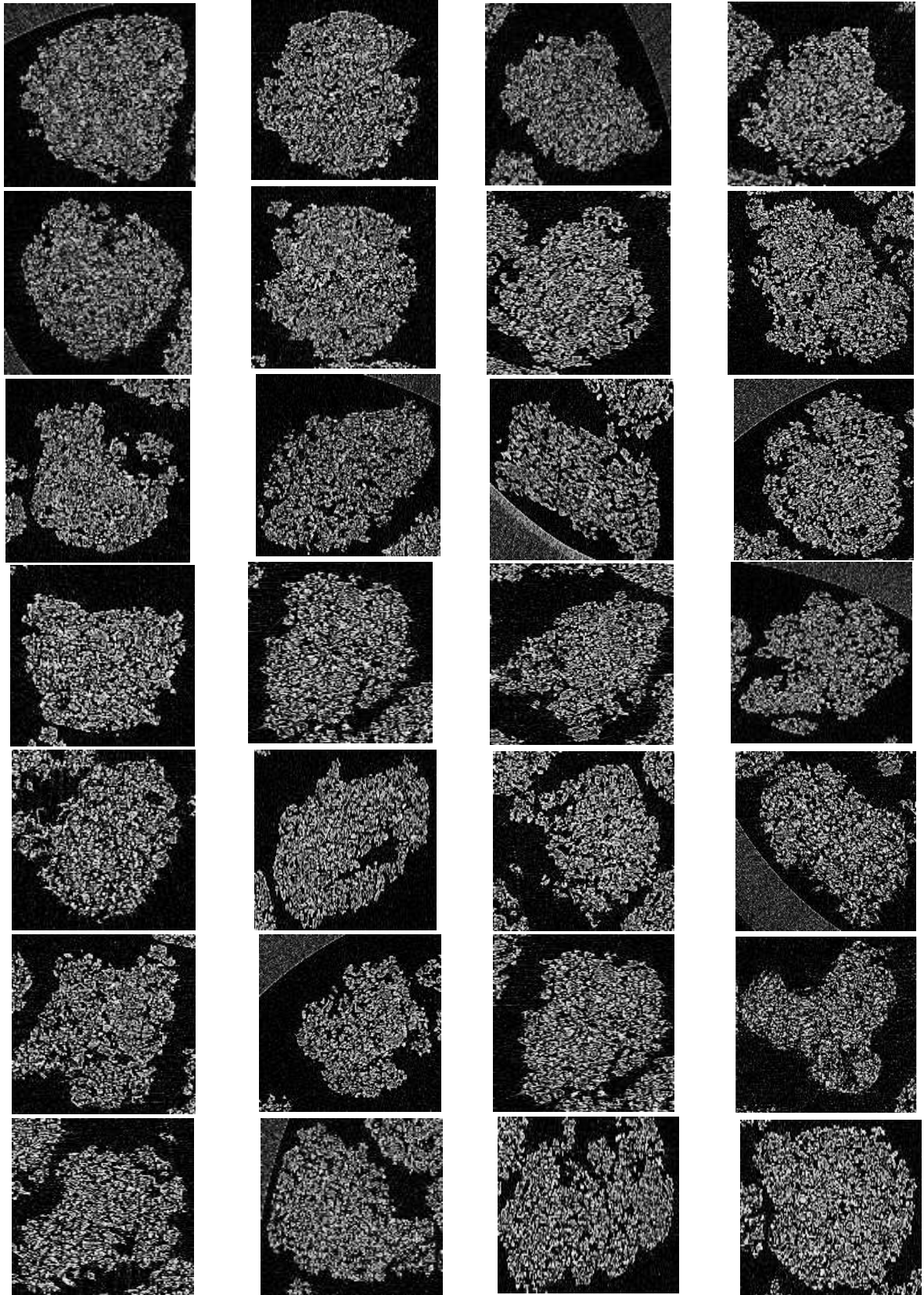


**Figure 143: X-ray images of granules prepared with 4KE elements in each screw at the twin screw granulation**

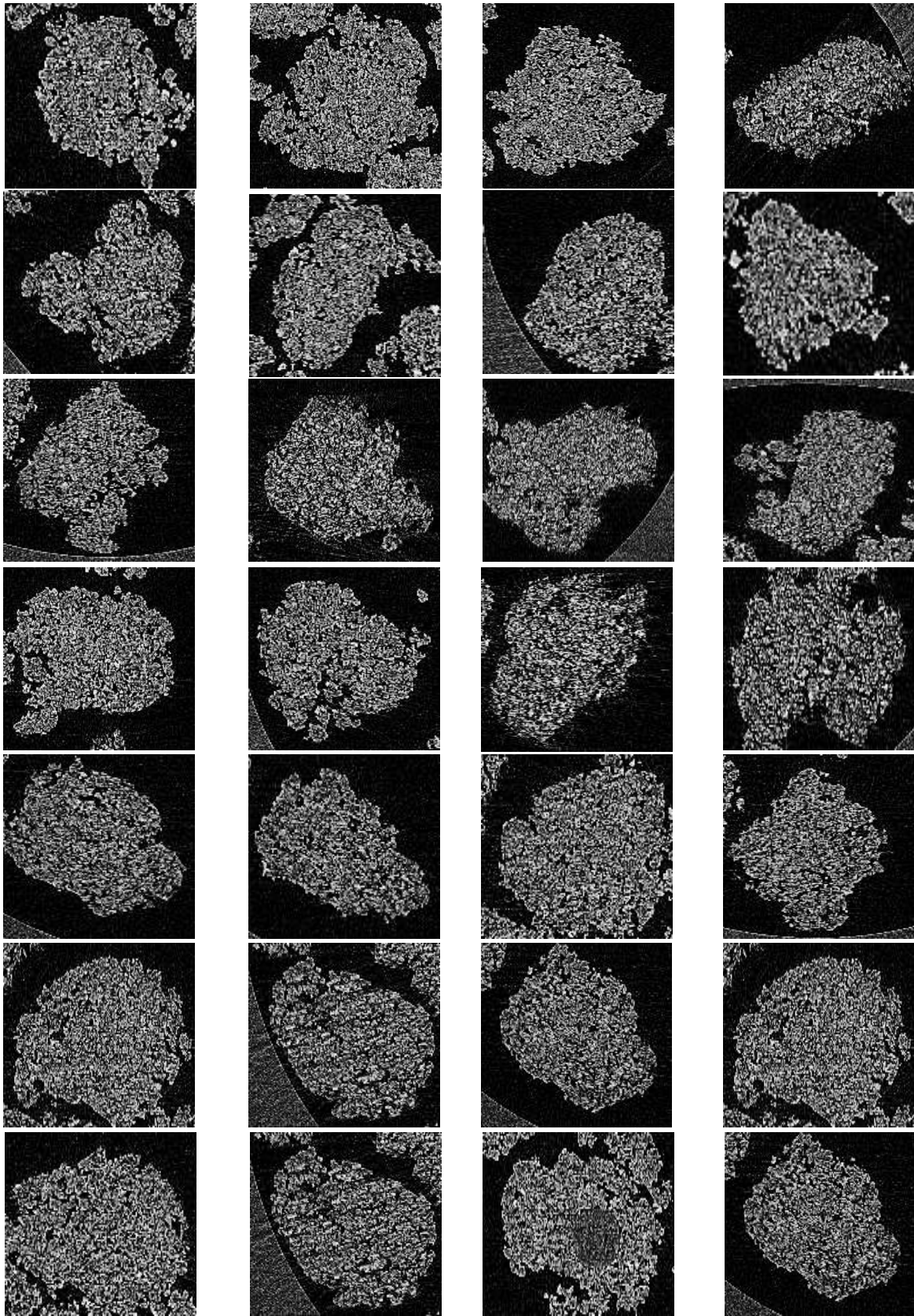


**Figure 144: X-ray images of granules prepared with 8KE elements in each screw at the twin screw granulation**



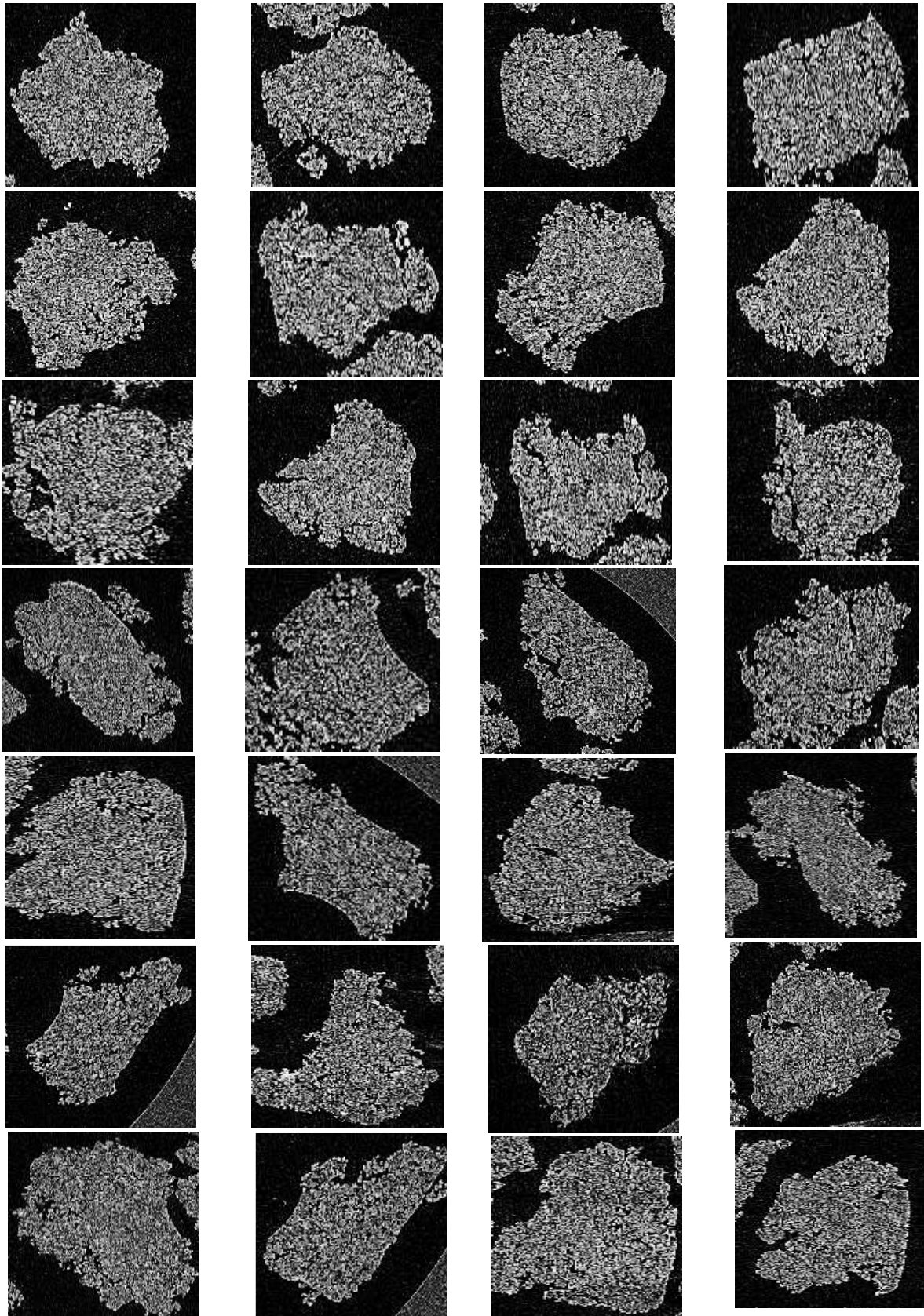


**Figure 145: X-ray images of granules prepared with 16KE elements in each screw at the twin**



# THE LIMITATIONS OF NIR-CHEMICAL IMAGING FOR DETERMINATION OF TABLET MOISTURE CONTENT

Kawther F. Kadhim, Riyadh Al-Asady, Feng Li, James D. Litster & Agba D. Salman

Department of Chemical and Biological Engineering, University of Sheffield, Sheffield, S1 3JD, UK  
E-mail: kkadhim1@sheffield.ac.uk

## ABSTRACT

Determination of moisture content is important for many industrial sectors. It is used to ensure achieving the required quality of the final product. This paper aims at investigating the validity of using a non-destructive near infrared (NIR) chemical imaging (CI) technique as a tool to determine the moisture content of tablet surface. This technique enables visualizing the distribution of moisture content, as well as providing a quantitative information of the tablet surface moisture content. Although, this method enables fast assessment of moisture content, it is associated with some limitations that should be considered when using this technique for such application. This study attempts at highlighting these limitations such as the effect of surface roughness of the sample on the reliability of the NIR-CI result. In this study, the effects of tableting compression forces and moisture content on tablet surface roughness and hence its impact on NIR-CI was investigated.

## KEYWORDS

NIR- chemical imaging, Tablet surface moisture content, Surface roughness

## 1. INTRODUCTION

The production of tablets consists of several consecutive steps of processing the active pharmaceutical ingredients (API) and the excipients [1, 2]. One of the important parameters to control the quality of the tablet is the moisture content. This is usually determined by several techniques such as Karl Fischer titration, loss on drying (LOD) and near infra-red (NIR) [3]. The first two techniques can be used offline whereas the NIR can be used as both offline or online.

As reported by Manley [4], Frederick William Herschel discovered the first non-visible region, i.e. near-infrared (NIR) in 1800. Until 150 years later, the NIR techniques was then considered significantly. NIR spectroscopy is applied as a tool during process analytical technology (PAT) and quality control (QC) as the method of choice in various fields, i.e. agriculture, food, bioactives, pharmaceuticals, petrochemicals, textiles, cosmetics, medical applications and chemicals such as polymers [4]. In the literature, NIR spectroscopy technique has been used for monitoring and determining the moisture content of pharmaceutical products during the processes of fluid bed drying and spray drying [5-9]. Margot Fonteyn, et al [3] have used NIR spectroscopy in a fluid bed drying process to monitor and predict the end of drying process and moisture content of lactose granules. The work focused on the validation of an in-line NIR to quantify the moisture content in the six-segmented fluid bed dryer of a continuous from-powder-to-tablet manufacturing line (ConsiGma™ 25, GEA Pharma Systems nv, Wommelgem, Belgium).

The development of NIR chemical imaging, which combines NIR spectroscopy with digital imaging, enables both localisation and spectral (identification) information to be obtained simultaneously. Chemical imaging have the potential of describing distribution of constituents within a sample. It applied increasingly in pharmaceuticals and other applications [4]. Thus, Near infrared



chemical imaging (NIR-CI) is a powerful tool for providing a great deal of information on pharmaceutical samples, as the NIR spectrum can be measured for each pixel of the monitored area over a wide range of wavelengths [10]. It has been applied in a number of different pharmaceuticals fields e.g. drug release in the dissolution of the tablets [11] and uniformity of contents [12, 13, 14]. Spectral imaging or imaging spectroscopy combines two well-known methodologies, namely spectroscopy and imaging, to provide a new advantageous tool [15,16, 17]. It is a relatively new technique, and its full potential has yet to be exploited. The spectral information allows the detection and the ability to distinguish among many different objects, even if they have a similar colour externally. This permits one to label different entities in a sample simultaneously and to quantitatively analyse each entity. The advantage of NIR-CI technique is that the distribution of chemical surface composition in the product can be obtained, not just the bulk composition [16]. Moreover, a study conducted by Koide et al, [12] to analyse the ingredients distribution within the clarithromycin tablets using NIR-CI. Another study by Elkhider et al. [17] has looked at the impact of moisture content and pressure on the compaction and distribution of components within an ibuprofen and hydroxypropylmethylcellulose tablet with using Fourier-transform infrared spectroscopy (FTIR). They used this technique to study the distribution of components within the tablet. Verduyck et al. [15] have used NIR chemical imaging to get an understanding of how the granulation liquid (distilled water) is mixed and distributed with  $\alpha$ -Lactose monohydrate 200 M using continuous twin-screw granulation. The study reported that NIR chemical imaging has been demonstrated to be a fast and adequate measurement tool for enabling process visualization and therefore better understanding of a continuous twin-screw granulation system [15]. Moreover Ravn et al. 2008 [13] has compared common calibration approaches to study NIR-CI on the pharmaceutical dosage forms. The work focused on using different calibration method to process NIR-CI of tablets made of different powder mixed with API. The methods were compared to see which one would give the right chemical image contrast and so it was confirmed that partial least square (PLS) was found to be the best calibration method in their work.

In all above-mentioned literatures, the huge attention was only given to NIR-CI as it is being chemical free, fast, non-destructive and non-invasive technique and not considering that there is some limitations associated with the NIR-CI. In other words, there is a lack of information about the effect of surface roughness of the material being examined with NIR- CI technique on the reliability of the obtained result This paper therefore aims at highlighting the limitation of using NIR-CI technique to determine the moisture content in tablets surface.

## 2. MATERIALS AND METHODS

### Materials

$\alpha$ - Lactose monohydrate

$\alpha$ - lactose monohydrate (150M Lactopure® lactose, Nestle, Switzerland) was used in this study as a primary powder. Before each experiment, the lactose powder was conditioned in a humidity chamber (Binder KMF 240 climatic chamber, Binder, UK) for approximately 3 days at a relative humidity of 40 % and a temperature of 20°C. This was to eliminate the difference in the temperature and humidity of primary powder, which might affect the tableting process. Figure 1 shows the primary particle size distribution of the lactose monohydrate measured by the camasizer XT (Retsch Technology GmbH, Germany). The particle size parameters  $d_{10}$ ,  $d_{50}$  and  $d_{90}$  of this lactose powder measured to be 12.1, 50.9 and 114.5  $\mu\text{m}$  respectively.

chemical imaging (NIR-CI) is a powerful tool for providing a great deal of information on pharmaceutical samples, as the NIR spectrum can be measured for each pixel of the monitored area over a wide range of wavelengths [10]. It has been applied in a number of different pharmaceuticals fields e.g. drug release in the dissolution of the tablets [11] and uniformity of contents [12, 13, 14]. Spectral imaging or imaging spectroscopy combines two well-known methodologies, namely spectroscopy and imaging, to provide a new advantageous tool [15,16, 17]. It is a relatively new technique, and its full potential has yet to be exploited. The spectral information allows the detection and the ability to distinguish among many different objects, even if they have a similar colour externally. This permits one to label different entities in a sample simultaneously and to quantitatively analyse each entity. The advantage of NIR-CI technique is that the distribution of chemical surface composition in the product can be obtained, not just the bulk composition [16]. Moreover, a study conducted by Koide et al, [12] to analyse the ingredients distribution within the clarithromycin tablets using NIR-CI. Another study by Elkhider et al. [17] has looked at the impact of moisture content and pressure on the compaction and distribution of components within an ibuprofen and hydroxypropylmethylcellulose tablet with using Fourier-transform infrared spectroscopy (FTIR). They used this technique to study the distribution of components within the tablet. Verduyck et al. [15] have used NIR chemical imaging to get an understanding of how the granulation liquid (distilled water) is mixed and distributed with  $\alpha$ -Lactose monohydrate 200 M using continuous twin-screw granulation. The study reported that NIR chemical imaging has been demonstrated to be a fast and adequate measurement tool for enabling process visualization and therefore better understanding of a continuous twin-screw granulation system [15]. Moreover Ravn et al. 2008 [13] has compared common calibration approaches to study NIR-CI on the pharmaceutical dosage forms. The work focused on using different calibration method to process NIR-CI of tablets made of different powder mixed with API. The methods were compared to see which one would give the right chemical image contrast and so it was confirmed that partial least square (PLS) was found to be the best calibration method in their work.

In all above-mentioned literatures, the huge attention was only given to NIR-CI as it is being chemical free, fast, non-destructive and non-invasive technique and not considering that there is some limitations associated with the NIR-CI. In other words, there is a lack of information about the effect of surface roughness of the material being examined with NIR- CI technique on the reliability of the obtained result This paper therefore aims at highlighting the limitation of using NIR-CI technique to determine the moisture content in tablets surface.

## 2. MATERIALS AND METHODS

### Materials

$\alpha$ - Lactose monohydrate

$\alpha$ - lactose monohydrate (150M Lactopure® lactose, Nestle, Switzerland) was used in this study as a primary powder. Before each experiment, the lactose powder was conditioned in a humidity chamber (Binder KMF 240 climatic chamber, Binder, UK) for approximately 3 days at a relative humidity of 40 % and a temperature of 20°C. This was to eliminate the difference in the temperature and humidity of primary powder, which might affect the tableting process. Figure 1 shows the primary particle size distribution of the lactose monohydrate measured by the camasizer XT (Retsch Technology GmbH, Germany). The particle size parameters  $d_{10}$ ,  $d_{50}$  and  $d_{90}$  of this lactose powder measured to be 12.1, 50.9 and 114.5  $\mu\text{m}$  respectively.

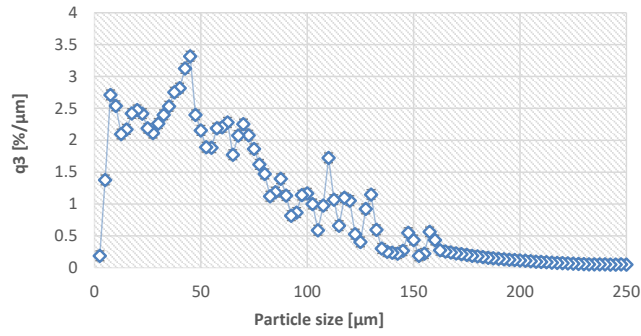


Figure 1: PSD of lactose monohydrate

### Powder Morphology

The powder shape and surface was examined using scanning electron microscopy (SEM). The lactose particles were nonconductive, hence, coated (for 36 seconds) with thin layer of gold using coating machine (Leica EM ACE200, Leica Microsystems, UK). Figure 2 shows the particle morphology of lactose monohydrate using SEM (JEOL IT100, JEOL, Japan). It can be seen that lactose primary particles tend to be taumahauk in shape.

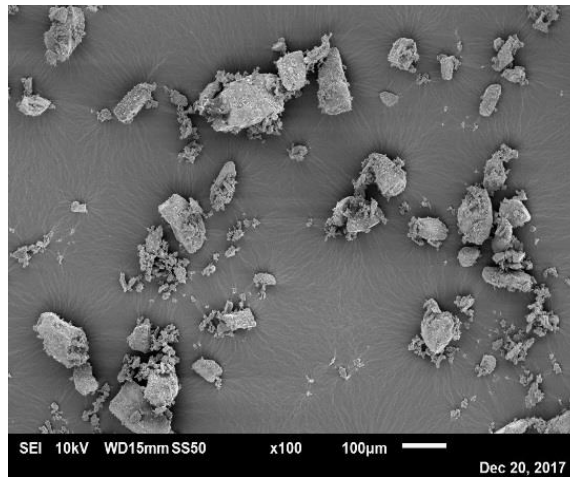


Figure 2: SEM of the primary particles of lactose monohydrates (150M lactopure) at 100 magnification

### 3. EXPERIMENTAL

#### Production of Tablets

Two sets of tablets were produced using the universal testing machine (Instron 3367, Germany) at a compaction speed of 1 mm/min with a die diameter of 30 mm. One tablets set used only for the calibration model of the chemical imaging. These were prepared using a compression force of 10 kN and four different percentages of water mixed by hand with the lactose powder. These water percentages were 0, 5, 10 and 15% of water. Each tablet weigh 3 g. The LOD of the produced tablets were then measured using Sartorius infrared moisture analyser (Sartorius, MA 37, Germany).The resultant moisture content values were 0.5, 4.7, 9.6 and 13.5% respectively. These values used to build the calibration model of the chemical imaging.

The other set of tablets were prepared in order to investigate the effect of surface roughness and moisture content on the reliability of the NIR-CI. Tablets with different moisture of 5, 10 and 12 moistures content % at different compression forces of 5, 10 and 15 kN were prepared. The LOD of these tablets were also measured by the moisture analyser to be 4.7, 9.6 and 10.7% respectively.

#### Chemical Imaging Equipment and Software

NIR spectral chemical imaging (Chemical imaging, Helios optimizer, EVK DI KERSCHHAGGL GmbH) was used to acquire a spectral image of each tablet. Figure 3 illustrates a schematic diagram of the chemical imaging machine used in this study. The spatial resolution is 312 pixels. The chemical imaging records spectral images in the visible and near-infrared range of 1000-2500 nm with a spectral resolution of approximately 30  $\mu\text{m}$ . The light intensity was controlled to be the same throughout the entire experiment by using the same voltage. This is to avoid variation in the result. The software, which was used in this work, is called SQALAR. This software was used to process the spectral images taken by Helios camera and convert it into a quantitative chemical imaging (QCI) images in which quantification of the moisture content at the sample surface can be obtained.

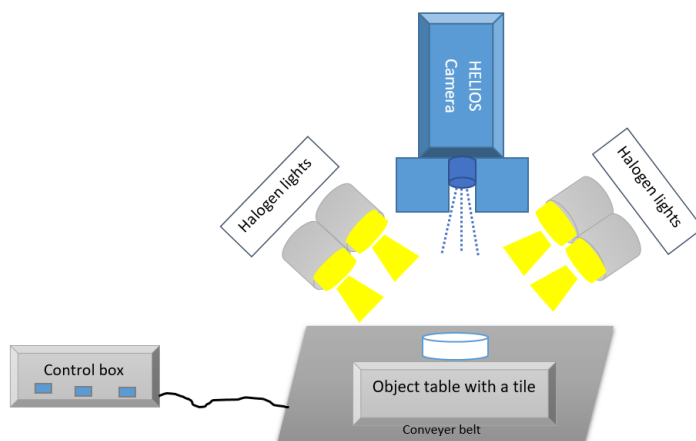


Figure 3: Schematic of the NIR chemical imaging equipment used in this study

### Quantitative calibration model (QCI) for NIR-CI experiment

In order to start using chemical imaging as a technique to quantify the moisture content of the tablet surface, a calibration model was needed. Different moisture content of tablet were used to build the calibration model; 0.5%, 4.7%, and 9.6% and 13.5% moisture content. The obtained tablets were then directly scanned by chemical imaging. Spectral information was then obtained for each scanned image. The Spectral data was first analysed by partial least-squares analysis (PLS), and then the pixel spectra were converted into a meaningful distribution map of moisture contents under the quantitative chemical imaging model (QCI). Figure 4 shows the resultant QCI images of the tablets that made up the calibration model. Having prepared the calibration model, the tablets with different moisture content and compression forces were put into the calibration model for final QCI determination. In the model scale bar, the red colour represents the highest moisture content whereas the blue colour represents the lowest moisture content.

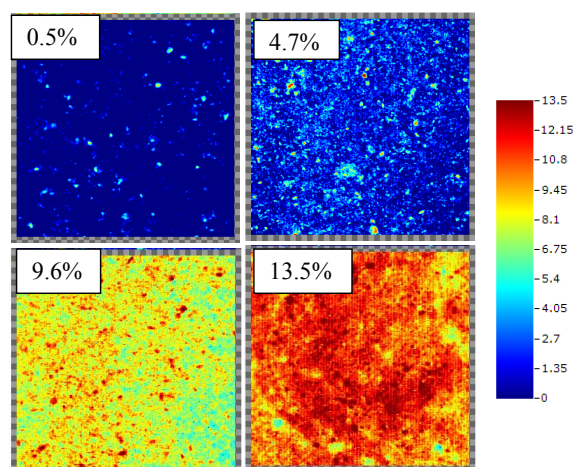


Figure 4: Tablet QCI images of the calibration model

### Surface Profile Measurement

Following the chemical imaging scans for the tablets produced with different compression forces and moisture contents, a digital microscope (Keyence VHX-5000) was then used to measure the surface profiles of the tablet. For the surface profile measurement of the tablet, a horizontal line was selected across an area within the centre of the tablet. A file from this measurement was then generated and extracted as a comma-separated values (CSV) document and therefore profiles were drawn. Surface roughness values ( $Ra$ ) therefore was then calculated using Eq. 1.

$$Ra = \frac{A_1 + A_2 + \dots + A_N}{L} \quad \text{Eq. (1)}$$

Where  $Ra$  is the universally recognised parameter of roughness.  $L$  is evaluation length of the line.  $A_1, A_2, \dots, A_N$  represents the maximum valley and peak respectively in the profiles. Figure 5 shows schematic diagram of the  $Ra$  representation.

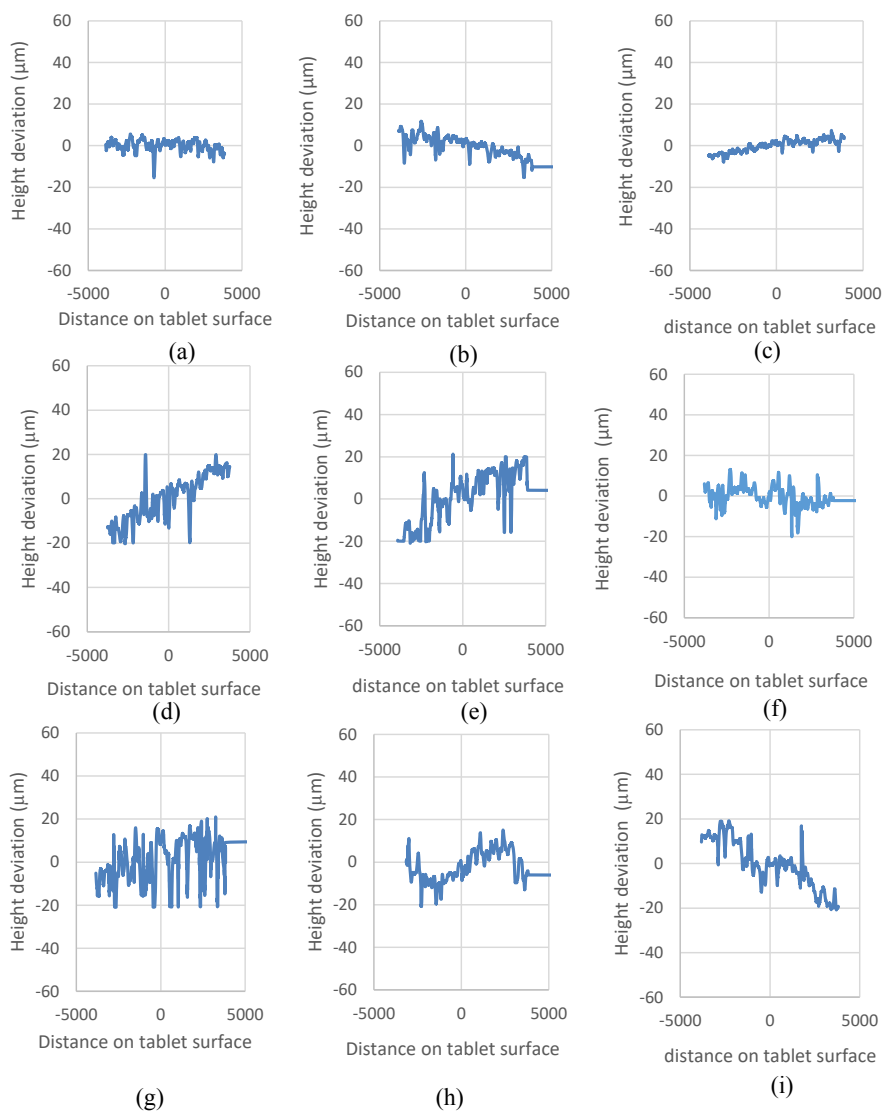


Figure 6: Surface profiles of tablet produced at different moisture content and compression forces (a) 4.7 % M-5kN (b) 4.7 %M-10 kN (c) 4.7 %M-15 kN (d) 9.6% M- 5 kN (e) 9.6 %M-10 kN (f) 9.6 %M-15 kN (g) 10.7 % M-5 kN (h) 10.7 % M-10 kN (i) 10.7%-15 kN

Figure 7 shows images (Raw (Upper) and QCI (Lower)) of three tablets produced with 4.7% moisture content using different compression forces of 5, 10 and 15 kN. Figure 8 and 9 shows the same for the tablet produced with 9.6 % and 10.7% moisture content respectively. In the color scale bar, the two extremes colors (blue and red) represents dry and wet tablet respectively.

For tablet produced with 4.7, 9.6 and 10.7 % moisture content at different compression forces. It can be noticed generally from these figures that as the compression forces increases, the moisture content/color intensity of the tablet surface increases even though similar moisture content was used when compressing the wet tablet at different load. This is could be a signature of the surface roughness effect and not the moisture content. This was seen in all the different moisture content used. Also, by looking at the Figures, it can be seen that there is black spots in the raw images which indicates the presence of holes as circled in the raw image (solid circle) and on the QCI (dotted circle). These showed different colour with respect to the blue colour of the major area of the tablet surface. This is a clear evidence that the roughness of the surface influences the result of the chemical imaging. This can be considered as a limitation of using the NIR-CI in such application.

Moreover, it can be generally seen from the Figure that surface with holes appeared to be always red in colour, and the peaks/debris appeared to be always blue in colour, this is also true for the tablet edges, which are usually higher than the surface in the middle of the tablet. This explains why always the edges appear to be blue although it is at similar moisture content when scanned.

Figure 10 shows the calculated surface roughness (Ra) as a function of compression force for different moisture contents. Ra values were calculated based on Eq. 1 in the experimental section. It can be seen from the Figure that as the compression force increases the surface roughness (Ra) decreases. However, as the moisture content increases, the surface roughness increases. In other word, as the compression force increases, the tablet surface become smoother and hence the moisture content determined by chemical imaging is getting close to the real moisture content of the tablet. This is because the colour of the chemical images indicates the moisture content with less influence of surface roughness.

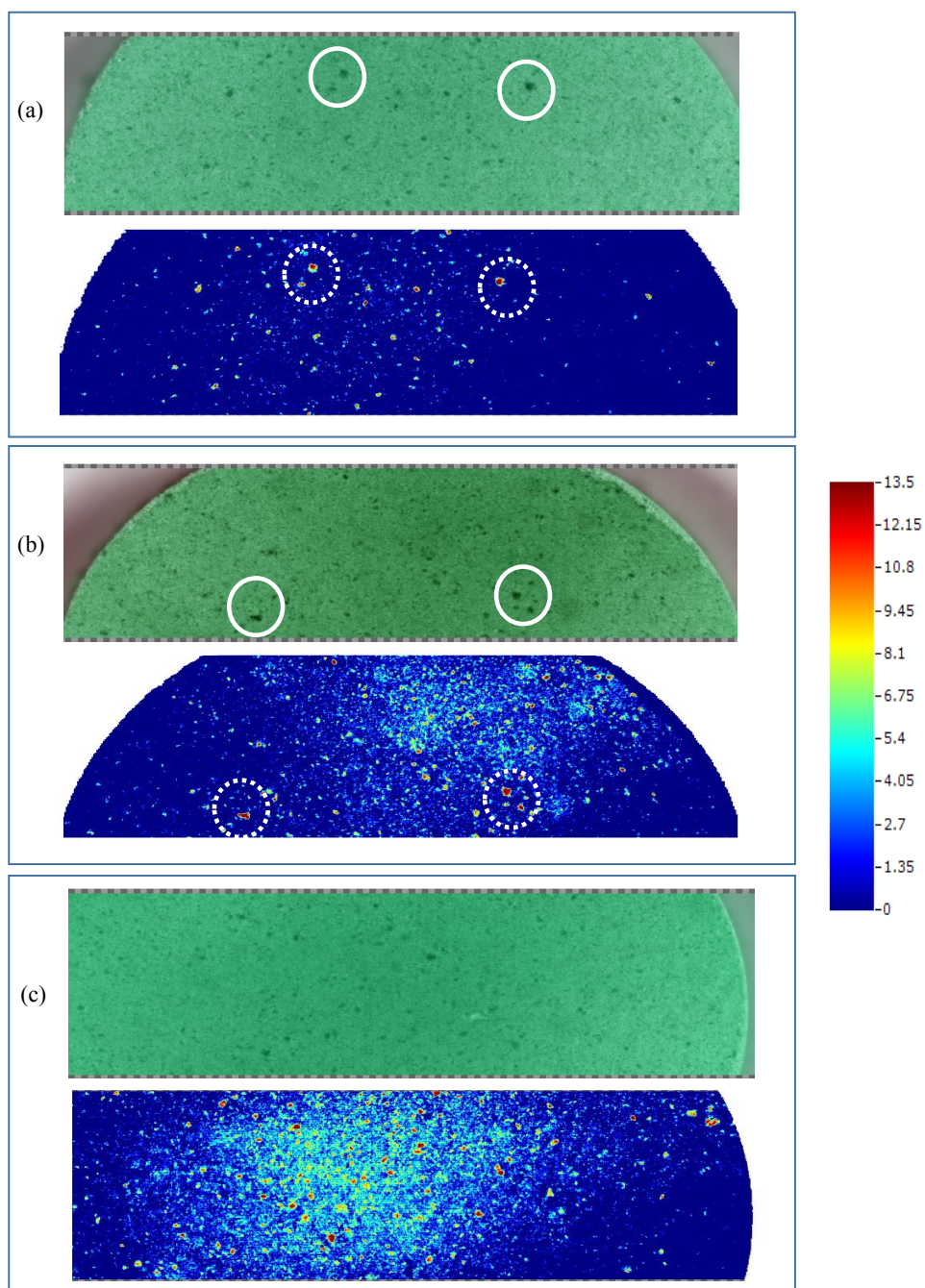


Figure 7: Raw image taken by the chemical imaging (Top) along with the corresponding QCI image (Bottom) for tablet produced with 4.7% moisture content at (a) 5kN (b)10kN (c) 15kN



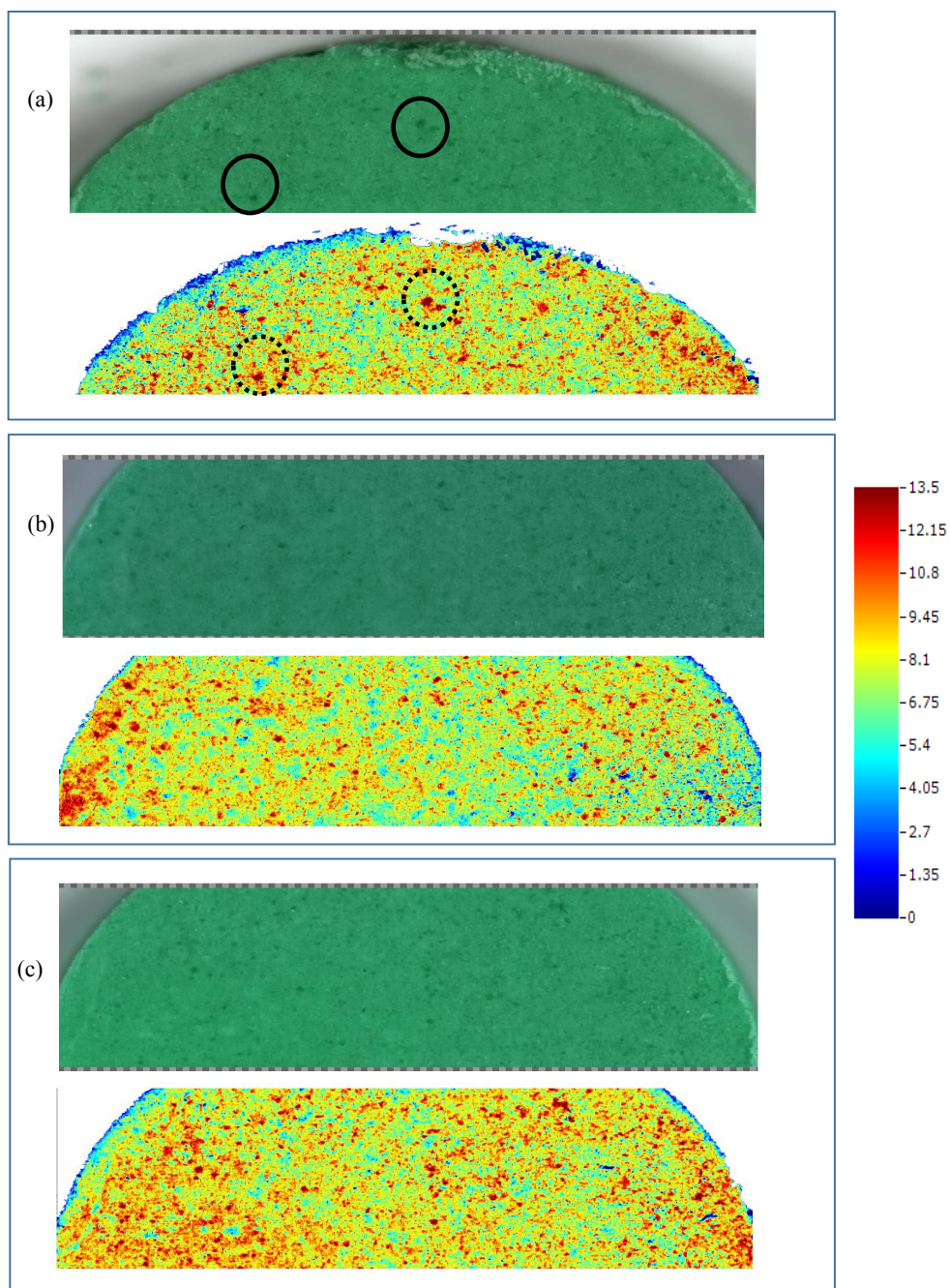


Figure 8: Raw image taken by the chemical imaging (upper) along with the corresponding QCI image (lower) for tablet produced with 9.6% moisture content at (a) 5kN (b)10kN (c) 15kN

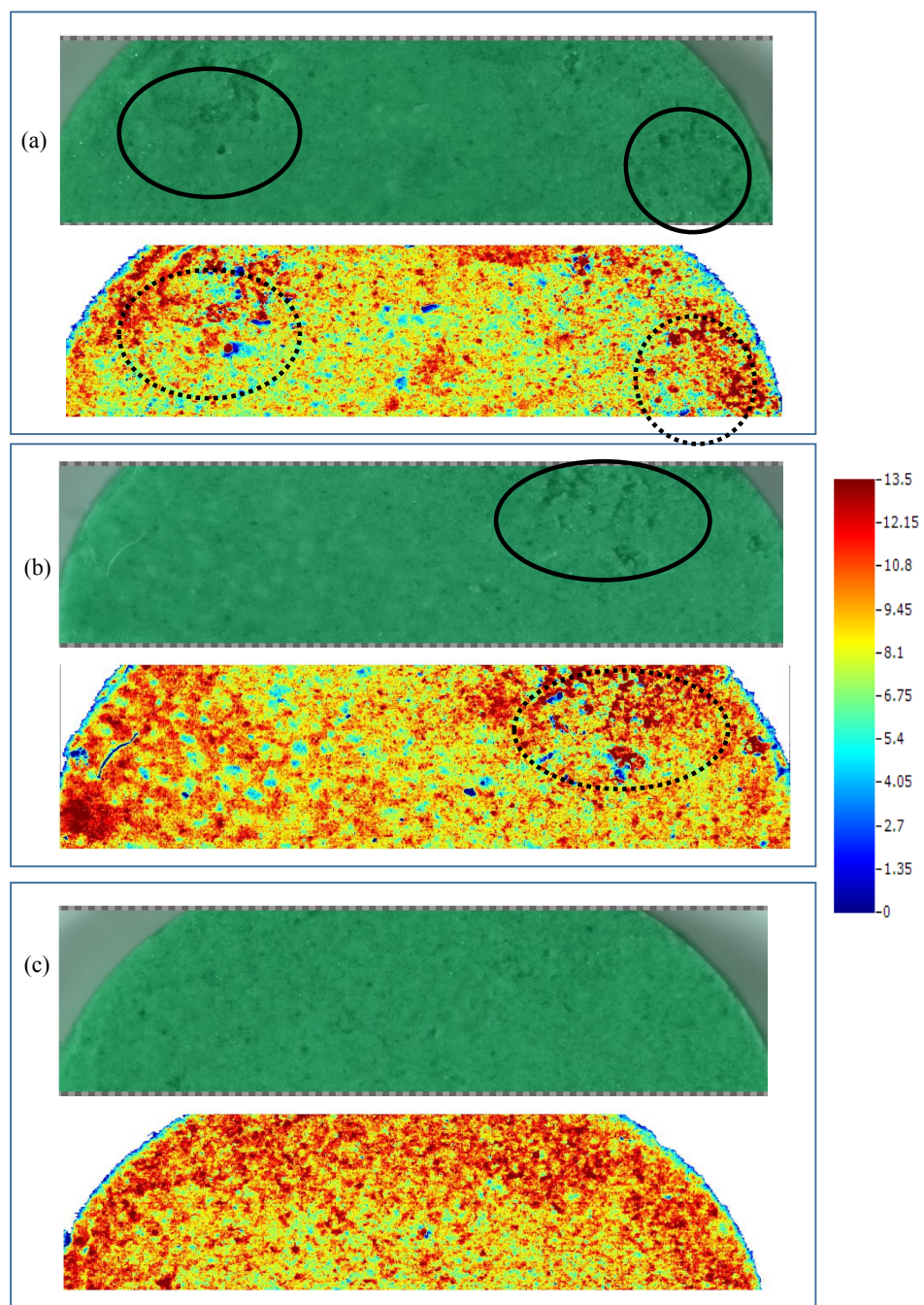


Figure 9: Raw image taken by the chemical imaging (Upper) along with the corresponding QCI image (Lower) for tablet produced with 10.7 % moisture content at (a) 5kN (b)10kN (c) 15kN

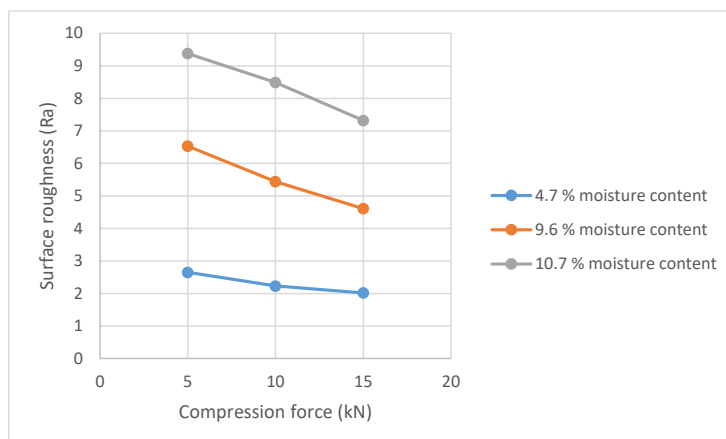


Figure 10: calculated surface roughness at different moisture content and compression forces

## CONCLUSION

This work highlighted the limitation of using the chemical imaging technique in determination of tablet moisture content. Tablet of different surface roughness were produced by using different compression forces and different moisture content.

It was found that the surface roughness highly influences the result of chemical imaging when determining the moisture content of the tablet and therefore misleading the result. It was also found that increasing the compression force and decreasing the moisture content caused a decrease in the tablet surface roughness.

## REFERENCES

- [1] S.T.F.C. Mortier, S.Van, H.K.Cierkens, K.V.Gernaey, P.S.B.De, B.T.De, B.I.Nopens, A GLUE uncertainty analysis of a drying model of pharmaceutical granules. *European Journal of Pharmaceutics and Biopharmaceutics*, 2013. 85(3 PART B), pp.984–995.
- [2] S.T.F.C.Mortier, T.D.Beer, K.V.Gernaey, J.Vercruysse, M.Fonteyne, J.P.Remon, C.Vervaeet, I.Nopens, Mechanistic modelling of the drying behaviour of single pharmaceutical granules. *European Journal of Pharmaceutics and Biopharmaceutics*, 2012. 80(3), pp.682–689.
- [3] M.Fonteyne, D.Gildemyn, E.Peeters, S.T. Mortier, J. Vercruysse, K.V. Gernaey, C.Vervaeet, J.P.Remon, I.Nopens, T.De.Beer, Moisture and drug solid-state monitoring during a continuous drying process using empirical and mass balance models. *European Journal of Pharmaceutics and Biopharmaceutics*, 2014.87(3), pp.616–628.
- [4] M. Manley, Near-infrared spectroscopy and hyperspectral imaging: non-destructive analysis of biological materials, 2014. *Chem. Soc. Rev.*, 43(24), pp.8200–8214.

- [5] P. Frake, D. Greenhalgh, S.M. Grierson, J.M. Hempenstall, D.R. Rudd, Process control and end-point determination of a fluid bed granulation by application of near infra-red spectroscopy, *Int. J. Pharm.* 151 (1997) 75–80.
- [6] A. Hartung, M. Knoell, U. Schmidt, P. Langguth, Role of continuous moisture profile monitoring by inline NIR spectroscopy during fluid bed granulation of an Enalapril formulation, *Drug Dev. Ind. Pharm.* 37 (2011) 274–280.
- [7] F.J.S. Nieuwmeijer, M. Damen, A. Gerich, F. Rusmini, K. van der Voort, H. Vromans, Granule characterization during fluid bed drying by development of a near infrared method to determine water content and median granule size, *Pharm. Res.* 24 (2007) 1854–1861.
- [8] A. Peinado, J. Hammond, A. Scott, Development, validation and transfer of a Near Infrared method to determine in-line the end point of a fluidised drying process for commercial production batches of an approved oral solid dose pharmaceutical product, *J. Pharm. Biomed. Anal.* 54 (2011) 13–20.
- [9] J. Rantanen, S. Lehtola, P. Ramet, J.P. Mannermaa, J. Yliruusi, On-line monitoring of moisture content in an instrumented fluidized bed granulator with a multi-channel NIR moisture sensor, *Powder Technol.* 99 (1998) 163–170.
- [10] J.M. Amigo, J. Cruz, M. Bautista, S. MasPOCH, J. Coello, M. Blanco, Study of pharmaceutical samples by NIR chemical-image and multivariate analysis 2008, *TrAC - Trends in Analytical Chemistry*, 27(8), pp.696–713.
- [11] E. Hernandez, P. Pawar, G. Keyvan, Y. Wang, N. Velez, G. Callegari, A. C. Bozena, M. K. Fernando, J. M. Rodolfo, R. J. Romanach, Prediction of dissolution profiles by non-destructive near infrared spectroscopy in tablets subjected to different levels of strain, *Journal of Pharmaceutical and Biomedical Analysis* 2016.117, pp.568–576.
- [12] T. Koide, Y. Yamamoto, T. Fukami, N. Katori, H. Okuda, Y. Hiyama, Analysis of Distribution of Ingredients in Commercially Available Clarithromycin Tablets Using Near-Infrared Chemical Imaging with Principal Component Analysis and Partial Least Squares. *Chemical & Pharmaceutical Bulletin*, 2015. 63(9), pp.663–668.
- [13] C. Ravn, E. Skibsted & R. Bro. Near-infrared chemical imaging (NIR-CI) on pharmaceutical solid dosage forms-Comparing common calibration approaches. *Journal of Pharmaceutical and Biomedical Analysis*, 2008. 48(3), pp.554–561.
- [14] A. Kumar, J. Vercruyssen, M. Toiviainen, P. E. Panouillot, M. Juuti, V. Vanhoome, C. Vervaet, J. P. Remon, K. V. Gernaey, T. D. Beer, I. Nopens, Mixing and transport during pharmaceutical twin-screw wet granulation: Experimental analysis via chemical imaging. *European Journal of Pharmaceutics and Biopharmaceutics*, 2014. 87(2), pp.279–289.
- [15] J. Vercruyssen, M. Toiviainen, M. Fonteyne, N. Helkimo, J. Ketolanen, M. Juuti, U. Delaet, I. V. Assche, J. P. Remon, C. Vervaet, T. D. Beer, Visualization and understanding of the granulation liquid mixing and distribution during continuous twin screw granulation using NIR chemical imaging. *European Journal of Pharmaceutics and Biopharmaceutics*, 2014. 86(3), pp.383–392.
- [16] G. Elmasry & J.P. Wold, High-speed assessment of fat and water content distributions in fish fillets using online imaging. *Journal of Agricultural and Food Chemistry*, 2008. 56, pp.7672–7677.
- [17] N. Elkhider, Chan. K.L.A. & S.C. Kazarian, Effect of moisture and pressure on tablet compaction studied with FTIR spectroscopic imaging. *Journal of Pharmaceutical Sciences*, 2007. 96(2), pp.351–360.

